AN INVESTIGATION OF THE BEHAVIOUR OF COUPLED SHEAR WALL STRUCTURES

by

Tien Dich Nguyen

A thesis submitted to the Faculty of Graduate Studies and Research in partial fulfillment of the requirements for the degree of Master of Engineering

Dept. of Civil Engineering & Applied Mechanics
McGill University
Montreal, Que.
Canada

March 1976

TABLE OF CONTENTS

ABSTRACT

This research program examined the behaviour of small-scale models of four-storey reinforced concrete coupled shear walls under monotonically increasing loads until failure. Methods of analysis briefly presented include:

(1) the Lamina Method,

(2) the Equivalent Frame Method,

(3) the Finite Element Method, and

(4) the Photoelastic Method

A method for direct model testing of coupled shear walls was developed in this study. The experimental set-up for this method consisted of a loading frame, a bracing system, a load distributor for an upper triangularly distributed load pattern, and a load transmission system to transfer a tensile (pull) force to the specimen. An ultimate load analysis using the Lamina approach was carried out to check the ultimate strength of the test specimens. Complete load-deflection curves for all four storeys and complete load-rotation curves for all four coupling beams and two walls, as well as strain values at selected positions, were obtained. Diagonal reinforcement pattern showed less distress and is therefore more suitable in transferring the load for medium and deep coupling beams. All test specimens showed significant ductility proving that if properly detailed, shear wall structures can absorb large amounts of energy and are suitable to resist earthquakes.

RÉSUMÉ

La présente recherche consiste en l'étude du comportement de modeles à l'échelle réduite, d'un mur de cisaillement jumelé de quatre étages, en béton armé, soumis à une charge croissante jusqu'à la rupture. Plusieurs méthodes d'analyses ont été brièvement présentées, notamment les quatre méthodes suivantes: (1) le remplacement des poutres d'accouplement par un "médium" continu et uniform de consistance équivalente à la rigidité des poutres, (2) la méthode du cadre équivalent, (3) l'idéalisation par éléments finis et enfin, (4) la photoélasticité.

Une méthode d'expérimentation directe a été développée pour les besoins de cette étude. Le montage expérimental se composait d'un cadre de chargement, d'un système d'appuis, d'un répartiteur de charge au niveau supérieur pour une distribution triangulaire des charges et enfin d'un mécanisme pouvant transmettre une force de tension a l'échantillon représentatif. Une vérification de la capacité ultime des prises d'essais a été effectuée par la méthode "Lamina" qui correspond à la première des méthodes spécifiées ci-dessus.

Les courbes complètes de charge-déflexion pour les quatre étages ainsi que les courbes de charge-rotation pour les quatre poutres d'accouplement et les deux murs ont été obtenues; de plus les valeurs des deformations à différents endroits prédeterminés ont aussi été

procurées. Une disposition en diagonale, du renforcissement dans les poutres d'accouplement, s'est avérée beaucoup plus efficace qu'une armature horizontale et, par conséquent, plus appropriée pour le transfert de charge dans des poutres dont l'épaisseur est de moyenne à profonde.

Toutes les prises ont démontrées une ductilité remarquable prouvant ainsi la grande capacité qu'a ce type de mur de cisaillement à absorber l'énergie: ce qui les rend aptes à resister aux tremblements de terre.

ACKNOWLEDGEMENTS

The author wishes to express his deep appreciation to Professor M.S. Mirza for the direction, advice and encouragement he gave to this work, and to Professor R.G. Redwood for providing the departmental assistantships, and other necessary facilities.

He is also grateful to Professor J. Udd for making available his photoelastic equipment; to Y. Faucher for his initial ideas of the loading frame; to B. Cockayne and the technical staff of the Concrete Laboratory for their assistance in building the loading equipment and the test specimens.

Special thanks go to Miss J. N. Richards for typing the final thesis.

LIST OF FIGURES

LIST OF TABLES

LIST OF TABLES (continued)

NOTATIONS

A	total cross-sectional area of walls 1 and 2.
A_e	equivalent cross-sectional area for "stiff-end" section.
A_f	equivalent cross-sectional area for middle portion of the coupling beams.
A_g	gross-sectional area of concrete.
A_{gN}	gross-sectional area of concrete of model structures.
A_{cr_1}	cracked cross-sectional area of wall 1.
A_{cr_2}	cracked cross-sectional area of wall 2.
A_{cr}	total cracked cross-sectional area of walls 1 and 2.
A_s	steel area.
A_{sM}	steel area for model structures.
A_t	transformed total area of the section.
A_{tN}	transformed total area of the section of the model structures.
A_1	cross-sectional area of wall 1.
A_2	cross-sectional area of wall 2.
A_ρ	cross-sectional area of the coupling beams.
$\{A\}$, $\{B\}$	vectors of coefficients.
C	distance to extreme edges from the neutral axis of individual wall.
C'	distance to extreme edges from common neutral axis of both walls.
E	Young's modulus of elasticity.
E_M	Young's modulus of elasticity for model structures.
E_c	concrete modulus of elasticity.
E_s	steel modulus of elasticity.

NOTATIONS (continued)

F	fringe constant.
G	modulus of rigidity.
H	total height of the structure.
H_M	total height of the model structure.
I_e	equivalent second moment of area for "stiff-end" section.
I_f	equivalent second moment of area of middle portion of the connecting beams.
I_{cr_1}	cracked second moment of area of wall 1.
I_{cr_2}	cracked second moment of area of wall 2.
I_{cr}	total cracked second moment of area of walls 1 and 2.
I_M	second moment of area of model structures.
I_1	second moment of area of wall 1.
I_2	second moment of area of wall 2.
I	total second moment of area of walls 1 and 2.
I_ρ	second moment of area of the coupling beams.
I_x	reduced second moment of area of a cracked beam.
I'_x	equivalent reduced second moment of area of a cracked beam.
K_1, K_2	wall bending stress factors.
K_3	connecting beam stress factor.
K_4	deflection factor.
L	linear dimension for prototype structures.
L_M	linear dimension for model structures.
M_o	total external cantilever moment.
$M_{1,0}$ $M_{2,0}$	moments induced by external load only in walls 1 and 2.
M_ρ	moments generated in the walls by separation forces.

NOTATIONS (continued)

M_{q1}, M_{q2}	moments generated by lamina forces in walls 1 and 2.
M_1, M_2	final bending moments on walls 1 and 2.
$M_{b,u}$	ultimate moment capacity of the coupling beams.
$M_{1,u}$ $M_{2,u}$	ultimate moment capacity at the base of walls 1 and 2.
P	point load at the top of structure, also point load for prototype structures.
P_M	point load for model structures.
P_{cr}	point load at cracking.
P_{cr_M}	point load at cracking for model structures.
Q_i	shear force acting on the coupling beam i.
$T_{(x)}$, $T_{1(x)}$ $T_{2(x)}$	axial force in the walls.
T_u	wall axial force at ultimate load.
$\{U\}$	vector of nodal displacement.
V	total external shear force.
V_p	shearing force generated in the walls by separation forces.
V_u	ultimate shear force across a coupling beam.
$V_{b,u}$	ultimate shear strength of the coupling beams.
V_1, V_2	final shear force on walls 1 and 2.
$V_{1,0}$, $V_{2,0}$	shear force induced by external load only in walls 1 and 2.
W	total external lateral load on coupled shear wall structure, also dead weight for prototype structures.
W_{cr}	total external load at cracking.
W_{cr_N}	total external load at cracking for model structures.

NOTATIONS (continued)

W_M	dead weight for model structures.
W_1, W_2	proportion of external load acting on walls 1 and 2 respectively.
W_e	external load at elastic limit of structural behaviour.
W_u	total external triangular ultimate load on coupled shear wall structure.
W_{u_M}	total external triangular ultimate load on coupled shear for model structures.
W_y	external triangular load which causes all lamina to yield.
$\Delta W'$	triangular load increment to cause wall 1 to attain its ultimate capacity.
$\Delta W''$	triangular load increment to cause wall 2 to attain its ultimate capacity.
Z	a stiffness ratio.
a_i, b_i	coefficients in displacement functions.
b	width of a coupling beam.
d	effective depth of a beam.
d'	distance from the centroid of flexural reinforcement to adjacent edge of beam.
d_a	lamina displacement at the cut due to wall axial force.
d_b	lamina deflection caused by flexure and shear.
d_f	lamina deflection owing to lamina flexure.
d_m	lamina displacement caused by the flexural rotation of coupled walls.
d_s	lamina displacement caused by shear.
e	length of "stiff end" section in the equivalent frame.
f	half length of middle portion of the connecting beams in the equivalent frame.
f'_c	cylinder crushing strength of concrete.

NOTATIONS (continued)

f_y	yield strength of steel.
h	storey height.
ℓ	distance between centroidal axes of coupled shear walls.
ℓ_1, ℓ_2	distance from axis of coupled shear wall structure to centroidal axes of walls 1 and 2 respectively.
$n = \frac{E_s}{E_c}$	= modular ratio.
$p(x)$, $p(\xi)$	lamina separation force per unit length.
$q(x)$, $q(\xi)$	lamina shear force per unit length.
q_i	lamina shear force per unit length at beam i level.
q_u	ultimate lamina shear force per unit length.
s	distance between inner faces of coupled shear walls or span length of coupling beams.
t	overall depth of a beam.
u	dead load per unit length.
u'	a displacement function.
v'	a displacement function.
v	nominal shear stress = V/bd.
w	external distributed load.
w_M	external distributed load for model structures.
x	distance from the top of a wall.
y	lateral deflection.
y_M	lateral deflection of model structures.
y_o	lateral deflection at the top of the shear wall structure.
y_o'	lateral deflection at top of structure caused by $\Delta W'$.
y_o''	lateral deflection at top of structure caused by $\Delta W''$.

NOTATIONS (continued)

y_e	lateral deflection of shear walls at the elastic limit.
y_{py}	lateral deflection of the walls at full plastification of laminas.
$\alpha, \beta, \gamma, \mu$	constants from the governing differential equation of the Lamina method.
$\mu' = \frac{\Delta u}{\Delta y}$	= ductility factor.
Δu	deformation at ultimate load.
Δy	deformation at yield load.
$\xi = \frac{x}{H}$	: specific distance.
λ	linear scale factor.
σ	stress at extreme edges.
ρ	flexural steel content.
$\rho' = \frac{P}{W}$	= constant load ratio.
ρ_w	web steel content.
ω	$\rho \frac{f_y}{f'_c}$
ν	Poisson's ratio.

I. INTRODUCTION

1.1 Introduction

In many tall buildings shear walls are constructed to provide a major part of the required strength and stiffness for lateral loading resulting from gravity, wind and earthquake effects. Recently, other structural systems such as frames, tubes, and tubes within tubes have also satisfactorily met the strength requirement and drift limitations of high-rise buildings. It is usually up to the designer to select the basic structural system to suit the height and functions of the building and the preferable mode of deformation. However, up to a certain height, shear wall structures are the most economical and the most effective system in resisting lateral forces. Shear walls are not only required for strength and stiffness requirements in buildings, but also for other human and functional requirements such as core walls for elevator shafts, stairwells and separation walls in apartment buildings.

Windows, doors and service ducts require that certain shear walls be provided with openings. A regular position of openings causes rows of connecting beams. Depending on the sizes of these connecting beams and the relative beam-wall stiffnesses, the overall behaviour of a coupled shear wall system tends to that of two separate walls or that of a single wall.

In addition to the limit states for strength and deflection, the ductility requirement arises for seismic design. In the past, many national building codes have treated shear walls as stiff and brittle elements not suitable for structures in earthquake prone regions. The Structural Engineers' Association of California[1] defined a numerical coefficient K that reflected the properties of the materials, the type of construction, damping, ductility and energy-absorption capacity of the structure. It suggested a K value of 1.33 in the calculation of earthquake load for box systems in which the lateral forces are resisted by shear walls. The comparative value of K allowed for a ductile moment resisting space frame resisting lateral loads is 0.67 suggesting that sufficient attention should be paid to ductility of component elements in the design of structural systems. The ductility of a coupled shear wall system is dependent on the ductility of the coupling beams or slabs and that of the walls themselves.

The fundamental behaviour of typical shear wall structures has been identified in numerous studies, in which the techniques of elastic analysis have been used or suitably modified to evaluate internal load distribution, stresses and deformations. However, at present only limited experimental data is available from which the range of validity of such analysis, as applied to reinforced concrete shear walls, could be assessed. In the following parts of experimental work, models of coupled shear walls are tested under monotonically increasing static loads. Loads are applied at floor levels using an upper triangular distribution. For design purposes, this pattern of loading is considered to be a static equivalent of earthquake loads in the first mode of vibration.

1.2 Previous Studies on Coupled Shear Walls

The widespread use of shear walls in multistorey buildings has fostered investigations into the basic behaviour of such structures. During the last decade, numerous studies on elastic analysis of coupled shear wall structures have been carried out while very little experimental work was done to examine the post-cracking behaviour of these structures.

The earlier successful attempts to solve the coupled shear wall problem were due to Chitty[2], Beck[3], and Rosman[4], who assumed that the discrete system of connecting beams or floor slabs may be replaced by an equivalent continuous medium. By assuming that the cross beam has a point of contraflexure at midspan, and does not deform axially, the behaviour of the system can be defined by a single second-order differential equation with a general closed form solution.

Later, by considering separately the cantilever action of individual walls, and composite cantilever action of the two walls, Coull and Choudhurry[5] presented Rosman's solution as graphical charts which enable a rapid evaluation of stresses and deflections in coupled shear walls for use in design offices.

A comprehensive series of photoelastic investigations of single storey walls containing rectangular openings and subjected to a single racking load, has been made by Kokinopoulos[7]. Curves have been produced, showing the effect of geometry of the panel on its stiffness, and the maximum tensile stress induced.

Different methods have been attempted to solve arbitrary systems of shear walls acting in conjunction with frames. An early computer program for analysis of multi-storey framed structures was extended by Clough, King and Wilson for three dimensional structures. The program, which used the stiffness method of analysis, was designed to include flexural, shear and axial distortions of the members; however, the floor slabs were considered to be rigid in their own plane and therefore the axial deformation of the beams was neglected.

These effective computer programs for solving frame problems paved the way to "the equivalent frame" method for analysing coupled shear wall problems. Schwaighogher[9] developed a table for the equivalent section of the stiff-ended beams connecting the equivalent column to the coupling beams.

From the point of view of ductility, Allen, Jaeger and Fenton[10] classified shear walls into three categories: the shear-shear wall, the moment-shear wall, and the ductile moment-shear wall. The ductile moment-shear wall is essentially an axially loaded flexural member having a minimum ductility factor of three. In an analytical study they noted that ductility of a ductile moment-shear wall increases with a decrease in axial load or with an increase in the flange area-gross wall cross-sectional area ratio, and it decreases with a decrease in the concrete strength, and remains relatively constant with changes in the main steel area. Suitable design techniques have been suggested to achieve ductile behaviour by considering the following factors:

(a) Minimum tension steel to ensure a "well-behaved" moment--curvature relationship: Besides the vertical and horizontal temperature steel requirements for a wall, the ductile-moment shear wall must have concentrations of reinforcing steel at each end of the wall, which should be tied as the longitudinal reinforcing steel in a column.

(b) Prevention of a premature shear failure before bending failure: The wall should be designed for an increased shear strength.

(c) Development of full moment capacity of wall at foundation: Foundation should be designed for ultimate moment capacity and adequate anchoring of the reinforcement.

(d) Prevention of a premature bond failure of the tension steel before bending failure.

(e) Construction joint details: Use of the 1971 ACI Code containing reinforcing steel requirements for shear friction was suggested.

(f) Decrease in the concrete strength: To be certain of the design ductility and strength to be attained, it was recommended that the value of concrete strength used in the calculations should be somewhat less than the specified concrete strength.

Jaeger et al.[11] solved the problem of elastic multiple shear walls connected by a large number of horizontal beams subjected to lateral loads. A reasonably accurate method for analyzing three-dimensional multiple shear wall buildings was extended to study the dynamic behaviour of the structures.

Mirza and Jaeger[12] studied the behaviour of two-storey coupled shear wall slab structures using small scale direct models. Two series of 1/10 scale shear walls coupled with two levels of slabs were constructed and tested. The study showed that shear walls behaved as individual deep beams and failure occurred in a shear compression mode with a ductility factor (ratio of ultimate strain to yield strain) of four and above. The wall size had a significant effect on the ultimate strength of the assembly. With improved reinforcing details, the shear-compression mode of failure can be either delayed or eliminated to obtain a more ductile flexural failure. The value of K was determined to be the same at 0.67.

In New Zealand, Paulay[13] tested a number of $\frac{3}{4}$-scale relatively deep and short spandrel beams for cyclic, near ultimate, alternating static loading. Rotations were applied to the beams by means of end blocks which simulated parts of coupled walls. Diagonal cracking across the beams was reported.

Paulay[14] later tested two one-quarter scale, seven storey reinforced concrete coupled shear wall models. He used identical wall reinforcement for the two models but varied the steel reinforcement in the coupling beams, one with the conventional parallel reinforcement (at top and bottom) and the other with cross-reinforcement following the stress trajectories. The distress in the concrete due to shear at the beam-wall interface was found to be not as severe in the cross-reinforced beams as in the conventionally reinforced beams with parallel steel reinforcement (top and bottom). Corresponding ductility factors of four to twelve were estimated for both models.

Recently, Mamet[16] at McGill University, has extended the finite element program developed by Mehrotra and Mufti[17] for a complete three-dimensional analysis of tall buildings by considering floors as substructures. He accounted for the flexural and in-plane deformations of the elements which were assumed to behave linear elastically. This program can be used for a large variety of usual building configurations comprising of slabs, shear walls, columns, beams, diagonal braces, etc. Openings in the walls and floors are taken into account, along with the effects of torsion, axial load and shear deformations. The mesh used in this program was a rectangular parallelepiped grid. Two original formulations were developed, a set of new displacement functions for the bending of rectangular elements and a new finite element treatment of the analysis of plane shear wall structures and their interaction with plane frames.

The finite element method has been utilized and made more versatile by Wilson[20] with a static analysis program for three-dimensional solids. This program called SSAP and its later revisions for dynamic analysis facilitated the solution of shear wall structures for both static and dynamic loads.

1.3 Scope of the Present Investigation

Though coupled shear walls have been used widely in high-rise buildings in earthquake prone regions and other areas, the understanding of their behaviour does not even come close to that of frame structures. The interest in understanding the behaviour of coupled shear wall systems has increased significantly over the past decade and a corresponding increase in research activity can be noted in the technical literature. The initiative of the University of Southhampton in organizing the first international symposium on tall buildings and shear wall structures in 1966[18] was a highlight in the efforts to promote knowledge in this field. More recently, two symposia held at the Buffalo and Dallas ACI conventions in 1971 and 1972[19] dealt with various aspects of analysis and design of tall concrete buildings, and clearly showed the need for more research in understanding the behaviour of shear wall structures in earthquake regions.

New techniques of elastic analysis of coupled shear wall systems have been developed to predict their behaviour. Most of these techniques can be modified to accommodate the plastification of certain parts of the structure. However, they can hardly cope with the real structures where brittle behaviour of concrete due to its cracking characteristics violates the assumption of isotropy and that of plane sections remaining plane.

There is very little experimental data on multistorey coupled shear walls subjected to earthquake loadings. Not much has been done on the post-elastic behaviour and the ductility of the reinforced concrete coupled shear wall systems.

A lack of understanding in this field can cause great damages to the occupants of the buildings not properly designed. Especially in high risk earthquake regions, a need for such an understanding is unquestionable.

This research program was developed with the purposes:

(a) to study the inelastic behaviour of coupled shear wall structures;

(b) to develop suitable techniques for model studies of the behaviour of reinforced concrete coupled shear walls.

This study forms a part of the on-going shear wall research program at McGill University. In the subsequent chapters, different methods of coupled shear wall analysis are developed and reviewed. A photoelastic study was also carried out before the reinforced concrete model study to check the stress patterns and trajectories in these shear wall configurations.

II. METHODS OF ANALYSIS OF COUPLED SHEAR WALLS

2.1 Introduction

A few methods of analysis of shear wall structures have appeared in the technical literature during the past several years. Most of the analysis methods have involved some forms of idealization or equivalence of all or part of the structure for purposes of simplification.

To determine the internal forces and moments in the various elements of a shear wall structure, certain idealizations need to be introduced. All methods of analysis which will be discussed in the following sections are based on the assumption that the material is (a) homogeneous, (b) isotropic, and (c) linear elastic. From the designer's point of view, the most important methods of analysis are:

(1) The Lamina Method[4]

(2) The Equivalent Frame Method[9]

(3) The Finite Element Method[20]

(4) The Photoelastic Analysis[21]

(5) Model Analysis[22]

Most of the basic understanding of shear walls has been achieved with the aid of the Lamina method especially through the efforts of Rosman[4], Beck[3], and Coull[5]. It was recognized that the deformation contributions due to bending and shear in the connecting beams, and due to bending and axial load in the walls, are significant and have been incorporated in this analysis of high-rise buildings. Presently the Lamina theory is used in design offices for analysis of building structures with regular shear wall configurations for which design aids are available.

The versatile "Equivalent Frame Method" has become very popular due to the ease with which it can be combined with the analysis of the "frame" part of the structure. The basic concept is the replacement of a given shear wall by a frame which behaves in the same manner as the given shear wall. This is achieved by suitably selecting the cross-sectional properties of the various elements of the frame. The method of analysis is basically the same as that for frame analysis and can be easily solved with the help of a large computer.

In recent years the Finite Element Method has been used successfully for the analysis of shear wall and shear wall-frame problems.[23] This method has proved to be reasonably accurate and advantageous in most of the cases. Different plane stress programs can be used with a wide choice of finite elements and the accuracy depends on the mesh used. A finer mesh would be more accurate though it can result in a higher cost due to the increased computer time involved.

The photoelastic method is useful in illustration of the stress trajectories and in the location of regions of stress concentration. However, this method is limited in its application to linear elastic systems.

2.2 Elastic Methods of Analysis

2.2.1 The Lamina Analysis

(a) Development of the Method

The following derivation of the elastic lamina analysis is largely based on the Beck-Rosman approach. Besides the assumption of material behaviour already stated in section 2.1, the lamina analysis makes the following further assumptions:

(1) All openings are of the same size.

(2) The sectional properties of the walls do not vary with the height of the structure.

(3) The sectional properties of all coupling beams are the same, with the possible exception of the uppermost coupling beam which can have half the stiffness of the coupling beams at the lower levels.

(4) The axial deformations of the coupling beams are neglected.

(5) The shear deformations of the walls are neglected.

(6) Each of the coupling beams has a point of contraflexure at its midspan.

(7) The external lateral load can be expressed as a continuous function of the distance x, which is measured from the top of the structure (Fig. 2.1).

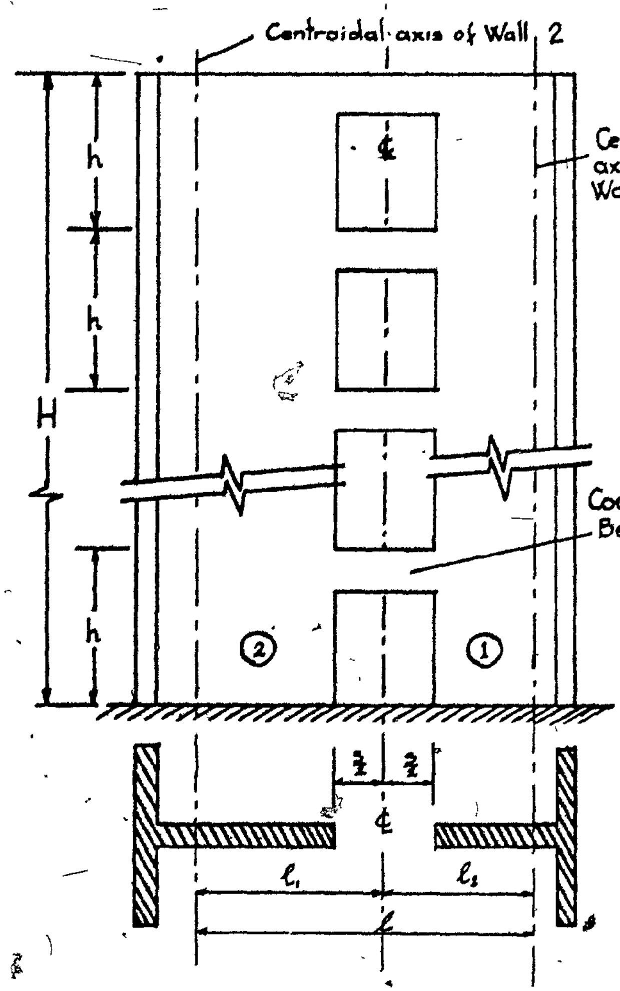

Fig. 2.1, Wall Dimensions

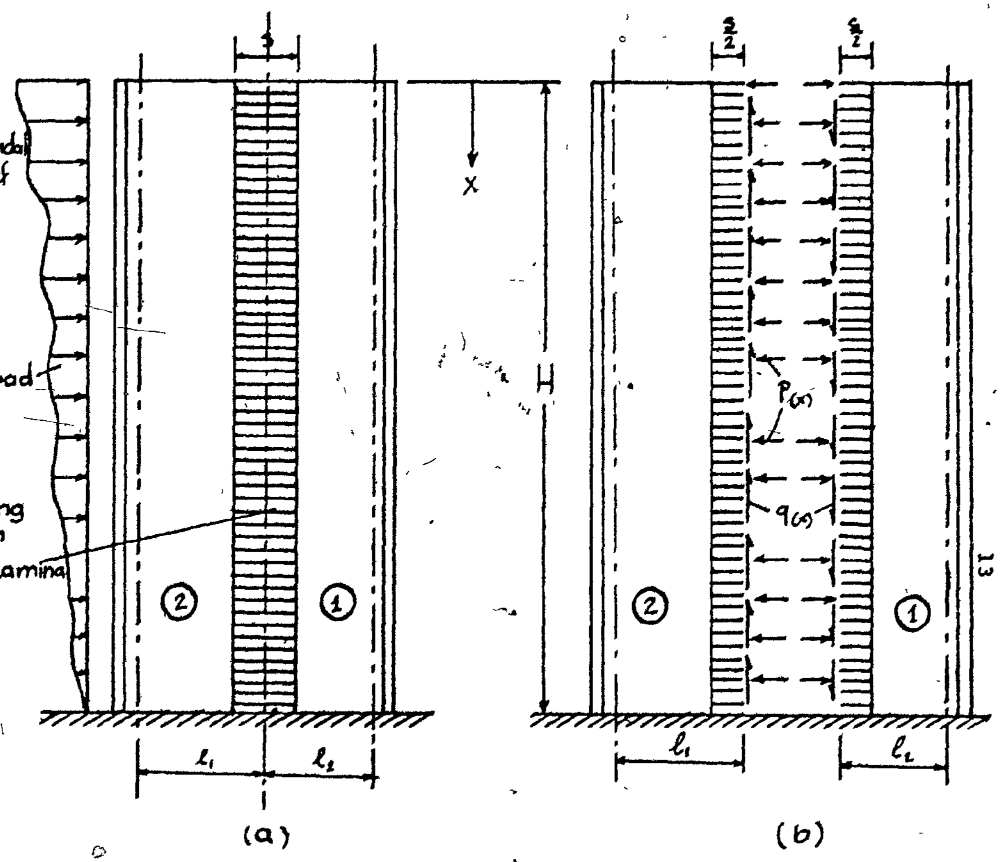

Fig. 2.2, The Laminar Model Structure

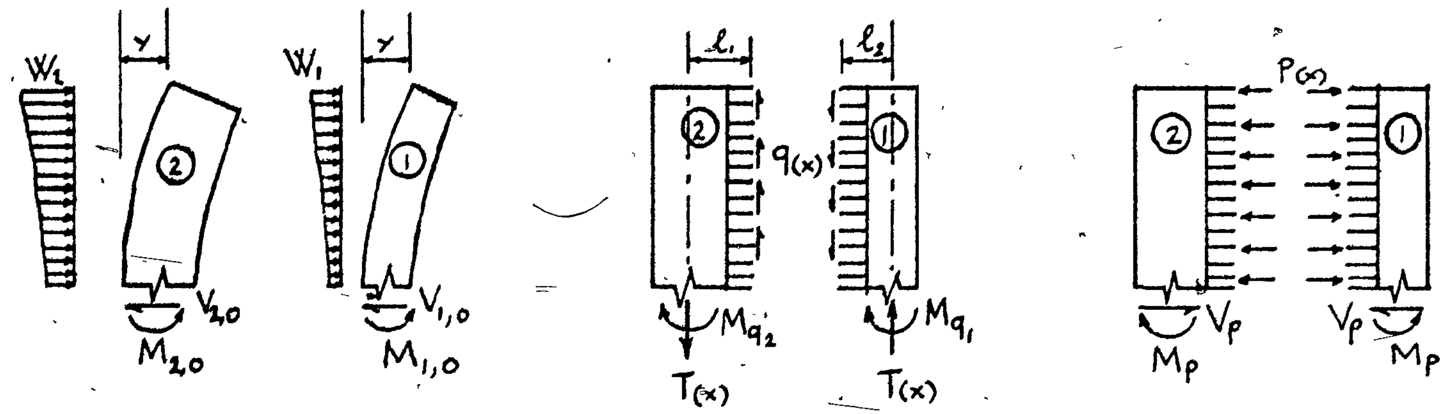

Fig 2.3 Wall Actions

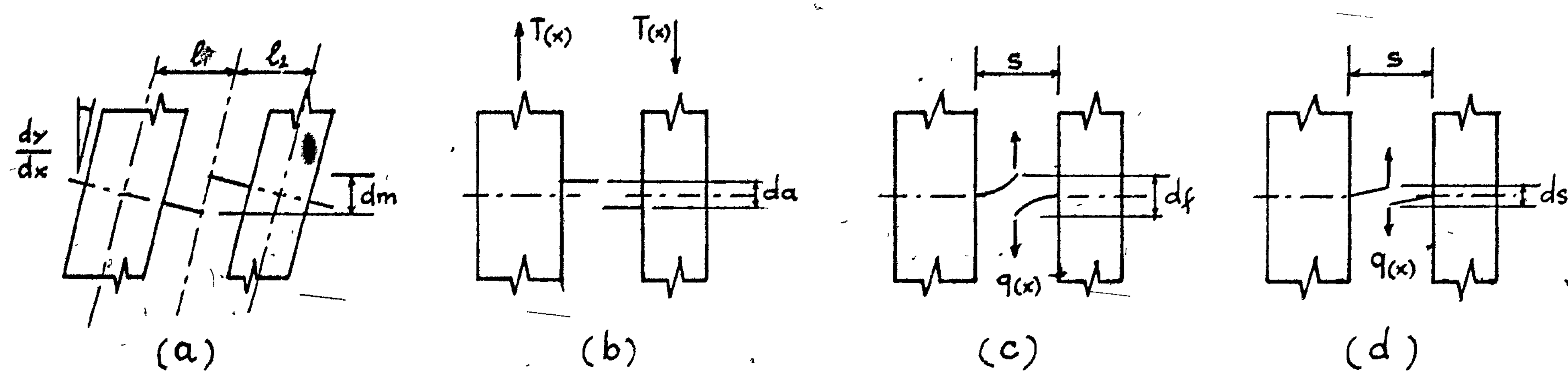

Fig. 2.4, Deformation and Discontinuity in a Cut Lamina

The properties of the substitute connecting medium of length dx are selected in such a way that

$$\text{Area of the lamina} = \frac{A_\rho}{h}\,dx$$

$$\text{Second moment of area of the lamina} = \frac{I_\rho}{h}\,dx$$

where A_ρ and I_ρ are the cross-sectional area and the second moment of area respectively, of the discrete beams.

The actions, such as shear force and axial force, are similarly replaced by a continuous distribution, referred to as "lamina shear", or "shear flow", in terms of force per unit length, and "separation force".

It has been assumed that the points of contraflexure are located at the beam midspans. Also, the lamina shear and separation forces are taken as positive when acting in the direction shown in Fig. 2.2.b.

If W = the total external lateral load

V = the total external shear at any level

M_o = the total external cantilever moment at any level (a continuous function of x)

I_1, I_2 = the second moments of areas of walls 1 and 2 respectively

I = the sum of the second moments of area of walls 1 and 2 $= I_1 + I_2$

then, the basic relationships between the distributed forces between the two walls are:

$$W_1 = \frac{I_1}{I} W \quad \text{and} \quad W_2 = \frac{I_2}{I} W \tag{2.1}$$

$$V_{1,0} = \frac{I_1}{I} V \quad \text{and} \quad V_{2,0} = \frac{I_2}{I} V \tag{2.2}$$

Since the axial deformations in the coupling beams are assumed to be negligible, the deflections of the cantilever walls are the same at every level. Hence, the moment M_o is distributed to each wall in proportion to its flexural rigidity:

$$M_{1,0} = \frac{I_1}{I} M_o \quad \text{and} \quad M_{2,0} = \frac{I_2}{I} M_o \tag{2.3}$$

From equilibrium of a given segment of each wall, the axial force $T_1(x)$ or $T_2(x)$ is equal to the resultant of the laminar shear:

$$T_1(x) = T_2(x) = \int_o^x q(x)\,dx = T(x) \tag{2.4}$$

The final moments M_1 and M_2 in the walls can be calculated from the external moment and the axial force by:

$$M_1 = \frac{I_1}{I} [M_{1,0} - \ell T(x)] \tag{2.5a}$$

$$M_2 = \frac{I_2}{I} [M_{2,0} - \ell T(x)] \tag{2.5b}$$

where ℓ is the distance from the neutral axis of wall 1 to the neutral axis of wall 2.

Shear forces in the walls can be determined as the difference between distributed shear and shear force generated by the separation force in the lamina:

$$V_1 = V_{1,0} - V_p \tag{2.6a}$$

$$V_2 = V_{2,0} - V_p \tag{2.6b}$$

Determination of the separation force V_p is discussed later.

In deriving the basic differential equation for this method, the lamina is considered cut at its mid-length. The displacements and actions at the cut ends of the lamina are caused by the bending and axial deformations of the walls, and bending and shear deformations of the lamina itself. The displacement due to flexural deformations of the walls is (Fig. 2.4a):

$$d_m = \ell \frac{dy}{dx} = \frac{\ell}{EI} \int_x^H M_o dx - \frac{\ell^2}{EI} \int_x^H T(x) dx \tag{2.7}$$

The displacement due to axial deformations of the walls is (Fig. 2.4b):

$$d_a = \frac{1}{E} \left(\frac{1}{A_1} + \frac{1}{A_2} \right) \int_x^H T(x) dx \tag{2.8}$$

The displacement of the lamina due to flexural deformations is (Fig. 2.4c):

$$d_f = \frac{hs^3 q(x)}{12EI_\rho} \tag{2.9}$$

The displacement of the lamina due to shear deformations is:

$$d_s = \frac{Fhs}{GA} q(x) \tag{2.10}$$

where

F = the shape factor and is 1.2 for rectangular section,

G = the modulus of rigidity.

From the four diagrams shown in Fig. 2.4, it is evident that the compatibility at the cut of the lamina is satisfied when

$$d_m - da - df - ds = 0 \tag{2.11}$$

By substituting appropriate terms from Equations (2.7), (2.8), (2.9), (2.10):

$$\frac{\ell}{EI} \int_x^H M_o dx - \frac{\ell^2}{EI} \int_x^H T(x)\,dx - \frac{1}{E}\left(\frac{1}{A_1} + \frac{1}{A_2}\right) \int_x^H T(x)\,dx - \frac{hs^3}{12EI_x} q(x) = 0 \tag{2.12}$$

As the axial force is the accummulation of laminar shear, it follows from Eq. (2.4) that

$$\frac{dq(x)}{dx} = \frac{d^2T(x)}{dx^2} \tag{2.13}$$

The basic differential equation can be written in the following form:

$$\frac{d^2T(x)}{dx^2} - \alpha^2 T(x) = - \gamma M_o \tag{2.14}$$

in which

$$\alpha^2 = \left(\frac{1}{A_1} + \frac{1}{A_2} + \frac{\ell^2}{I} \right) \left(\frac{12Ix}{hs^3} \right) \tag{2.15}$$

and

$$\gamma = \frac{12\ell Ix}{I\ hs^3} \tag{2.16}$$

The solution of this equation yields the axial force T(x) induced in the walls:

$$T(x) = A \ \sinh\alpha x + B \ \cosh\alpha x + T_\rho(x) \tag{2.17}$$

where

$$T_\rho(x) = \frac{\gamma}{\alpha^2} \left(M_o + \frac{d^2M_o}{\alpha^2 dx^2} + \frac{d^4M_o}{\alpha^4 dx^4} + \ldots \right) \tag{2.18}$$

is a particular solution.

The integration constants can be found from the boundary conditions and the moment function, M_ρ .

The moment and shear force generated by the separation forces of the lamina can be determined from the axial force in the walls using the following relationships:

$$M_\rho = \frac{I_1\ell_2 - I_2\ell_1}{I} T(x) = CT(x) \qquad (2.19)$$

$$V_\rho = \frac{dM_\rho}{dx} = C\frac{dT(x)}{dx} = Cq(x) \qquad (2.20)$$

(b) Boundary conditions

The integration constants are found from the following two conditions:

(i) the axial force at the top of the wall must be zero, i.e.

$$T(x) = 0 \quad \text{when} \quad x = 0$$

(ii) if the wall is fixed at its base

$$q(x) = \frac{dT(x)}{dx} = 0 \quad \text{when} \quad x = H$$

Letting $\beta = \alpha H$, one obtains the following expressions:

$$A = T_\rho(o) \tanh\beta - \frac{1}{\beta\cosh\beta} \frac{dT_\rho(x)}{dx} \tag{2.21}$$

$$B = - T_\rho(o) \tag{2.22}$$

where

$T_\rho(o)$ = the value of particular integral when x is zero.

(c) <u>The External Load</u>

The moment intensity for an upper triangular distributed load is expressed as

$$M_o = WH\ (\ \xi^2 - \frac{\xi^3}{3}\ ) \tag{2.23}$$

in which W = the total triangular load

and $\xi = \frac{x}{H}$ $(0 < \xi < 1)$

For this load, only the first two terms of the particular integral are non-zero, which involve the zero and second order differentials. Therefore

$$T_\rho\ (\xi) = \frac{\gamma WH^3}{\beta^2} [\ \xi^2 - \frac{\xi^3}{3} - \frac{2}{\beta^2} (1 - \xi)\ ] \tag{2.24}$$

and

$$T_\rho(o) = \frac{2\gamma WH^3}{\beta^4} \tag{2.25}$$

$$\frac{dT_\rho(o)}{dx} = -\frac{2\gamma WH^2}{\beta^4} \tag{2.26}$$

and

$$\frac{dT_\rho(H)}{dx} = \frac{\gamma WH^2}{\beta^2}\left(1 - \frac{2}{\beta^2}\right) \tag{2.27}$$

For design purposes, the equivalent seismic load includes also a point load at the top of the structure. Therefore, the additional moment is

$$M_o = PH\xi \tag{2.28}$$

Hence:

$$T_\rho(\xi) = \frac{\gamma PH^3}{\beta^2}\xi \quad \text{and} \quad \frac{dT(o)}{dx} = \frac{dT(H)}{dx} = \frac{\gamma PH^2}{\beta^2} \tag{2.29}$$

The solution for the triangularly distributed load and a point load is obtained by substituting the appropriate values of the sum of the above two load cases into the integration constants of Eqs. (2.21) and (2.22). These values are then substituted into the equation of the unknown axial force (2.17) and (2.18) to obtain:

$$T(\xi) = \frac{\gamma WH^3}{\beta^2}\left[\frac{2}{\beta^2}\tanh\beta\,\sinh\beta\xi + \frac{\sinh\beta\xi}{\cosh\beta} \times \left(\frac{2}{\beta^3} - \frac{1}{\beta} - \frac{\rho}{\beta}\right) - \frac{2}{\beta^2}\cosh\beta\xi - \frac{\xi^3}{3} + \xi^2 + \frac{2}{\beta^2}(1 - \xi) + \rho'\xi\right] \tag{2.30}$$

where $\rho' = \frac{P}{W}$, the constant load ratio.

The shear force per unit length is obtained from:

$$q(\xi) = \frac{dT(\xi)}{Hd\xi} = \frac{\gamma WH^2}{\beta}\left[\frac{2}{\beta^2}\tanh\beta \quad \cosh\beta\xi\right.$$

$$+ \frac{\cosh\beta\xi}{\cosh\beta}\left(\frac{2}{\beta^2} + \frac{1}{\beta} - \frac{\rho'}{\beta}\right) - \frac{2}{\beta^2}\sinh\beta\xi \quad +$$

$$\left.\frac{1}{\beta}(2\xi - \xi^2) - \frac{2}{\beta^3} + \frac{\rho'}{\beta}\right] \tag{2.31}$$

Integrating twice and by introducing the boundary conditions for this case, one obtains:

$$y = \frac{WH^3}{EI}\left\{\frac{1}{60}\left(\frac{\gamma\ell}{\alpha^2} - 1\right)\left[\xi^5 - 5\xi^4 + 15\xi - 11 -\right.\right.$$

$$\left.10\rho(\xi^3 - 3\xi + 2)\right] - \frac{\gamma\ell}{\alpha^2\beta^4\cosh\beta}\left[\left(\sinh\beta\xi - \sinh\beta\right) \times\right.$$

$$\left(2\sinh\beta + \frac{2}{\beta} - \beta - \rho\beta\right) - 2\cosh\beta\left(\cosh\beta\xi - \cosh\beta\right) -$$

$$\left.\left.\frac{\beta^2\cosh\beta}{3}\left(\xi^3 - 3\xi^2 + 3(\xi - 1)\left(\frac{2}{\beta^2} - \rho'\right) + 2\right)\right]\right\} \tag{2.32}$$

The deflection at the top of the structure is obtained by putting $\xi = 0$:

$$Y_o = \frac{WH^3}{EI} \left\{ (1 - \frac{\gamma \ell}{\alpha^2})(\frac{11}{60} - \frac{\rho'}{3}) - \right.$$

$$\frac{\gamma \ell}{\alpha^2 \beta^4} \left[2 \quad \cosh\beta - \tan\beta \quad (2 \quad \sinh\beta + \frac{2}{\beta} - \beta - \rho'\beta) \right.$$

$$\left. \left. - \beta^2 (\rho' + \frac{2}{3}) \right] \right\} \qquad (2.33)$$

Reactions at the ends of a coupling beam situated at $x = x_1 + \frac{h}{2}$ are obtained from the relationships:

$$V = \int_{x_1}^{x+h} q(x)\,dx \qquad (2.34)$$

$$M_{max} = \frac{V_s}{2} \qquad (2.35)$$

2.2.2 <u>The Equivalent Frame Method</u>

The Equivalent Frame method has certain advantages over the Lamina method. It is applicable to almost all tall shear wall structures encountered in engineering practice, such as shear walls with one or several rows of openings, stepped shear walls, and shear wall-frame structures.

Because the analysis of frames is quite well-developed, and since the engineers are reasonably familiar with computerized solutions, replacement of shear wall by equivalent frames and the use of existing computer programs constitute the basic attractive features of this method. Its main advantages are:

(a) simplicity and efficiency,

(b) applicability to almost any shear wall configuration,

(c) such usual limitations as constant floor to floor height and constant size of openings are not a limitation in this method,

(d) the method is capable of handling horizontal loading of any type (uniform load, triangular load, or joint loads of any magnitude) at any locations in the structure besides any vertical loading (therefore the performance of a shear wall due to gravity loading can easily be assessed),

(e) the entire external loading on the building can be properly apportioned to the various shear wall bents.

Equivalent frames can also be found for other frame-type structures with a large number of bays, and even for column and slab structures. The accuracy depends on the relative stiffness of different members of the structure and whether axial deformation can be ignored or not.

If one compares the deformations under load in a coupled shear wall and in a plane frame with the same number of stories, then it is observed that a shear wall can be simulated by an "equivalent frame" which has the following characteristics:

(a) The center lines of the wall sections and of all connecting beams form the "equivalent frame".

(b) The cross-sectional characteristics of all columns in the equivalent frame are identical with those of the corresponding wall sections.

(c) The center portions of all beams have the same cross-sectional area as the connecting beams of the shear wall structures; any corrections in the deflection should be reflected in the value of the moment of inertia I_ρ.

(d) The end sections of the beams which do rotate but do not bend should theoretically possess infinitely large areas and infinitely large second moments of area.

The infinitely large cross-sectional areas and second moments of area of the stiff end of the beams may cause some difficulties in computation. Hence, it has been suggested[9] for the use of an equivalent cross-sectional area A_e and the second moment of area I_e for the "stiff ended" section and the same A_f and I_f for the middle portion of the connecting beams (Fig. 2.5). If e/f represents the ratio of the length of the stiff ended to the half-length of center portion, Table 1 can be used to determine A_e and I_e.

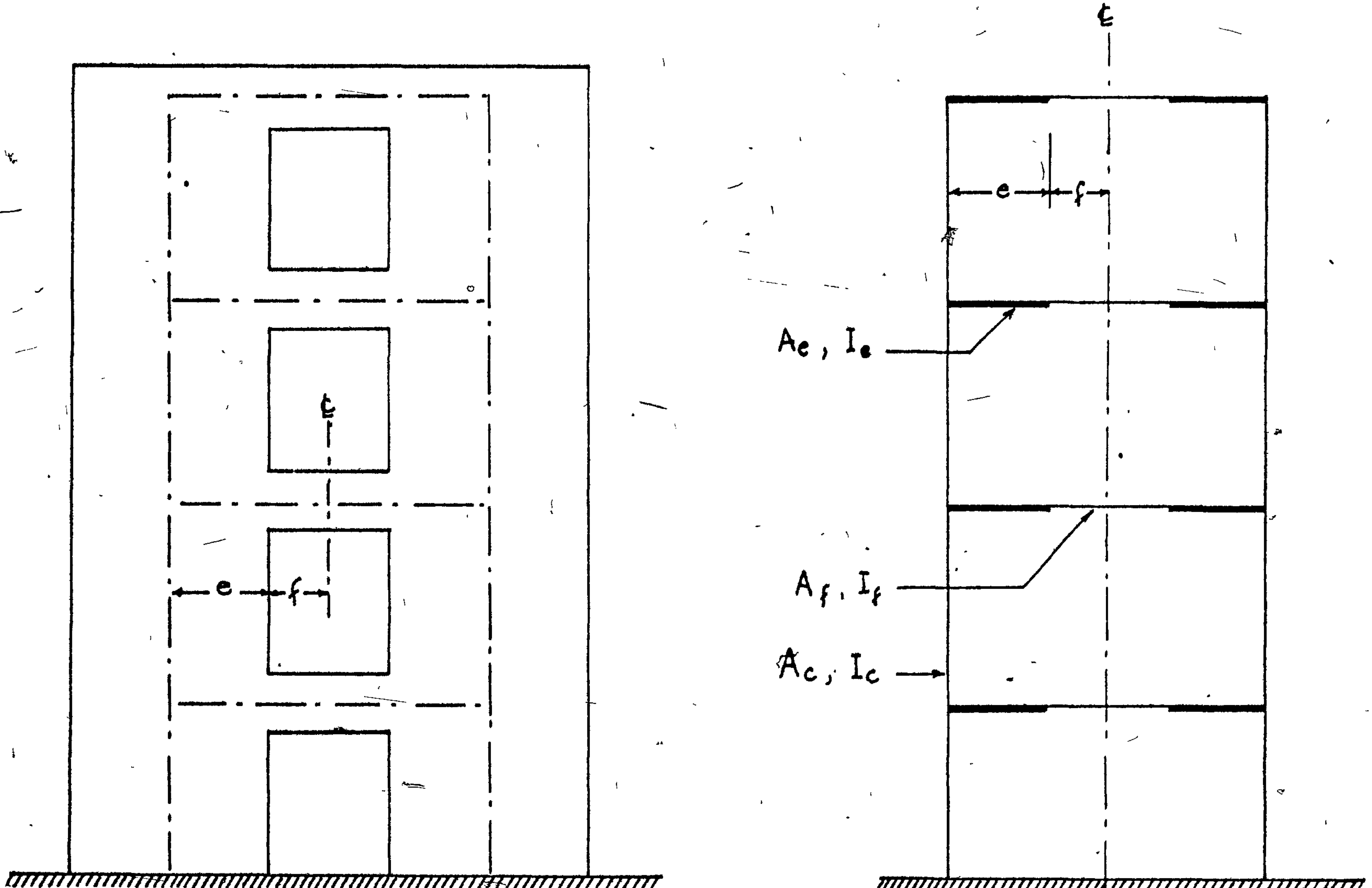

a) Shear Wall

b) Equivalent Frame

Fig. 2-5. The Equivalent Frame Method

TABLE 2.1 Equivalent Area and Second Moment of Area

e/f	A_e/A_f	I_e/I_f
0.5	50	238
1.0	100	700
2.0	200	2600
3.0	300	6300
5.0	500	21500

Schwaighofer[9] showed that with these ratios of areas and second moments of area, the deformations of the rigid connecting links are within an error limit of one percent, and hence an overall error in the moments and forces of the walls and beams would be of the order of 0.1 percent.

The shear wall is now properly simulated by a frame and can be analyzed using a suitable frame program which takes into account the effect of axial loads in the walls, and shear in the connecting beams besides the flexural effects.

The equivalent frame method is applicable not only in the analysis of coupled shear wall problems but also in the analysis of shear wall frame structures. A single shear wall can also be replaced by an equivalent frame with a single column connected to other frames by means of rigid arms. Solutions can be obtained by using any standard frame analysis program with a little hand calculation and minimum data input for computers.

2.2.3 The Finite Element Method

The Finite Element Method has been recently applied to shear wall analysis. It has certain advantages over other methods because of its ability to account for:

1. variation of thickness of shear walls,
2. irregularities in loading, body forces, etc.,
3. irregularities in the geometry of the openings,
4. variation in material properties.

This method consists of dividing a structure arbitrarily into elements whose material properties and general behaviour are known. Finite element analysis is normally carried out using the stiffness method of analysis which is described in many texts[26].

Triangular, quadrilateral and rectangular elements have been used successfully for analysis of shear wall problems. Commonly used element for such problems is the constant stress triangle in which the stresses are assumed to be constant throughout. It has the advantage of permitting easy representation of irregular geometrical shapes.

Because of the constant stress assumption, however, a large number of small elements are necessary in zones of rapid change of stress. The number of elements required to simulate a common shear wall, approximately 20 storeys high with one or more openings in each storey, makes the analysis cumbersome and costly.

Elements within which the assumed displacement functions permit greater freedom than the donstant stress triangular element are not uncommon. This is most often achieved by introducing one or two nodes along each side of the element in addition to those at the corners. Hansteen[27], for instance, has developed such a triangular element within which cubic variations of displacement are permitted, while compatibility is satisfied between adjacent elements. This element proved satisfactory for shear wall analysis, but it has the disadvantage of leading to a large band width (the maximum difference between node numbers within any element of the structure). For programs in which the entire banded portion of the stiffness matrix is stored, there is a serious limitation on the number of nodes that can be accommodated.

An alternative approach is a rectangular element with two degrees of freedom at each node, and an increased number of displacement within the element[28]. The displacement functions u' and v' consist of the following polynomials:

$$u' = a_0 + a_1x + a_2y + a_3xy + a_4y^2 + a_5xy^2 + a_6y^3 + a_7xy^3 \tag{2.26}$$

$$v' = b_0 + b_1x + b_2x^2 + b_3x^3 + b_4y + b_5xy + b_6x^2y + b_7x^3y \tag{2.27}$$

The vector of nodal displacements becomes:

$$\{U\} = \{u'_1 \; v'_1 \; \frac{\partial u'}{\partial y_1} \; \frac{\partial v'}{\partial x_1} \quad u'_2 \; — \; \frac{dv'}{\partial u_4}\}^T \tag{2.28}$$

can be related to the vector of coefficients

$$\{A\} = \{a_0 \; a_1 \; — \; a_7 \; b_0 \; — \; b_7\}^T \tag{2.29}$$

by the relationship: $\{U\} = [B]\{A\}^T$ (2.30)

A rectangular element with a rotational degree of freedom at each node has been used by MacLeod to overcome the difficulty of combining line elements in bending with constant stress elements. This element is most suitable for slender connecting beams, which can be represented by line elements in bending. The actual value of the in-plane rotational stiffness at a point in a plate will normally be high especially when compared with the stiffness of line elements which might be attached at the point. This is one reason why this degree of freedom is normally neglected.

Tocher and Hartz suggested a triangular plane stress element with six degrees of freedom represented by u, v, $\partial u/\partial x$, $\partial v/\partial y$, $(\partial u/\partial y + \partial v/\partial x$, $\frac{1}{2}(\partial u/\partial y - \partial v/\partial x)$. The greater the number of degrees of freedom per node, the greater will be the accuracy for a given mesh division. However, this must be set against the resulting increase in computational effort required for solution.

For practical shear wall analysis the finite element method is generally expensive in special circumstances. It is, however, useful for testing more approximate analysis techniques. The method is particularly valuable for analyzing the important effects of foundation flexibility, or the now common arrangement of a coupled shear wall supported at ground floor level in a frame structure.

2.2.4 Photoelastic Study

Besides the finite element method, photoelasticity is another powerful method of stress analysis which requires the physical construction of a model. The variety of problems that can be solved by use of photoelasticity, its simplicity, and the advantages of an instantaneous pictorial representation of stress, make the photoelastic method of considerable value to designers and researchers.

The photoelastic method was used in this study of coupled shear walls with the following objectives:

(a) To obtain a complete picture of stress distribution within a four-storey coupled shear wall model.

(b) To study the load transferring mechanism across the coupling beam system.

A loading device was constructed to transmit the load at four-storey levels to simulate an upper triangularly distributed load. The stress trajectories across the beams in this study provided information to design steel reinforcement pattern for the reinforced concrete models in this study.

(a) Model Material and Construction

Columbia Resin 39 was used to construct the model because of its easy machinability, lack of residual stress and high transparency. Effects of prolonged loading is quite pronounced in CR-39 and it is not possible to give any fixed stress-strain relationship without introducing the time factor. According to a previous study[21] at McGill University, the properties of CR-39 are listed as:

Young's modulus, $E = 3 \times 10^5$ psi

Poisson's Ratio, $\nu = 0.42$

Strength (tensile) = 600 psi

Proportional limit = 3000 psi

Fringe constant F = 84 lbs/in/fringe of principle stress difference

Coefficient of Thermal Expansion = 72×10^{-6} in/in/°F

An aluminium template of $\frac{1}{15}$ scale of the reinforced concrete prototype was cut in the laboratory. Using this template, a CR-39 photoelastic model of ¼" thickness was later cut. The size of the model was ¼" x 4" x 2.6" with four .6" x .7" holes spaced at 1 in. (storey height) and three beams of .3" x .6" and a top beam of .26" x .6" (Fig. 2. 6).

(b) <u>The Photoelastic Bench</u>

A standard photoelastic bench with rail-mounted components was used for this study. The polarizer and analyzer, which are the nearer and farther filters for transmitting plane polarized light, were graduated in degrees and were capable of being rotated about an axis conforming with the optical path. Perpendicular tracks on which the quarter wave plates could be moved in and out of the optical path were a design feature of the instrument.

The biaxial loading frame used was connected to two hydraulic pumps; one for applying loads in a horizontal direction and the other for applying a vertical load. Only the horizontal load application was used,

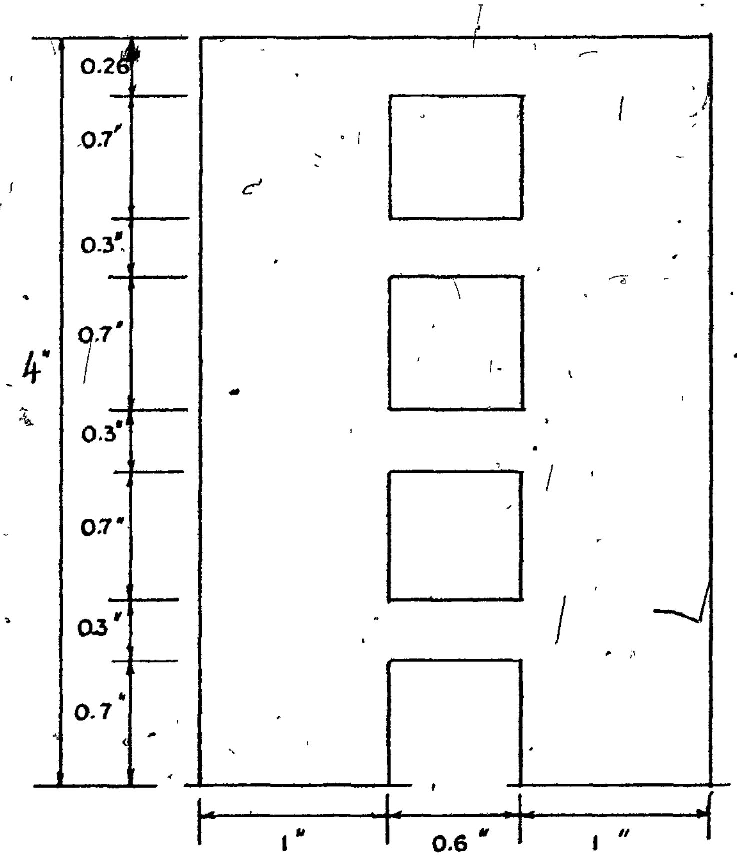

Fig. 2.6 The Photoelastic model

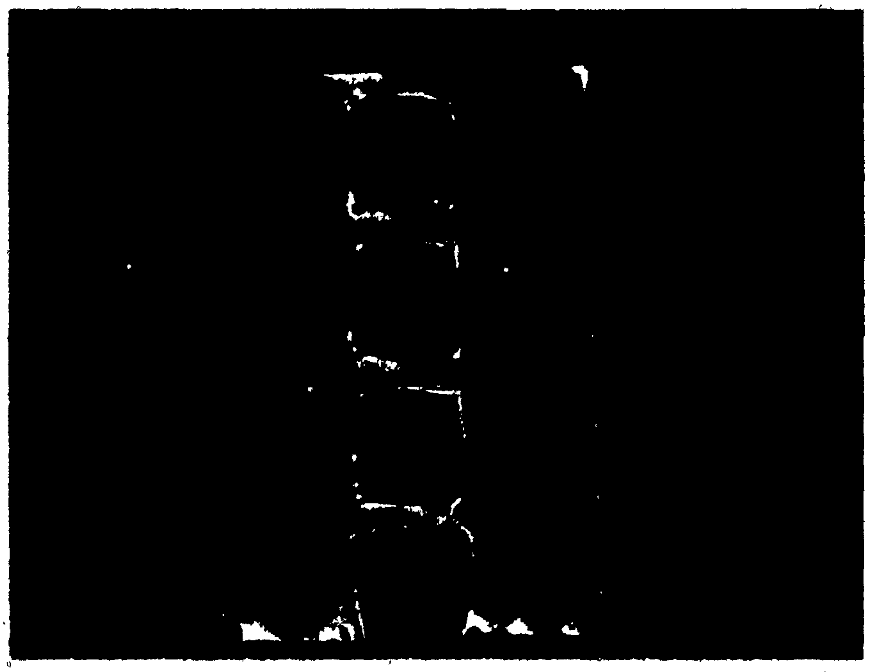

Fig. 2.7 Photoelastic specimen under 0 psi loading

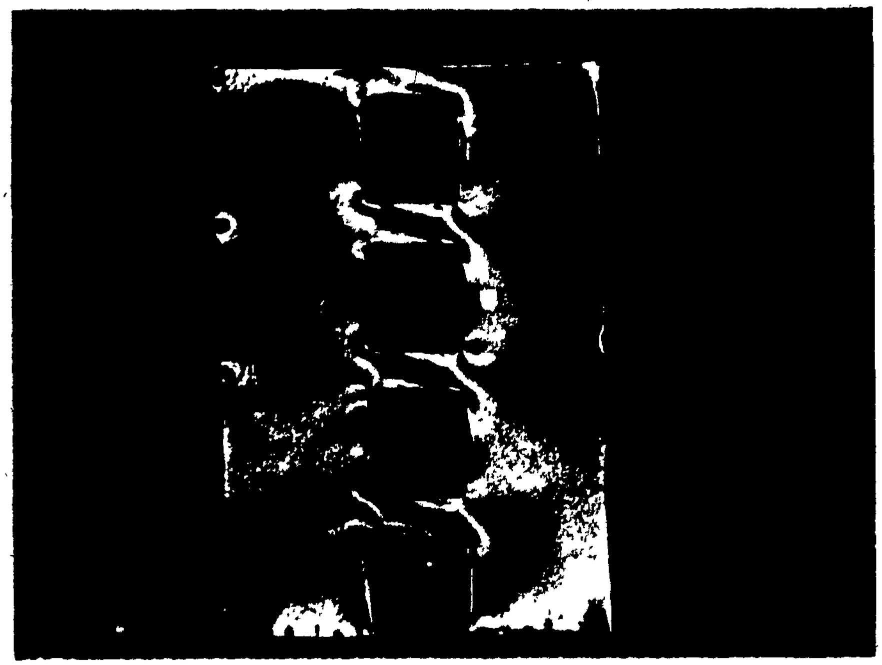

Fig. 2.8 Photoelastic specimen under 50 psi jack pressure

Fig. 2.9 Photoelastic specimen under 100 psi jack pressure

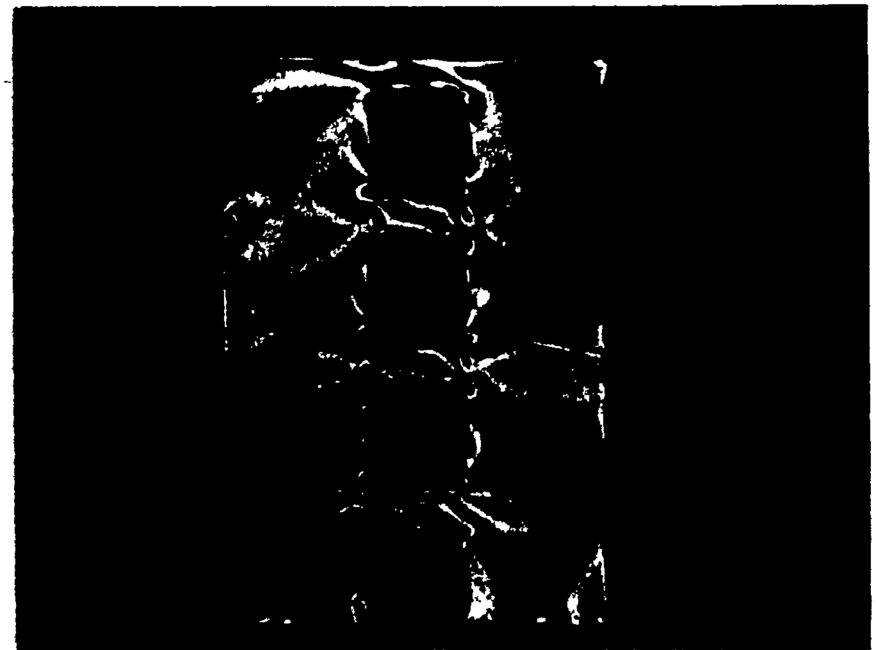

Fig. 2.10 Photoelastic specimen under 250 psi jack pressure

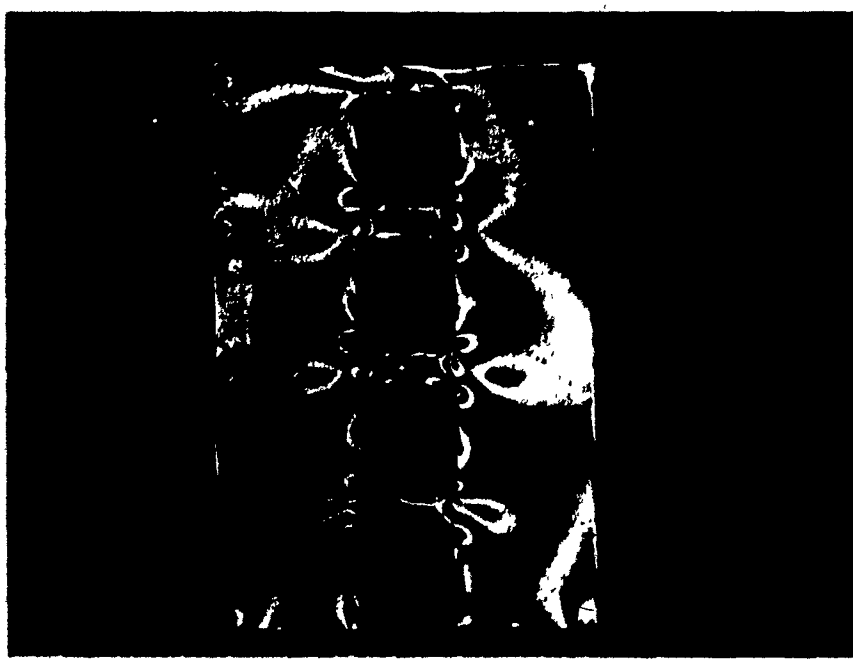

Fig. 2.11 Photoelastic specimen under 350 psi jack pressure

with a loading device mounted on the vertical side, which can distribute the load into four point load to correspond to an upper triangular distributed load pattern.

The photoelastic specimen was a $\frac{1}{15}$ scale model of the reinforced concrete model later studied or a $\frac{1}{150}$ scale model of prototype structure.

<u>Observations</u>: During the course of loading, the initial unloaded specimen and four loading increments of 50, 100, 250, and 350 psi of jack pressure were photographed. The unloaded specimen shows some effect of initial stresses due to the cutting and filing effects.

Some isochromatic fringe photographs are shown in the photographs in Figs. 2.7 to 2.10. The reader's attention is drawn to the progressive development of the fringe patterns. Points of particular interest are at the corners of the openings and the cross fringes in the coupling beams. These colored isochromatic fringes are lines of constant relative retardation along which the maximum shear stress, or the difference between the principal stresses, is constant. The photoelastic study also shows that the load transfer in medium and deep coupling beams is principally along the diagonal across the beam. This brings up the question of more effective steel design and supports Paulay's suggestion[13] that cross reinforcement is more effective in transferring load in coupling beams.

2.3 Accuracy of Existing Methods

The results of these stress and deflection analyses from the existing shear wall analysis methods were noted by many investigators to be in good agreement with experimental results using elastic materials, such as plexiglass or steel. The finite element method has also been used as a check to other methods. The continuous lamina approach has received a great deal of attention and would seem to have reached a stage where further developments in analytical methods are not likely to result in basic improvements in design techniques.

However, the major limitations of the technique arises from the basic assumptions regarding the regularity of dimensions, opening locations and structural properties throughout the height of the coupled shear wall system. If the wall system is not regular, whether through changes in the wall thickness or concrete strength, or changes in the number or location of bands of openings, the analysis becomes considerably more complex. Since the deviation of this method, it has been continually modified to account for certain special cases:

(a) variation of cross sections of the walls, which causes stepped coupled shear walls,

(b) flexible foundation conditions,

(c) inelastic and dynamic analysis.

The assumptions of all existing methods ignore the effects of local deformations at the beam-to-wall junctions on the stiffness of coupling elements. Introduction of correction factors have been attempted to account for these local deformations. One method is to consider deflection due to end moment in a cantilever beam as the sum of the effects of the wall and the bracket

$$\theta_m = \theta_c + \theta_w$$

$$= \frac{Mb}{EI} + \frac{6M}{Et^2}$$

$$\Delta_m = \Delta_c + s\theta_w + \Delta_w$$

$$= \frac{Mb^2}{2EI} + 6Ms/Et^2 + 0.8M/Et$$

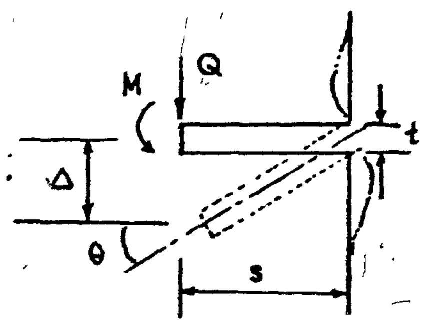

Fig. 2.12
Deformation of beam-wall junctions

The stress concentrations at these points of local deformations would be released very fast due to the cracking and crushing of the concrete. This effect would cause an early softening of the structure, and hence a deviation from the results of the analysis.

III. EXPERIMENTAL PROGRAM

3.1 Introduction

The experimental program consisted of building the loading frame and the loading arrangement simulating a statical equivalent of the earthquake loading to test the reinforced concrete shear wall models. The objectives of this experimental study were:

(1) to develop techniques for building and testing suitable direct models of coupled shear walls;

(2) to study the behaviour of reinforced concrete shear walls when subjected to lateral loads.

A simple method for tests of coupled shear walls under monotonically increasing loads was developed. The testing procedure can be suitably modified to include the effects of vertical loads and reversal of applied loads, besides examining the different load distribution patterns.

3.2 Description of the Test Specimens

Three coupled shear walls, each four storeys high, were tested with concentrated loads at the floor levels to simulate earthquake loads (upper triangular loading). These one-tenth scale model specimens were built using micro-concrete and annealed reinforcing steel wires[22].

The walls were reinforced with one layer of steel wires, while the beams were reinforced with two layers of steel, one on each side of the wall reinforcement.

The dimensions of test specimens Nos. 1 and 2 were as follows:

Wall cross-section	=	15" x 1.25"
Wall height	=	59.4"
Beam dimensions	=	4.5" x 9" x 1.25"
Dimensions of top beam	=	3.9" x 9" x 1.25"

In test specimen No. 1, the external face of the shear wall was reinforced with three D4 wires while the internal face was reinforced with one D2.5 wire. This reinforcement pattern is similar to that in real structures which are required to resist applied lateral loads in both directions (Fig. 3.1).

Another two D2 wires were provided at equal spacing as shown in Fig. 3.1. Horizontal shear reinforcements were provided with deformed wires of 0.005 in^2 cross section. The spacings of these wires were 1.5 in. centres in the lowest storey, 2.5 in. centres in the second storey, and 3 in. centres in the upper two storeys (Fig. 3.1).

All four connecting beams were reinforced with two D2 wires at the top and the bottom faces (Fig. 3.1). A minimum concrete cover of 0.2 in. was maintained throughout the specimen.

The reinforcement in the walls of test speciman No. 2 was similar to that of test specimen No. 1, except that it is proportioned for loading in one direction only as shown in Fig. 3.2. The reinforcing steel at the inside edge of the compression wall consisted of two D2.5

wires (which is twice that in specimen No. 1) while the reinforcement at the outside edge consisted on only one D4 wire, as shown in Fig. 3.2.

The dimensions of test specimen No. 3 were as follows:

Wall cross-section	=	16" x 1.25"
Wall height	=	60"
Beam dimensions	=	7" x 1.25" x 7"

The reinforcement pattern is shown in Fig. 3.3. Details of dimensions and reinforcement of the walls and beams are also given in Tables 3.1, 3.2, and 3.3. These coupled shear walls were designed according to the continuous lamina method with the help of the design charts reproduced in Appendix B. Properties of the materials are given in later sections. In the conventional design process, coupled shear walls are assumed to have only in-plane stiffness and are considered to be flexible in a direction perpendicular to the wall. Also, the interaction of the shear wall assembly with other elements such as floor slabs or frames was neglected in the experimental work. However, to prevent lateral buckling and to keep the applied loads in the plane of the shear walls, lateral bracing was provided as described in section 3.5.4.

3.3 The Formwork and Casting of Concrete

The formwork for the coupled shear wall models consisted of two platforms as shown in Fig. 3.4, and the base block form as shown in Fig. 3.5.

The formwork was put on six rollers so that it could be easily moved in the process of assembling the reinforcement or concreting. The lower platform was braced underneath by four 3" x 3" wooden diagonals as shown in Fig. 3.4. The upper platform was supported along the perimeter and along the beam positions (Fig. 3.4). After assembling, the formwork was coated with a waterproof paint. The shape of the shear wall model was laid out on the upper platform and 1.25" x 0.5" plexiglass pieces. These plexiglass pieces were connected to the upper platform by means of screws. Wall reinforcements were held in position by small metal wires which were strung across the width of form and the plexiglass pieces.

The test specimens were cast in one operation for the walls, beams, and the base block in the horizontal plane (Figs. 3.6 - 3.10).

3.4 Material Properties

3.4.1 The Micro-concrete

The micro-concrete mix was designed for a compressive strength of 4000 psi at an age of 14 days for Specimen No. 1 and 4000 psi at an age of 28 days for the remaining two specimens. High-early strength cement (Type III) was used for all specimens. The aggregates consisted of four narrowly graded crushed quartz sands (passing sieves #16, #24, #40 and #70). The details of mixes used for the three specimens are given in Table 3.1. The variations of micro-concrete compressive and tensile strengths with water-cement ratio are shown in Figs. 3.11 to 3.14 (ref. 22).

Fig. 3.1: REINFORCEMENT PATTERN OF SHEAR WALL MODEL NO. 1

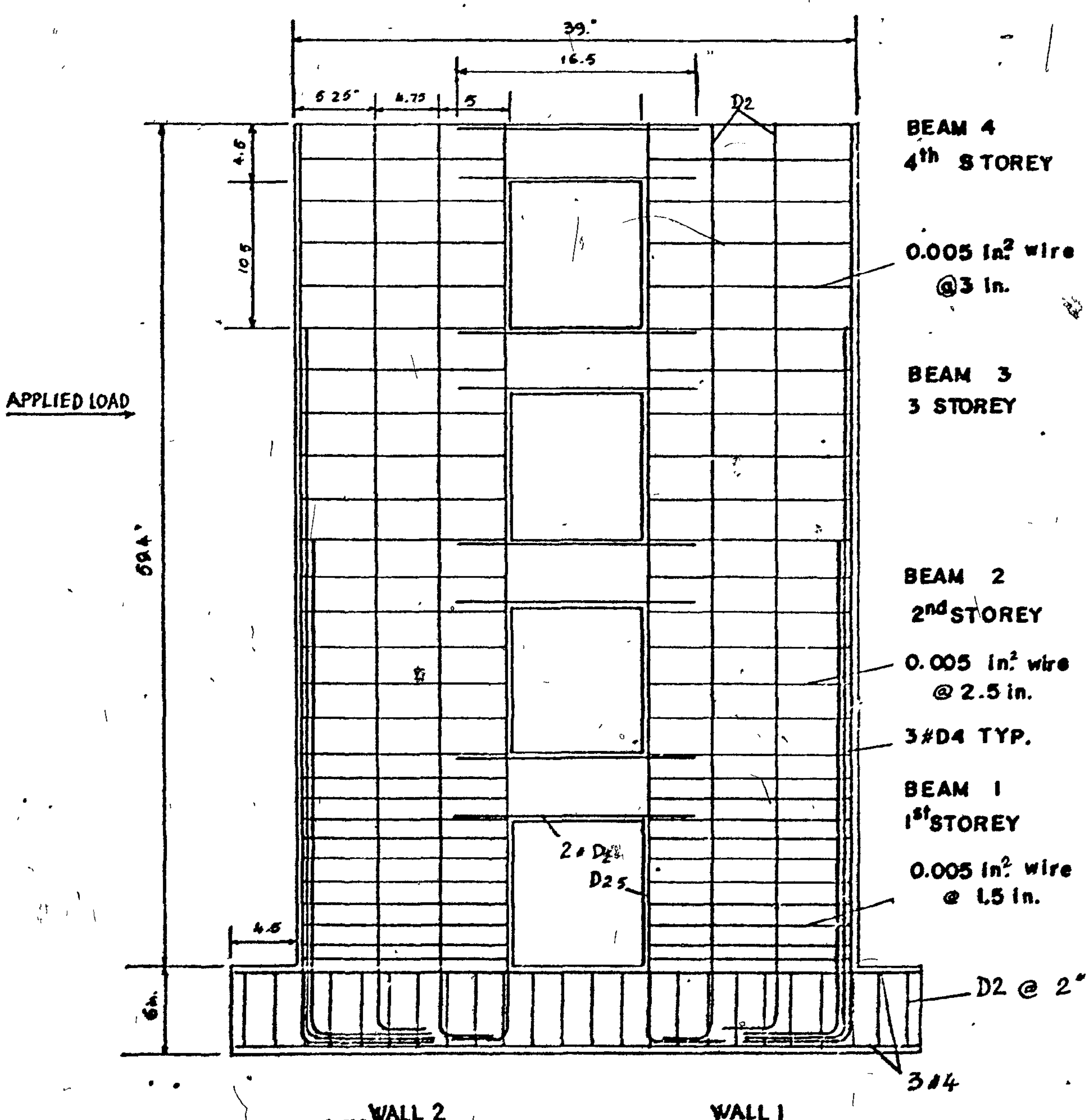

Fig. 3.2: REINFORCEMENT PATTERN OF SHEAR WALL MODEL NO. 2

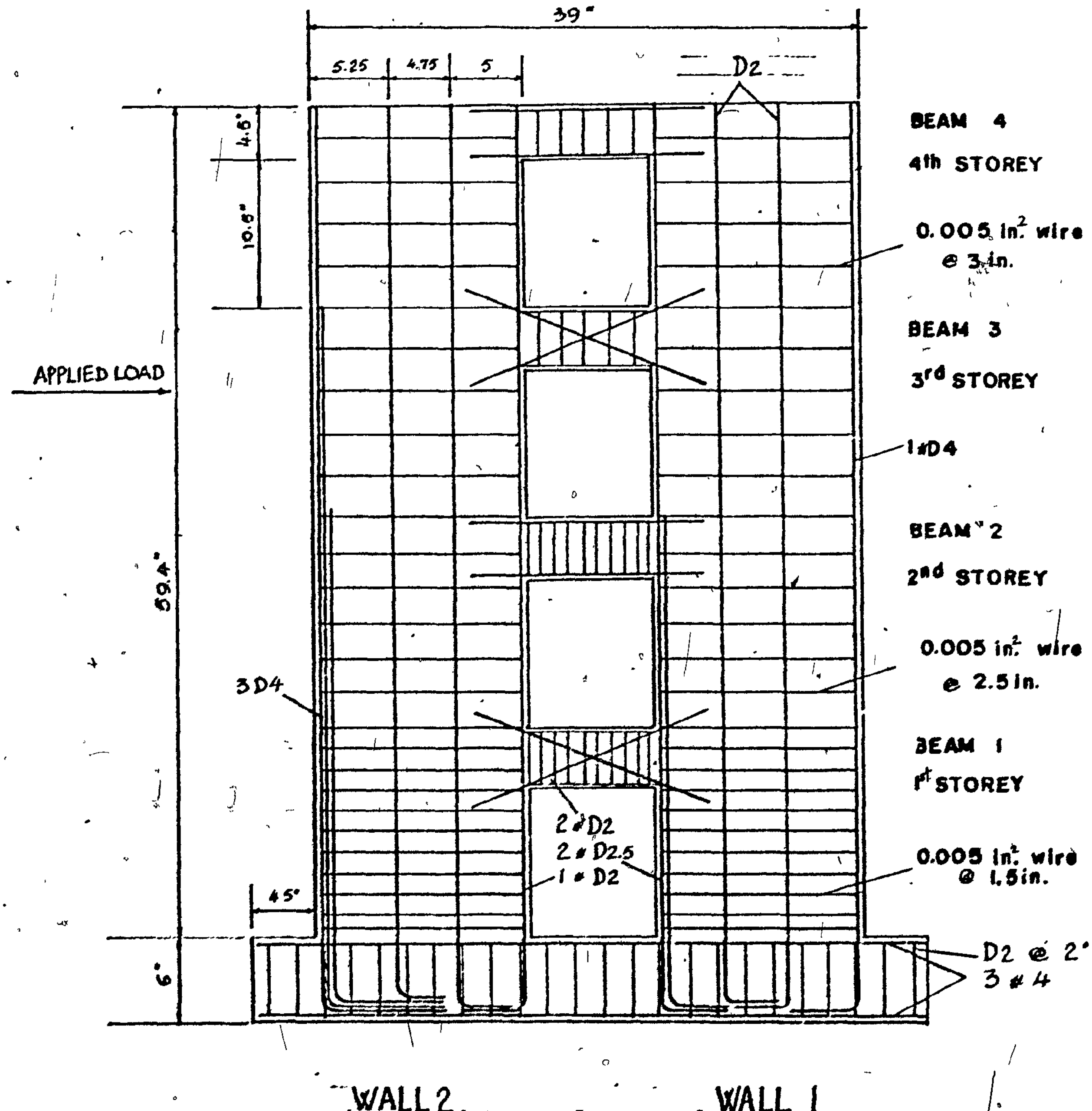

Fig. 3.3: REINFORCEMENT PATTERN OF SHEAR WALL MODEL NO. 3

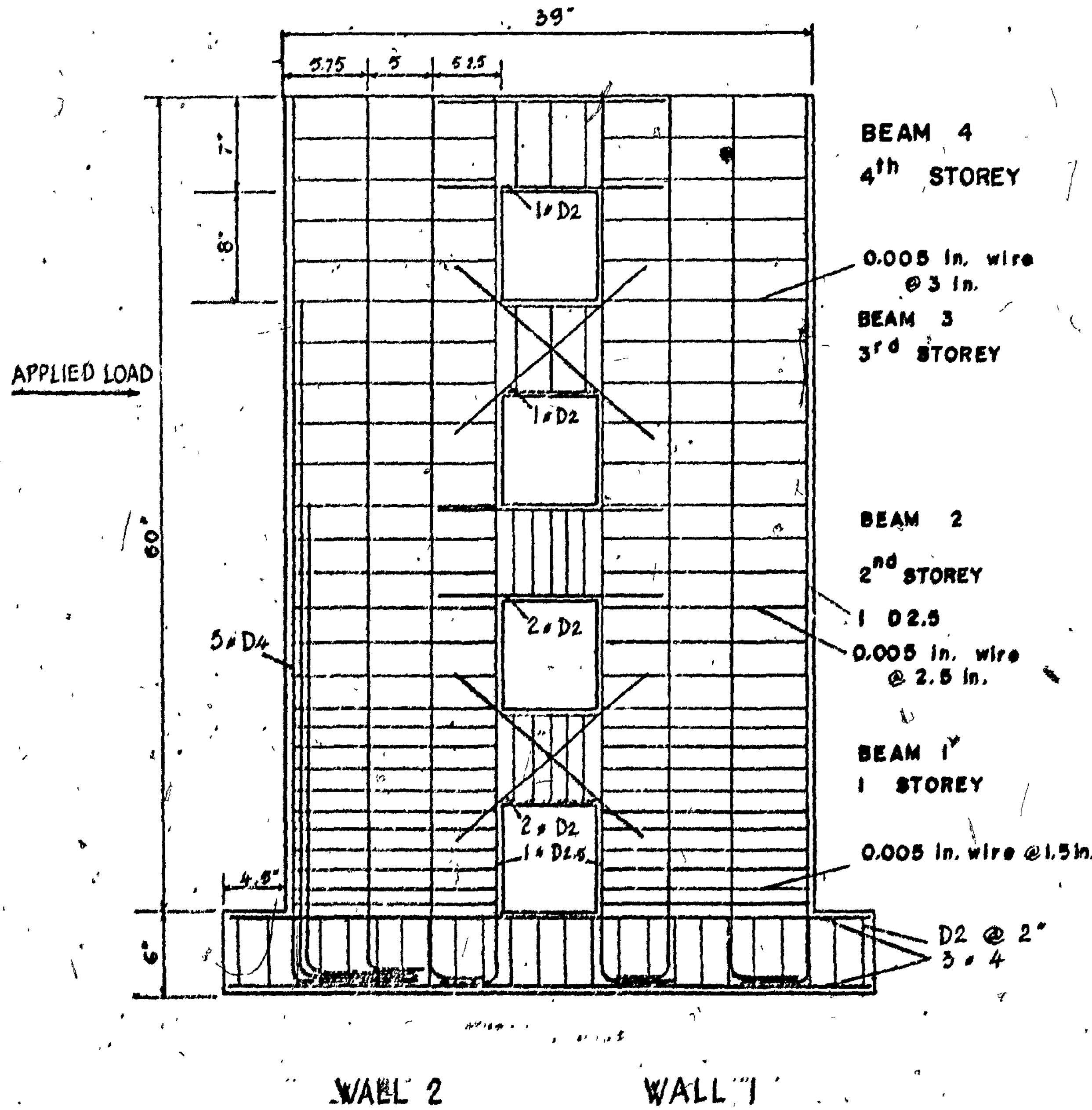

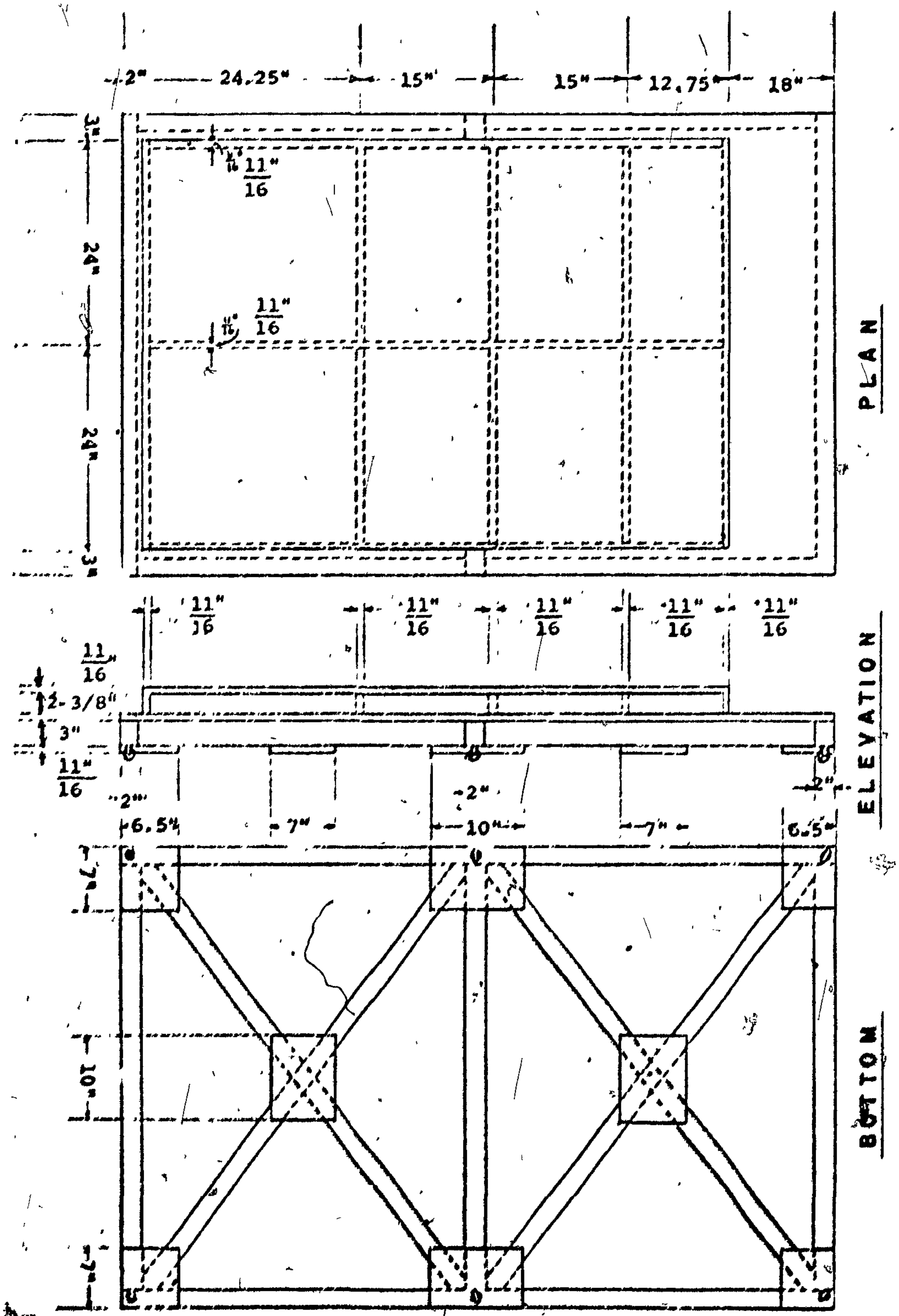

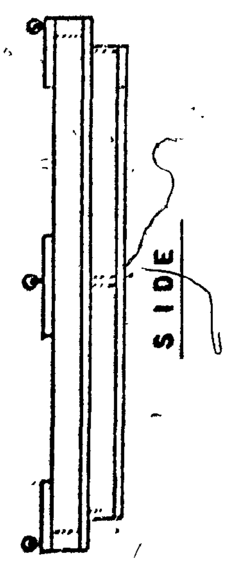

Fig. 3.4: FORMWORK FOR COUPLED SHEAR WALL SPECIMENS

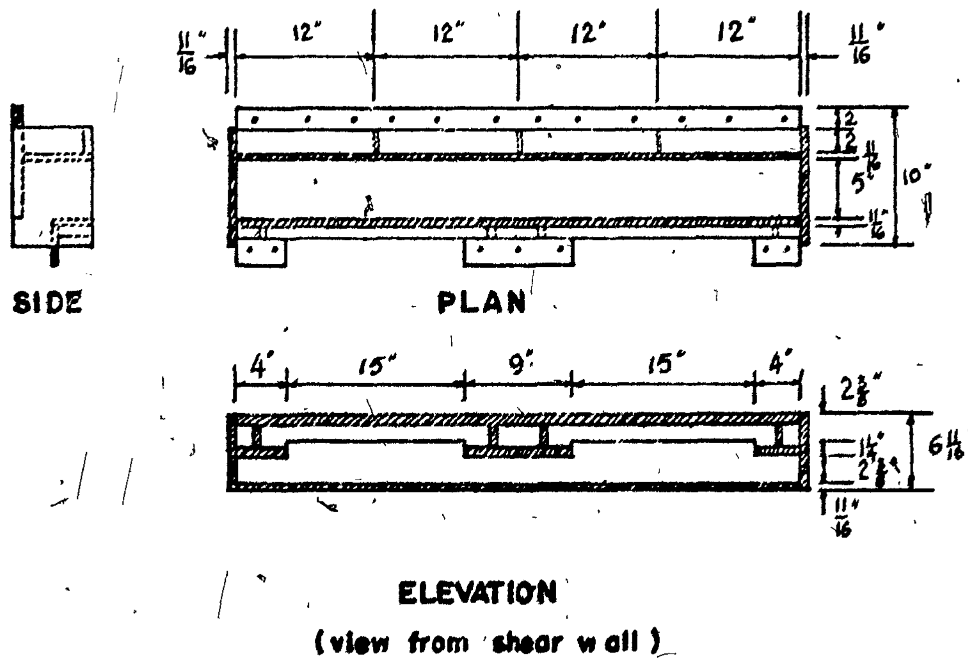

Fig. 3.5: BASE BOX

(for horizontal casting)

Fig. 3.6 Reinforcement pattern of shear wall No. 1.

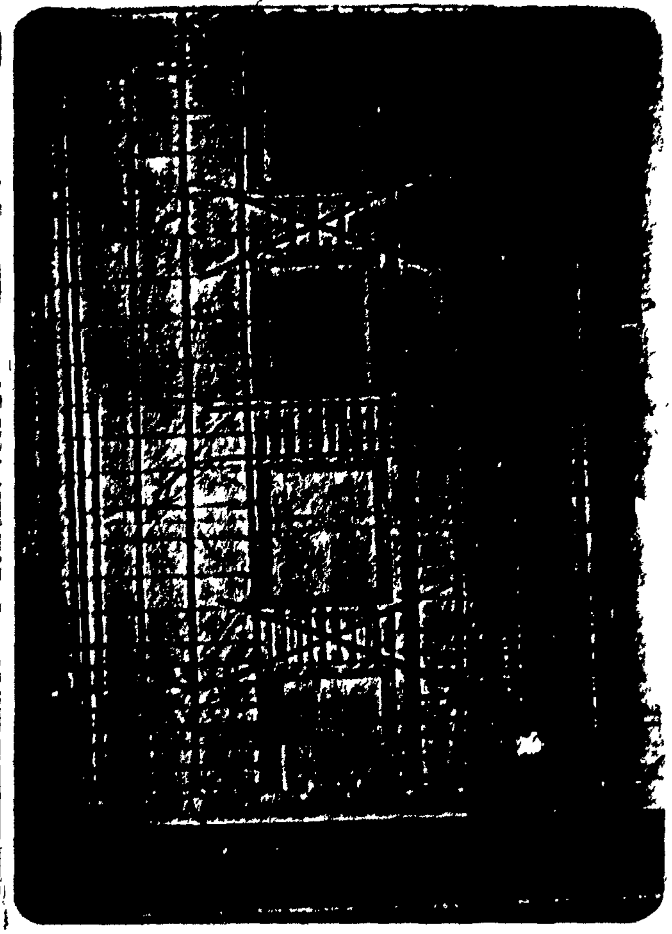

Fig. 3.7 Reinforcement pattern of shear wall No. 2

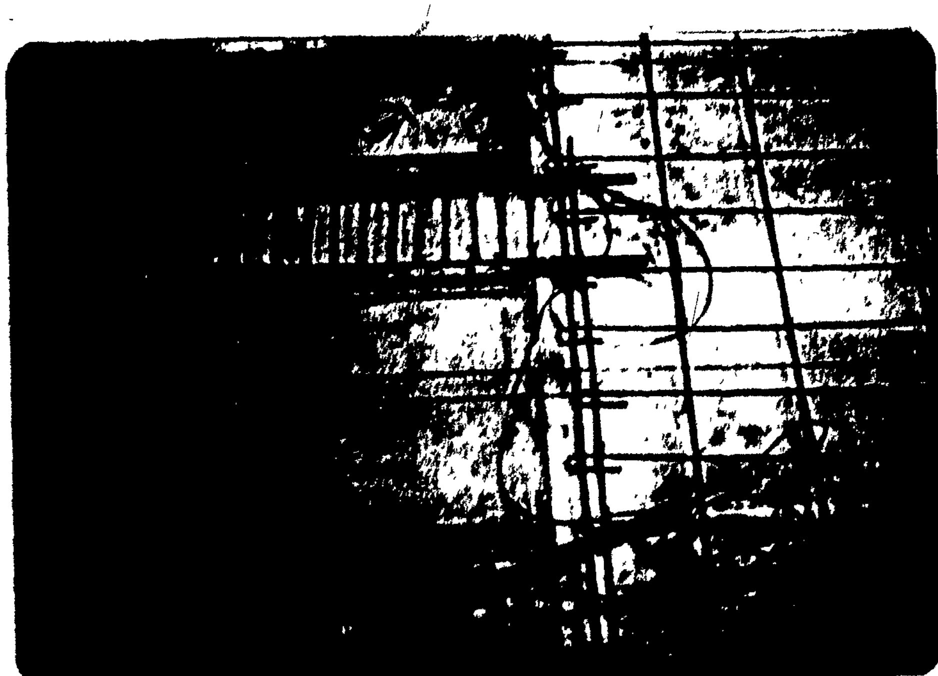

Fig. 3.8 Reinforcement pattern of the beams of shear wall No. 2

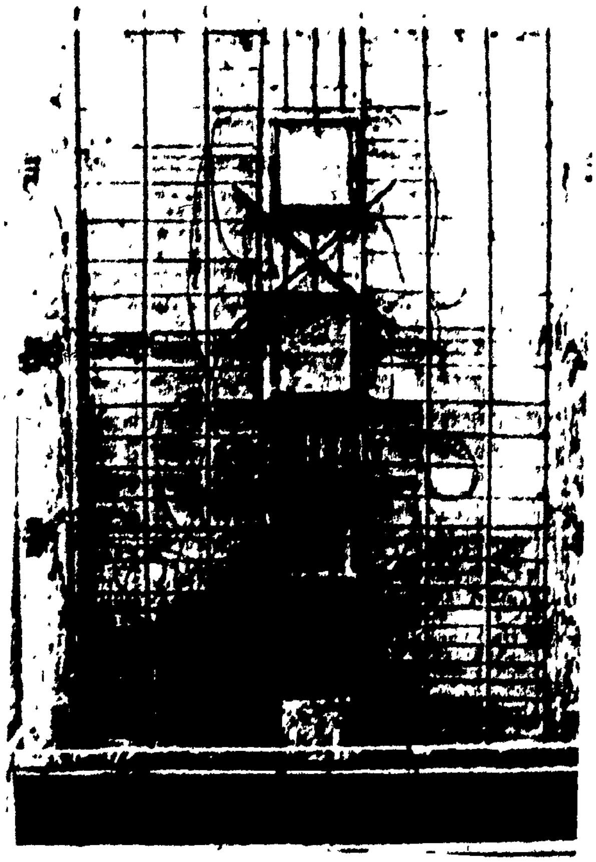

Fig. 3.9 Reinforcement pattern of shear wall No. 3

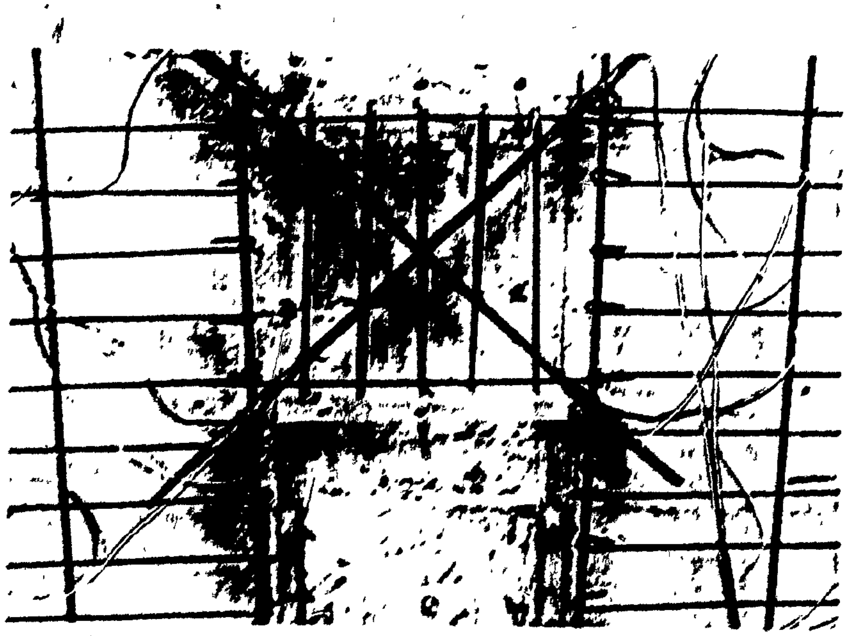

Fig. 3.10 Reinforcement pattern of the 1st level of shear wall No. 3

TABLE 3.1 Mix Proportion and Strength of Concrete for Three Coupled Shear Wall Models (2" x 4" cylinders)

Specimen	W/C ratio	A/C ratio	Crushed quartz sand proportion by weight				Specimen age at testing	No. of cylinder	Ultimate compressive load (lbs)	Compressive strength (psi)
			#16	#24	#40	#70				
								1	17200	
								2	11400	
								3	18600	
#1	0.60	3.25	35%	30%	25%	10%	55 days	4	18400	5200
								5	18800	
								6	15600	
								7	15000	
								1	11300	
								2	13600	
								3	15400	
#2	0.70	3.60	35%	30%	25%	10%	40 days	4	13300	4000
								5	10600	
								6	11850	
								7	12300	
								8	12700	
								1	12900	
								2	13700	
#3	0.70	3.60	35%	30%	25%	10%	62 days	3	15400	4300
								4	12200	
								5	15620	
								6	11900	

TABLE 3.2 Summary of Properties of Prototype Vessel Concrete and Properties of Mortar Model Micro-concrete (After Mirza, Ref. 22)

	28 day cured wet concrete		90 day cured wet concrete		90 day cured dry concrete	
	Average	Range (% of mean)	Average	Range (% of mean)	Average	Range (% of mean)
Prototype Vessel Concrete						
Modulus of elasticity, psi	3.2×10^6	25.0	3.4×10^6	8.8	3.5×10^6	8.6
Poisson's ratio	0.22	36.4	0.18	66.7	0.18	55.6
Compressive strength, psi	6810	8.3	7540	4.7	8060	7.7
Splitting tensile strength, psi	461	9.5	575	7.0	635	6.9
Modulus of rupture, psi	750	2.1	818	2.1	747	6.8
Unit weight, [a] lb/ft	147.3	1.0	147.8	0.7	145.3	1.2
Mortar Model Concrete						
Modulus of elasticity, psi	3.8×10^6		4.2×10^6		4.3×10^6	
Poisson's ratio					0.18[b]	
Compressive strength, psi	6840	17.3	6960	23.6	7010	35.1
Splitting tensile strength, psi	761	9.9	743	18.9	762	12.1
Modulus of rupture, psi	803	23.2	1189	23.5	1014	31.4
Adjusted modulus of rupture, [c] psi	698		1035		882	

a) Unit weights were based on 6 x 12 in. cylinders only.

b) Poisson's ratio was obtained from dry specimens at an age of 270 days.

c) Because of a significant size effect, modulus-of-rupture data for 3 in. deep beams are generally about 15% above data for 6 in. deep beams. The adjusted modulus values reflect this difference and provide a better basis for comparison with prototype concrete values.

Concrete was prepared and mixed with water only ten minutes before being placed in the forms, and then vibrated for about three minutes on a vibrating table. The concrete was moist-cured with wet burlap from one to two weeks. The compressive strengths of the micro-concrete were obtained using 2 x 4 in. cylinders. These cylinders were tested at the same time as the parent specimens and the strengths are detailed in Table 3.1.

After the curing period, each specimen was carefully removed from the formwork by first cutting the tensioned wires, unscrewing and removing the plexiglass pieces, unscrewing and removing the base block forms. It was then transferred to a lifting table to be prepared for instrumentation.

3.4.2 The Reinforcement

(a) Steel Properties

The properties of steel which must be considered in simulating the prototype steel reinforcement in small-scale models are the yield and ultimate strength, its ductility, and bond characteristics (ref. 24 and 25).

Recent McGill work[22] has used deformed steel wires obtained from the Lundy Fence Company, Dunnville, Ontario, in sizes ranging from D2 to D10. The chemical composition of this wire steel is as follows:

Carbon	0.13%
Phosphorous	0.007%
Sulfur	0.028%
Manganese	0.68%
Silicon	0.15%

The effects of heat treatment, cold drawing, bond characteristics, are described in detail in Ref. (22). It was noted that after annealing, followed by air cooling of D2, D2.5 and D4 wires at temperatures between 1100°F and 1500°F, the yield strength was lowered from 80 or 90 ksi to a value between 35 and 45 ksi, and the percentage of elongation was increased from 3 or 6 percent to a value between 18 and 28 percent. Temperature above 1200°F did not have any additional effect on the yield or ultimate strengths as well as the percentage of elongation.

All reinforcement wires used in the three coupled shear wall models were heat treated at 1200°F for 60 min. by a local company. The stress-strain characteristics of the wires used in this investigation are shown in Figs. 3.15 to 3.18.

Experimental investigations by Harris et al.[25], Mirza and McCutcheon[24], and Hsu[22], have shown that sufficient bond resistance can be achieved with reasonable ratios of embedment length to reinforcement diameter, L/d, even for the small smooth wires commonly used for model reinforcement. The comparison of ultimate bond stress indicated that suitably deformed wires will have pull-out bond strengths reasonably close to those measured for prototype bars. Therefore one cannot expect bond to be a significant problem in this study.

TABLE 3.3 Steel Percentage of the Beams of Three Specimens

	Cross-section	$\frac{s}{t}$ ratio	type of reinf.	main steel percentage ρ	vertical steel percentage
Test specimen no.1					
Beam 1	1.25x4.5	2	parallel	.744	0.
Beam 2	1.25x4.5	2	parallel	.744	0.
Beam 3	1.25x4.5	2	parallel	.744	0.
Beam 4	1.25x3.9	2.3	parallel	.856	0.
Test specimen no.2					
Beam 1	1.25x4.5	2	crossed	.744	.924
Beam 2	1.25x4.5	2	parallel	.744	.924
Beam 3	1.25x4.5	2	crossed	.744	.462
Beam 4	1.25x3.9	2.3	parallel	.856	.462
Test specimen no.3					
Beam 1	1.25x7.0	1	crossed	.470	.594
Beam 2	1.25x7.0	1	parallel	.470	.594
Beam 3	1.25x7.0	1	crossed	.235	.357
Beam 4	1.25x7.0	1	parallel	.235	.357

TABLE 3.4 Details of the Wall Steel Reinforcement

	WALL 1					WALL 2				
	steel at outside edge	steel at inside edge	vertical shear steel	Total vertical steel	Horizontal steel	steel at outside edge	steel at inside edge	vertical shear steel	Total vertical steel	Horizontal steel
Specimen No.1										
1st storey	.64	.133	.21	.983	.277	.64	.133	.21	.983	.277
2nd storey	.64	.133	.21	.983	.166	.64	.133	.21	.983	.166
3rd storey	.43	.133	.21	.773	.139	.43	.133	.21	.773	.139
4th storey	.21	.133	.21	.553	.139	.21	.133	.21	.553	.139
Specimen No.2										
1st storey	.21	.267	.21	.687	.277	.64	.133	.21	.983	.277
2nd storey	.21	.267	.21	.687	.166	.64	.133	.21	.983	.166
3rd storey	.21	.133	.21	.553	.139	.43	.133	.21	.773	.139
4th storey	.21	.133	.21	.553	.139	.21	.133	.21	.553	.139
Specimen No.3										
1st storey	.125	.125	.20	.45	.277	.60	.125	.20	.925	.277
2nd storey	.125	.125	.20	.45	.166	.60	.125	.20	.925	.166
3rd storey	.125	.125	.20	.45	.139	.40	.125	.20	.725	.139
4th storey	.125	.125	.20	.45	.139	.20	.125	.20	.525	.139

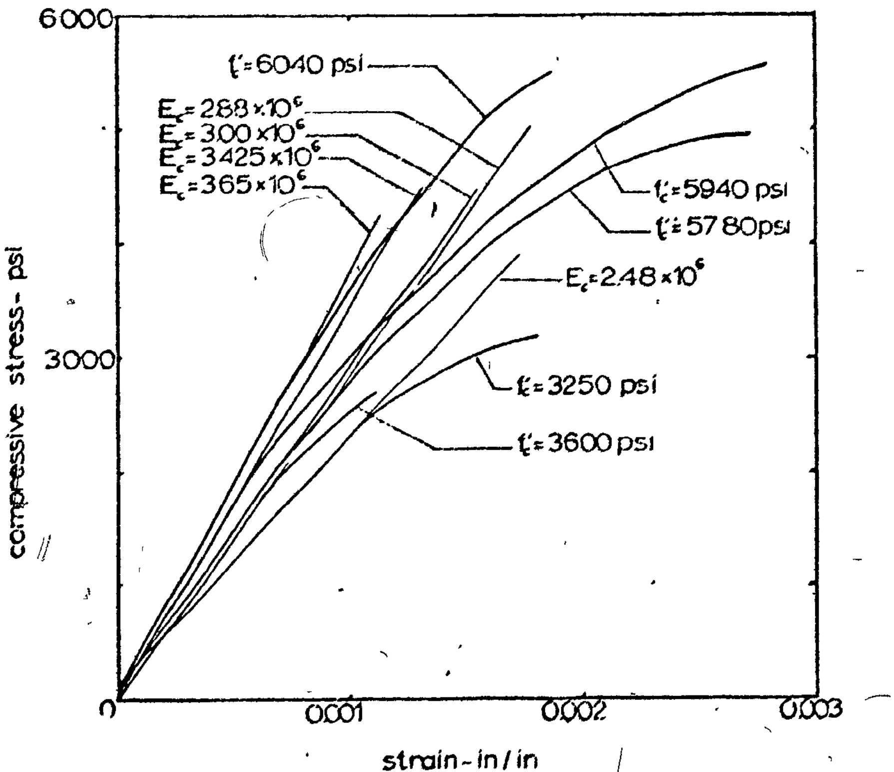

fig. 3.11 : COMPRESSION STRESS-STRAIN CURVES MICROCRETE (AFTER MIRZA, REF. 22)

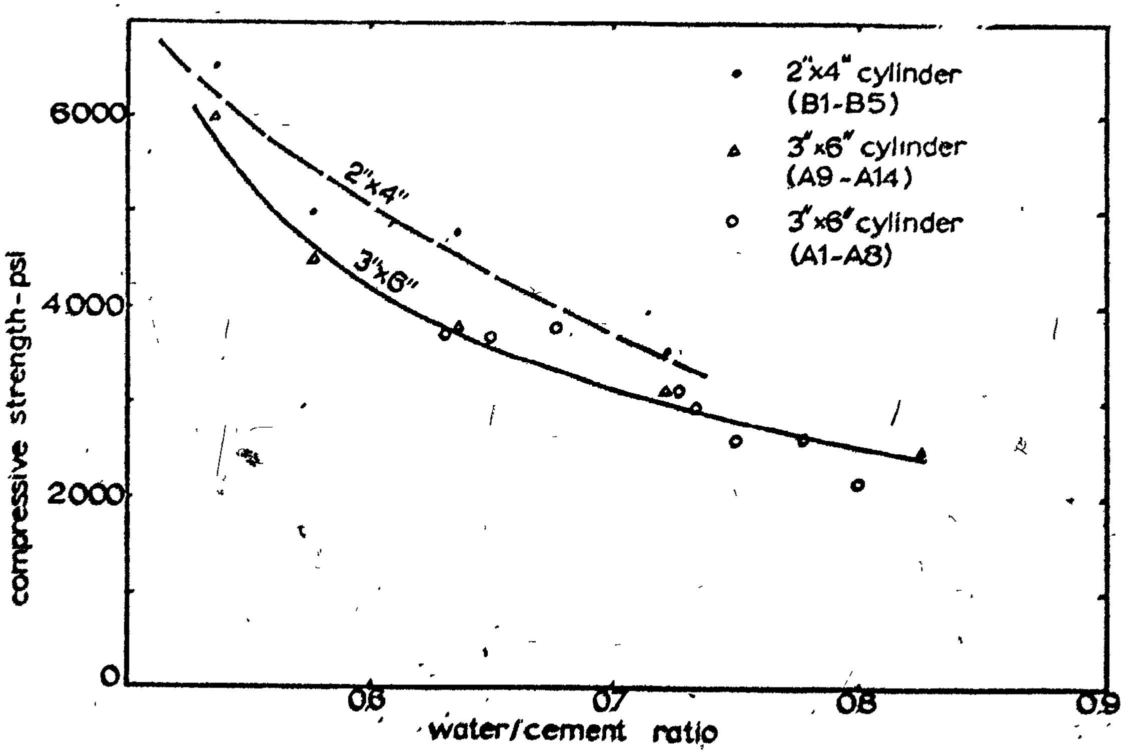

fig. 3.12 : VARIATION OF COMPRESSIVE STRENGTH WITH WITH WATER CEMENT RATIO (AFTER MIRZA, REF. 22)

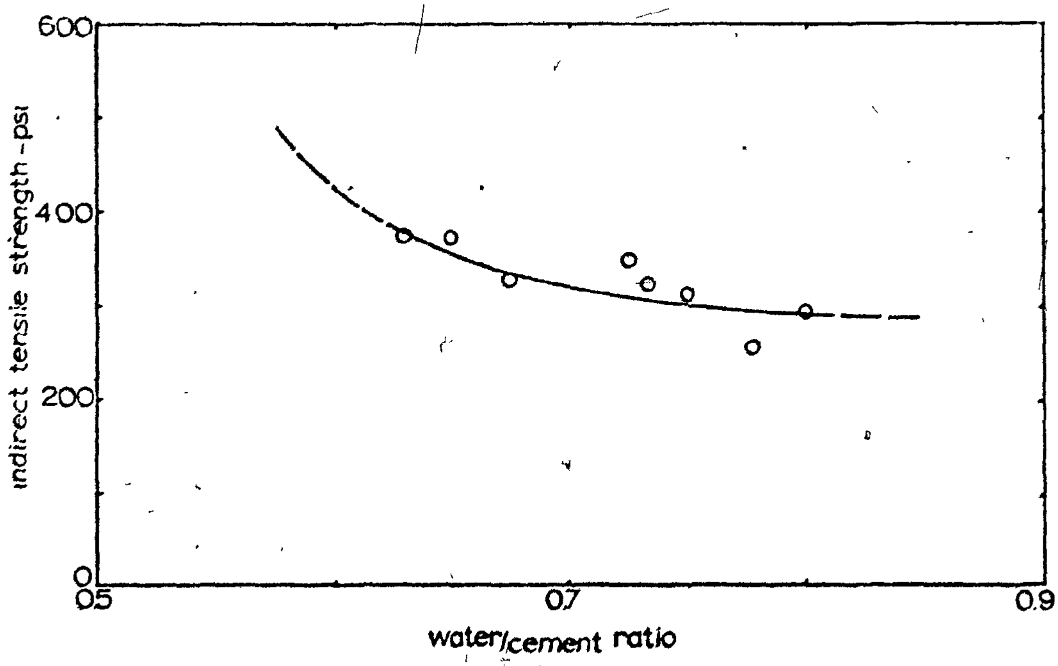

fig. 3.13 : VARIATION OF TENSILE STRENGTH WITH WATER-CEMENT RATIO (AFTER MIRZA, REF. 22)

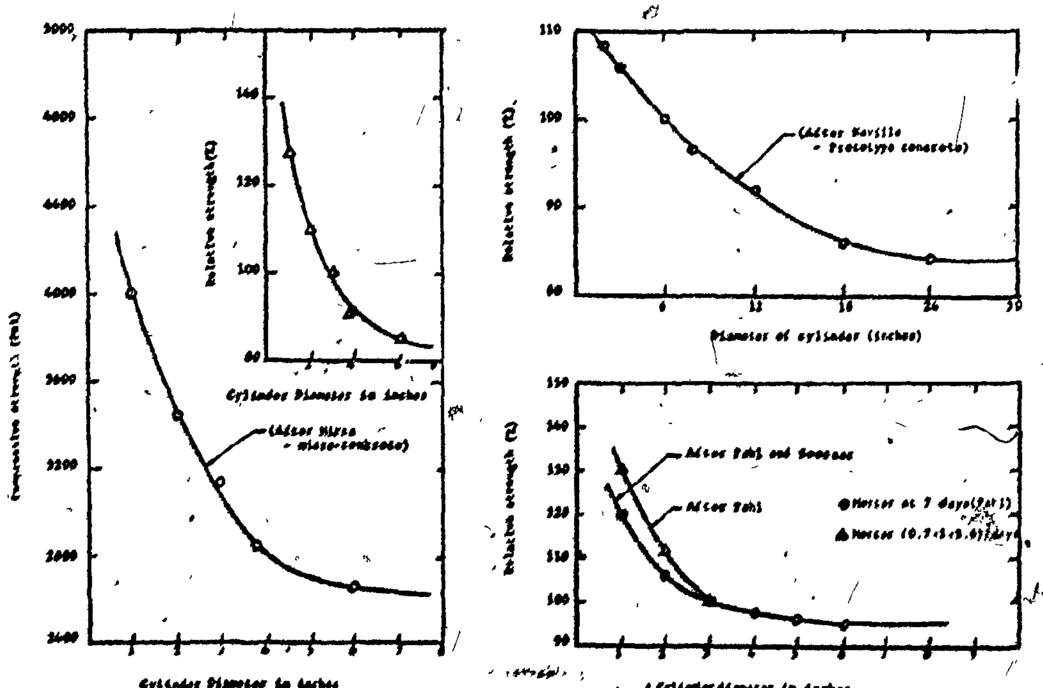

fig. 3.14 : SIZE EFFECT COMPRESSIVE STRENGTH (REF. 22)

Fig.3-15 _ The Stress Strain Curve of D4 Wires

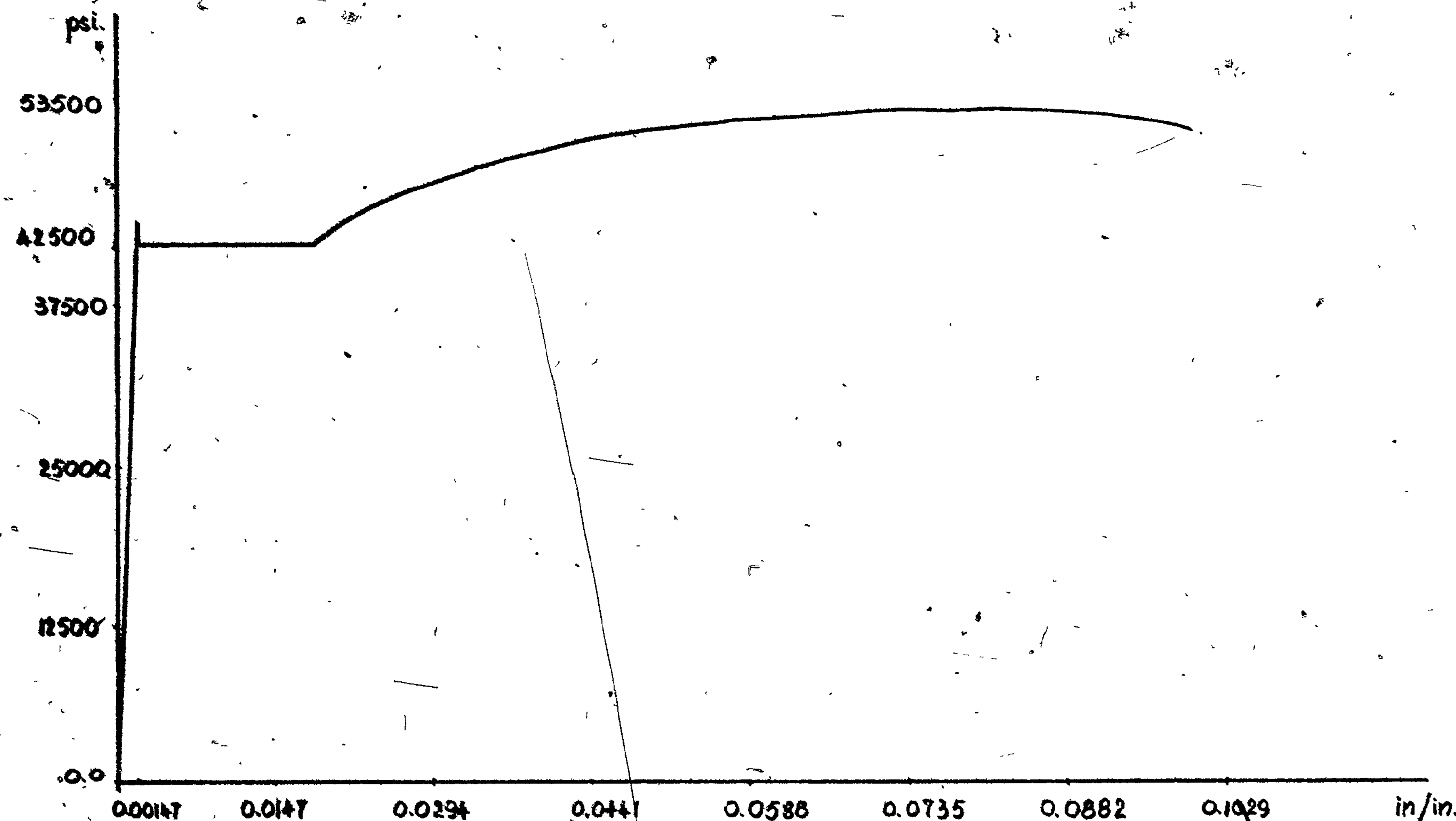

Fig.3-16: The Stress Strain Curve of D2.5 Wires

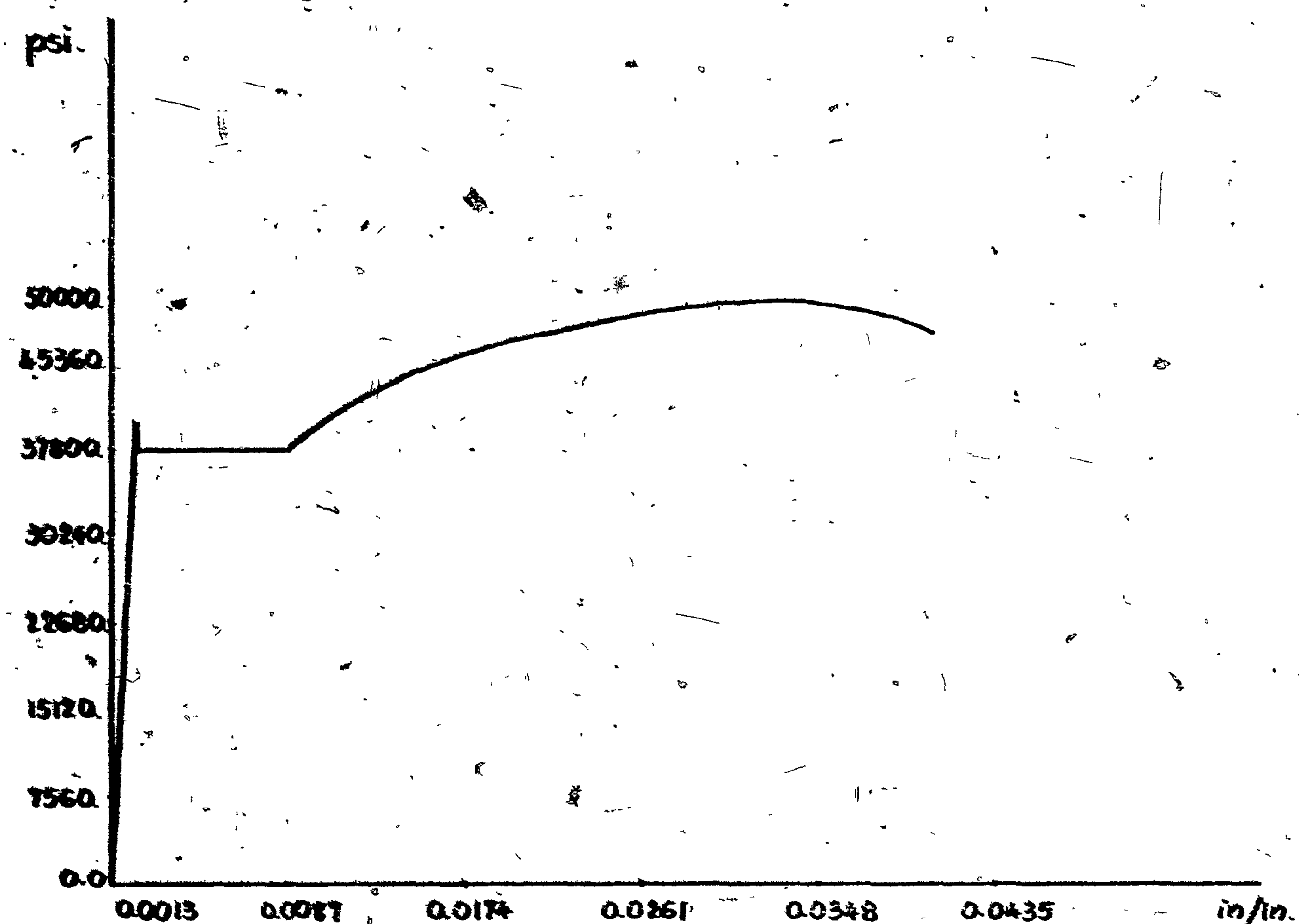

Fig. 3-17 : The Stress-Strain Curve of D2 Wires

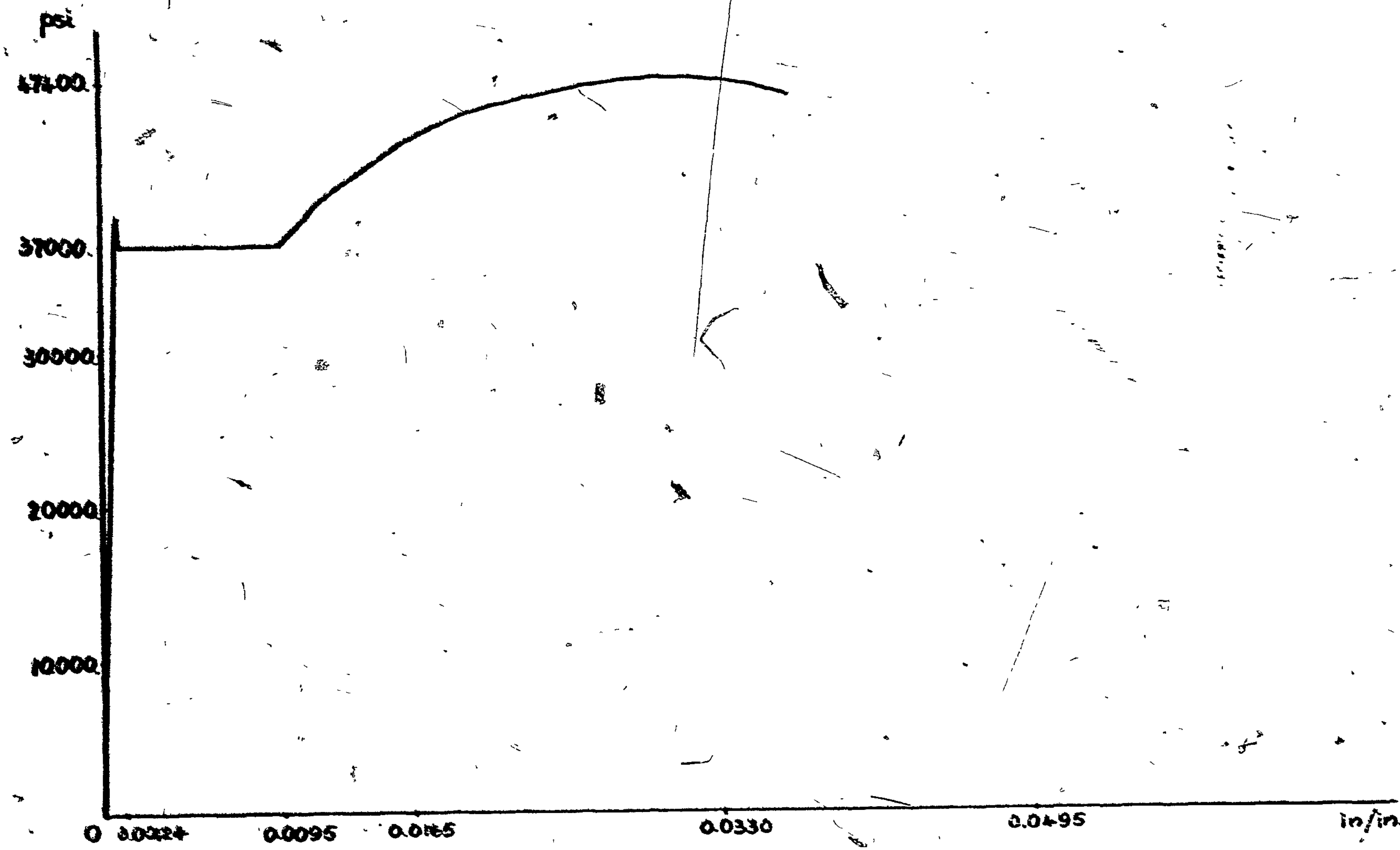

Fig. 3.18: The Stress-Strain Curve of 0.005 Wires

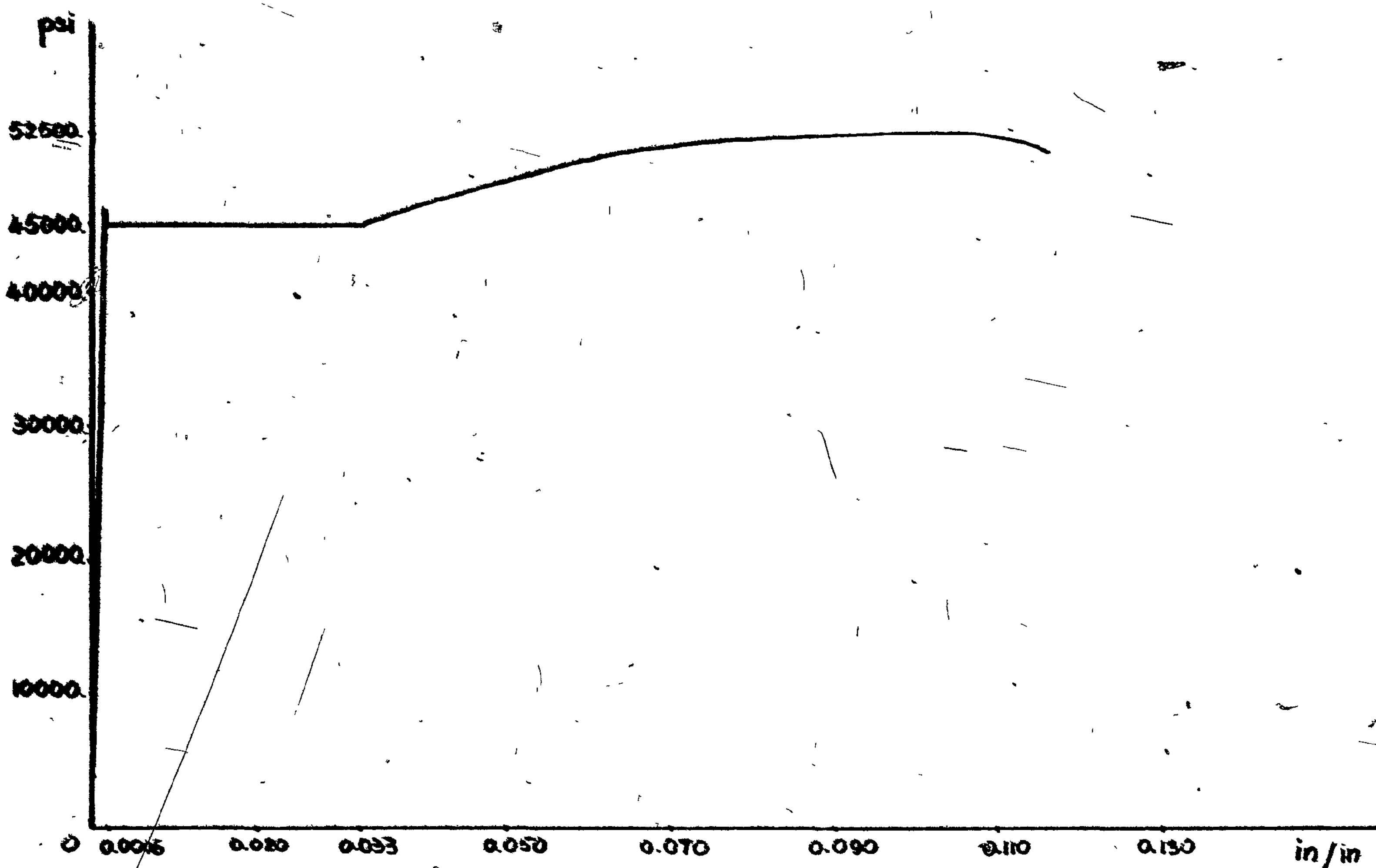

(b) Assembly of the Reinforcement

The reinforcement for the base block of the shear wall model was first assembled. It consisted of three #4 bars at the top and the bottom of the beam. The vertical shear reinforcement consisted of closed D2 wire stirrups at 2 in. spacing.

The reinforcement for the walls was then assembled in the horizontal plane and was supported by tensioned wires as described earlier. Finally, the reinforcement details for the specimens are shown in Figs. 3.1 to 3.3.

In specimens nos. 2 and 3, the first and the third level connecting beams were reinforced with "cross-reinforcement" (similar to that used by Paulay, ref. 13) to compare the behaviour of these beams with that of beams with the conventional parallel reinforcement. This pattern of reinforcement was also selected to follow the stress trajectories deduced from the photoelastic studies described in Chapter II.

3.5 Loading System

3.5.1 Loading Frame

The loading frame was designed for the following considerations.

(a) The loading frame was required to be large enough to contain the model.

(b) The loading frame was to have adequate stiffness and stability under a maximum load of 20 kips which was applied by means of a jack. A part of the applied load is taken by the rubber block mounted on the other end of the frame (Fig. 3.19).

(c) Lateral bracing for the test specimen was provided at different levels with sufficient stiffness to prevent buckling.

To satisfy the above requirements, the loading frame was built to consist of two parallel frames, 6 in. apart. Each frame, 12ft . in width and 12 ft. high, was constructed from four channels, two C15x33.9 horizontally and two C12x25 vertically. A two-way hydraulic jack was installed on one side, bearing on these two frames. A 12x12x18 in. rubber block was mounted on the other side of the frame. The behaviour of this rubber block under compressive loading is shown in Fig. 3.22.

3.5.2 Load Distributor

The experience gained from the use of the aluminum load distributor in the photoelastic study was used in designing this load distributor. This device (Fig. 3.20) was built with two steel plates 4" x ¾" and 4" x ½" in size. Bolts of ¾" diameter were used at three pre-determined locations along vertical bars as pin connectors for load transmission. The load distributor was designed to achieve the following:

(a) To distribute the lateral forces into four point loads at the floor levels, according to a triangularly distributed load (Fig. 3.21),

(b) To transmit the load without any local buckling,

(c) To reduce friction by placing the loading device on rails mounted on the two angles at a specified level.

3.5.3 The Load Transmission System

The applied force was transmitted to the test specimen through the load distributor by a pulling force generated by the two-way hydraulic jack as shown in Fig. 3.19. The load distributor was connected to the hydraulic jack by two ¾" diameter threaded rods and a universal joint to permit rotation of the system as it moved horizontally. The load distributor was connected to the rubber block on the other side by means of a one-inch diameter steel rod.

To measure the force transmitted, four load cells were placed along the load transmission line (Fig. 3.19): load cell no. 1 at the hydraulic jack to measure the total load exerted on both the test specimen and the rubber block, load cells nos. 2 and 3 at the two sides of the specimen to check the balancing of loads on the two sides, and load cell no. 4 on the one-inch diameter rod connected to the rubber block.

The load applied to the specimen at any stage can be calculated by subtracting the force on the rubber block from the total load.

3.5.4 Lateral Bracing

The coupled shear wall system was braced at the following three levels:

(i) mid-beam 1 level at 12.75 in. from base

(ii) mid-beam 2 level at 27.75 in. from base

(iii) between storeys 3 and 4 at 51 in. from base.

The bracing system consisted of rollers welded to threaded rods and then bolted to the horizontal angles attached to the loading frame at two ends. The bracing system proved to be effective.

3.6 Instrumentation

Instrumentation equipment consisted of dial gauges and strain gauges. Dial gauges with least counts of .0001 were used to measure rotations and deflections of the walls and beams, as shown in Figs. 3.23 to 3.25.

Two types of electric resistance strain gauges were used for measuring strains: surface strain gauges and internal or embedded strain gauges. The types of strain gauges used in the three specimens are: embedded PL-2 gauges (on first specimen only), embedded J.M. type ZF 1A, and surface TML type PL-10 on the concrete. The advantage of strain gauges is their adaptability to automatic and continuous reading of strain values. Positions of strain measurement are shown in Figs. 3.23 to 3.25.

3.7 Test Procedure

All load cells were calibrated 24 hours prior to testing on the "Instron" loading machine. Calibration curves for the four load cells used in three tests are detailed in Appendix A. The test procedure for coupled shear wall models consisted of the following steps:

1. The concrete shear wall specimen was carefully lifted and placed on a steel plate $13\frac{1}{2}$" x 54" x $\frac{1}{2}$" which is bolted to the channels

FIG. 3.19. SKETCH OF SPECIMEN, LOADING FRAME AND LOADING DEVICE

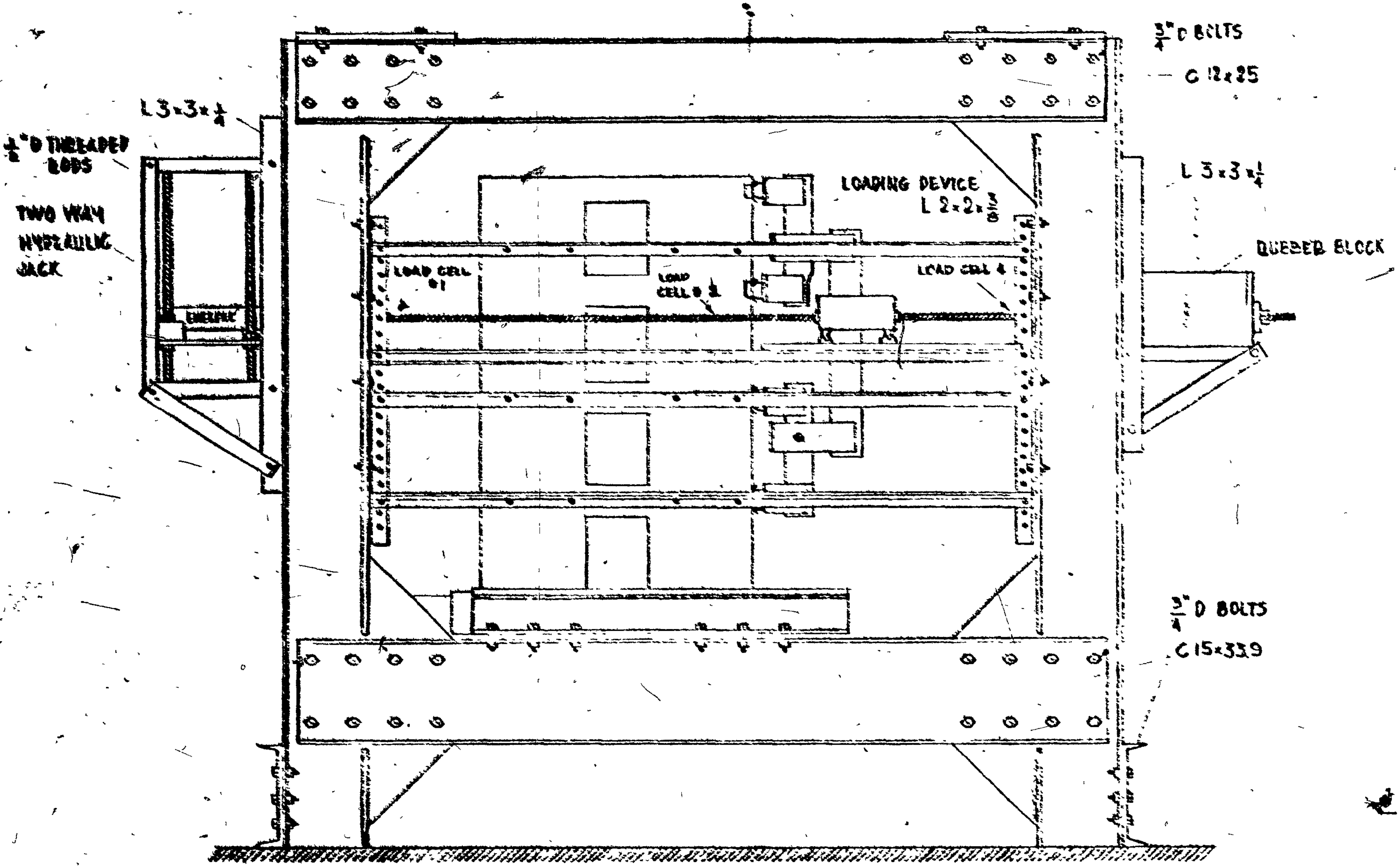

SCALE = 1/10

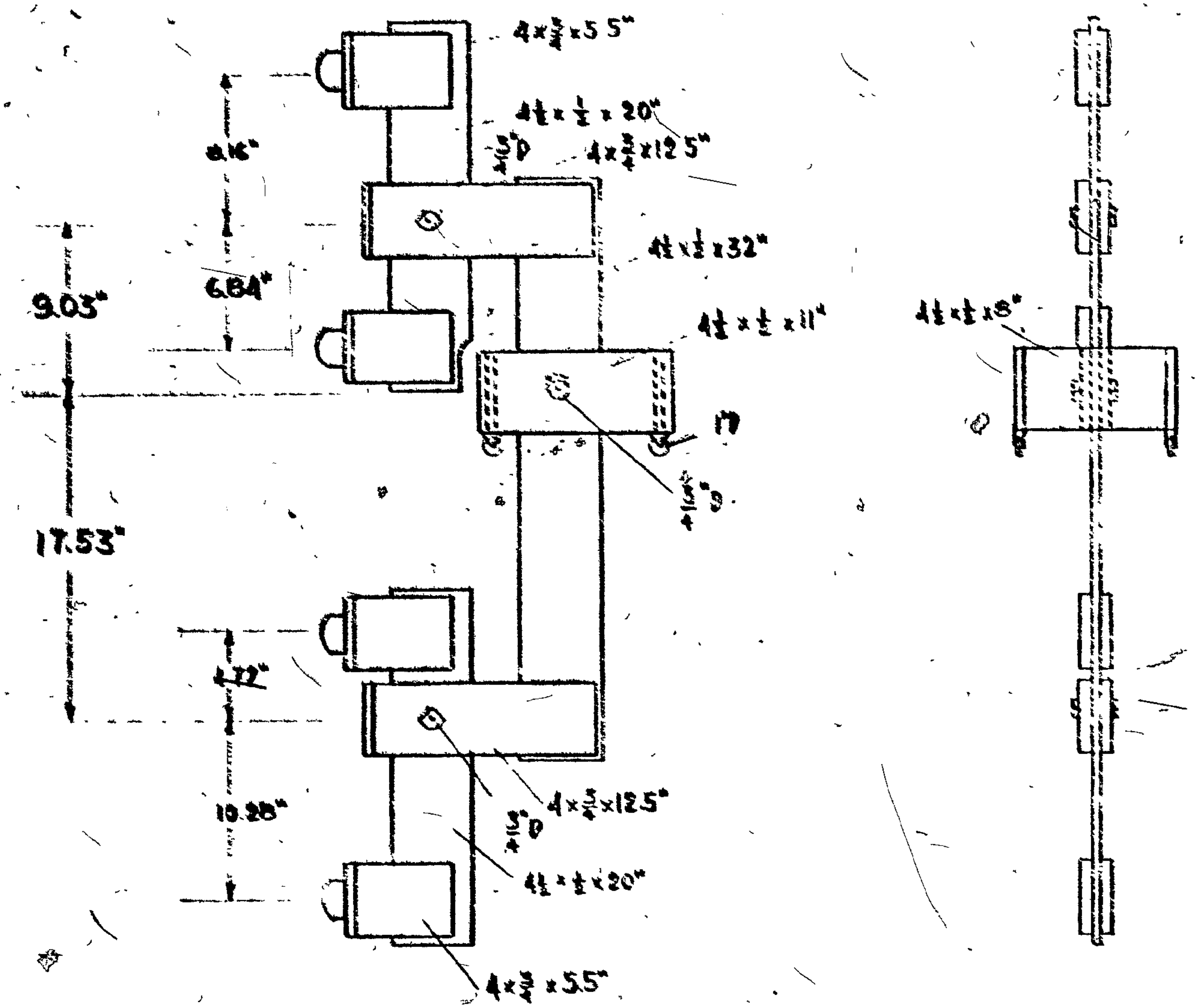

FIG. 3-20: THE LOAD DISTRIBUTOR

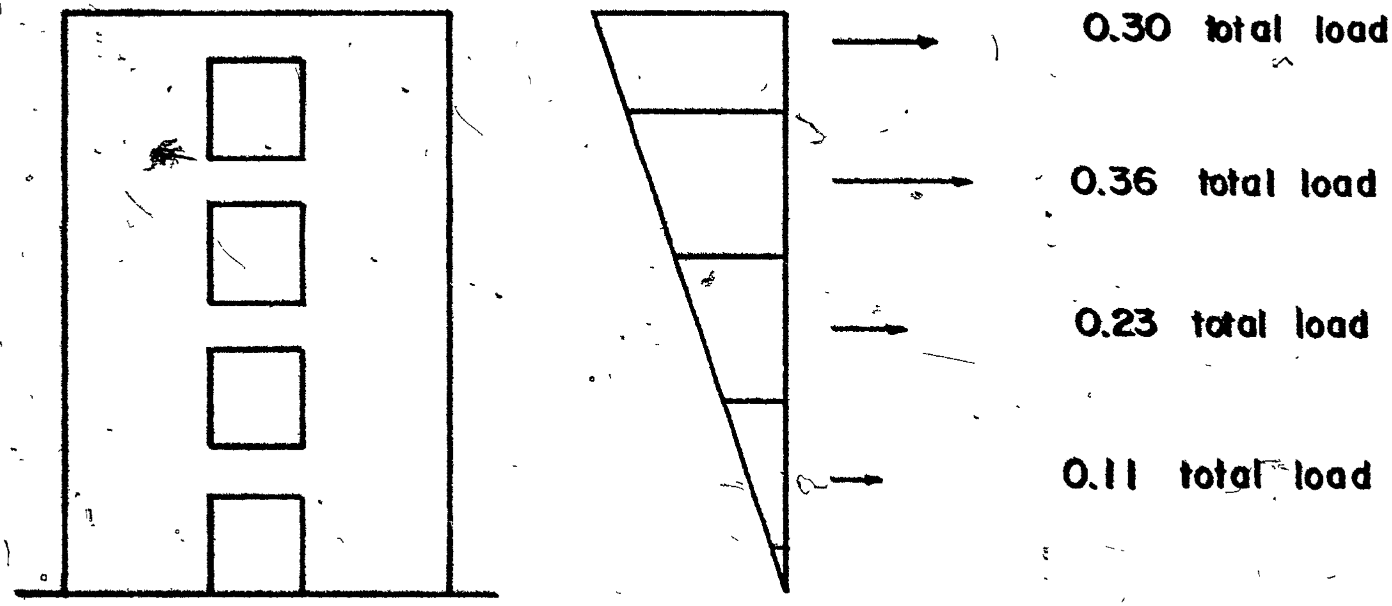

FIG. 3.21: DISTRIBUTED LOAD LUMPED BY THE LOAD DISTRIBUTOR

Fig. 3-22 Load-Deflection Curve of the Rubber Block

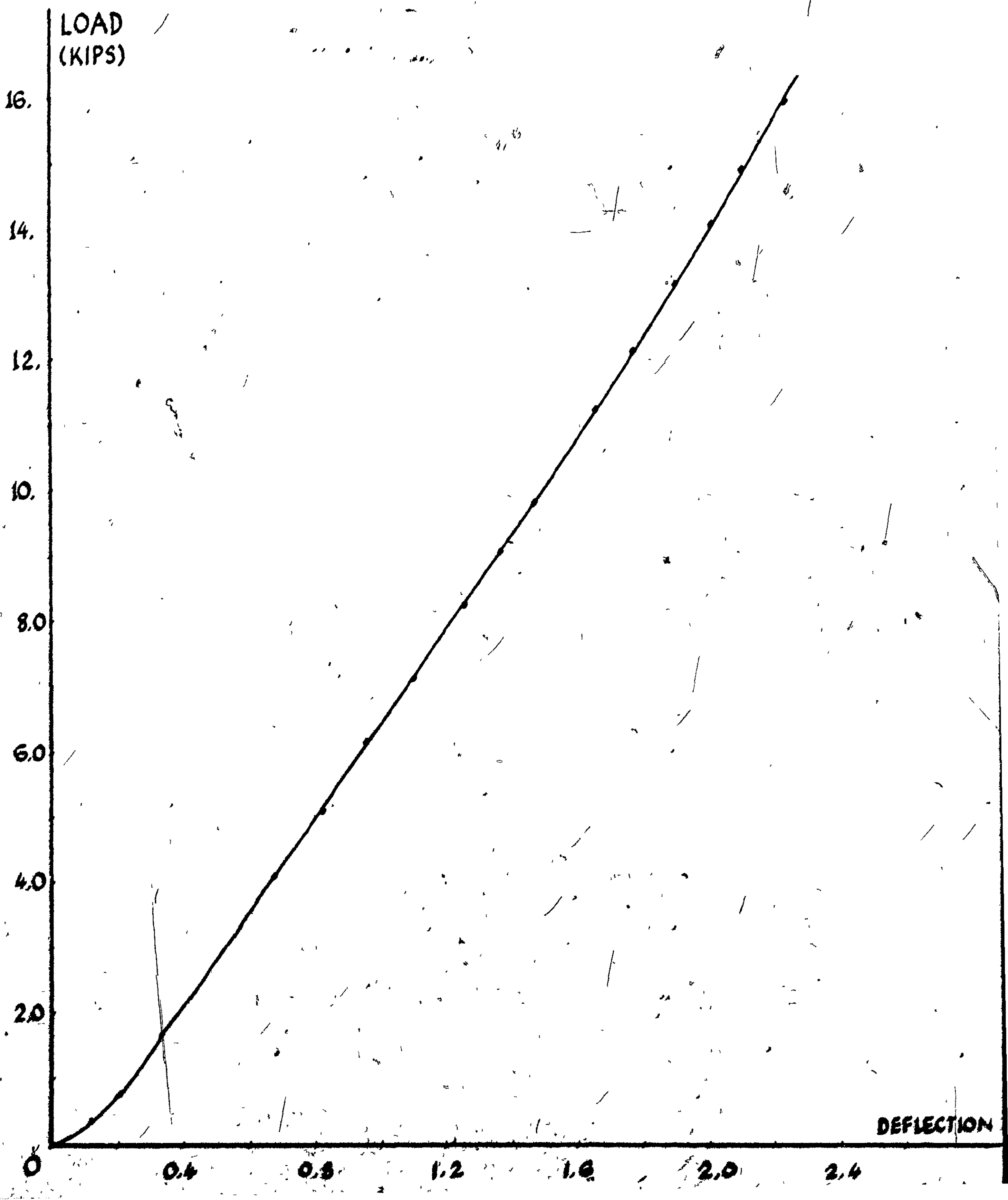

FIGURE 3.23: INSTRUMENTATION DETAILS OF SPECIMEN N°1

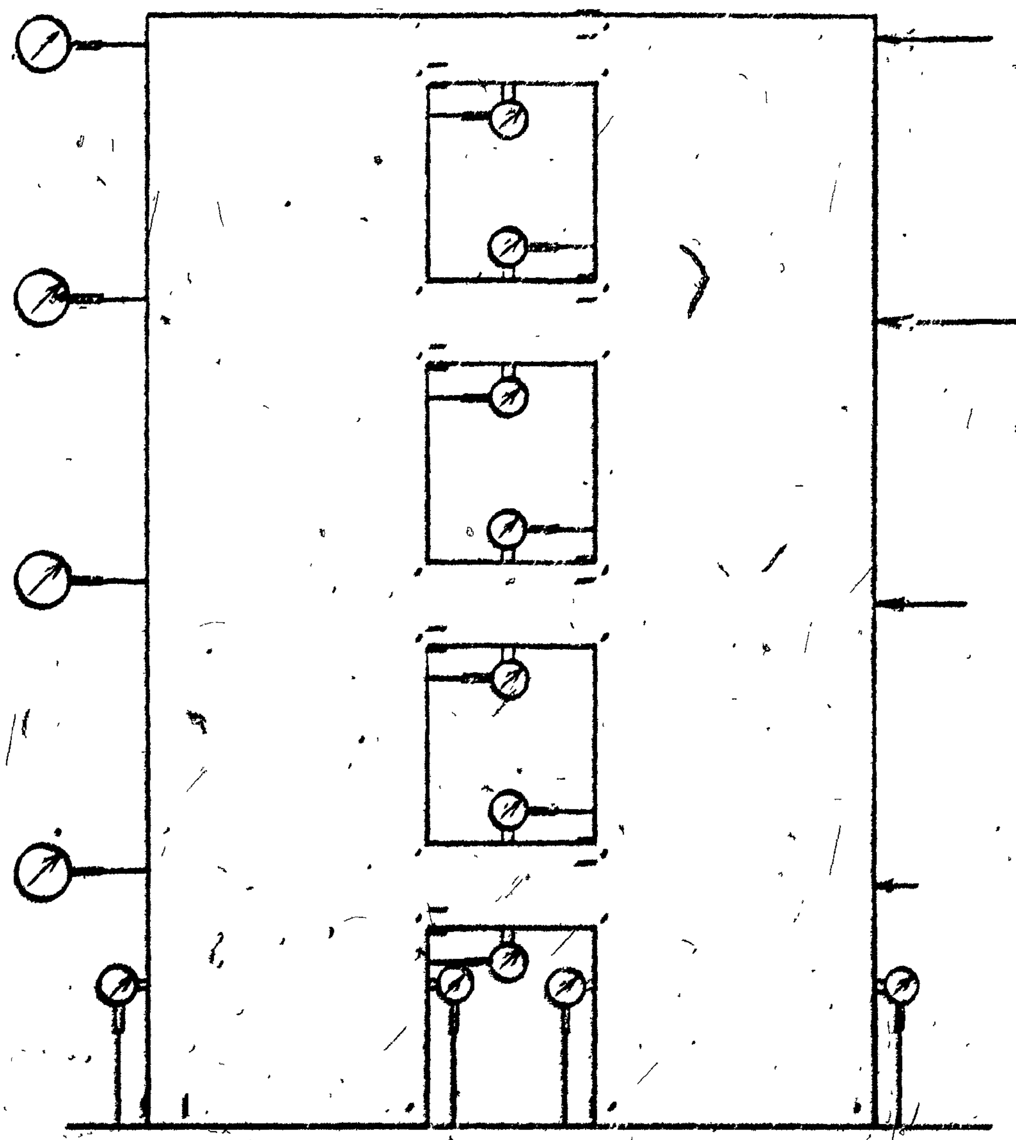

DIAL GAUGE

IMBEDDED STEEL STRAIN GAU

CONCRETE STRAIN GAUGES

SCALE = 1/10

FIG. 3.24: INSTRUMENTATION DETAILS OF SPECIMEN Nº 2

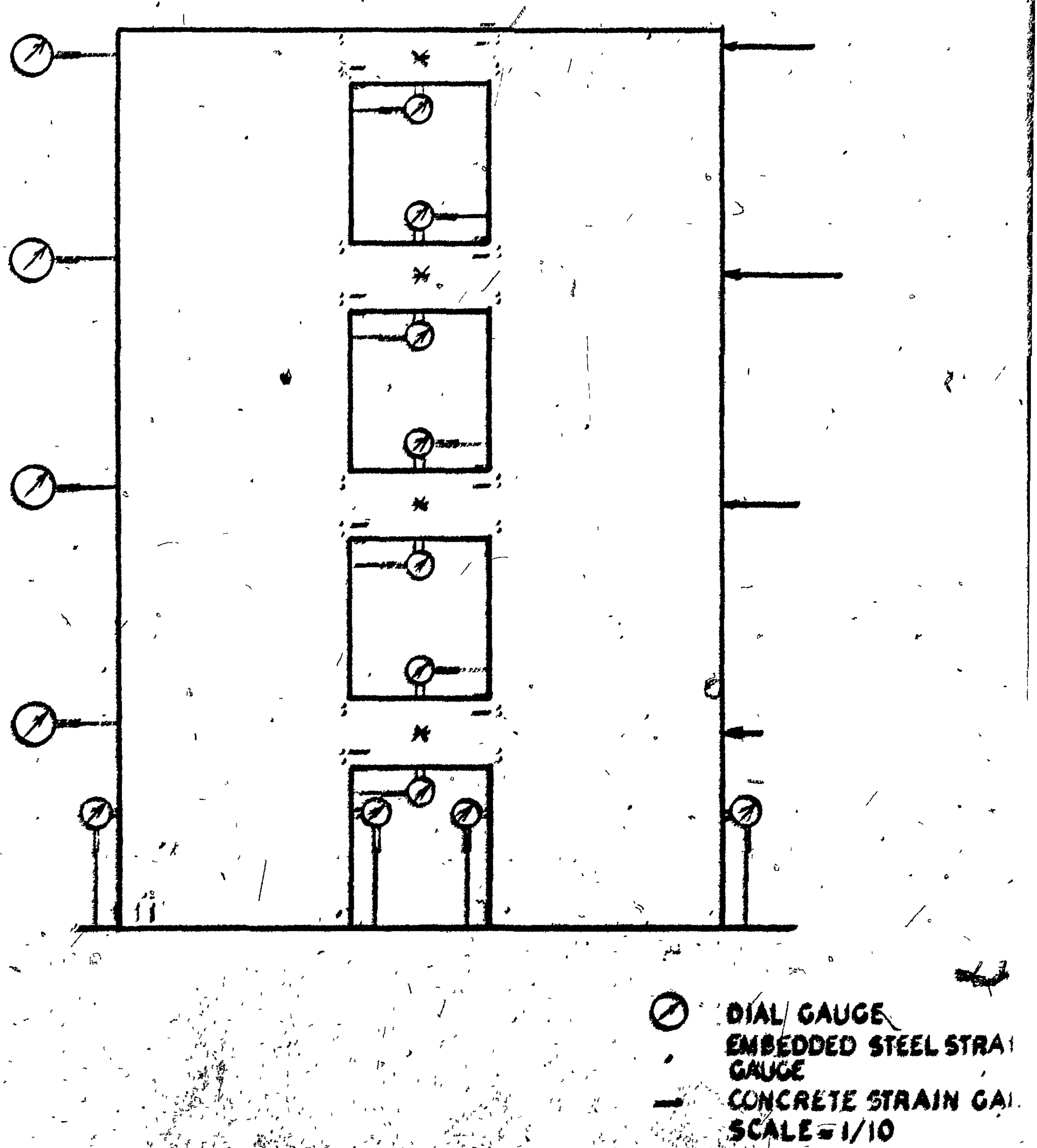

FIG. 3.25: INSTRUMENTATION DETAILS OF SPECIMEN Nº3

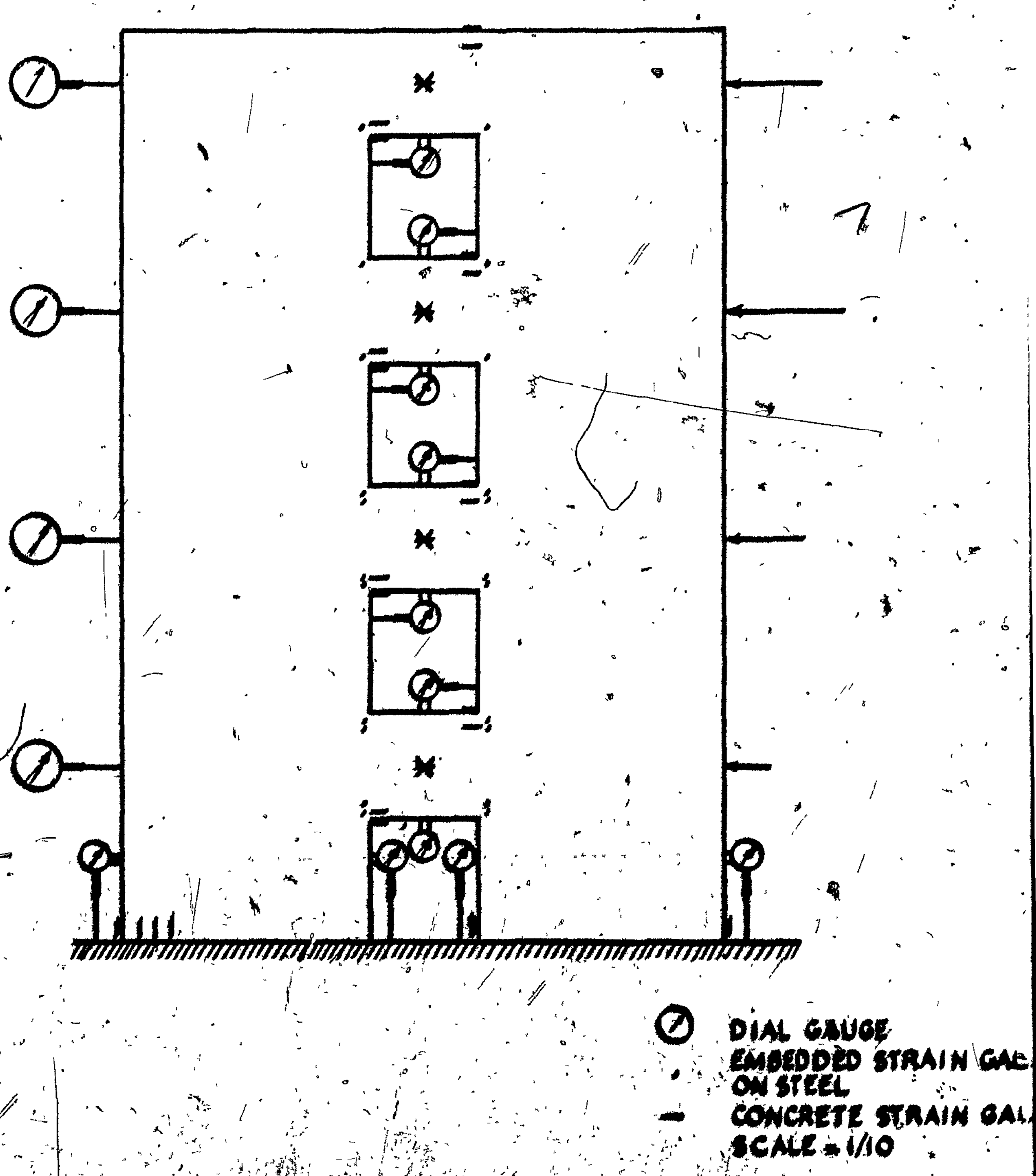

of the loading frame together with two clamping devices (Fig. 3.26). These clamping devices were made of two angles $3\frac{1}{2}$" x 5" x $\frac{1}{2}$" and $2\frac{1}{2}$" x $3\frac{1}{2}$" x $\frac{1}{2}$" welded at mid-height of each angle in such a way to make the clearance equal the height of the base block of 6 in.

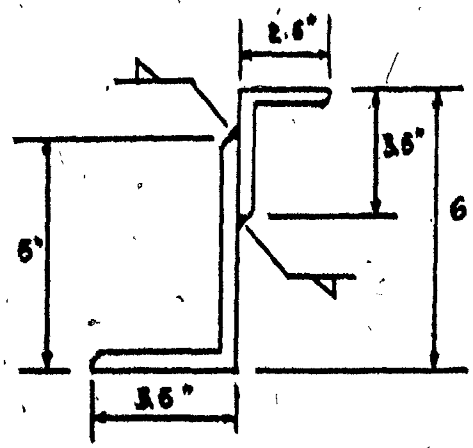

Fig. 3.26 The clamping device

2. Four pairs of 2" x 2" x $\frac{3}{8}$" angles were mounted on two sides of the loading frame. Three of these pairs were used to support the bracing rollers and the remaining one pair of angles was used to support the loading device. (Fig. 3.19).

3. The load distributor was moved carefully on rollers to make full contact with the shear wall assembly through four curved steel bearings mounted at the four storey levels along the height of the wall.

4. Sixteen dial gauges were used for measuring deflections. These were carefully set up (Figs. 3.23 to 3.25) and initial readings were recorded before applying any load. Four of these gauges were used to measure lateral displacements of the wall at the beam levels. Seven of these gauges were used to measure the rotation of mid-length sections of the four coupling beams. Four other gauges were used to measure the rotation of a section a distance $\frac{d}{2}$ above the base and one gauge was used to measure the uplifting of the end of the base block. All dial gauges attached to the specimen were mounted on plexiglass arms $\frac{1}{4}$" x $\frac{3}{4}$" x $1\frac{1}{8}$" glued to the beams and $\frac{1}{4}$" x $\frac{3}{4}$" x $\frac{3}{4}$" glued to the walls.

5. The line of action of the load was then checked. All joints between the ¾" dia. threaded rods were securely connected.

6. The bracing rollers on both sides of the shear wall were tightened. These rollers were required to remain in contact with the concrete surface without exerting any significant pressure on it.

7. Load was applied in increment of 0.5 kip. To achieve the required load levels, each strain indicator of the load cells was set to a specified strain reading. When the top deflection exceeded 0.05 in. in each loading step, this deflection value was used as the controlling factor for further experimental work (Figs. 3.26 and 3.27).

8. The readings of the strain gauges and dial gauges were taken three minutes after each load increment was applied. For specimen no. 1, at the beginning of loading, the pump had to be adjusted slightly to maintain constant loads. The walls and the beams were examined for the appearance and propagation of cracks which were traced with a marking pen and the ends marked with the number of the loading step.

9. Just before failure, all dial gauges were removed to prevent any damage.

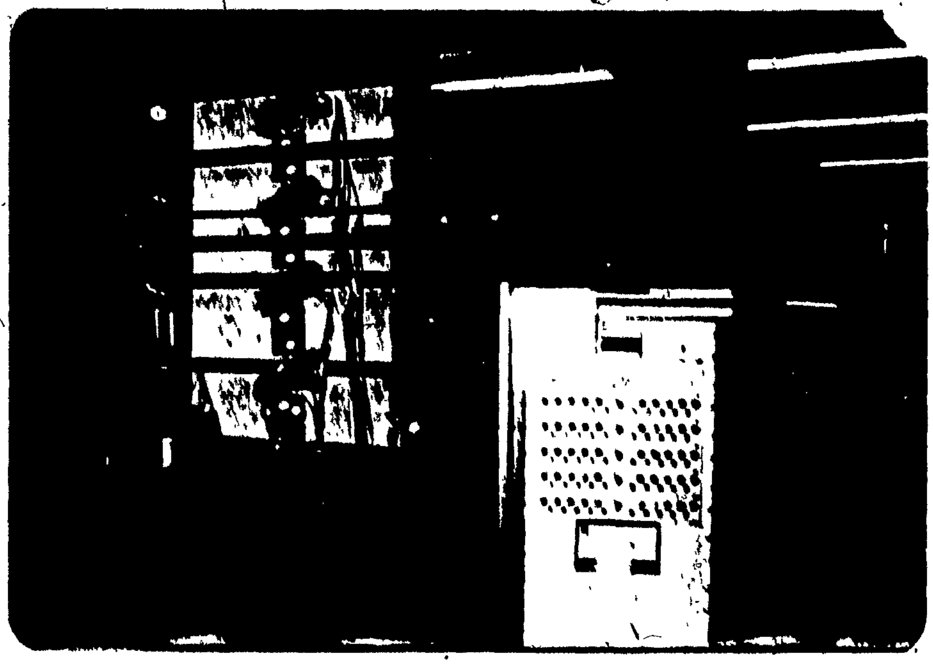

Fig.3.27A: Experimental set-up of specimen no. 3

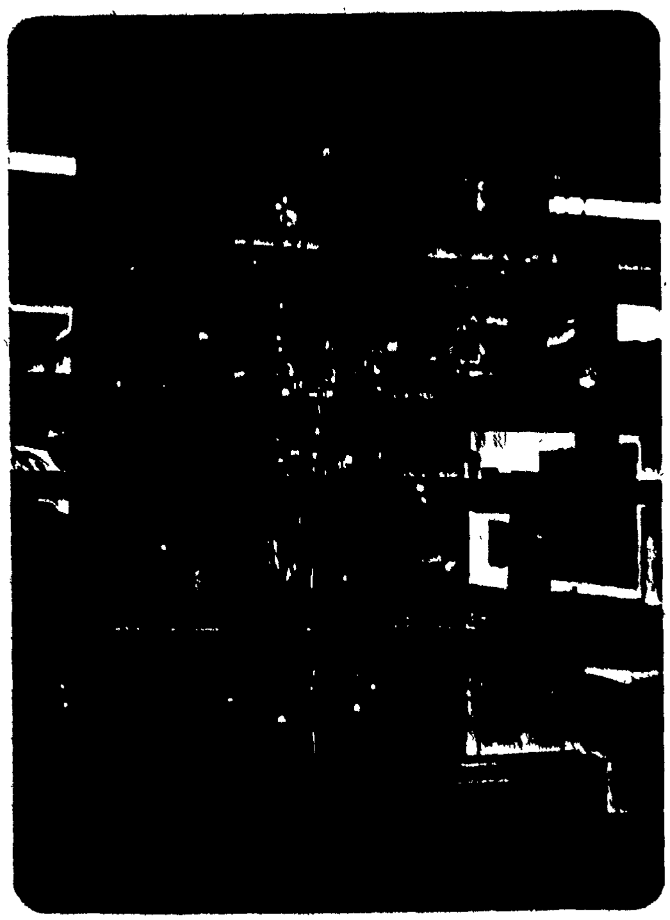

Fig.3.27B: Specimen no. 2 - under testing

IV. THE BEHAVIOUR OF THE TEST SPECIMENS

4.1 General Behaviour

During the last decade, several investigators have studied the elastic behaviour of coupled shear walls. Small scale models constructed from perspex, steel, celluloid, aluminum, etc., have been used in the design of economical shear wall structures to resist the seismic forces.

In studying the energy-absorption capacity of coupled shear walls, direct models constructed from reinforced concrete have been used successfully by Paulay[14] and Faucher[30]. Paulay used two direct one-quarter scale models of seven-storey reinforced concrete coupled shear walls to study the effect of the different type of reinforcing patterns for the coupling beams on the overall behaviour. He observed the damage to be much less in the model with diagonally reinforced beams than in the model with conventionally reinforced beams. Full capacity of the connecting beams was achieved and maintained during the test and finally the wall failed at its base. Considerable ductility was observed for both specimens with only moderate loss of strength under progressive reversed loading[14].

In recent years, some analytical work has been conducted to predict the behaviour of coupled shear walls after yielding or local failure of some parts or all of the critical sections. Paulay[29] used his approximate elasto-plastic analysis technique to analyse an eighteen storey coupled shear wall. His analysis led to a complete description of the behaviour of the structure at any stage of loading. The results of Paulay's study are reproduced in Figs. 5.1 and 5.2.

Effects of cracking on the beam and wall actions are shown in Fig. 5.1. Curves A indicate the results of a conventional analysis, assuming uncracked sections while curves B show the internal actions calculated after making an allowance for the loss of stiffness caused by cracking in the coupling elements. Curves C indicate the effect of reduced stiffness of the lamina and wall 2 (tension wall).

According to Paulay's results, the maximum tensile force in the coupled shear walls occurs at the wall base, while the laminar shear attains a maximum value of roughly one-fourth of the height from the base. This accounts for the reduction of the stiffness of the coupling elements due to cracking. Fig. 5.1 also shows that after cracking of the lamina and wall 2, these actions increase again to a slightly higher value. However, these values are much less than the corresponding maximum values for the uncracked section on account of the additional cracking of wall 2 (ref. 29).

Figures 5.2 a and b show values of moments and rotations along the wall height as yielding spreads through the total height of the lamina and at the base of wall 2. The location where maximum rotation occurs in the lamina gradually moves upwards from approximately a quarter height point at the onset of yielding to a point at approximately mid-height at a stage when the laminas are fully plastified and the capacity of walls 1 and 2 is attained.

Figure 5.2c shows a theoretical load-deflection curve obtained by Paulay using the approximate elasto-plastic analysis. He assumed identical properties for all coupling beams. If the ultimate strength of the coupling beams was varied according to the elastic laminar shear, the transition from elastic to plastic behaviour of all laminas would occur at about the same load. Thus, point 3 in Fig. 5.2.c would approach point 2 and would result in a smaller ultimate strength for the structure as a whole[29].

This direct model study was undertaken to examine the effects of cracking and yielding of the laminas and walls and the influence of the various patterns of connecting beam reinforcement on the overall behaviour of coupled shear walls. The details of the test set-up and the instrumentation used were presented in Chapter III. The test data consisted of the following:

(i) Load-deflection curves at all four storey levels

(ii) Load-rotation curves for all four connecting beams

(iii) Strain values at selected positions.

Some typical data is presented graphically in the following sections and the rest of the data is included in Appendix C.

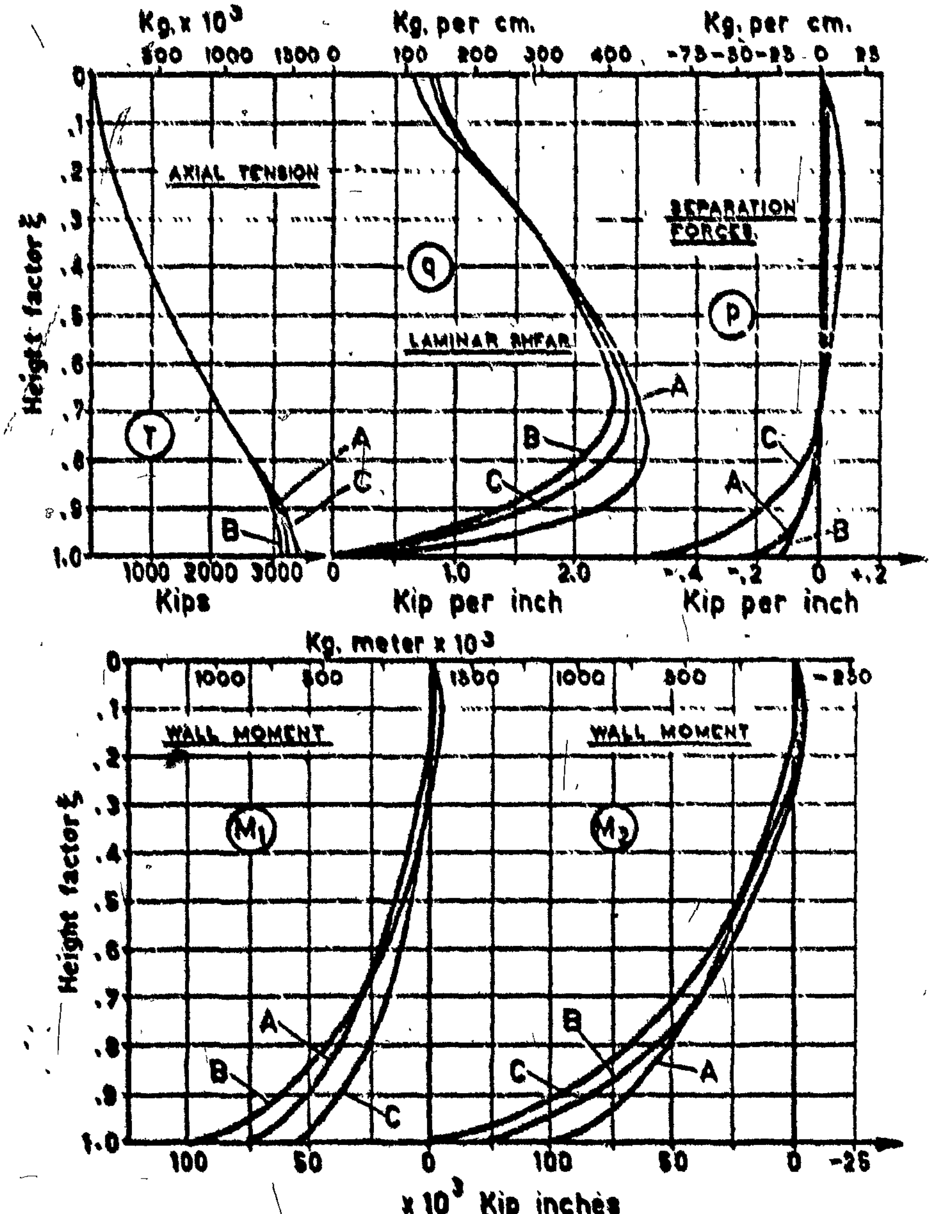

FIG. 4.1 EFFECTS OF CRACKING ON THE INTERNAL ACTIONS
(after Paulay, Ref. 29)

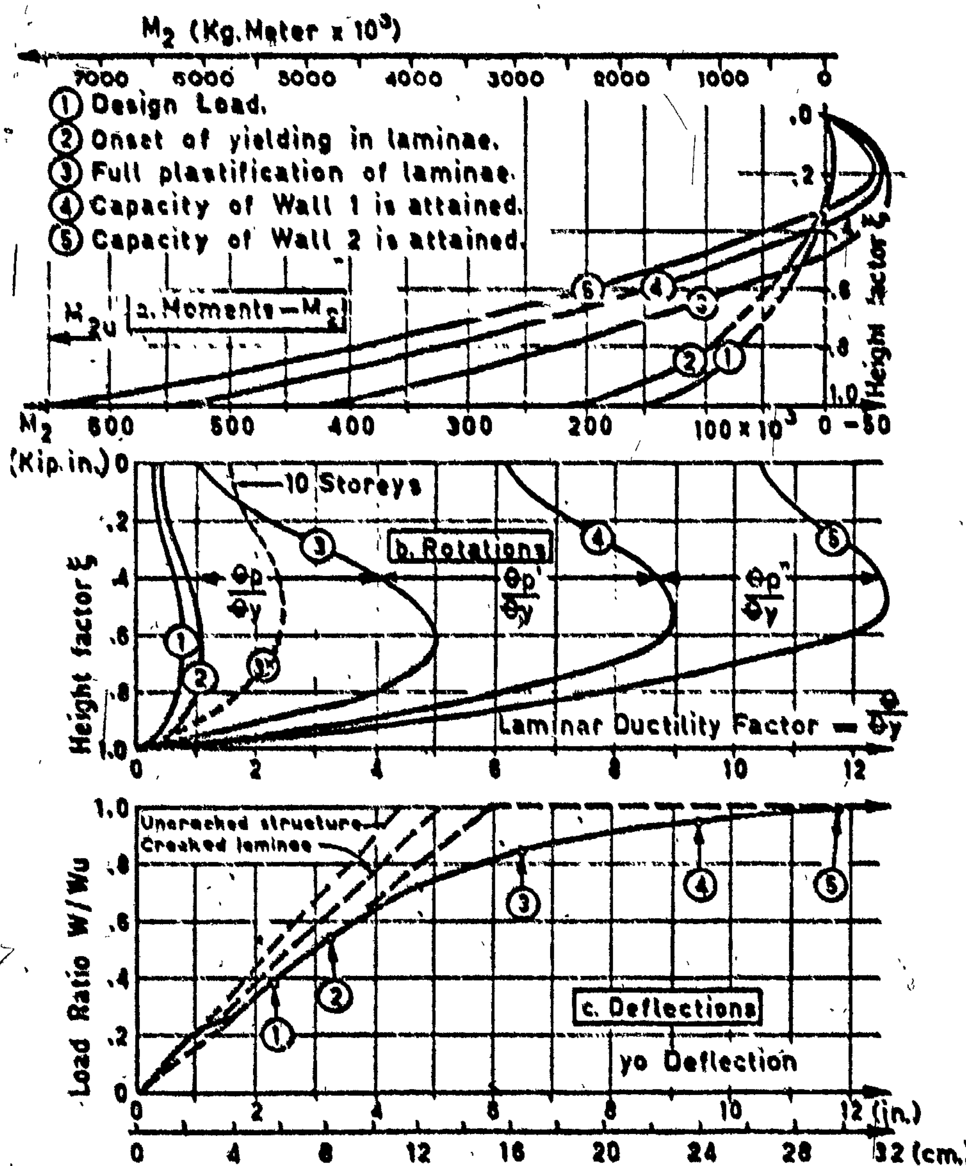

FIG. 4.2 RESULTS OF AN ELASTO-PLASTIC ANALYSIS OF AN 18-STOREY SHEAR CORE (after Paulay, Ref. 29)

4.2 Behaviour of Test Specimen No. 1

The reinforcement pattern and instrumentation details for test specimen no. 1 were described in Chapter III. This specimen was loaded in increments of 1 kip for the first four loading steps. Beyond this load, the test was continued using controlled increments of deflection at the top storey which were maintained constant at a value of 0.05 in.

Cracking was observed to start at a total applied load value of 3 kips (this was distributed in the form of four concentrated loads at the storey levels) (Fig. 4.3). The top storey deflection at this stage was observed to be 0.06 in. (Fig. 4.4). The deflections of lower storeys are also presented in Figs. 4.5 to 4.8. The rotation at the base of each shear wall was about 0.006 radian (this was measured at sections distant $\frac{d}{2}$ above the bases)(Figs. 4.9, 4.10). The concrete and steel strains at the base of wall 1 were approximately 150 x 10^{-6} and 170 x 10^{-6} respectively. The concrete and steel strain values at the base of wall 2 were about 220 x 10^{-6} and 780 x 10^{-6} respectively.

Figure 4.8 presents the load-deflection curves at various storey levels. All curves show a change in slope at a load value near three kips, indicating a reduction of the overall stiffness of the specimen due to cracking at the beam-wall junctions. Cracks appeared in the lower beams almost simultaneously; however, these were not significant. These cracks formed at an angle of approximately 30° with the vertical and were wider than the cracks in the upper beams. Rotations at mid-span sections of the four beams are shown in Figs. 4.11 to 4.14. Cracking patterns of these beams are shown in Figs. 4.15 to 4.19. A crack appeared in the top beam at a point where the beam reinforcement terminated. At a load value near 5 kips, this crack propagated downward into the wall and the beam as shown in Fig. 4.16. Near failure, the width of this crack and the cracks in the lower beams was in the neighborhood of ¼ in.

Cracks in wall 2 started first as diagonal tension cracks in the first storey at about 7" from the base at a load value near 5 kips. These cracks then propagated both ways to reach the outside edge of the wall where secondary flexural cracks started to form. Although most cracks concentrated in the first storey of wall 2 (Fig. 4.18), it was the rupture of the reinforcement at the inside edge of wall 1 that caused the load-deflection curve to drop off at a total load value around 5.4 kips (Fig. 4.19). The top storey deflection at this stage was 1.9 in.

Crushing of the concrete in wall 1 at the outside edge was observed at a load value of 5 kips. At this stage the cracks had propagated through approximately one-third of the wall depth. There was no significant crushing of the concrete at the inside edge of wall 2 (Fig. 4.18). Crushing of the concrete at the beam wall interfaces of lower beams was noticeable at the ultimate load (Fig. 4.17).

Further loading beyond a total load value of 5 kips caused more cracking in the wall bases. The steel reinforcement at all connecting beam-wall junctions and wall 2 base yielded at a total load value of approximately 5.1 kips (Fig. 4.4). The top storey deflection at this stage was 0.17 in. (Fig. 4.4) and the rotation at the midspan section of the beam at storey 1 was 0.0028 radian. The relative rotation at a section distant $\frac{d}{2}$ from the wall base was observed to be 0.0019 radian (Figs. 4.9, 4.10).

TABLE 4.1 Strain Gauges' Reading Values for Specimen No. 1 at Yield Load of 5 kips (Micro strain, x 10^{-6})

	Concrete strain Compression end	Steel strain Compression end	Steel strain Tension end
Wall 1	658	487	214
Wall 2	322	70	1487
Beam 1 (Wall 1 face)	190	565	555
Beam 1 (Wall 2 face)	257	-	-
Beam 2 (Wall 1 face)	264	260	1010
Beam 2 (Wall 2 face)	162	80	201
Beam 3 (Wall 1 face)	317	574	648
Beam 3 (Wall 2 face)	220	368	892
Beam 4 (Wall 1 face)	-	250	-
Beam 4 (Wall 2 face)	216	230	579

TABLE 4.2 Strain Gauges' Reading Values for Specimen No. 1 at Ultimate Load of 6.02 kips (Micro strain, $10^{-6}\mu$)

	Concrete strain Compression end	Steel strain Compression end	Steel strain Tension end
Wall 1	2166	765	175
Wall 2	799	515	359
Beam 1 (Wall 1 face)	1252	-	-
Beam 1 (Wall 2 face)	2365	-	-
Beam 2 (Wall 1 face)	-	463	-
Beam 2 (Wall 2 face)	2437	-	-
Beam 3 (Wall 1 face)	2560	904	-
Beam 3 (Wall 2 face)	1379	-	438
Beam 4 (Wall 1 face)	72	182	-
Beam 4 (Wall 2 face)	493	352	-

TABLE 4.3 Maximum Microstrain Values Recorded for Specimen No. 1 (and corresponding top deflection)

	Concrete strain Compression end	Steel strain Compression end	Steel strain Tension end
Wall 1	2926 (1.133)	1049 (2.3)	341 (1.733)
Wall 2	4490 (2.5)	740 (.77)	1542 (.263)
Beam 1 (Wall 1 face)	3656 (.444)	1056 (.64)	651 (.263)
Beam 1 (Wall 2 face)	4085 (2.4)	-	-
Beam 2 (Wall 1 face)	3961 (.59)	727 (2.5)	1109 (.263)
Beam 2 (Wall 2 face)	3613 (2.5)	627 (1.833)	317 (.351)
Beam 3 (Wall 1 face)	3186 (1.233)	1930 (1.333)	655 (.116)
Beam 3 (Wall 2 face)	1639 (1.233)	1781 (.734)	998 (.351)
Beam 4 (Wall 1 face)	84 (.734)	936 (1.633)	-
Beam 4 (Wall 2 face)	563 (1.433)	546 (2.5)	579 (.166)

FIG. 4.3: SPECIMEN NO. I CRACK PATTERN

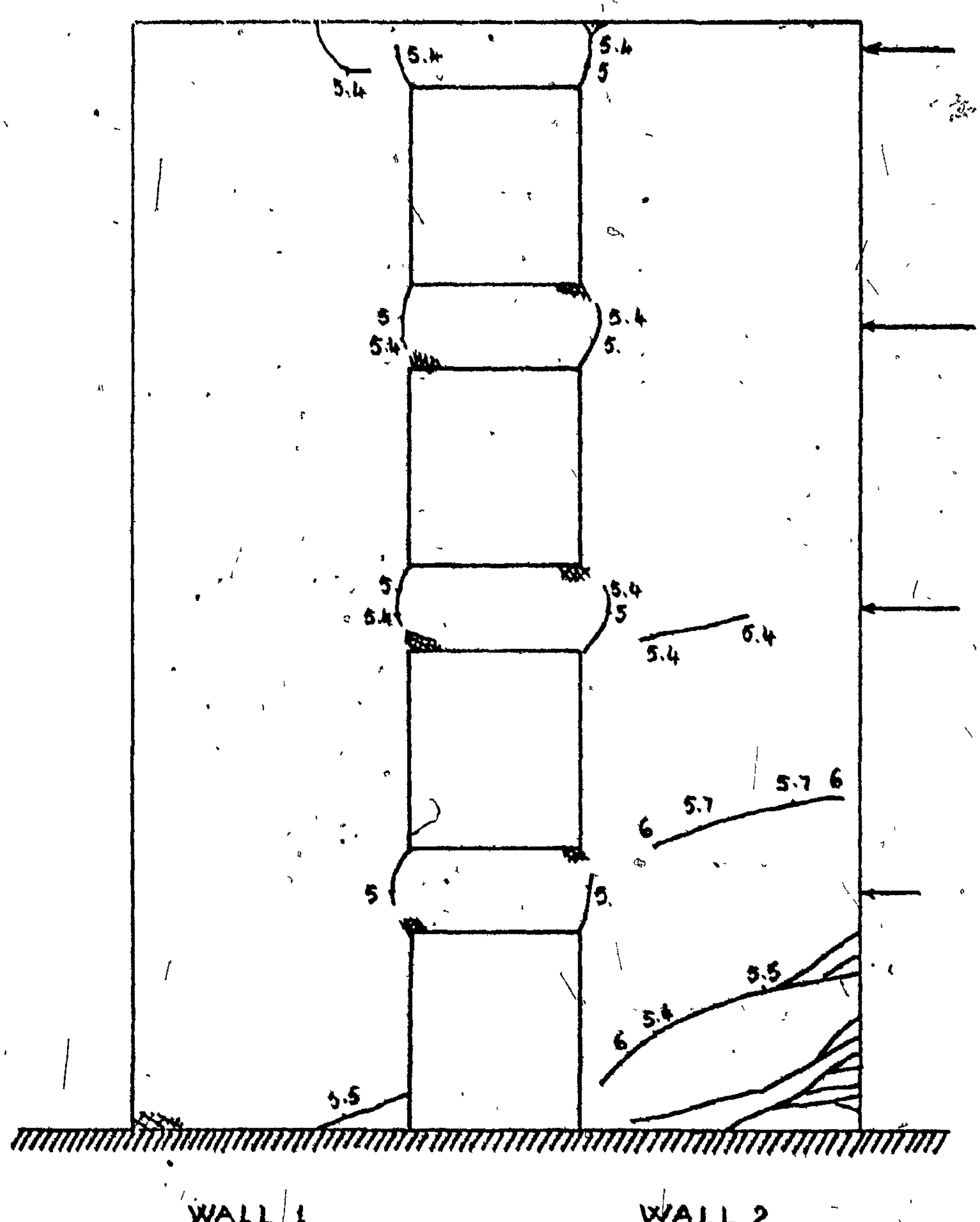

FIG. 4.4:

TOP STOREY DEFLECTION - Specimen No. 1

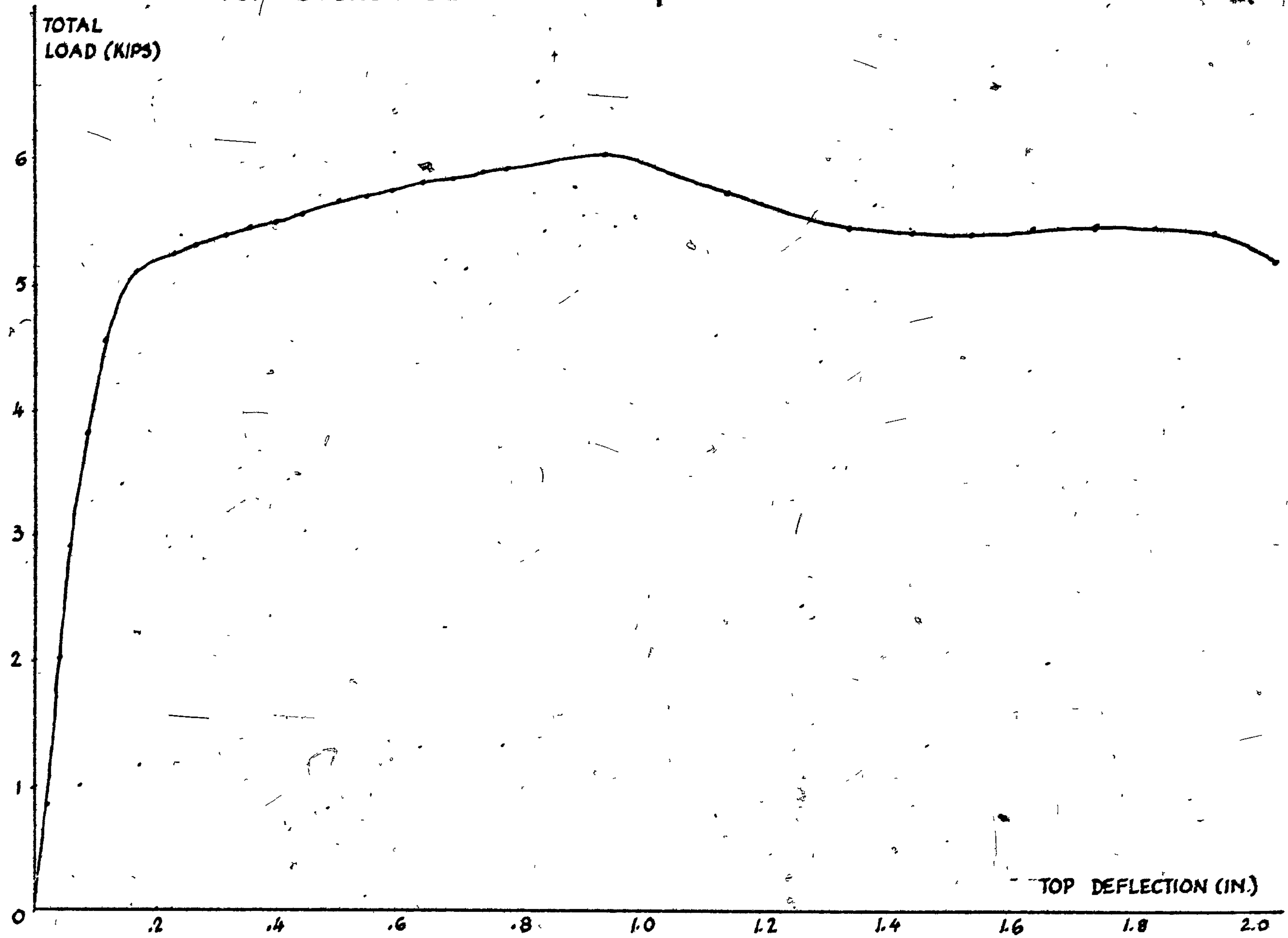

FIG. 4.5 :
Third Storey Deflection - Specimen No.1

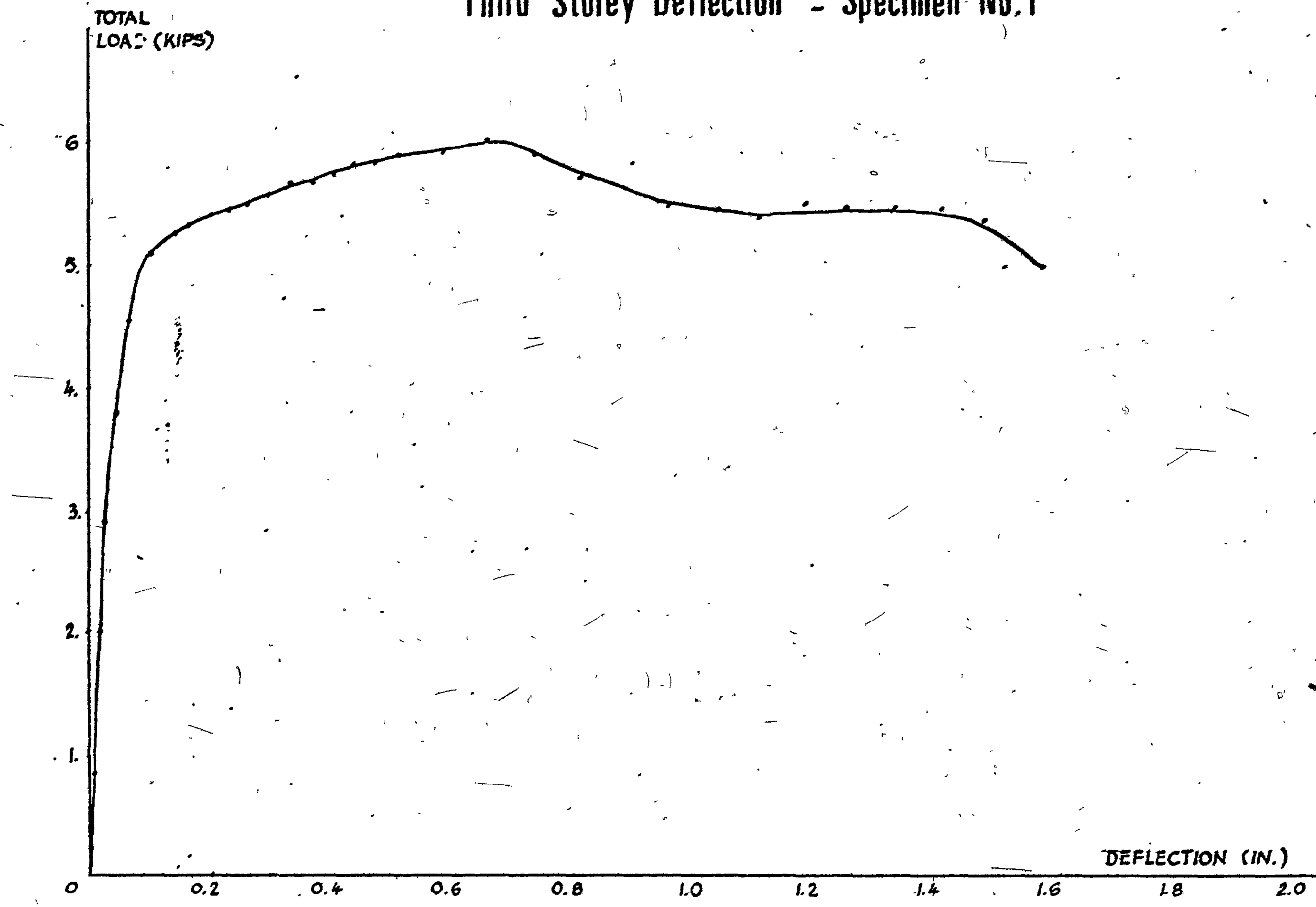

FIG. 4.6:
Second Storey Deflection - SPECIMEN NO. 1

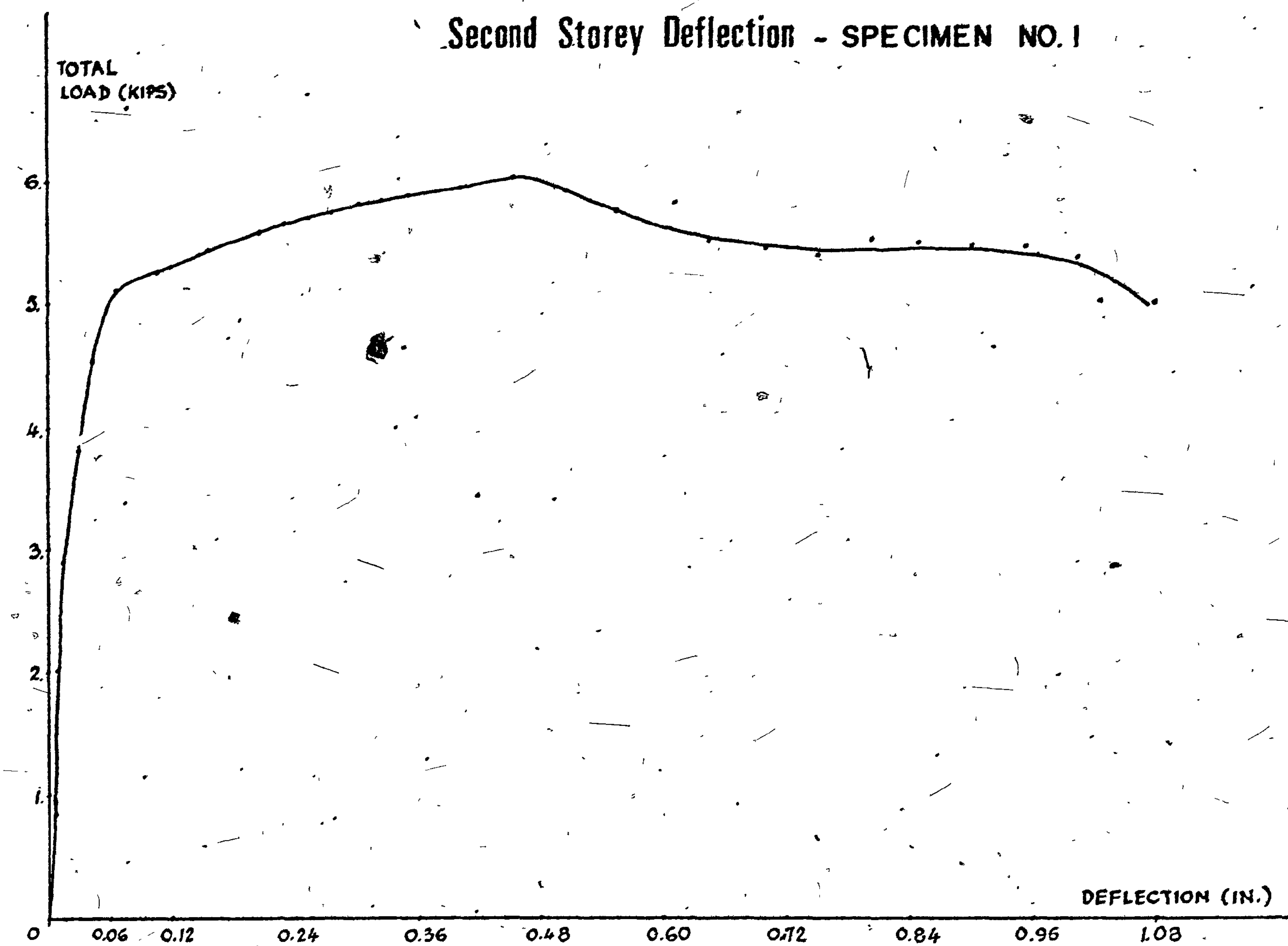

Fig. 4.7 : First Storey Deflection - SPECIMEN NO. I

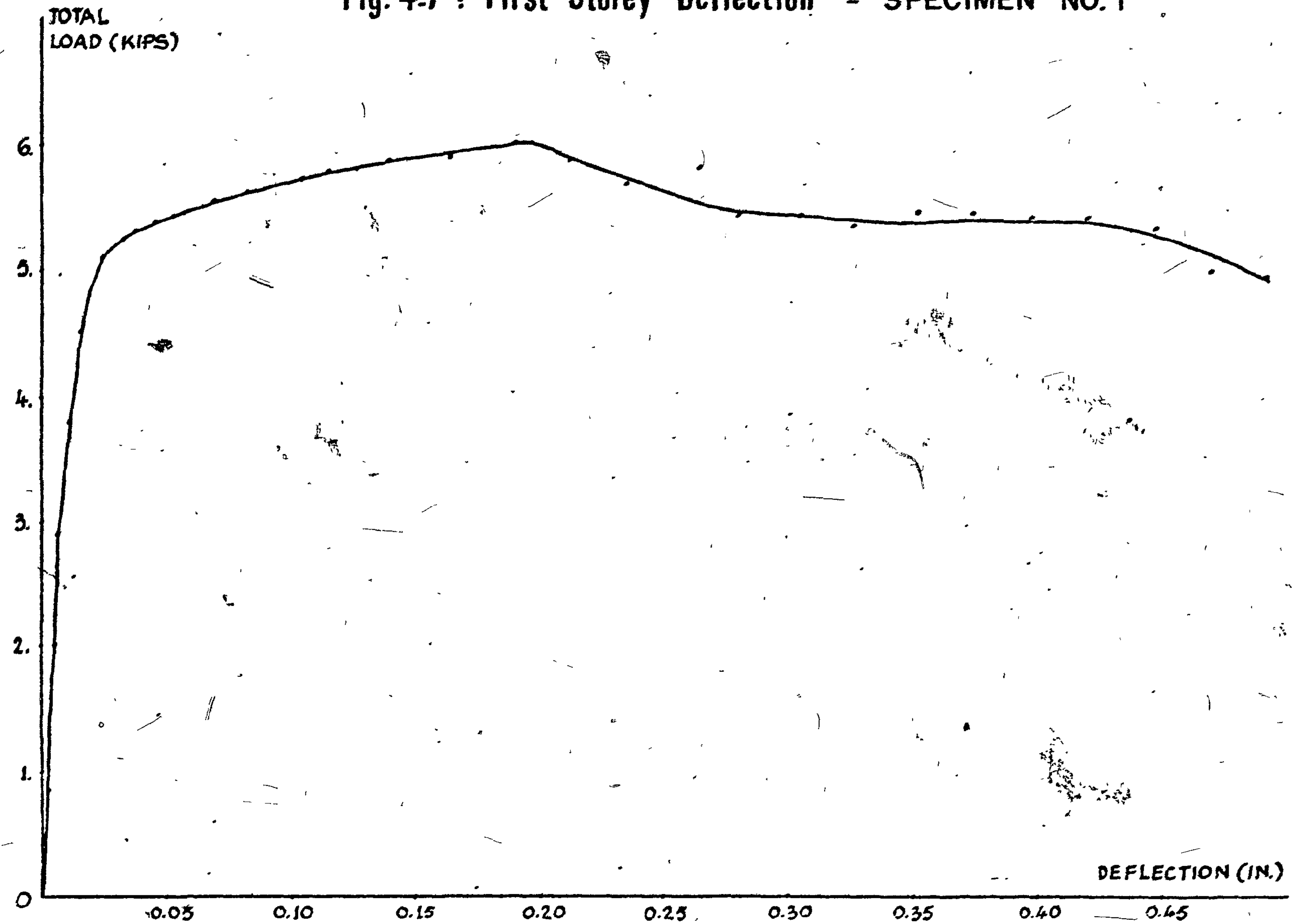

FIG. 4.8: DEFLECTION OF FOUR STOREY LEVELS - SPECIMEN NO. 1

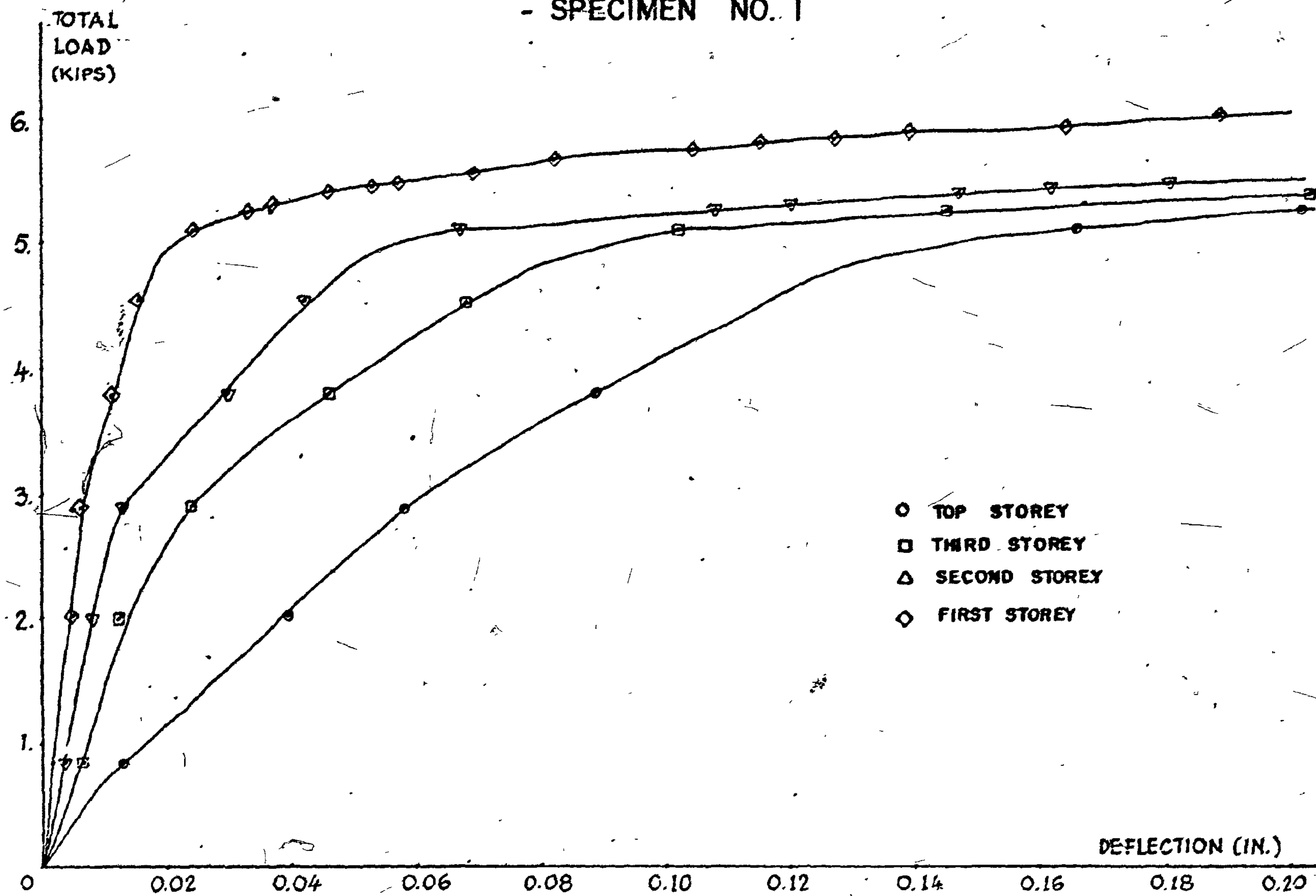

FIG. 4.9:

Wall 1 Rotation

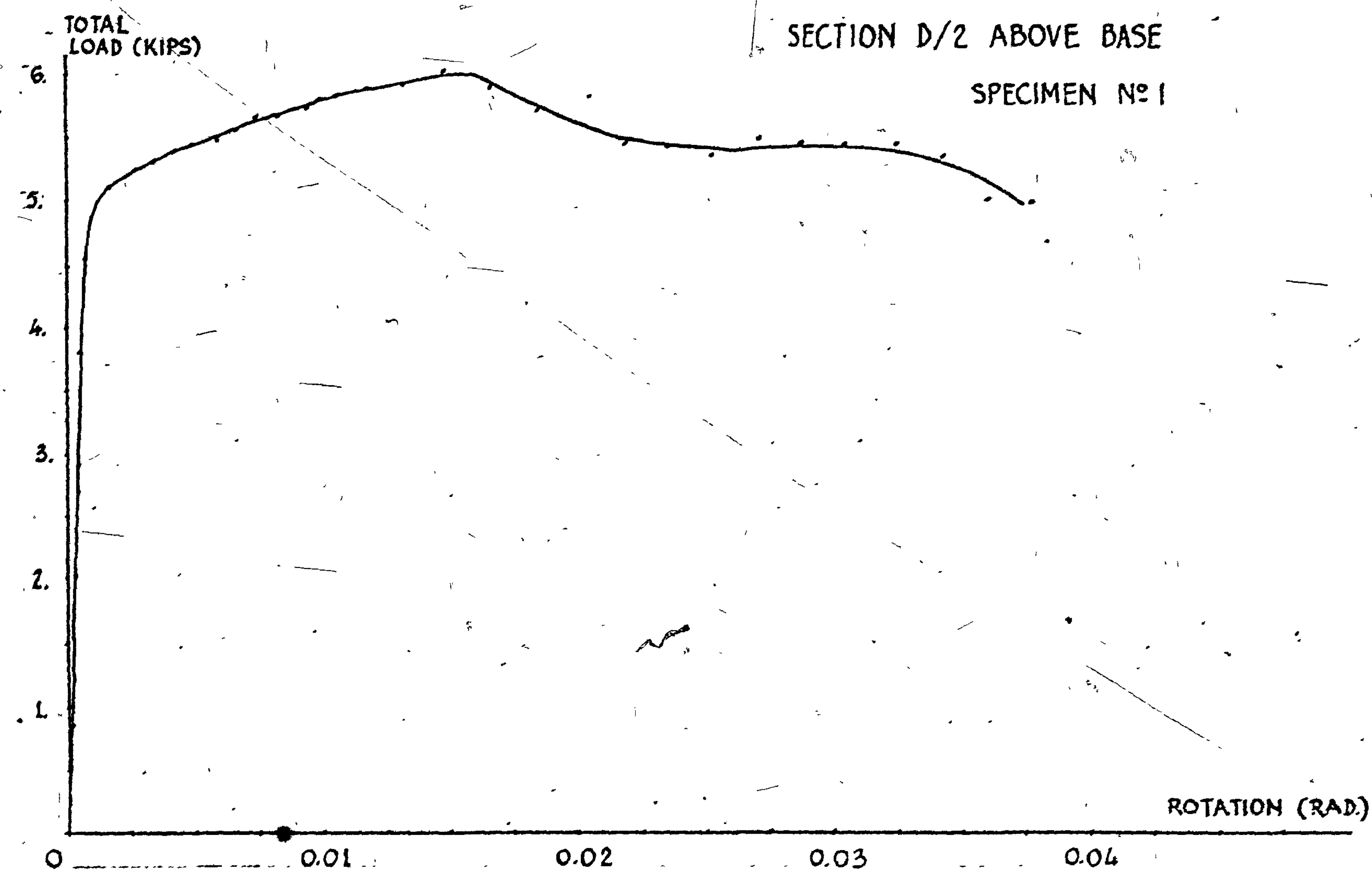

FIG. 4.10:

Wall 2 Rotation

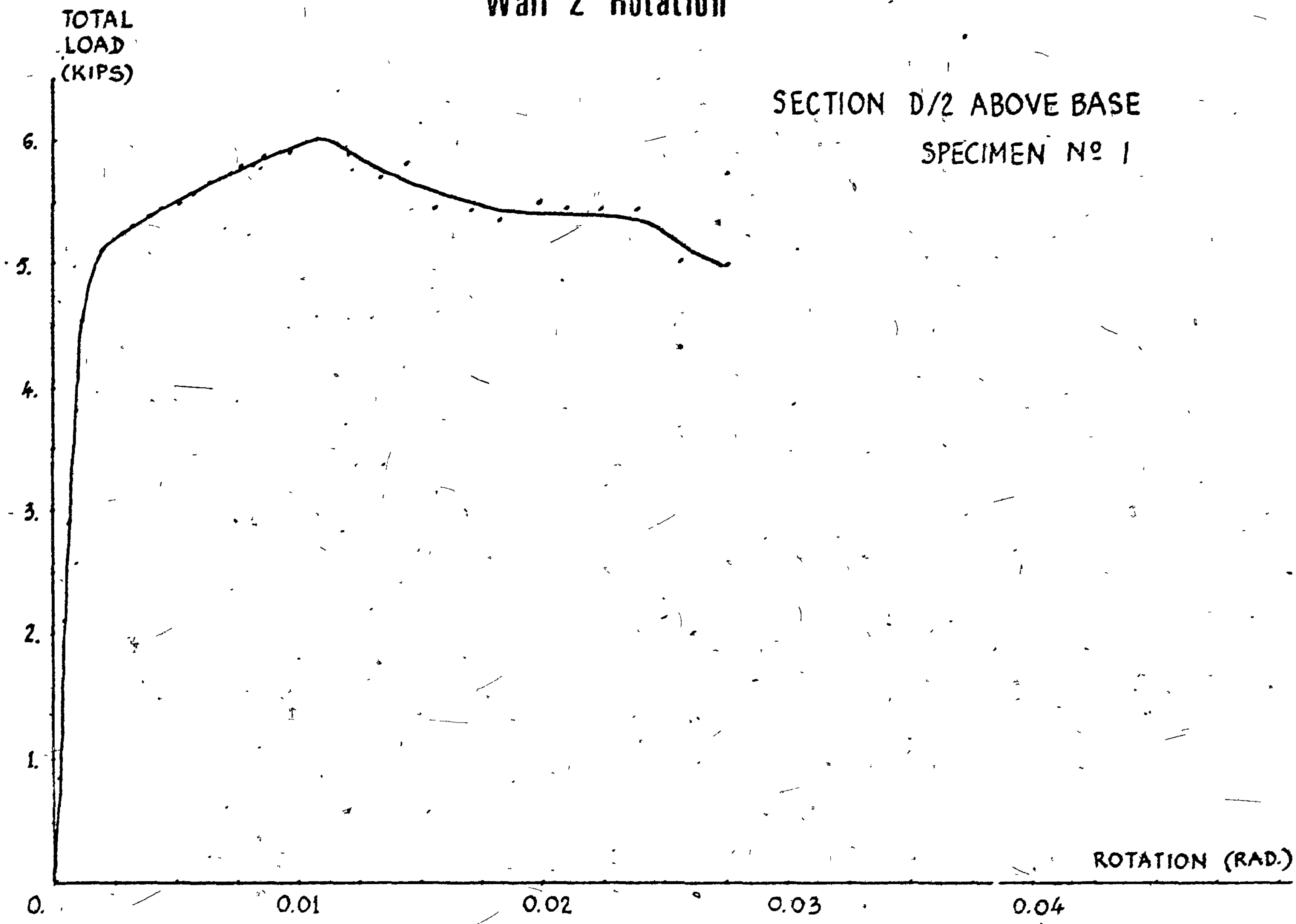

FIG. 4.11:
Beam 1 Rotation

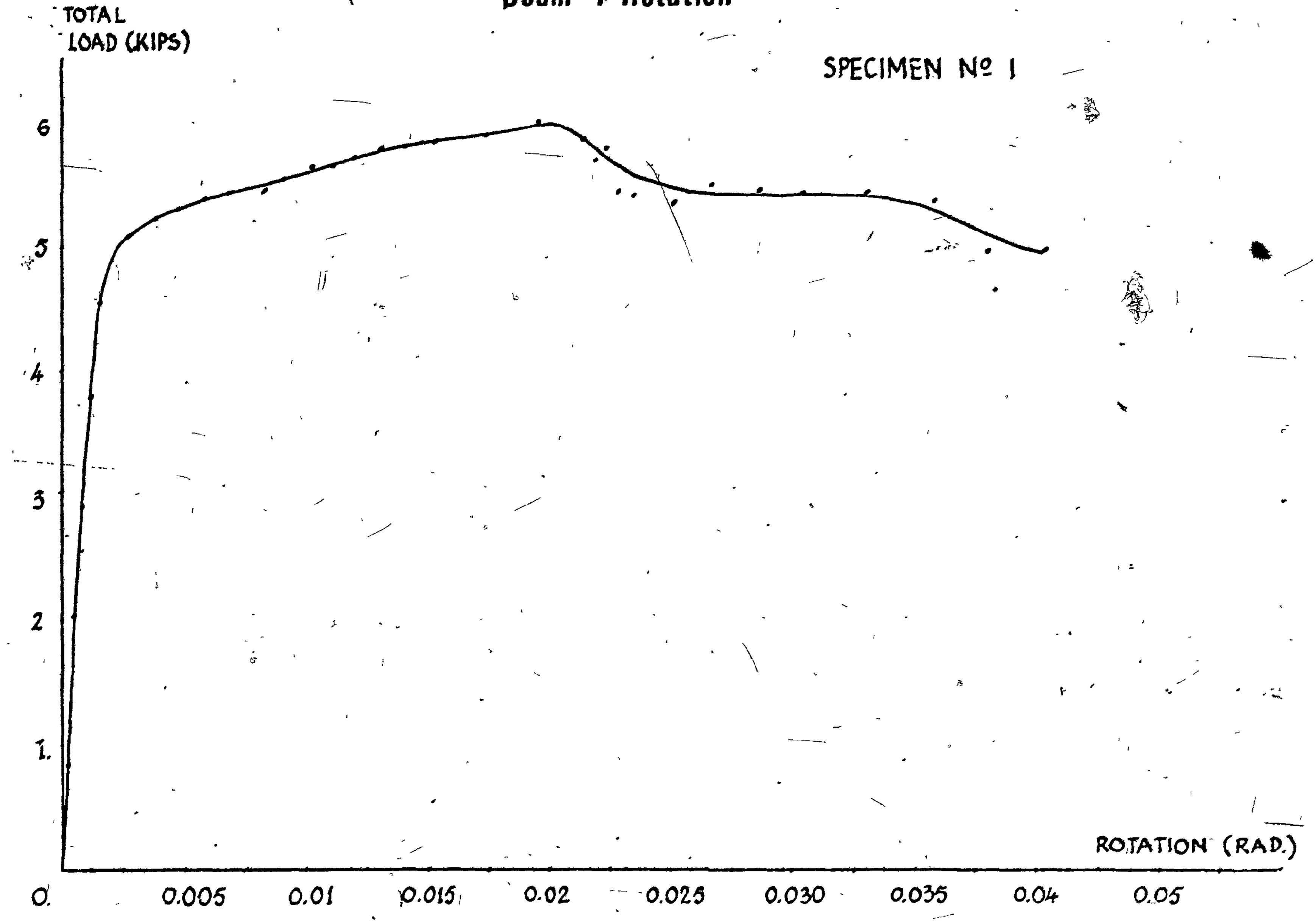

FIG. 4.12:
Beam 2 Rotation

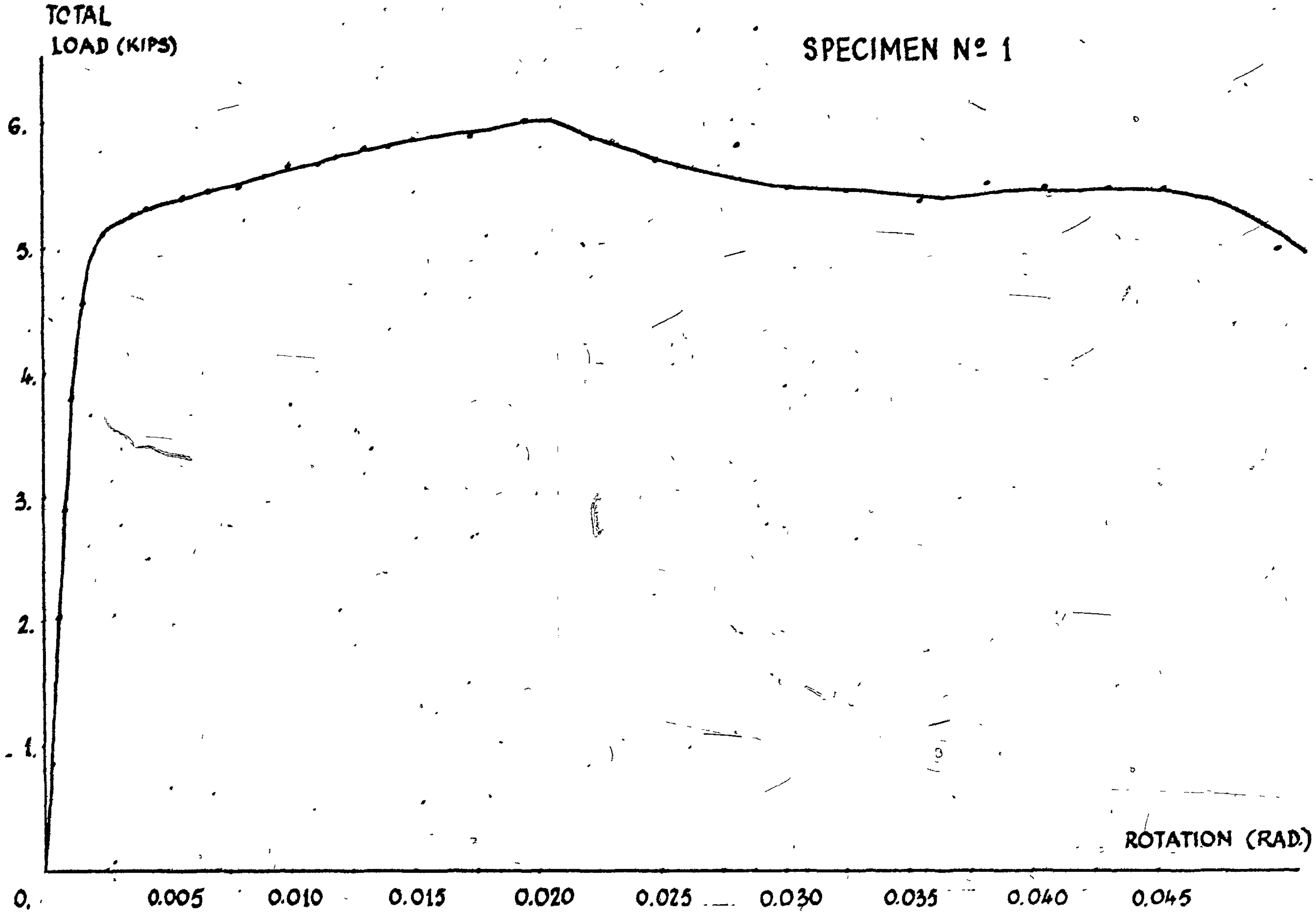

FIG. 4. 13:

Beam 3 Rotation

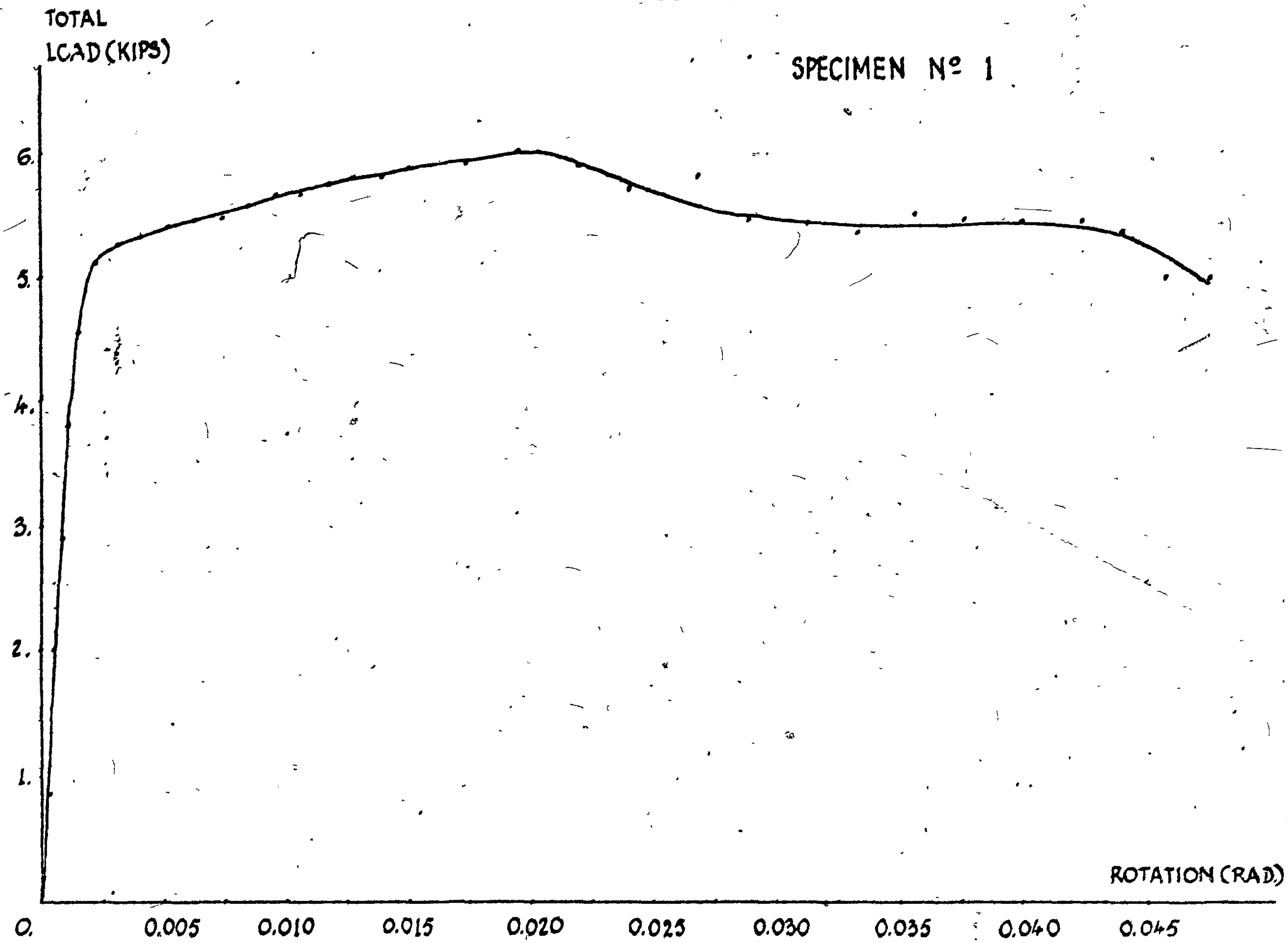

FIG. 4.14:
Beam 4 Rotation

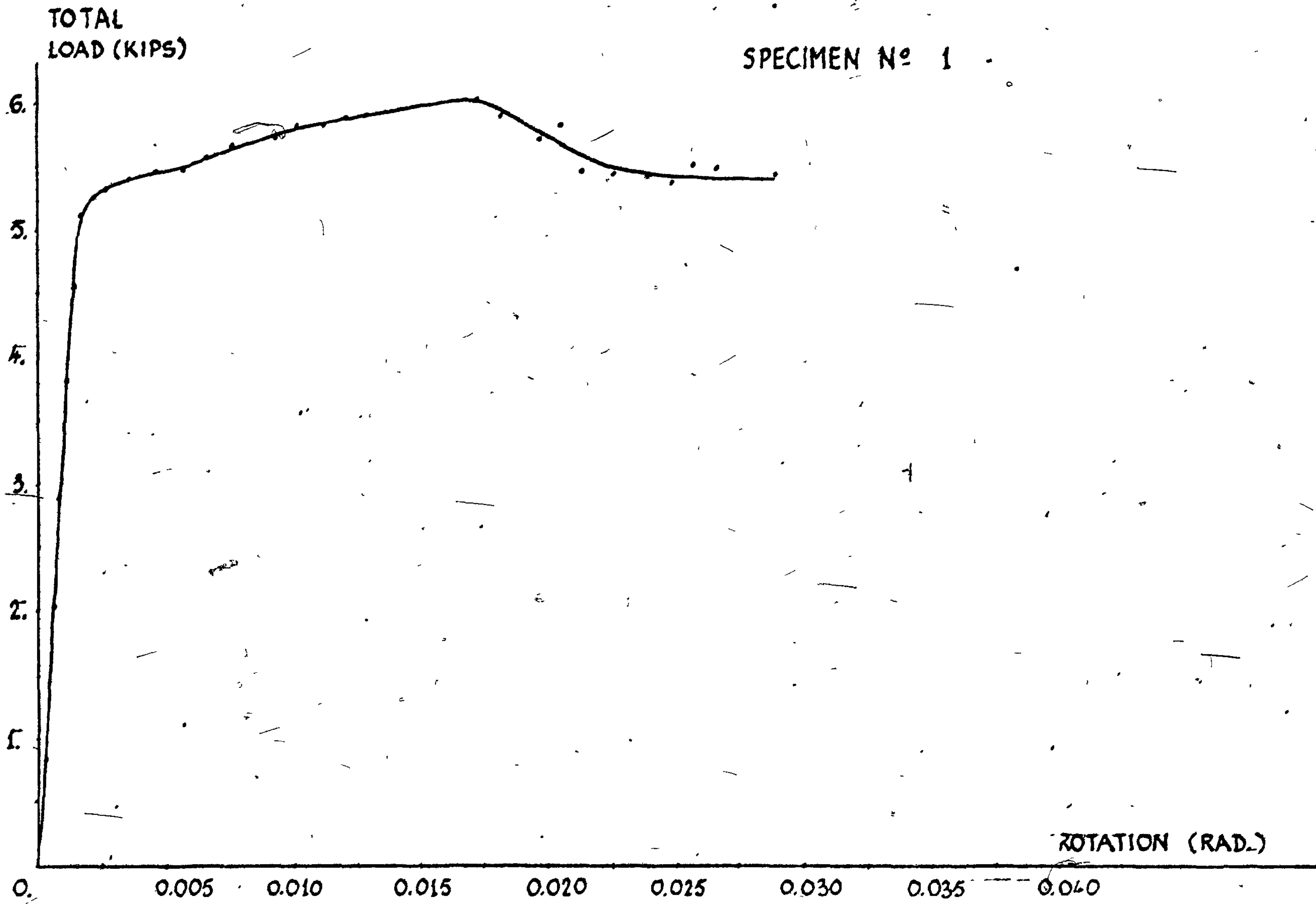

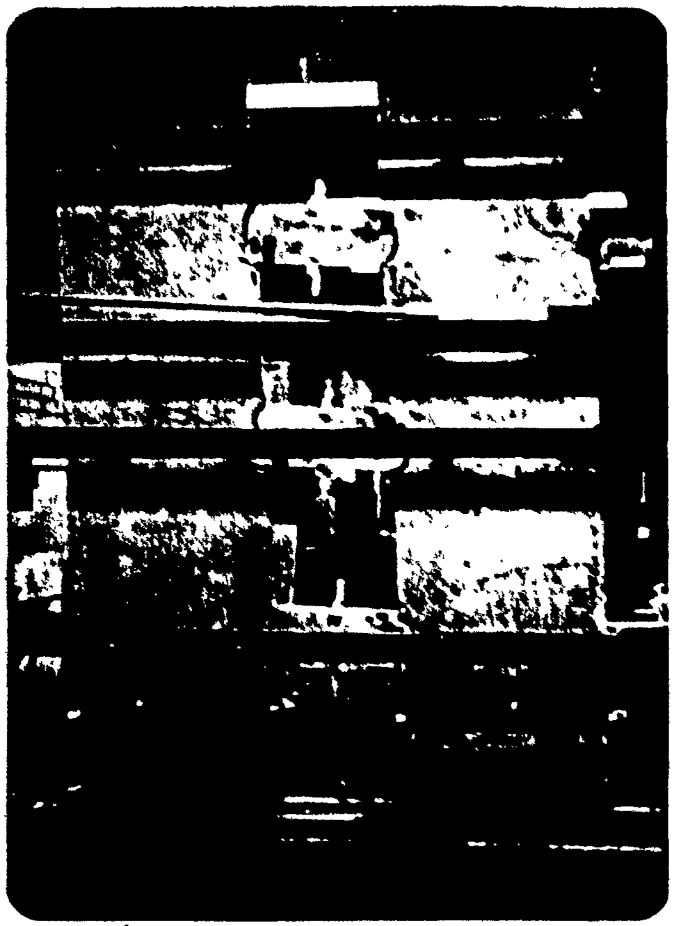

Fig. 4.15 Specinem No. 1 at failure

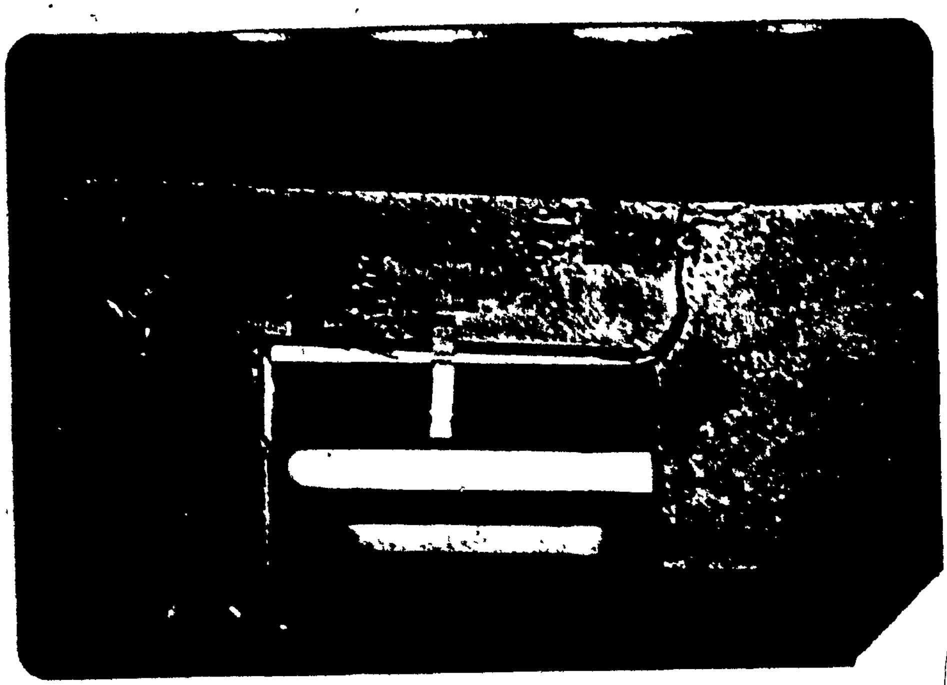

Fig. 4.16 Cracks in the top beam, Specimen No. 1

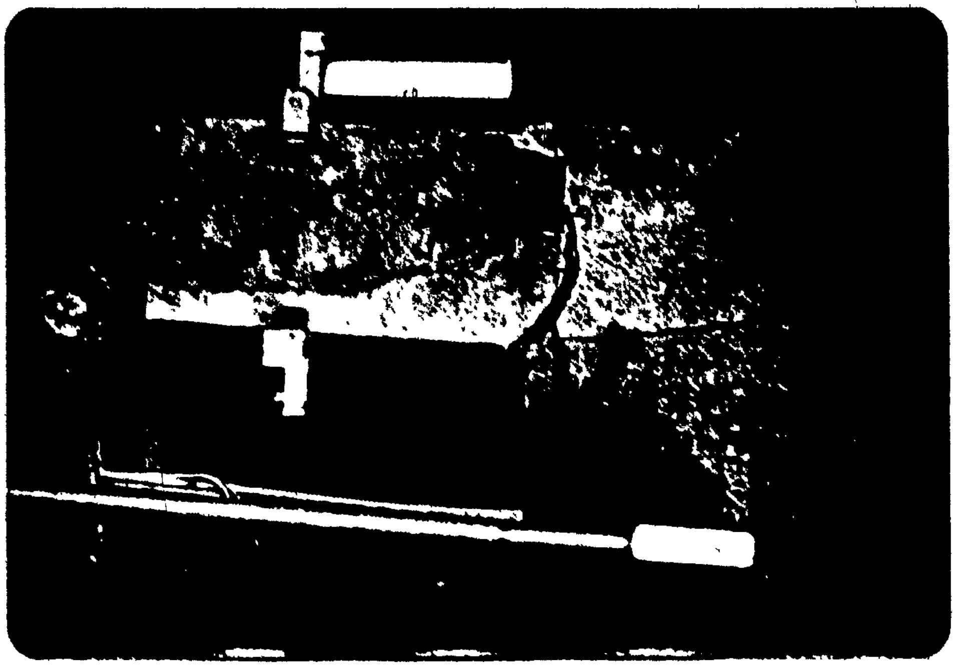

Fig. 4.17 Beam failure of Specimen No. 1

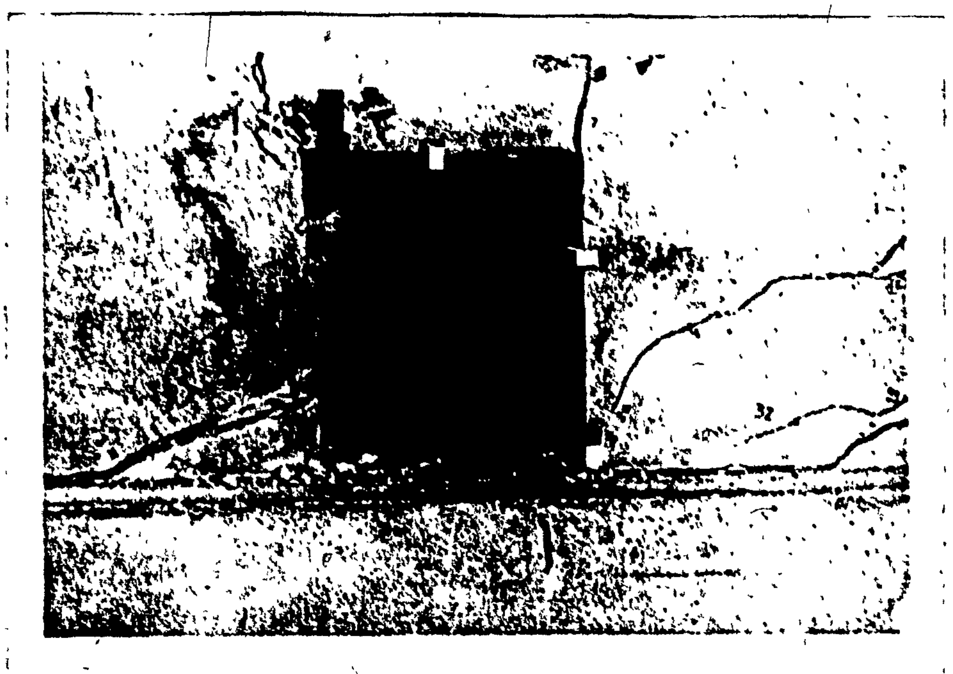

Fig. 4.18 Cracks in the bases

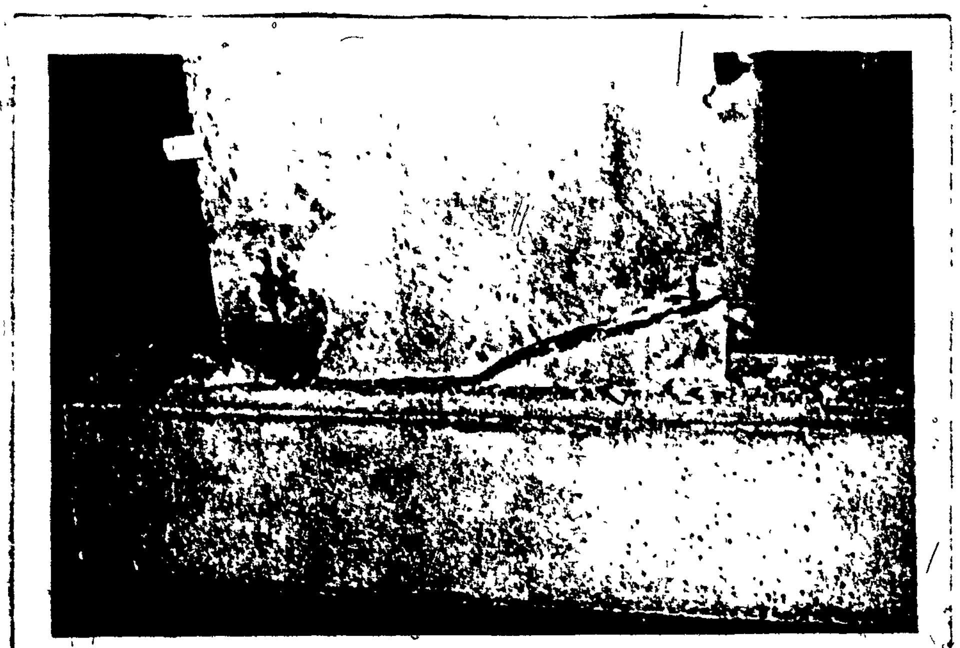

Fig. 4.19 Cracks and failure of Wall 1

Strain values at this load stage are shown in Table 4.1. The maximum concrete and steel strain values were observed to be 4090 x 10^{-6} and 1900 x 10^{-6} respectively (Table 4.3).

As the applied load was increased from 5.1 kips to 6.0 kips, the storey deflections increased almost linearly (Figs. 4.4 to 4.8); however, as expected, the overall stiffness had decreased considerably.

At this peak point of loading around 6.0 kips, the top storey deflection was observed to be 0.94 in. (Fig. 4.4). The ductility factor of roughly 6.5 was determined from the top level deflections. At failure stage, this ratio was roughly 14.3.

The specimen was considered to have failed when the tension reinforcement in wall 1 failed. At this stage, shear cracks in the first storey of wall 2 propagated to the outside edge and continued as flexural cracks. Cracks in lower beams opened wide (approximately ½ in. width) and the top storey deflection was approximately 1.9 in.

4.3 Behaviour of Test Specimen No. 2

The reinforcement pattern and instrumentation details of test specimen No. 2 were described earlier in section 3.2. This specimen was reinforced for one-way loading only (Table 3.9). Different reinforcement patterns were used for the coupling beams (Table 3.8).

This specimen was loaded in increments of 0.5 kip for the first ten loading steps. Afterwards, the test was controlled by 0.05 in. increments of the top storey deflection. Crack pattern of this specimen is shown in Fig. 4.20. Deflections of the four-storey levels are shown in Figs. 4.21 to 4.24.

Cracking was initially observed at a total applied load of 3 kips. The top storey deflection at this stage was 0.09 in. (Fig. 4.21) while the rotation at mid-span of the lower beams was around 0.0014 radian (Fig. 4.23). The relative rotations at a section distant $\frac{d}{2}$ (7.5 in.) from the base were 0.006 rad. and 0.009 rad. for wall 1 and wall 2 respectively (Figs. 4.23, 4.24).

Further loading to a total load value of 5.3 kips caused the specimen to reach the stage of complete yielding at all critical sections and the wall bases. At this stage, the top storey deflection was about 0.22 in. (Fig. 4.21) while the rotation at midspan of the lower beams was in the vicinity of 0.003 radian (Fig. 4.28). Relative rotation at section $\frac{d}{2}$ (7.5 in.) above the bases was 0.002 radian for both walls (Figs. 4.26, 4.27). Strain readings at this loading stage are detailed in Table 4.4.

As the applied load increased from zero to 5.3 kips, the slope of the load-deflection curve was observed to change twice - at total load values of 3 kips and 5 kips (Figs. 4.21 to 4.25).

After the load value of around 5 kips, the deflections increased more rapidly with further increase in load up to the ultimate load value of 6.02 kips. As for specimen no. 1, these changes in the elastic range indicated reductions of the overall stiffness of the specimen. This reduction of stiffness was caused by the onset of cracking at the beam-wall interfaces at a load value of around 3 kips. Further decrease in stiffness, as the applied load was increased from 3 kips to 5 kips, was due to the onset of yielding of the reinforcement in certain beams. The yielding of the wall reinforcement continued until a total load value of 5.3 kips (Fig. 4.21). Due to the delay of yielding of the tension reinforcement in wall 1, more cracks appeared in wall 2 base in this specimen than in specimen no. 1.

Cracks initiated at the shear wall-beam interfaces at a total load value just less than 5 kips. Additional diagonal shear cracks were also observed along the length of the beams at an inclination of around 30° with the vertical. These cracks continued to propagate and widen until the crushing of the concrete on the opposite face (Figs. 4.20, 4.33).

The measured rotations at midspan of the three lower beams were very close (Fig. 4.32). At ultimate load, the rotation of midspan of beam 4 was 0.018 radian compared to 0.024 radian for both beams 2 and 3 and 0.026 radian for beam 1.

In examining the rotational behaviour of the midspan sections of the connecting beams at failure (load value = 5.2 kips) with the corresponding top storey deflection of 2.9 in., the midspan rotation in beams 2 and 3 was 0.07 radian, while similar values for beam 1 and beam 4 were 0.06 radian and 0.05 radian respectively. It shows that the location of the section where the maximum rotation occurs, has shifted from storey 1 (roughly 25% of total height) at yielding of steel reinforcement (Fig. 4.32) to a location between beam 2 and beam 3 (roughly 50% of total height) at failure.

A crack formed in the lower corner of beam 4 – wall 2 interface propagated into wall 2 and reached the reinforcement on the upper edge of the beam at a load value about 5 kips (Fig. 4.35). The width of this crack was roughly ½ in. at ultimate load and approximately ¾ in. at failure. This crack propagated further along the beam reinforcement to cause bond failure to the top level beam.

Cracks appeared almost instantaneously in both the diagonal and parallel reinforced beams. However, the cracks in beams with diagonal reinforcement were not as wide and there was much less crushing of the concrete. This shows the superiority of the diagonal reinforcement over the conventional parallel reinforcement. Paulay has made a similar deduction from his experimental work[13]. The stress pattern and load transmission between the walls had been illustrated in the photoelastic study of Chapter II. Diagonal reinforcement is ideal for this pattern of transferring forces.

Diagonal tension cracks appeared in the first storey of the tension wall (wall 2) at a total load value of approximately 5 kips (Fig. 5.20). Flexural cracks appeared at the inside edge of wall 1 at a total load value of 5.5 kips (Fig. 4.20). Cracks were also observed in second storey of wall 2 at a load value near 5.5 kips (Fig. 4.20). However, these cracks did not open wide as the cracks in the first storey.

Crushing of the concrete on the outside edge of wall 1 and at the wall-beam junction occurred at a load value of approximately 6 kips. The concrete on the inside edge of wall 2 also crushed after another two loading steps.

The concrete strains in wall 1 and the steel strain in wall 2 at a load value of 5.3 kips were approximately 1100×10^{-6} in/in. and 1300×10^{-6} in/in., respectively. At this stage, the concrete and steel strains in the lowest beam were 1840×10^{-6} in/in. and 1880×10^{-6} in/in. respectively. Other strain values are detailed in Table 4.4.

As the applied load was increased from 5.3 kips to 6.7 kips, the top storey deflection increased almost linearly to about 1.44 in. (Fig. 4.21). The load-deflection behaviour at other storey levels was also almost linear in this range. At this loading stage, the maximum rotation at the midspan section of the lower beams was approximately 0.025 radian, and the relative rotation at a section distant $\frac{d}{2}$ from the wall base was about 0.022 radian (Figs. 4.26, 4.27).

Further loading beyond the maximum load caused the load to drop off slowly. At the maximum load of 6.02 kips, the ductility factor, which is the ratio of the deflection at ultimate load to that at yielding of steel reinforcement, was about 6.9. At failure, this ratio was approximately 14.3.

Failure of the lower beams was due to shear-flexure mode at the beam-wall interfaces. Failure of wall 1 was due to a flexural mode leading to rupture of the tension reinforcement. At this stage, the top storey deflection was approximately 2.9 in. Failure of wall 2 can also be categorized as the shear-flexure mode. Rupture of reinforcement in beams 2 and 3 occurred three loading steps after the rupture of wall 1 reinforcement. At this failure state, the top storey deflection exceeded 3 in.

TABLE 4.4 Strain Gauges' Reading Values for Specimen No. 2 at Yield Load of 5.3 kips (in Microstrain = $10^{-6}\mu$)

	Concrete strain Compression end	Steel strain Compression end	Steel strain Tension end
Wall 1	1096	-	-
Wall 2	155	-	1329
Beam 1 (Wall 1 face)	159	-	627
Beam 1 (Wall 2 face)	1839	435	1884
Beam 2 (Wall 1 face)	1218	225	1607
Beam 2 (Wall 2 face)	141	-	1448
Beam 3 (Wall 1 face)	162	-	-
Beam 3 (Wall 2 face)	132	451	268
Beam 4 (Wall 1 face)	1073	29	510
Beam 4 (Wall 2 face)	1453	339	1134

FIG. 4.20 : SPECIMEN NO. 2 CRACK PATTERN

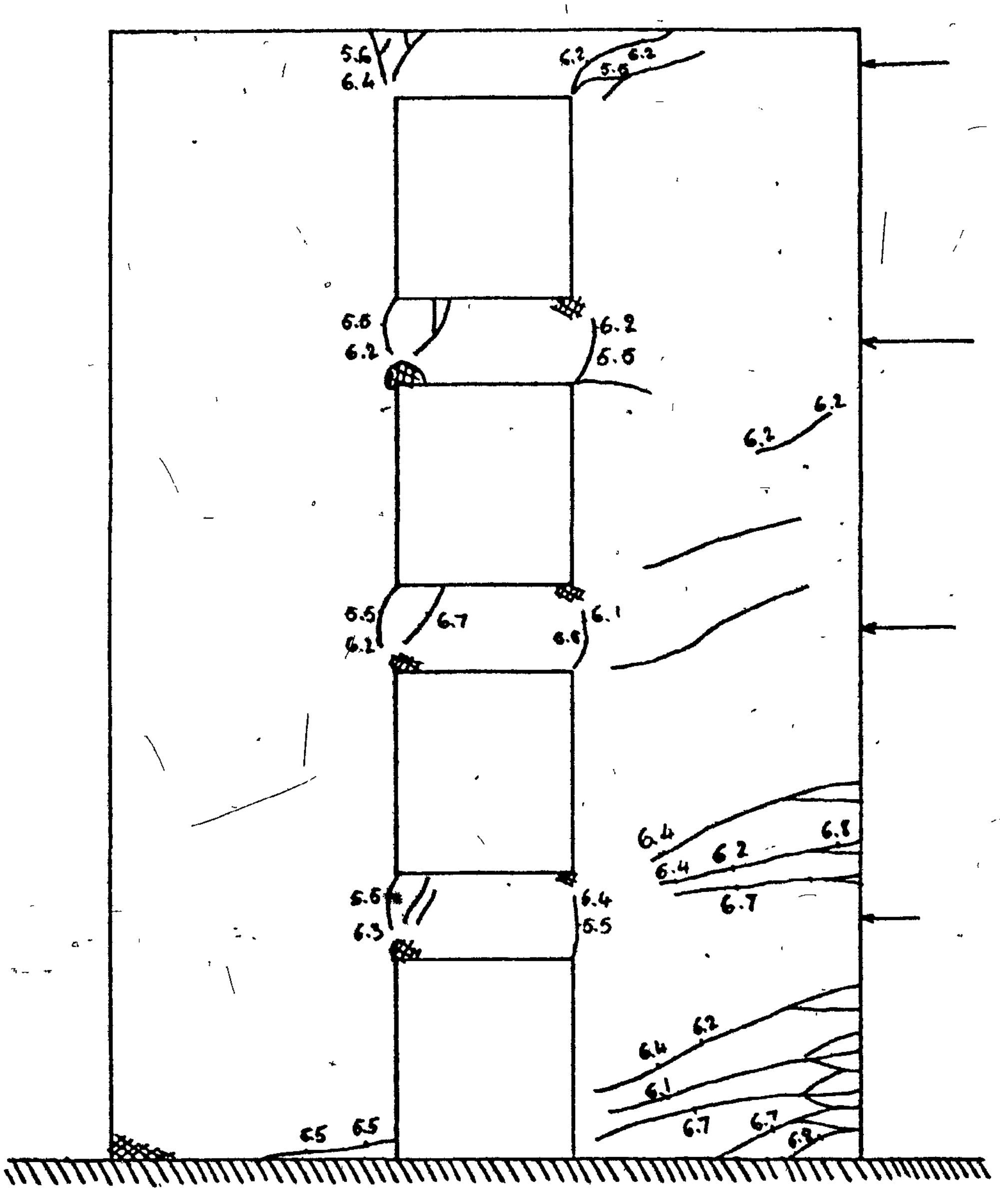

FIG. 4.21:

TOP STOREY DEFLECTION - SPECIMEN NO. 2

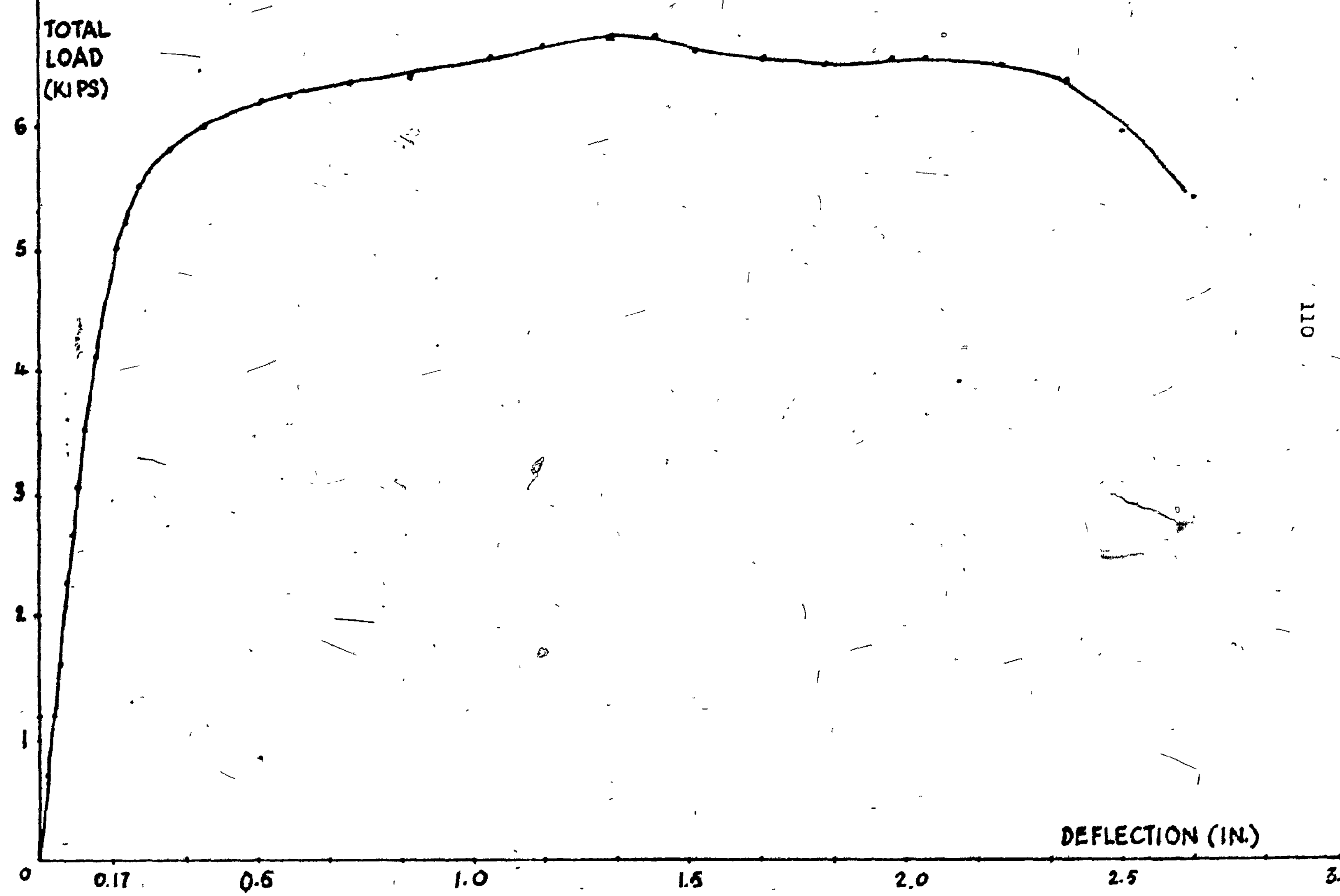

FIG. 4.22: THIRD STOREY DEFLECTION - SPECIMEN NO. 2

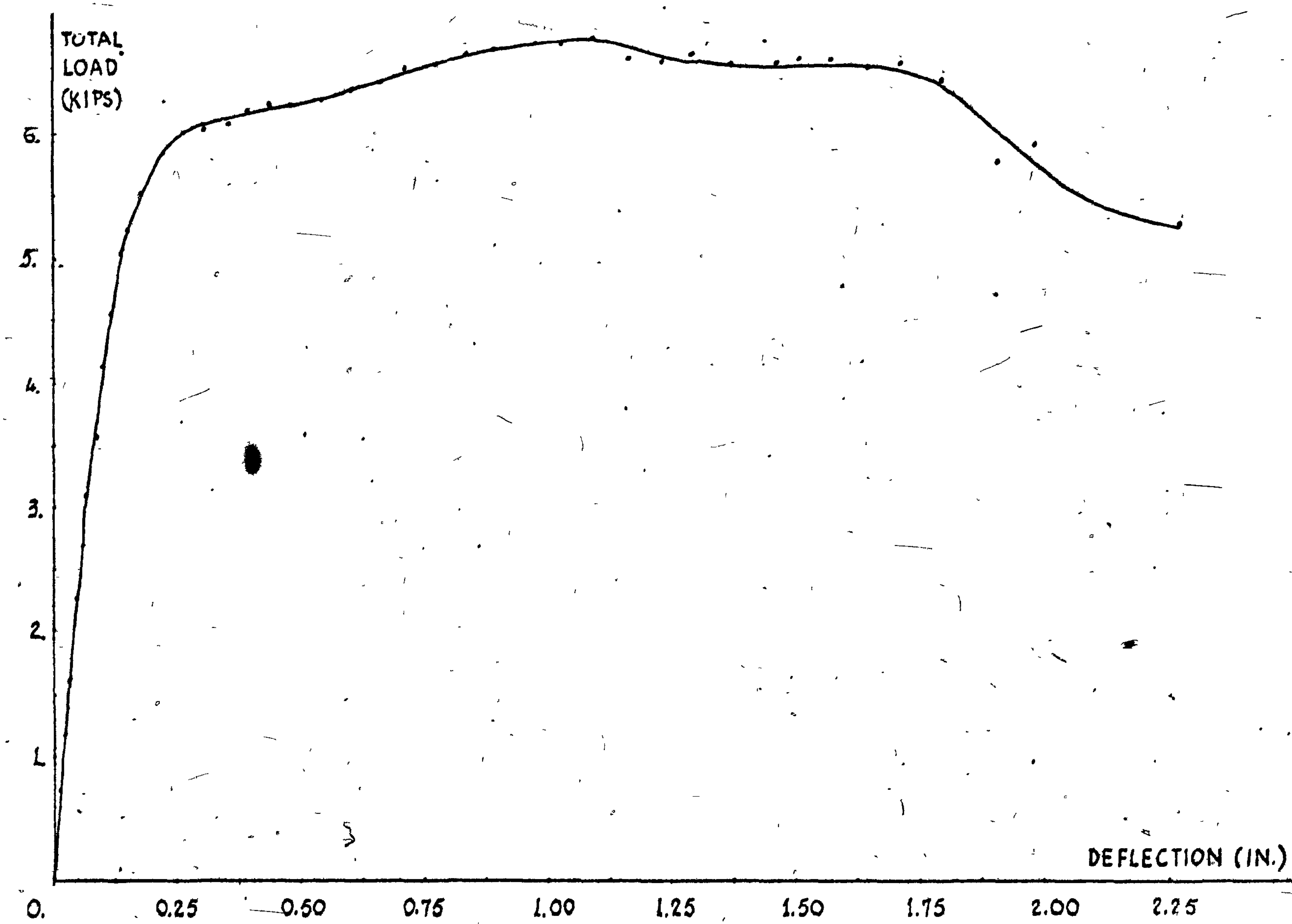

FIG. 4.23 : SECOND STOREY DEFLECTION - SPECIMEN NO. 2

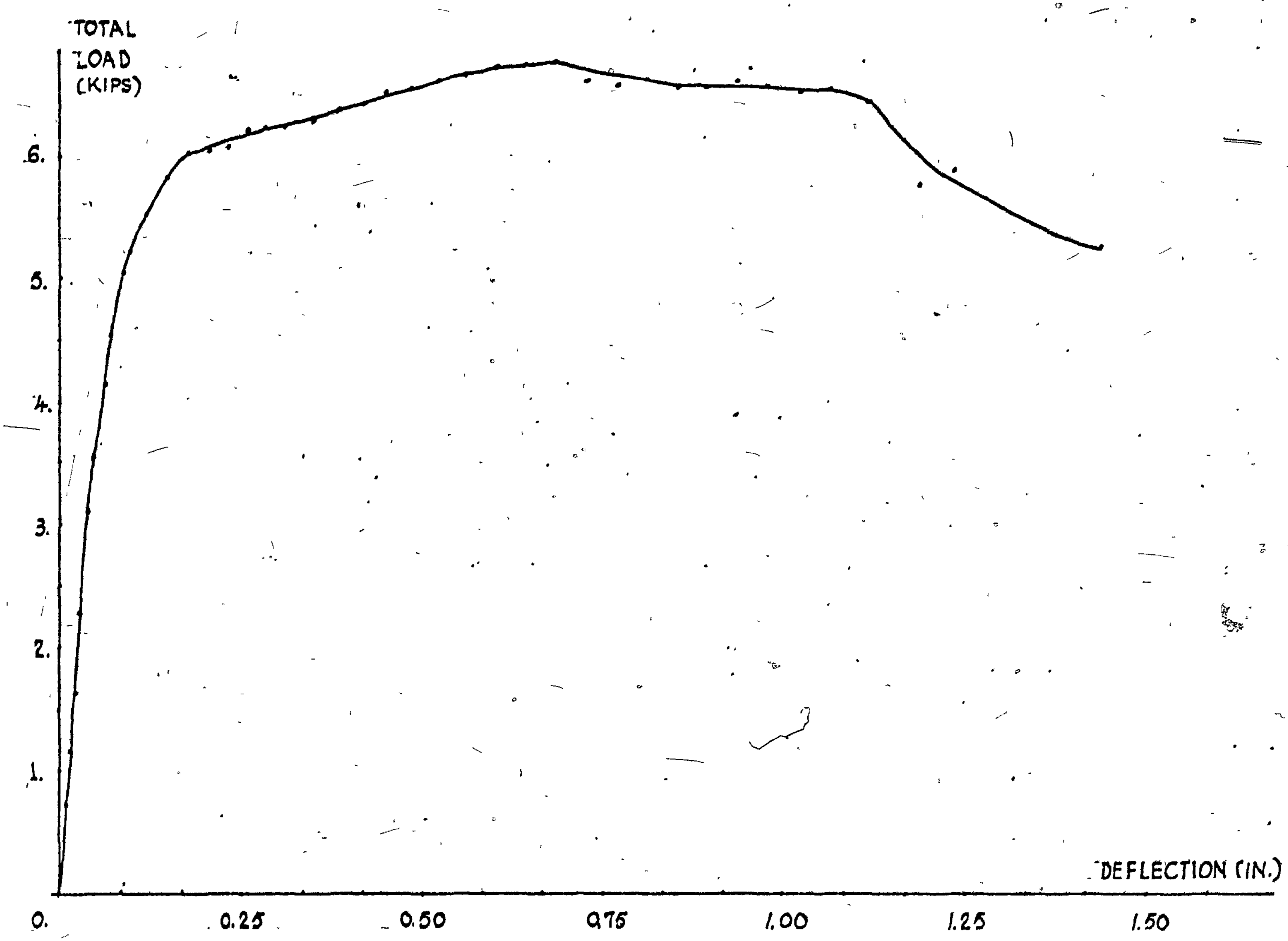

FIG. 4.24: FIRST STOREY DEFLECTION - SPECIMEN NO. 2

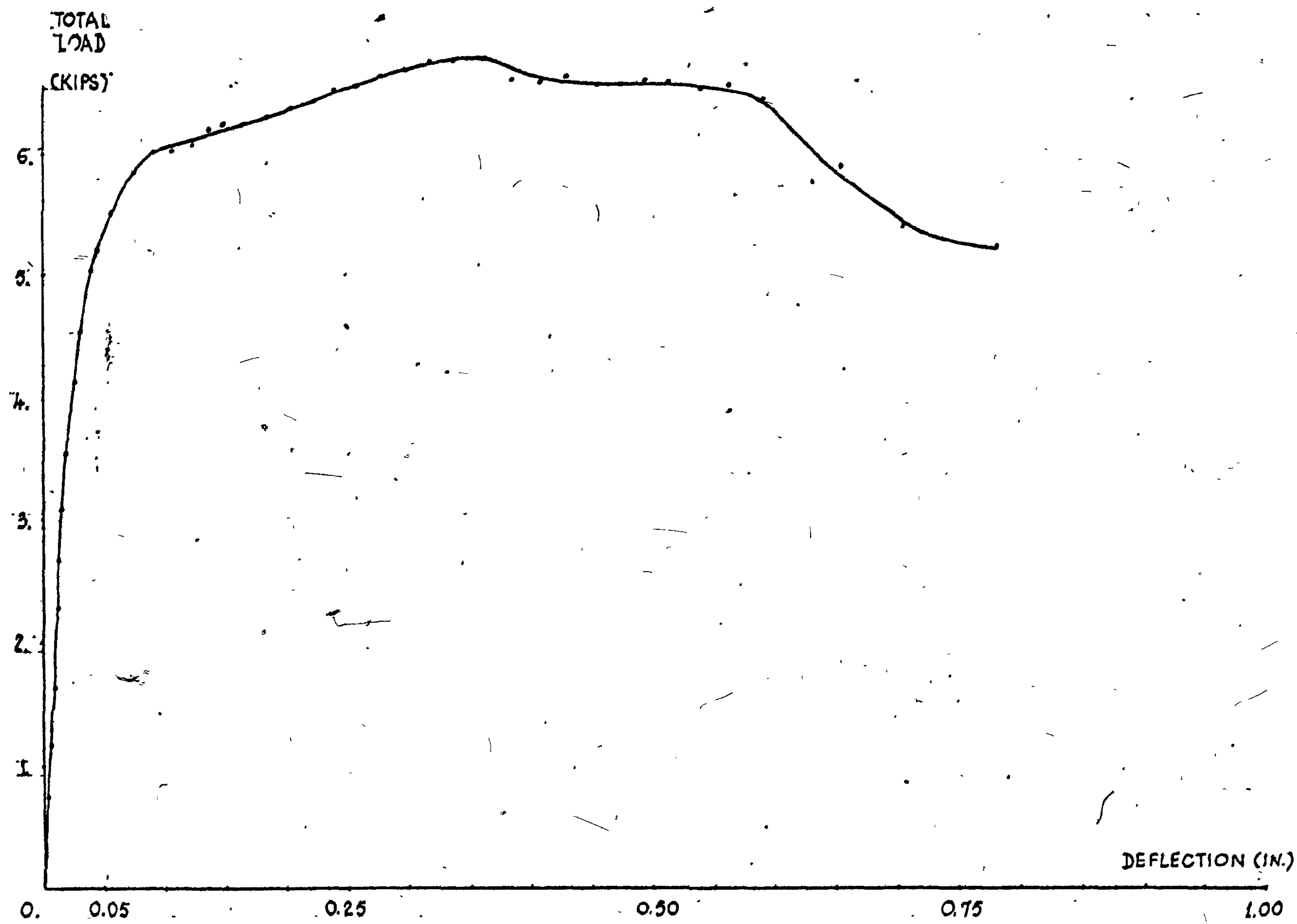

FIG. 4.25 : DEFLECTION OF FOUR STOREY LEVELS - SPECIMEN NO. 2

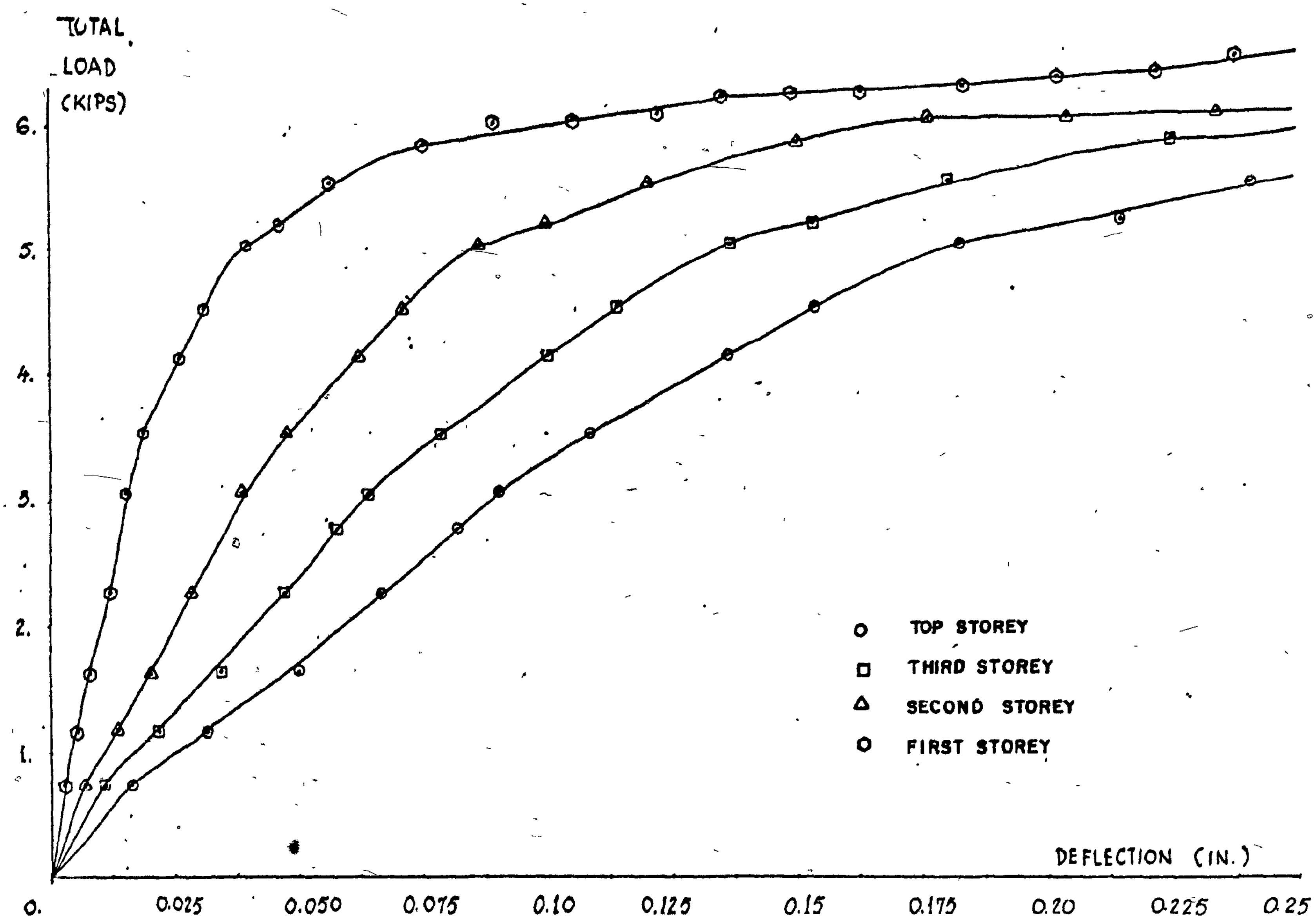

FIG. 4.26: WALL I ROTATION - SPECIMEN NO. 2

- SECTION D/2 ABOVE BASE -

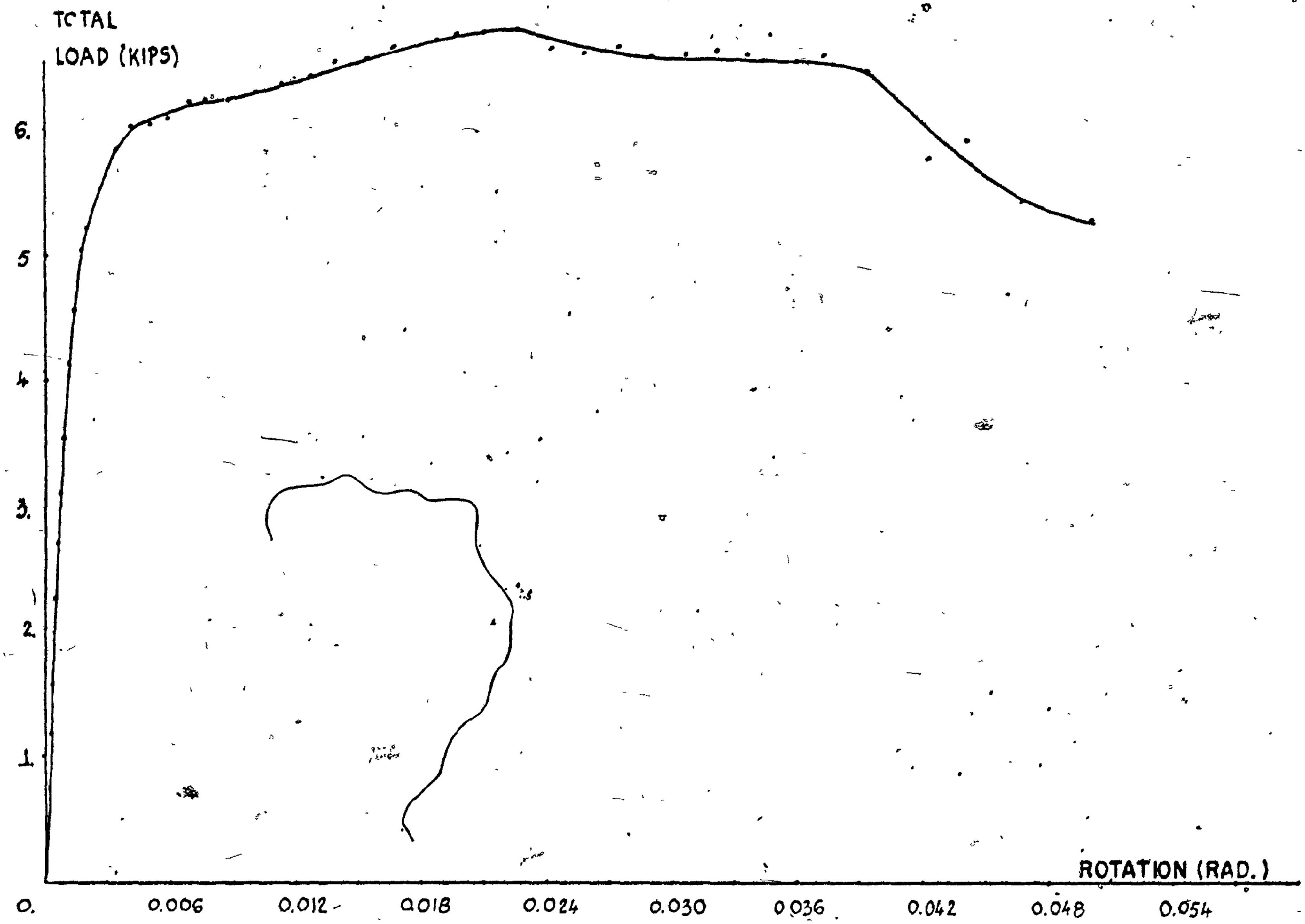

FIG. 4.27 WALL 2 ROTATION - SPECIMEN NO. 2

- SECTION D/2 ABOVE BASE -

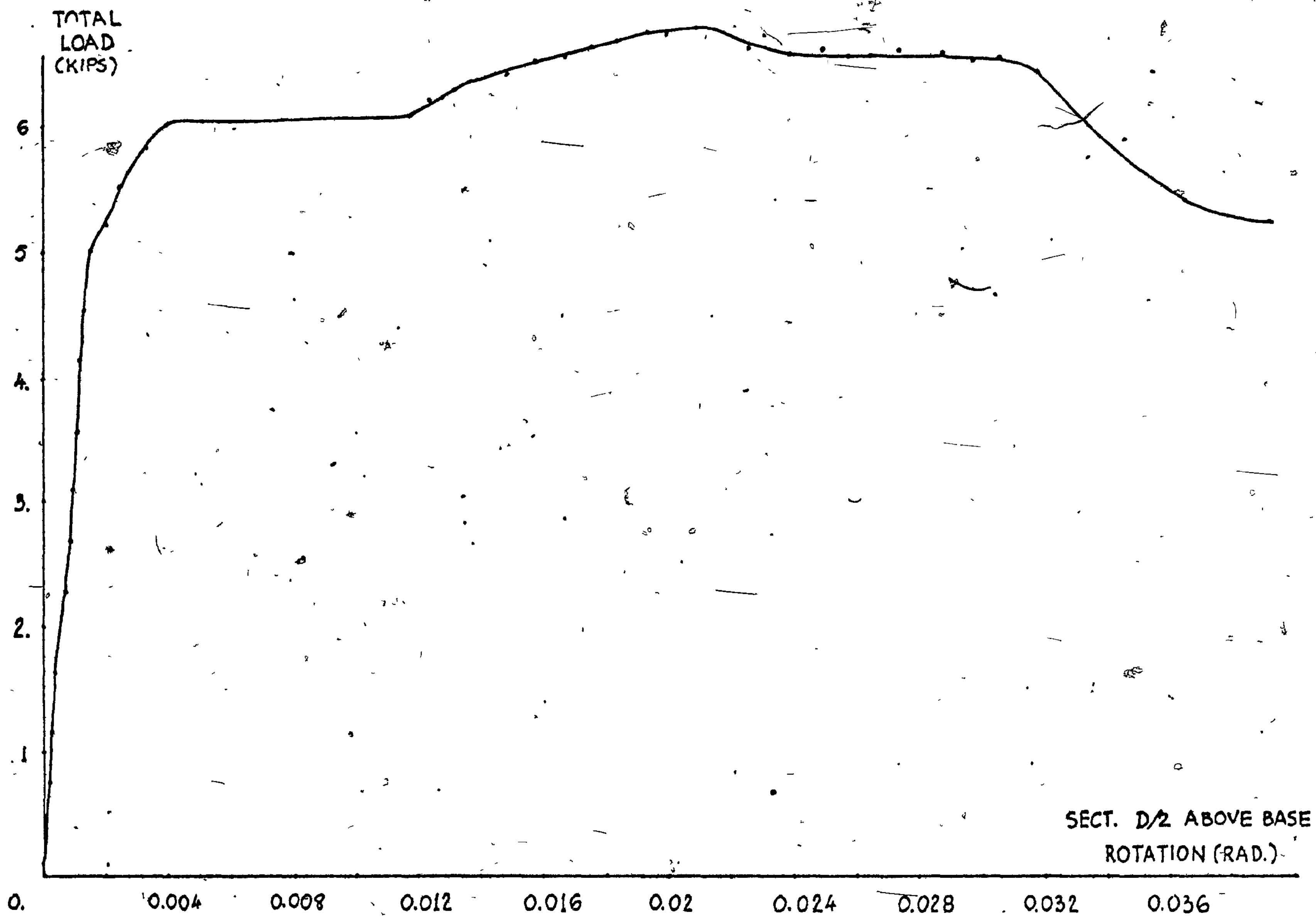

FIG. 4.28: BEAM I ROTATION - SPECIMEN NO. 2

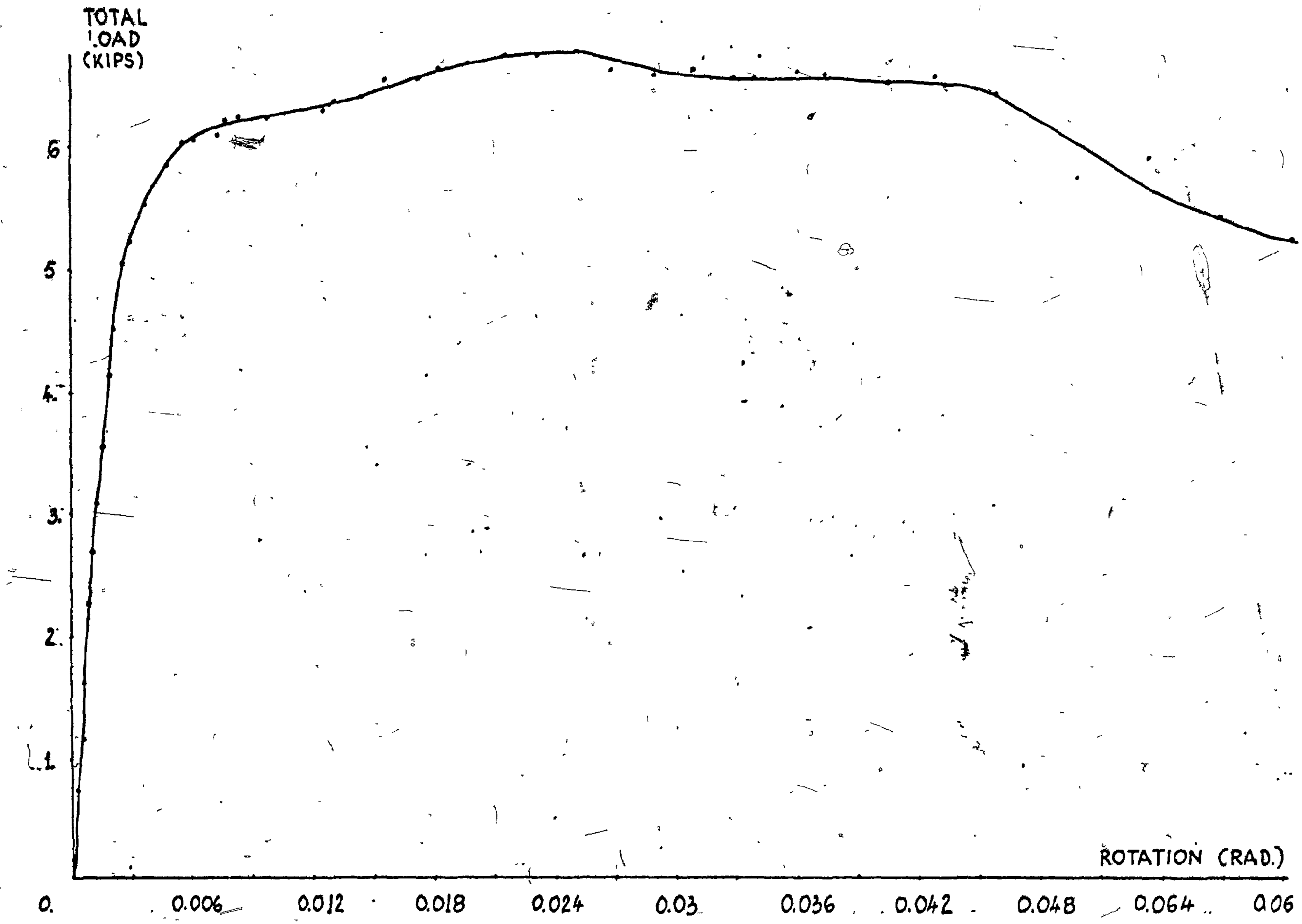

FIG. 4.29: BEAM 2 ROTATION - SPECIMEN NO. 2

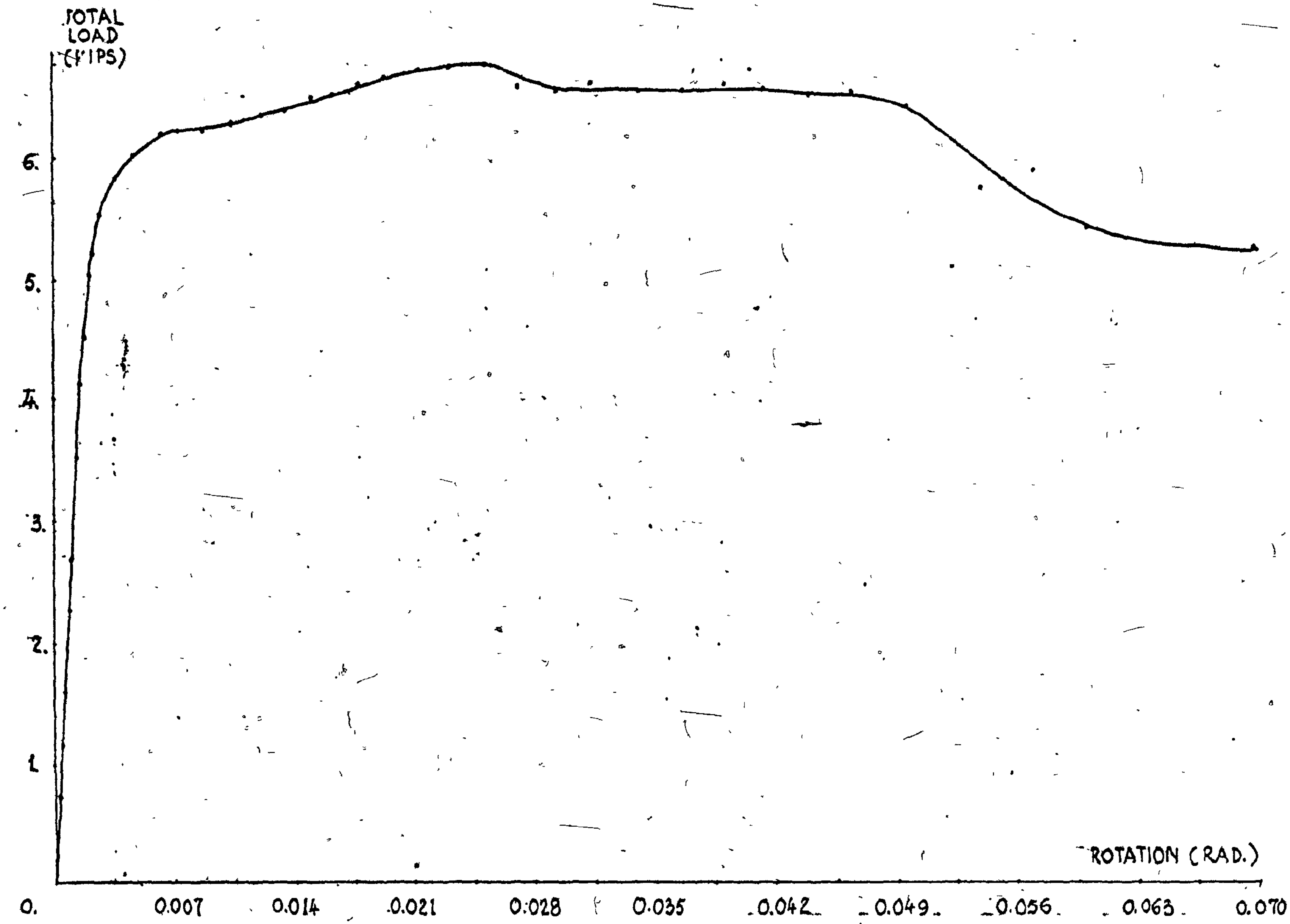

FIG. 4.30 : BEAM 3 ROTATION - SPECIMEN NO. 2

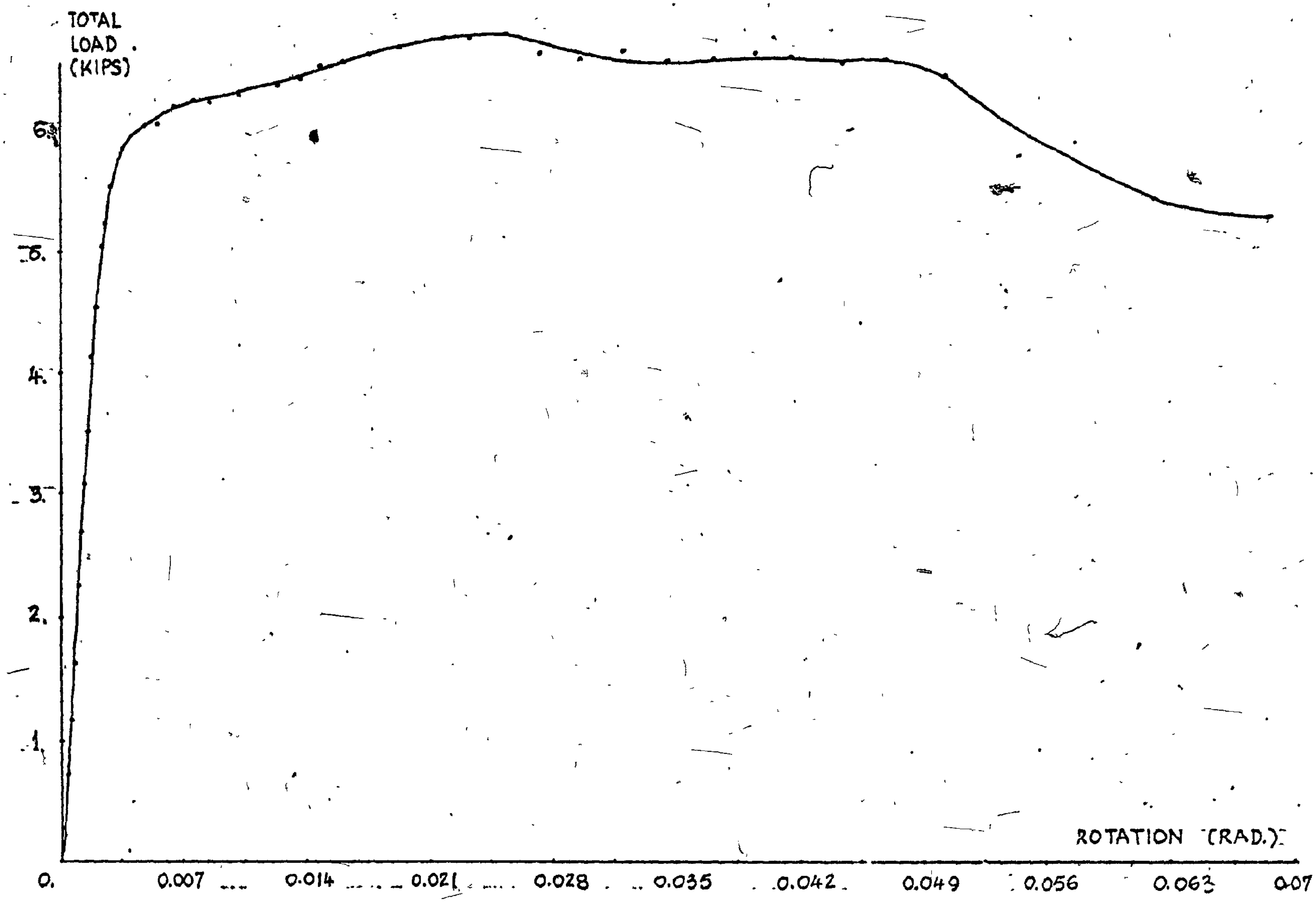

FIG. 4.31 : BEAM 4 ROTATION - SPECIMEN NO. 2

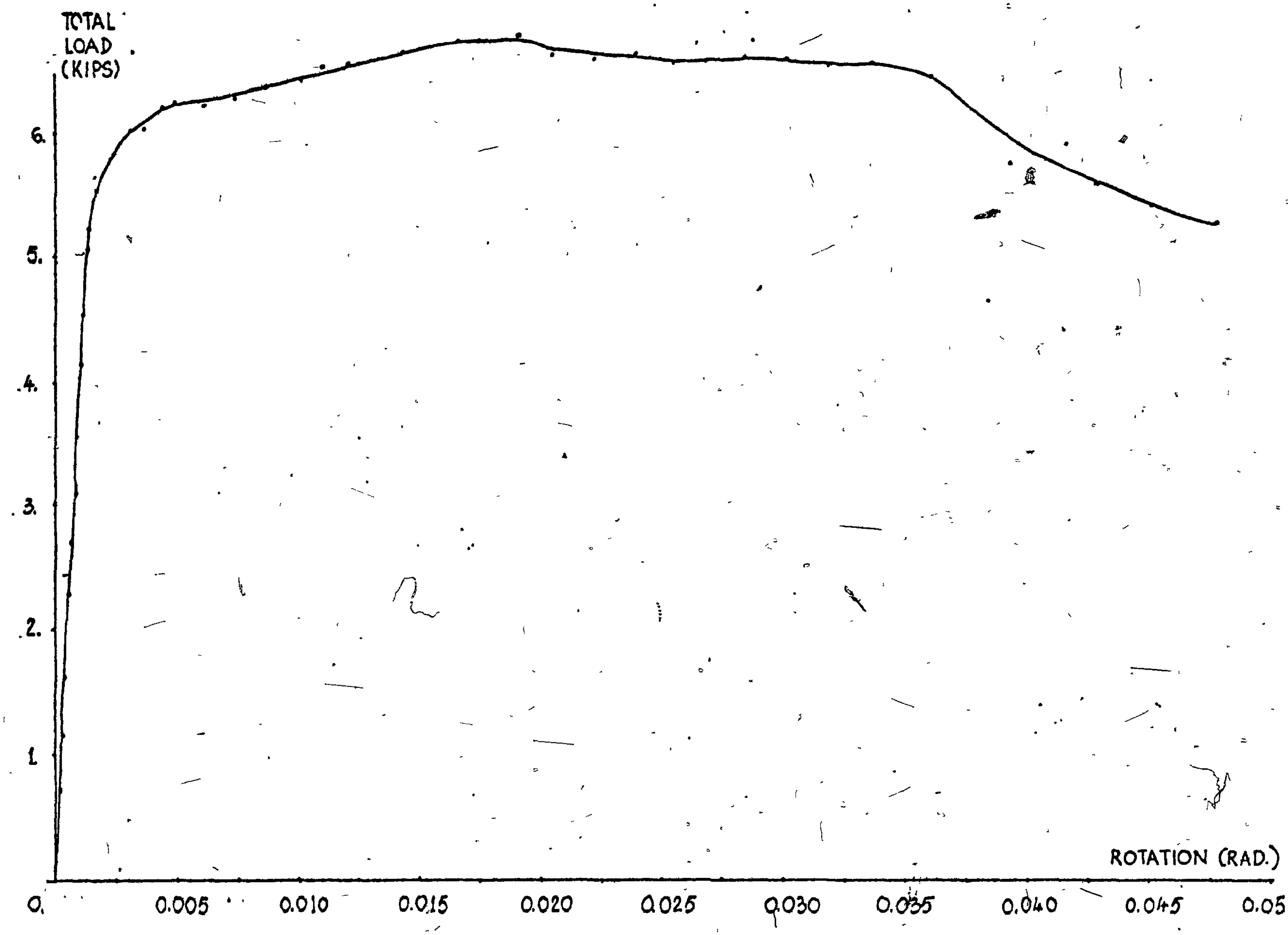

FIG. 4.32: ROTATION OF FOUR BEAMS - SPECIMEN NO. 2

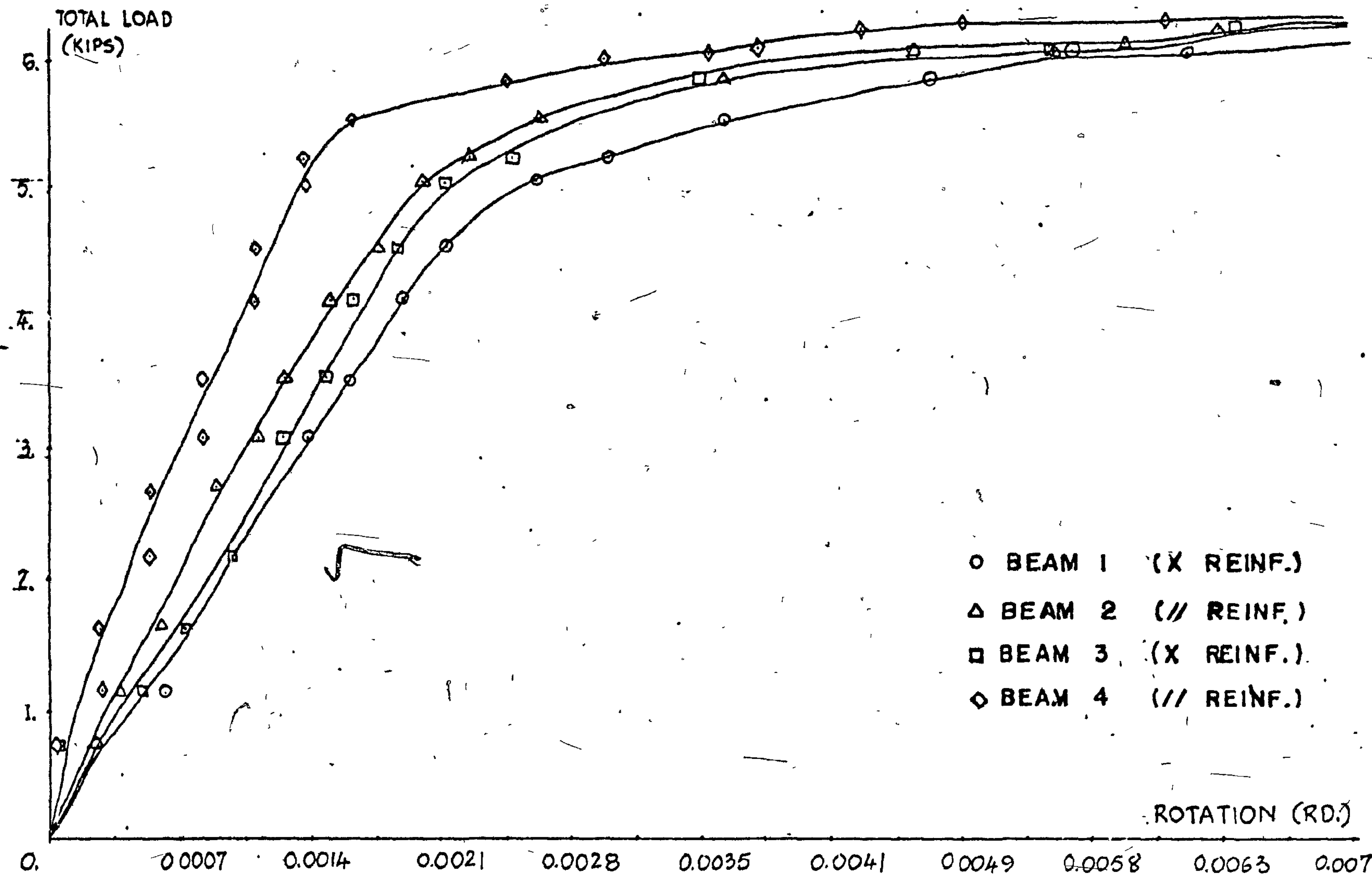

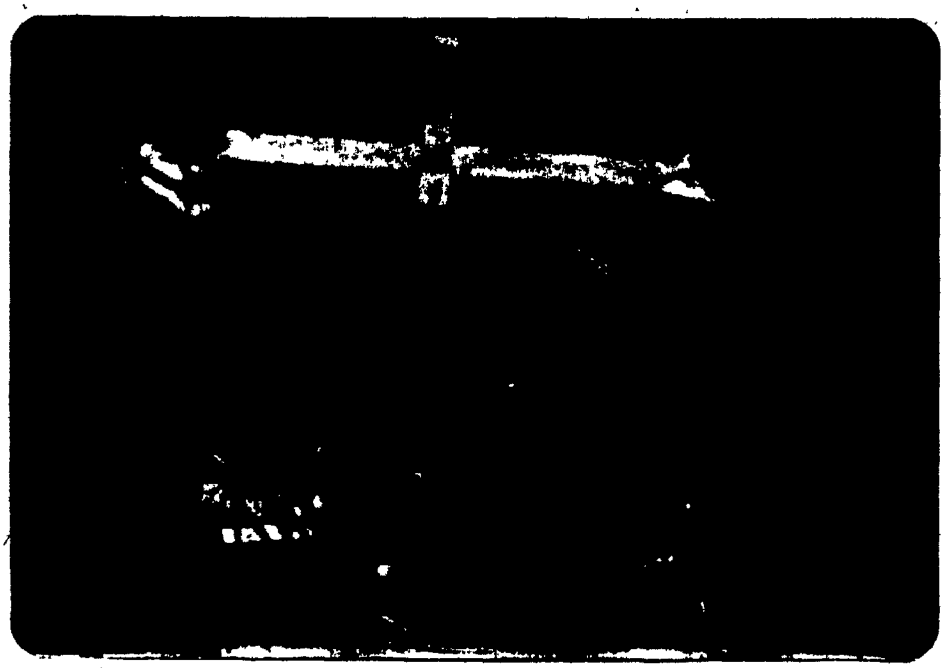

Fig. 4.33 Failure of lower beams, Specimen No. 2

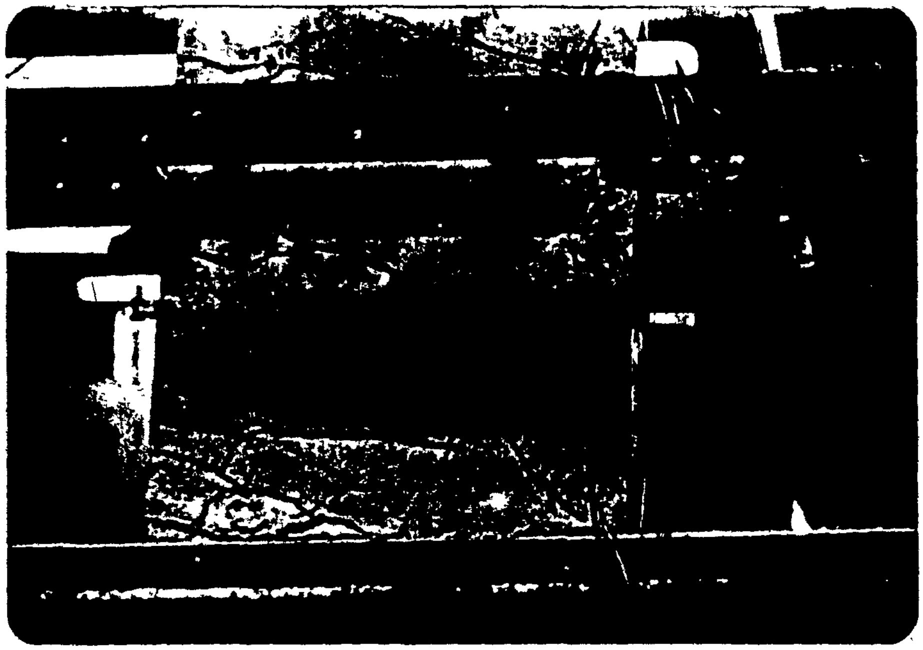

Fig. 4.34 Cracks in Wall 2 base, Specimen 2

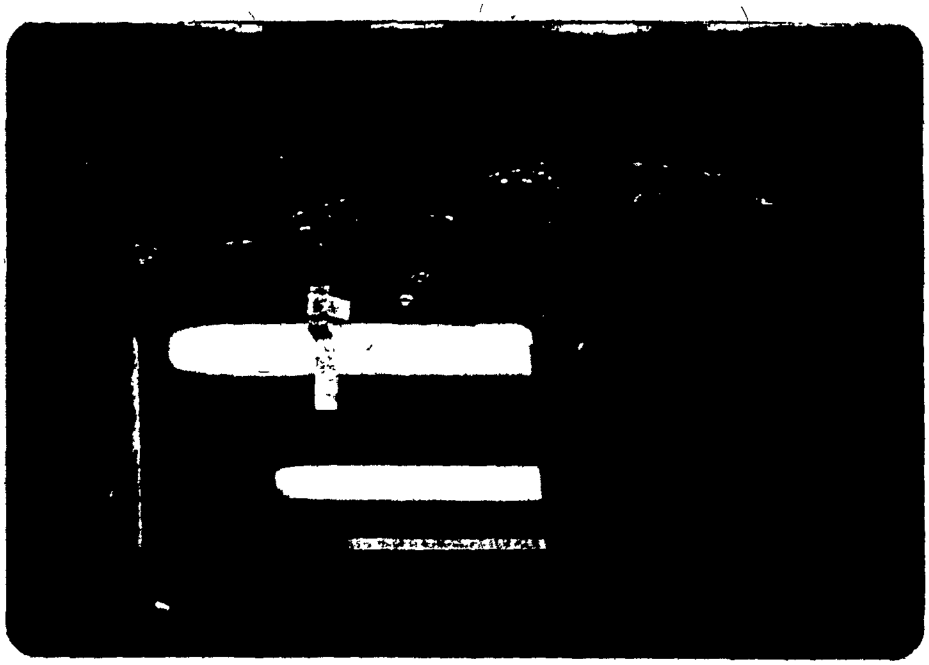

Fig. 4.35 Failure of top beam, Specimen 2

4.4 Behaviour of Test Specimen No. 3

Reinforcement pattern and instrumentation details of specimen no. 3 were described in section 3.2, and Tables 3.8 and 3.9. The span-depth ratio (s/t) of the coupling beams was one and the length of the coupling beams to the wall width (s/2e) ratio was 0.44 as described in Chapter III. Dimensions of the openings of this specimen were different from those of specimens nos. 1 and 2, and were described in Chapter III. The specimen was loaded in increments of 1 kip for the first five loading steps. Beyond this stage, the test was controlled by a top storey deflection increment of 0.05 in. Crack pattern of this specimen after loading is shown in Fig. 4.36.

The specimen behaved linearly up to a total load value of about 6.1 kips (Fig. 4.37). The behaviour of the other storeys was also almost linear in this range (Fig. 4.38). The corresponding top storey deflection at this stage was 0.30 in. Deformations of sections 5.75 in. from the wall base are presented in Figs. 4.39 and 4.40. Rotations of midspan sections of the four beams are also presented in Fig. 4.41.

The concrete and the steel strain (tension face of wall 2) values were 586×10^{-6} in/in. and 1760×10^{-6} in/in. respectively. At this stage, the concrete and the steel strains on the lowest beam were 955×10^{-6} and 1072×10^{-6} in/in. respectively. Other strain values are detailed in Table 4.5.

Diagonal tension cracks occurred in wall 2 at a total load value of 3.9 kips (Figs. 4.42, 4.43). Cracks also appeared as diagonal shear cracks in the second storey of wall 2 and as flexural cracks in the first storey of wall 1 at a total load value of approximately 5 kips (Fig. 4.42).

Although some very narrow diagonal cracks occurred at the corners of the lowest openings and in the middle of beam 1 in the elastic range of loading, these did not propagate. This cracking pattern was similar to the diagonal cracking pattern normally obtained in deep beams and in shear wall structures. Similar crack patterns were observed by Paulay in his tests[13].

As the applied load was increased beyond the yield load of 5.3 kips, the load-deflection curve leveled off (Figs. 4.37, 4.38). As the top storey deflection increased to roughly 0.6 in., the load increased very slowly and almost linearly up to a value of roughly 6.7 kips (Fig. 4.37).

Near maximum load, the rotation at a section at a height of 5.75 in. above the base of wall 1 was observed to be 0.008 radian (Fig. 4.39). As the cracks in wall 2 widened, axial deformation due to the net wall tension force at a section distant 5.75 in. from the base is shown on Fig. 4.40. At maximum load, beam 1 showed the largest rotational deformation of about 0.0011 radian at midspan (Fig. 4.41).

Further loading beyond the ultimate load of around 6.7 kips resulted in the widening of the cracks in wall 2. After a few loading increments, the cracks propagated through the depth of the wall. The vertical reinforcement of wall 1 ruptured at a load value of about 6.5 kips. The top storey deflection at this stage was 1.6 in.

The two vertical reinforcing wires next to the steel wire at the inside edge of wall 2 ruptured two loading increments after the rupture of the steel wire at the inside edge. However, this did not cause a collapse of the whole structure; they greatly reduced the stiffness and the lateral strength of the structure (Fig. 4.37). Ductility factors of approximately 2.1 and 5.7 were obtained from the ratios of the ultimate deflection and failure deflection to that of yield, respectively.

This specimen was considered to have failed when the diagonal tension cracks had propagated through the depth of the wall and the reinforcement ruptured. This tension failure of wall 1 occurred at a top storey deflection of approximately 2 in.

TABLE 4.5 Strain Gauges' Reading Values for Specimen No. 3 at Yield Load of 6 kips

	Concrete strain Compression end	Steel strain Compression end	Steel strain Tension end
Wall 1	586	549	1760
Wall 2	-	-	-
Beam 1 (Wall 1 face)	955	987	1072
Beam 1 (Wall 2 face)	295	610	555
Beam 2 (Wall 1 face)	518	623	-
Beam 2 (Wall 2 face)	98	268	393
Beam 3 (Wall 1 face)	109	-	-
Beam 3 (Wall 2 face)	114	215	-
Beam 4 (Wall 1 face)	69	62	-
Beam 4 (Wall 2 face)	56	-	-

FIG. 4.36: SPECIMEN NO. 3 CRACK PATTERN

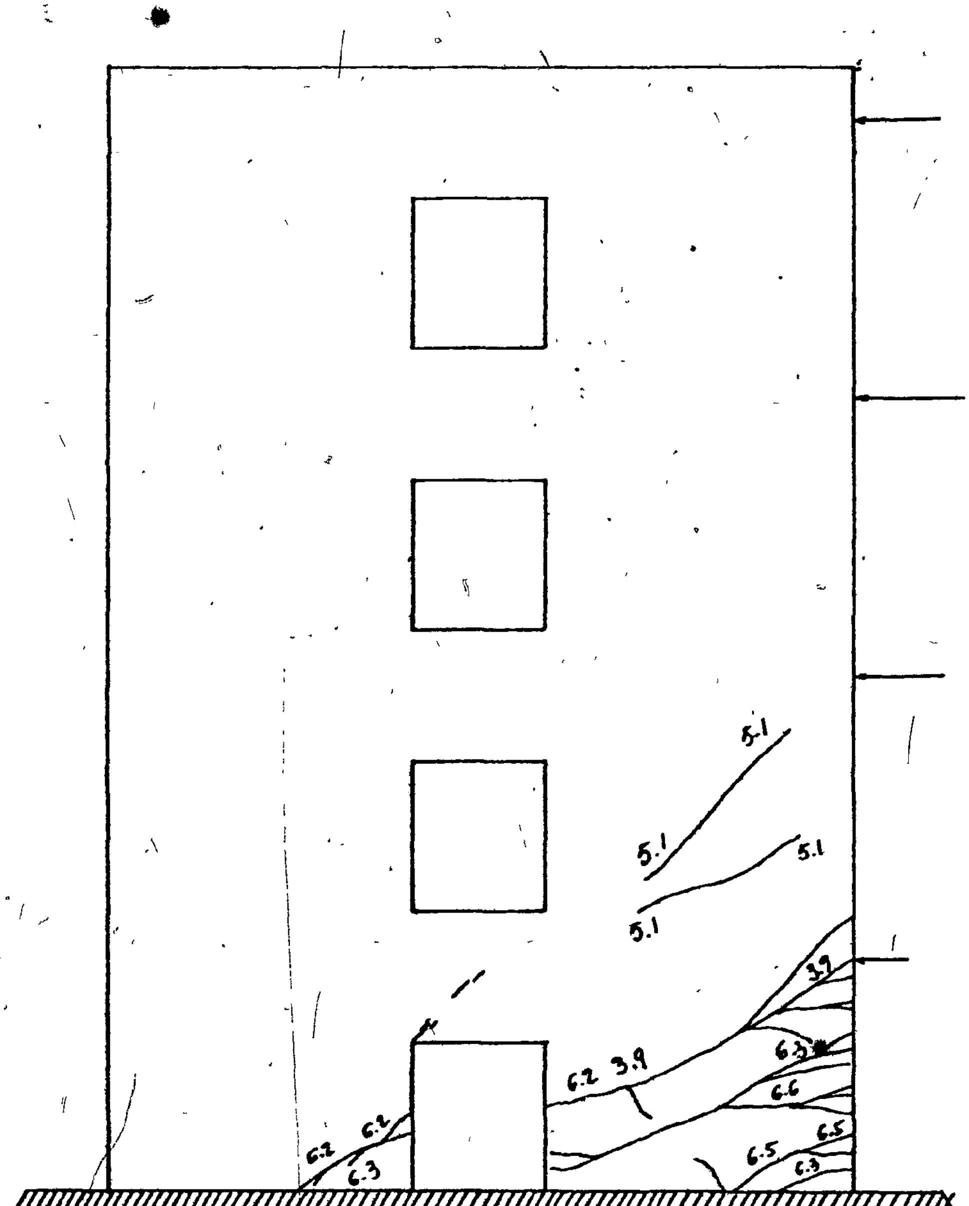

FIG. 4.37: TOP STOREY DEFLECTION - SPECIMEN NO. 3

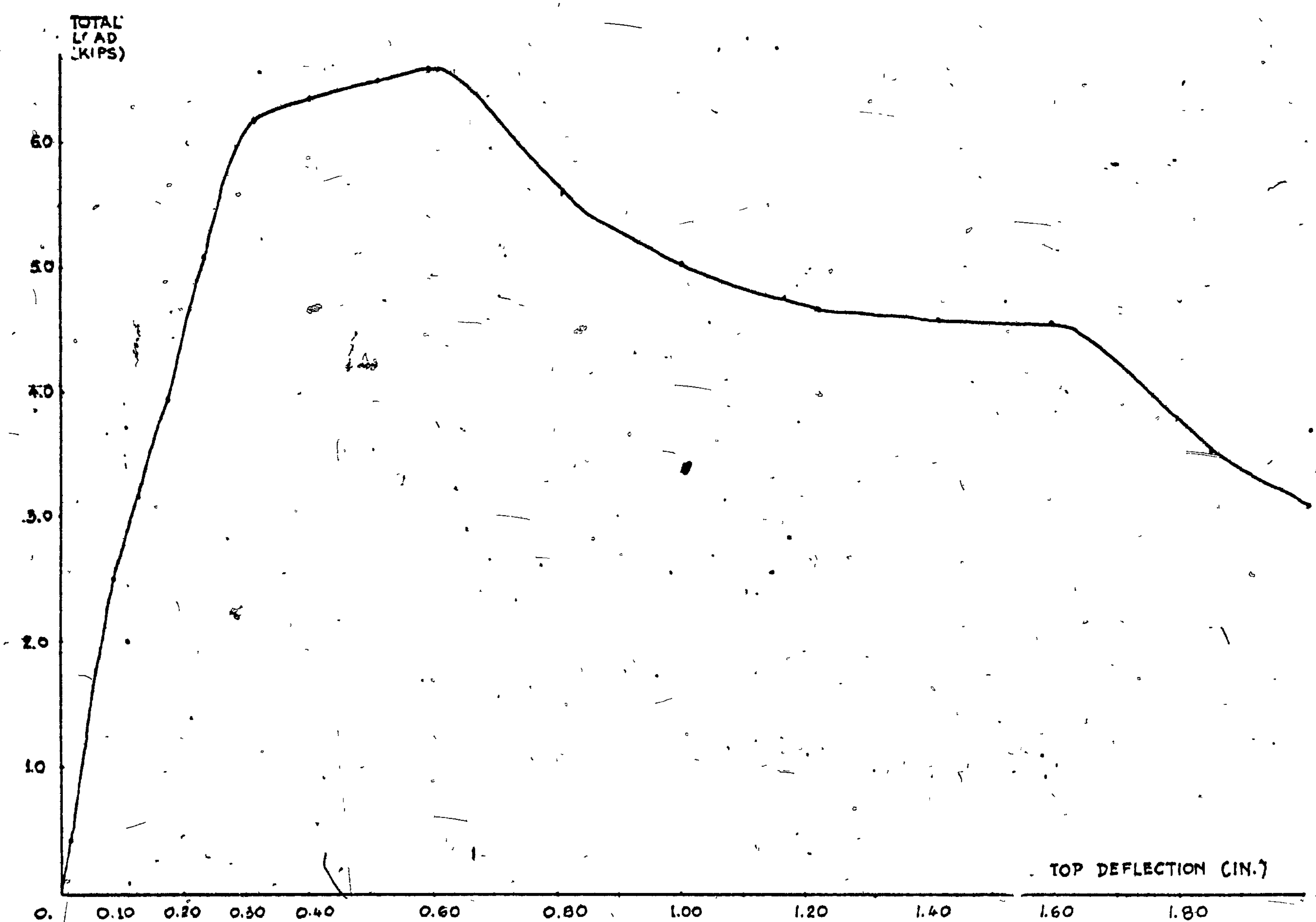

FIG. 4.38: DEFLECTION OF FOUR STOREY LEVELS - SPECIMEN NO. 3

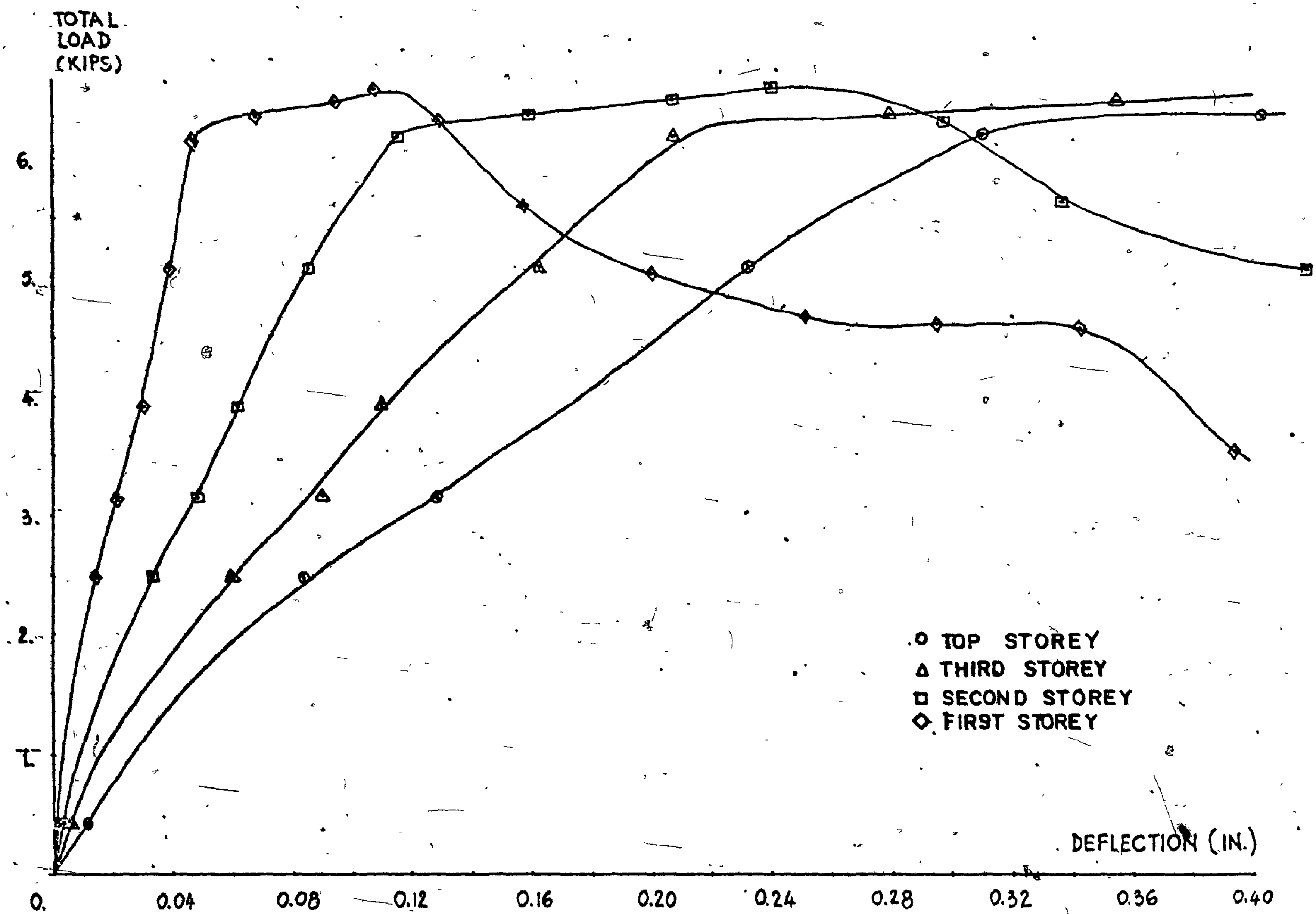

FIG. 4.39 : WALL I ROTATION - SPECIMEN NO. 3

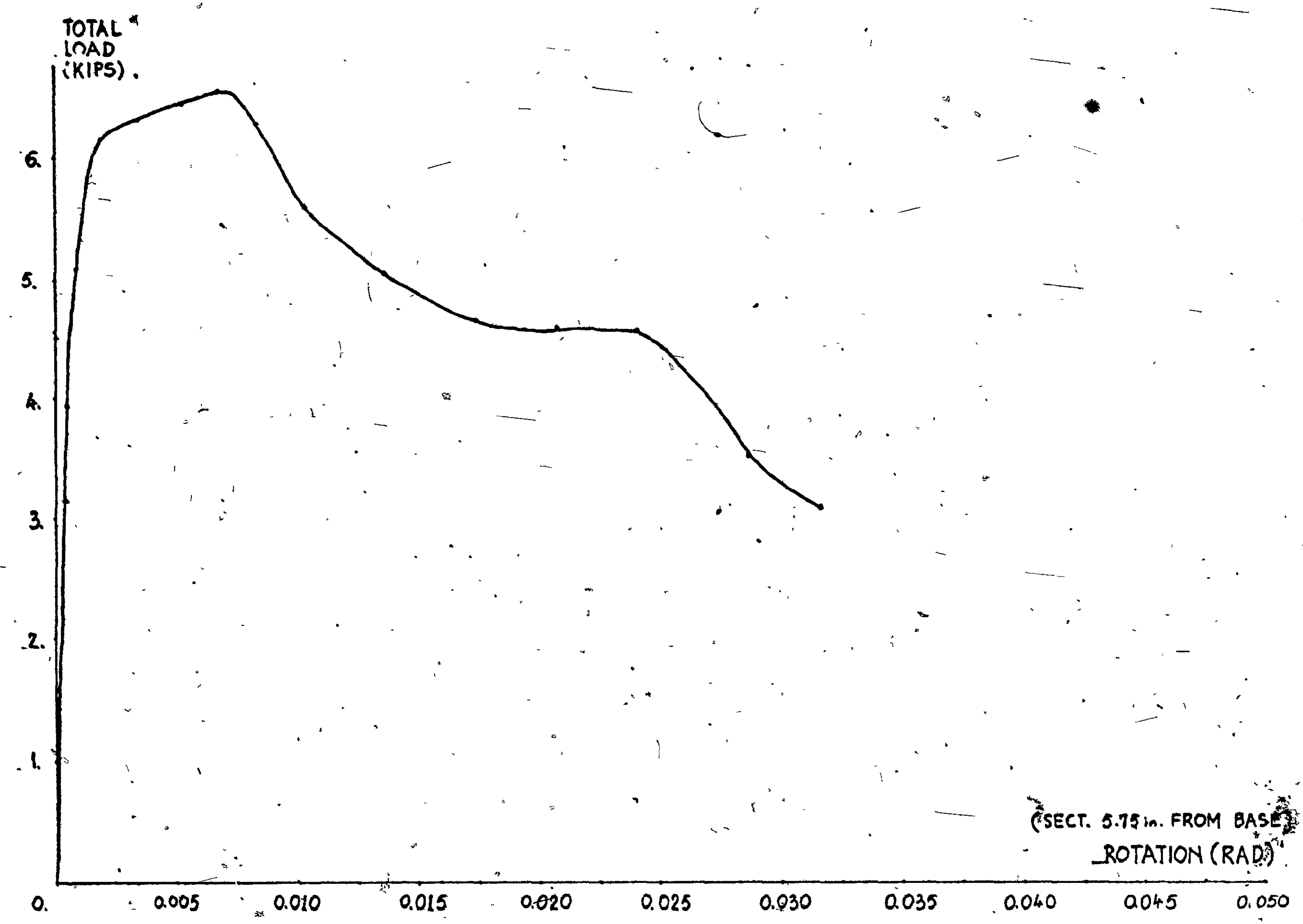

FIG. 4.40: WALL 2 DEFORMATION - SPECIMEN NO 3

(section distant 5.75 in. from base)

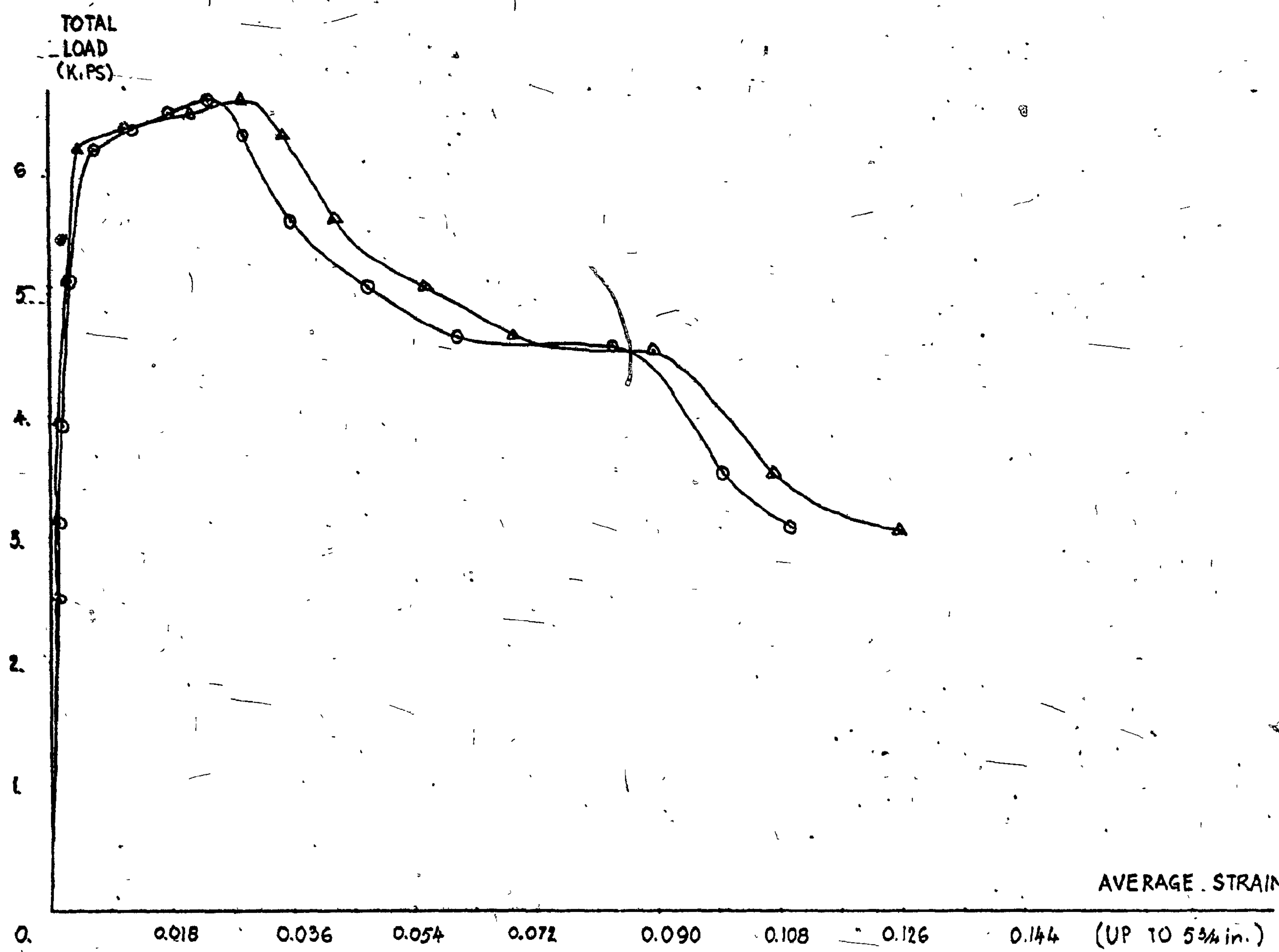

FIG. 4.41. ROTATION OF FOUR BEAMS - SPECIMEN NO. 3

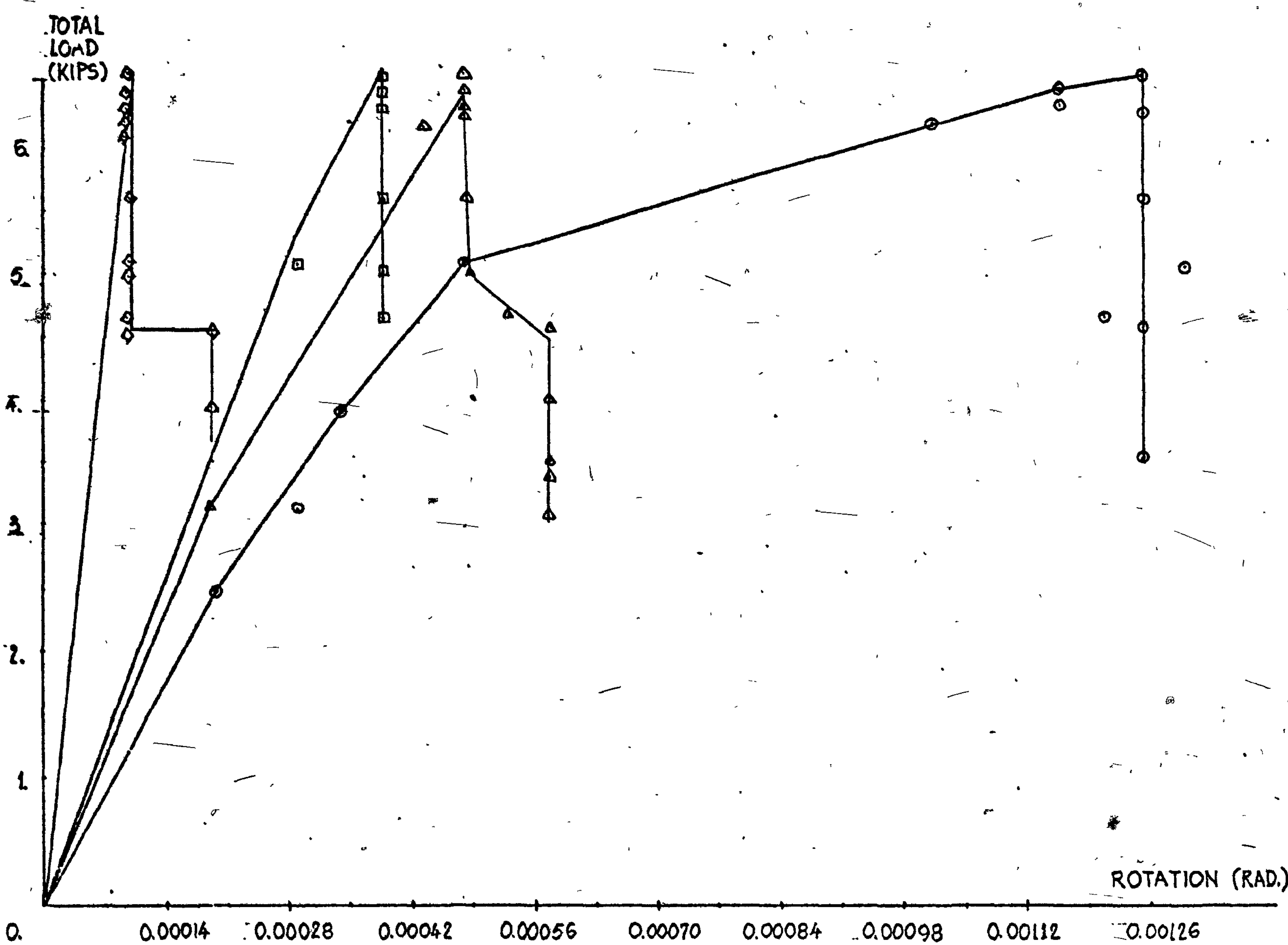

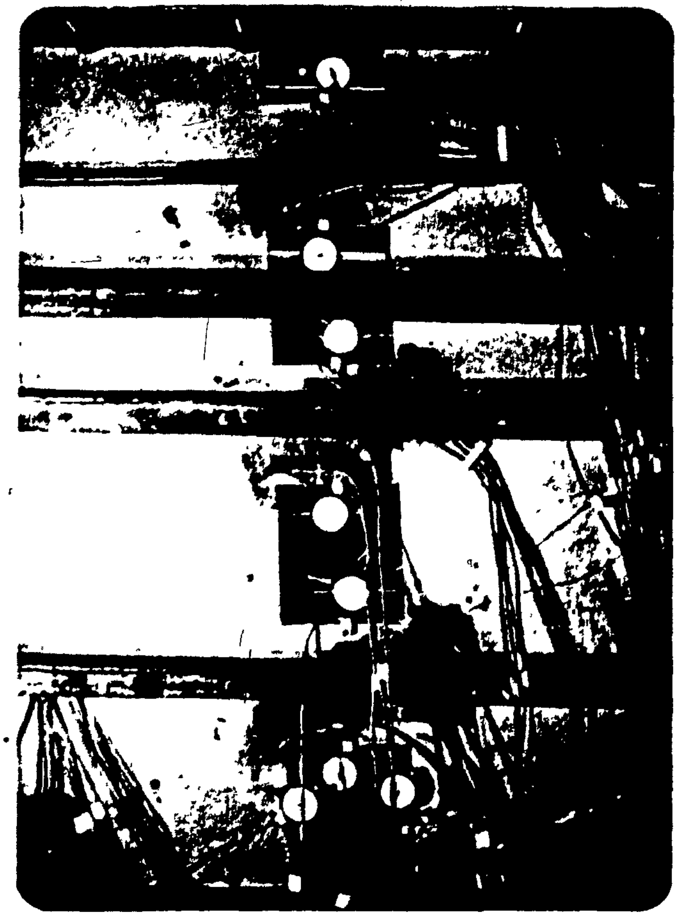

Fig. 4.42 Specimen No. 3 at failure

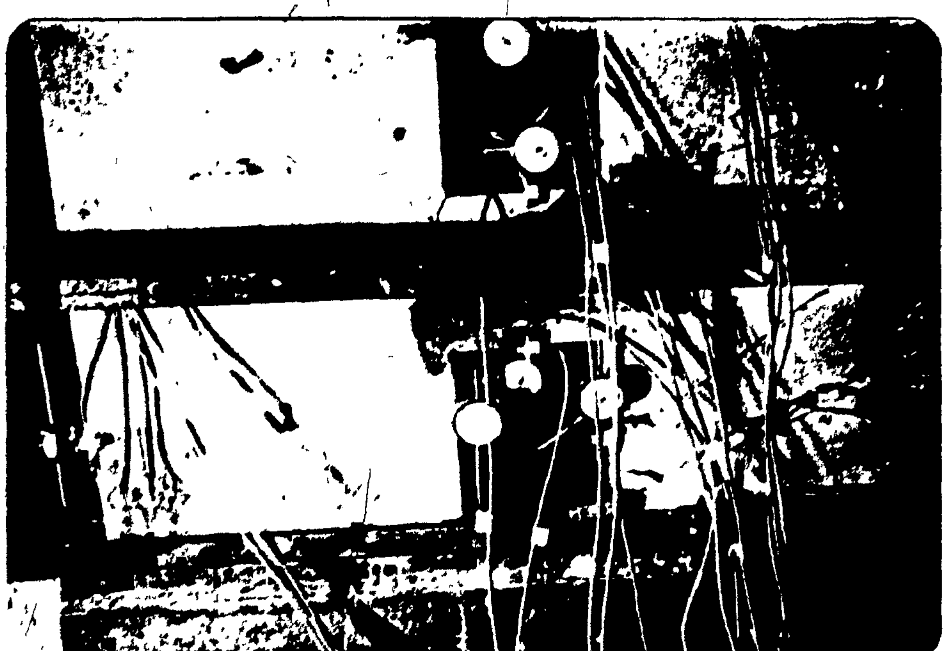

Fig. 4.43 Specimen No. 3 base of wall 2 failure

4.5 Summary

The load-deflection curves for all test specimens showed an almost linear behaviour within the elastic range. Changes in the overall stiffness of the specimens were caused by the cracking of concrete and the yielding of the reinforcement near the wall-beam junctions; yielding of the reinforcement at the wall base caused the load-deflection to level off. After the reinforcement at all critical sections had yielded, the specimens could sustain little or no more increase in applied lateral loads up to the ultimate load. This kind of behaviour is very similar to the elasto-plastic assumptions made in Paulay's analysis[29].

The large shearing forces across the coupling beams and the wall bases were responsible for an early onset of cracking in all test specimens. Cracking and yielding in the coupling beams reduced the stiffness of the overall structure, and this was reflected in the observed load-deflection curves.

According to Paulay's experiments and analysis[13], diagonal cracking has been observed to reduce the flexural stiffness to a much greater extent than flexural cracking. Diagonal reinforcement pattern was suggested for these coupling beams. It was also shown by Paulay that cracking of coupled walls was largely affected by axial load in the wall base. This axial load results from gravity loads and from the accummulation of laminar shears.

The position of maximum rotation in the coupling beams showed agreement with Paulay's elasto-plastic analysis results as stated in section 4.1. Rotations of mid-span sections of the coupling beams indicated a similar trend. The maximum rotational position tends to move upward from a location near quarter height beam in the elastic range to a location near mid-height at ultimate load. The ductility factors for specimens nos. 1 and 2 were 6.5 and 6.9, respectively, which are in excess of the necessary ductility factor of 4. This ductility is necessary to resist the earthquake disturbances. A moderate ductility factor of 2.1 was obtained for specimen no. 3.

Beams with diagonal reinforcement showed less damage (cracking, crushing of concrete) at failure when compared with the conventionally reinforced beams. Diagonal cracking in the deep coupling beams (specimen no. 3) was also found to agree with Paulay's observations. This inelastic deformation at the coupling beams and the wall bases is critical and must be considered to provide safety and adequate resistance to seismic loads.

V. ANALYSIS

5.1 Elastic Analysis of Test Specimens

The experimental results of the test specimens under lateral loads were analysed using the elastic lamina method. For a rapid evaluation of stresses and deflections of the specimens, design curves derived from the continuous lamina thoery were used. The design curves for uniformly distributed load, triangularly distributed load, and concentrated load at the top level, are reproduced in Appendix B.

The following quantities are required to use the design curves[5,6]:

$$\mu = 1 + \frac{AI}{A_1 A_2 \ell^2} \tag{5.1}$$

$$\alpha = \left[\frac{12\ I_\rho \ell^2}{hs^3 I} \mu \right]^{\frac{1}{2}} \tag{5.2}$$

$$\beta = \tfrac{1}{2} w\ell \left(\frac{12\ I_\rho}{hs^3} \right) \frac{1}{I} \tag{5.3}$$

The analysis of test specimens nos. 1 and 2 was carried out using the following data:

$$H = 59.4 \text{ in.}$$

$$A_1 = A_2 = 1.25 \times 15 = 18.75 \text{ in.}^2$$

$$A = A_1 + A_2 = 37.5 \text{ in.}^2$$

$$I_1 = I_2 = \frac{1}{12} \times 1.25 \times 15^3 = 350 \text{ in.}^4$$

$$I = I_1 + I_2 = 700 \text{ in.}^4$$

The second moment of area of the two wall sections about their common neutral axis is:

$$I' = 700 + 2 \times 18.75 \times 12^2$$

$$= 700 + 5400 = 6100 \text{ in.}^4$$

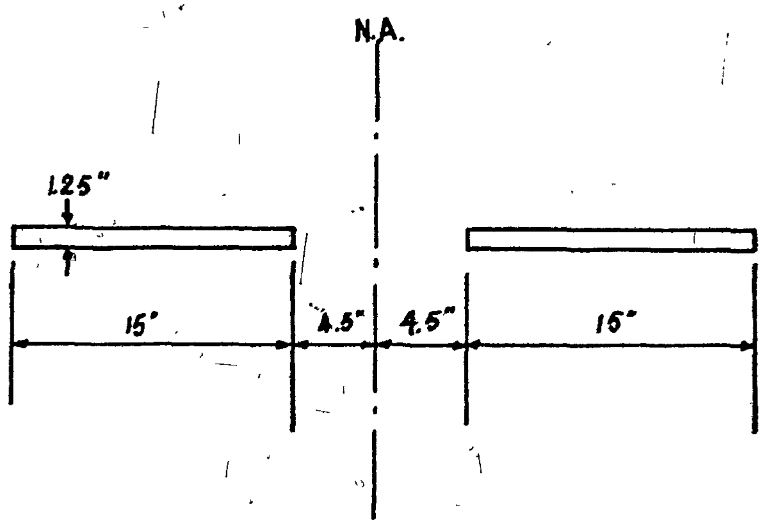

Fig.5.1A: Section of Wall 1 and Wall 2 of Specimens Nos. 1 and 2

The second moment of area of the connecting beams is:

$$I_p = \frac{1}{12} \times 1.25 \times 4.5^3 = 9.45 \text{ in.}^4$$

From equation (5.2) it follows that:

$$\alpha^2 = \frac{12\ I_p}{hs^3}\ \frac{\ell^2}{I}\ \mu = \frac{12 \times 9.45}{15 \times 9^3} \times \frac{24^2}{100} \times 1.13 = 0.00963$$

$$\alpha = 0.0981$$

whence $\alpha H = 0.0981 \times 59.4 = 5.83$

for a total applied load value at 3 kips, which is equivalent to a triangularly distributed load with a maximum value of 0.1 k/in. at the top. From design chart B.5, the percentage of individual cantilever action K_1 and the percentage of composite cantilever action K_2 is given by:

$$K_1 = 0.25$$

$$K_2 = 0.75$$

From design chart B.6, the average value of the connecting beam stress factor K_3 for triangularly distributed load for each storey is given by:

$K_3 = 0.16$ for the fourth storey

$K_3 = 0.25$ for the third storey

$K_3 = 0.32$ for the second storey

$K_3 = 0.29$ for the first storey.

The shear force acting on the coupling beams from the fourth storey level to the first storey level can then be calculated as:

$$Q_i \doteq hq_i = hs \frac{H}{\ell} \frac{1}{\mu} K_3 \tag{5.4}$$

hence:

$$Q_4 = hq_4 = 15 \times 0.1 \times \frac{59.4}{24} \times \frac{1}{1.13} \times 0.16 = 0.526\text{k}$$

$$Q_3 = hq_3 = 15 \times 0.1 \times \frac{59.4}{24} \times \frac{1}{1.13} \times 0.25 = 0.821\text{k}$$

$$Q_2 = hq_2 = 15 \times 0.1 \times \frac{59.4}{24} \times \frac{1}{1.13} \times 0.32 = 1.051\text{k}$$

$$Q_1 = hq_1 = 15 \times 0.1 \times \frac{59.4}{24} \times \frac{1}{1.13} \times 0.29 = 0.953\text{k}$$

Stresses at the extreme edges of the wall bases are calculated as the sum of the stresses due to composite cantilever action and individual cantilever action:

$$\sigma_A = \frac{2}{3} \times W \times H \left[\frac{C'_A}{I'} K_2 + \frac{C_A}{I} K_1 \right] \quad (5.5)$$

$$= \frac{2}{3} \times 3 \times 59.4 \left[\frac{19.5}{6100} \times 0.75 + \frac{7.5}{700} \times 0.25 \right] = 0.603 \text{ ksi}$$

$$\sigma_B = \frac{2}{3} \times W \times H \left[\frac{C'_B}{I'} K - \frac{C_B}{I} K_1 \right] \quad (5.6)$$

$$= \frac{2}{3} \times 3 \times 59.4 \left[\frac{4.5}{6100} \times 0.75 - \frac{7.5}{700} \times 0.25 \right]$$

$$\sigma_B = - 0.252 \text{ ksi}$$

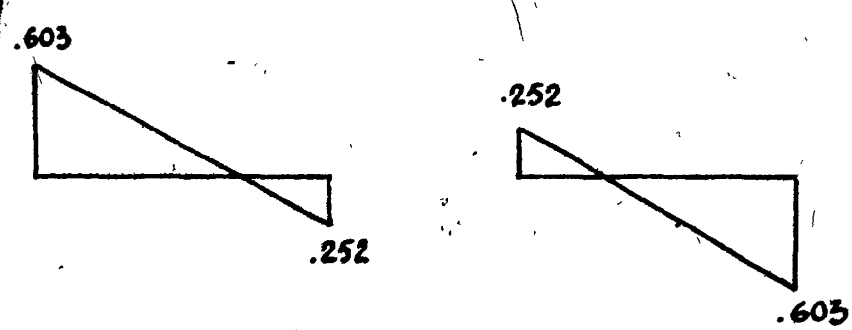

Fig. 5.1B: Stress distribution at wall bases of Specimens nos. 1 and 2

From design chart B.7, deflection factor K_4 is obtained:

$$K_4 = 0.19$$

Second moment of area of cracked sections of the wall bases are:

$$I_{1cr} = 62.2 \text{ in.}^4$$

$$I_{2cr} = 122.3 \text{ in.}^4$$

$$I_{cr} = 184.5 \text{ in}^4$$

Deflection at the top storey level is given by:

$$Y_{max} = \frac{11}{120} \times \frac{wH^4}{EI} K_4 \qquad (5.7)$$

Hence:

$$Y_{uncrack} = 0.0077 \text{ in.}$$

$$Y_{crack} = 0.0290 \text{ in.}$$

as compared to 0.06 in. and 0.086 in. obtained for specimens nos. 1 and 2 respectively, and 0.010 in. obtained from elastic finite element analysis. The experimental values are generally higher than the calculated values due to cracking in the connecting beams and the shear walls under applied loads.

Strain values obtained for specimen no. 1 are also plotted against the total applied load as compared to theoretical values obtained from Finite Element Analysis using SOLID SAP in Appendix D from Figs. D.2 to D.7. Concrete strains are noted lower than theoretical values while steel strains show higher values. This is due to the cracking effects at these critical sections where strain gauges were applied. On the average of concrete and steel strains, the strains at these locations show good agreement with the results from the finite element analysis.

The analysis of Test specimen no. 3 was carried out with the following wall and beam properties:

$$H = 60 \text{ in.}$$

$$A_1 = A_2 = 1.25 \times 16 = 20 \text{ in.}^2$$

$$A = A_1 + A_2 = 40 \text{ in.}^2$$

$$I_1 = I_2 = \frac{1}{12} \times 1.25 \times 16^3 = 426.67 \text{ in.}^4$$

$$I = I_1 + I_2 = 853.34 \text{ in.}^4$$

$$I_{cf} = 142 + 34 = 176 \text{ in.}^4$$

$$I' = 853.34 + 2 \times 20 \times 11.5^2 = 6143.33 \text{ in.}^4$$

$$I_\rho = \frac{1}{12} \times 1.25 \times 7^3 = 35.73 \text{ in.}^4$$

Evaluating the constants for the design charts as follows:

$$\mu = 1 + \frac{AI}{A_1 A_2 \ell^2} = 1 + \frac{40 \times 853.33}{20 \times 20 \times 23^2} = 1.16$$

$$\alpha^2 = \frac{12\, I_\rho}{hs^3}\, \frac{\ell^2}{I}\, \mu = \frac{12 \times 35.75}{16 \times 7^3} \times \frac{23^2}{853.33} \times 1.16 = 0.05628$$

hence: $\alpha = 0.237$

$\alpha H = 14.23$

From design chart B.5:

$$K_1 = 0.10$$

$$K_2 = 0.90$$

From design chart B.6, the average value of the stress factors K_3 for each storey are as follows:

$K_3 = 0.07$ for the fourth storey

$K_3 = 0.20$ for the third storey

$K_3 = 0.37$ for the second storey

$K_3 = 0.45$ for the first storey

For a total load value of 3 kips, the shear forces acting on the coupling beams from the fourth storey level to the first storey level are given by:

$$Q_4 = hq_4 = hw\,\frac{H}{\ell}\,\frac{1}{\mu}\,K_3 = 15 \times 0.1 \times \frac{60}{23} \times \frac{0.07}{1.16} = 0.23k$$

$$Q_3 = hq_3 = 15 \times 0.1 \times \frac{60}{23} \times \frac{1}{1.16} \times 0.20 = 0.674k$$

$$Q_2 = hq_2 = 15 \times 0.1 \times \frac{60}{23} \times \frac{1}{1.16} \times 0.37 = 1.247k$$

$$Q_1 = hq_1 = 15 \times 0.1 \times \frac{60}{23} \times \frac{1}{1.16} \times 0.45 = 1.517k$$

Stresses at the extreme edge of the wall bases are:

$$\sigma_A = \frac{2}{3} W_i H \left[\frac{C'_A}{I'} K_2 + \frac{C_A}{I} K_1 \right]$$

$$= \frac{2}{3} \times 3 \times 60 \left[\frac{19.5}{6143.33} \times 0.9 + \frac{8}{853.33} \times 0.1 \right]$$

$$= 0.455 \text{ ksi}$$

$$\sigma_B = \frac{2}{3} \times 3 \times 60 \left[\frac{3.5}{6143.33} \times 0.9 - \frac{8}{853.33} \times 0.1 \right]$$

$$= 0.051 \text{ ksi}$$

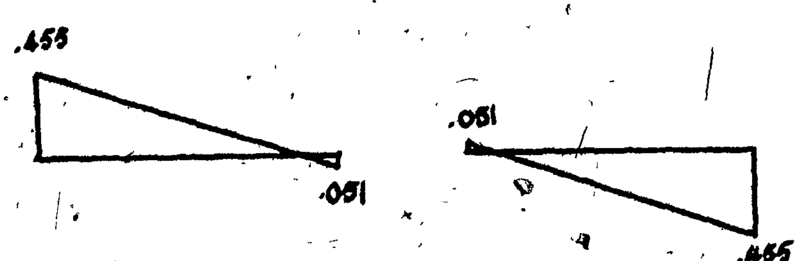

Fig. 5.2: Stress distribution at wall bases of Specimen no. 3

From design chart B.7, the parameter K_4 is given by:

$$K_4 = 0.16$$

and the top storey deflection y_{max} is:

$$y_{max} = \frac{11}{120} \frac{wH^4}{EI_{cr}} K_4 = \frac{11}{120} \times \frac{0.1 \times 60^4}{4000 \times 176} \times 0.16$$

$$= 0.027 \text{ in.}$$

The experimental value of deflection for specimen no. 3 at the top storey level was 0.12 in. at a total load value of 3 kips. The difference between the experimental and calculated values is again due to cracks which first formed in the first storey of shear wall no. 2. These cracks reached the inside edge first, which was reinforced with much lighter steel percentage than the outside edge. Thus, one can expect a much less stiff cracked section at the base of wall 2, and consequently a higher top storey deflection.

5.2 Ultimate Load Analysis

Prediction of the behaviour of coupled shear walls up to the maximum load can be carried out, using the ultimate load analysis suggested by Paulay[29]. This method accounts for a stagewise development of the collapse mechanism. A triangularly distributed load pattern is used in the analysis.

The ultimate moment capacity of the coupling beams is calculated as:

$$M_{b,u} = A_s f_y \, (d - d') \tag{5.8}$$

$$= 0.04 \times 37 \times 4$$

$$= 5.92 \text{ k in.}$$

The ultimate moment capacities of wall 1 and wall 2 are given by:

$$\omega_1 = \rho_1 \frac{fy}{fc} = 0.00276 \times \frac{37}{4} = 0.0256$$

$$\omega_2 = \rho_2 \frac{fy}{fc} = 0.0066 \times \frac{40}{4} = 0.0660$$

$$M_{1,u} = bd^2 \, f'_c \, \omega_1 \, (1 - 0.59 \, \omega_1) \tag{5.9}$$

$$= 1.25 \times 14.5^2 \times 4 \times 0.0256 \, (1-0.59 \times 0.0256)$$

$$= 26.5 \text{ in.}$$

$$M_{2,u} = bd^2 \, f'_c \, \omega_2 \, (1 - 0.59 \, \omega_2)$$

$$= 1.25 \times 14.5^2 \times 4 \times 0.066 \, (1 - 0.59 \times 0.066)$$

$$= 66.67 \text{ k in.}$$

The ultimate shear strength of the beams is:

$$V_{b,u} = \frac{2M_{b,u}}{3} = \frac{2 \times 5.92}{9} = 1.316 \text{ k.}$$

The ultimate laminar shear of the lowest beam level is:

$$q'_u = 1.316/20.25 = 0.065 \text{ k/in.}$$

For beams at other storey levels, this shear distribution is:

$$q_u = 1.316/15 = 0.088 \text{ k/in.}$$

The equivalent second moment of area of a cracked coupling beam is:

$$I'_x = 0.3 \times 9.45 = 2.835 \text{ in.}^4$$

Stage 1: Elastic Design Load

The elastic analysis was carried out in section 5.1 using design charts and a design load of 3 kips. The maximum elastic laminar shear at beam 1 level is:

$$q_{max} = 0.29 \times 0.1 \times \frac{59.4}{24} \times \frac{1}{1.13} = 0.0635 \text{ k/in.}$$

Stage 2: Elastic Limit of the Structure

The next increment of loading brings beam 1 to its elastic limit. This maximum elastic load is given by:

$$W_e^* = \frac{q'_u}{q_{max}} \; W = \frac{0.065}{0.0635} \times 3 = 3.07 \text{ kips}$$

The corresponding maximum laminar rotation and top level deflection are:

$$\theta'_y = \frac{hs^2 q_u}{12\, EI'_x} = \frac{15 \times q^2 \times 0.065}{12 \times 4000 \times 2.835} = 5.8 \times 10^{-4} \text{ rad.}$$

$$y_e = \frac{W_e}{W}\, y = \frac{3.07}{3} \times 0.0652 = 0.0667 \text{ in.}$$

Stage 3: Full Plastification of the Laminas

Further load increase causes other coupling beams to enter the plastic range with:

$$q_u = 0.088 \text{ k/in.}$$

and $$\theta_y = 7.84 \times 10^{-4} \text{ rad.}$$

Second moment of area of the cracked sections of the wall bases are:

$I_{1cr} = 62.2 \text{ in.}^4$, $A_{1cr} = .7 \times 20 = 14 \text{ in.}^2$

$I_{2cr} = 1.22.3 \text{ in.}^4$, $A_{2cr} = .7 \times 20 = 14 \text{ in.}^2$

$I_{cr} = 184.5 \text{ in.}^4$, $A_{cr} = 28 \text{ in.}^2$

It is assumed that that laminas possess bilinear elasto-plastic load rotation characteristics. At the end of this load increment the laminar plastification is assumed to have spread over the height of the structure while each beam sustains its yield capacity.

The critical stiffness ratio is defined as:

$$Z_c = \frac{\nu - 1}{1 - 0.19\nu} \qquad (5.10)$$

where

$$\nu = \frac{0.25}{0.616} = 4.058$$

$$Z_c = \frac{4.058 - 1}{1 - 0.19 \times 4.058} = 13.36$$

The stiffness ratio of the structure is:

$$Z = \frac{q_u H^2}{2\, sE\theta_y} \left(\frac{1}{A_1} + \frac{1}{A_2} + \frac{\ell^2}{I} \right) \qquad (5.11)$$

$$= \frac{0.088 \times 59.4^2}{2 \times 9 \times 4000 \times 7.84 \times 10^{-4}} \left(\frac{2}{14} + \frac{24^2}{184.5} \right)$$

$$= 17.96 > Z_c = 13.36$$

Thus, the uppermost lamina must just attain the yield rotation. The corresponding load is:

$$W_y = \frac{4\ s\ E\ I\ (Z + 1)}{\ell H^2}\ \Theta_y \tag{5.12}$$

$$= \frac{4 \times 9 \times 4000 \times 184.5 \times (17.96 + 1)}{24 \times 59.4^2} \times 7.84 \times 10^{-4}$$

$$= 4.66 \text{ kips.}$$

The top storey deflection at the end of this stage is given by:

$$Y_{\rho y} = \frac{H^3}{EI} \left\{ W_y \left(\frac{11}{60}\right) - \frac{\ell q'_u}{3} \right\} \tag{5.13}$$

$$= \frac{59.4^3}{4000 \times 184.53} \left\{ 4.66 \left(\frac{11}{60} \right) - \frac{24 \times 0.065}{3} \right\}$$

$$= 0.095 \text{ in.}$$

as compared to 0.13 in. and 0.16 in. obtained from experimental results for specimens nos. 1 and 2, respectively. The theoretical and experimental deflection values are also shown on the load-deflection curves of Fig. 5.3.

Stage 4: Ultimate Strength of Wall 1

A further load increment is assumed to cause wall 1 to attain its ultimate capacity in the presence of Tu axial tension. The critical moment at the base of the wall is obtained from:

$$M_1 = \frac{HI_1}{I_{cr}} \left[(W_y + \Delta W')\left(\frac{2}{3}\right) - 0.95\, \ell q_u \right] = M_{1,u} \tag{5.14}$$

assuming that both walls receive the load within the elastic limit until the end of this stage.

Solving for $\Delta W'$, one obtains:

$$\Delta W' = \left(\frac{M_{1,u}}{I_1 H} I + 0.95\, \ell q_u \right) \frac{3}{2} - W_y \tag{5.15}$$

$$= \left(\frac{26.5 \times 184.5}{59.4 \times 62.2} + 0.95 \times 24 \times 0.088 \right) \frac{3}{2} - 4.66$$

$$= 0.33 \text{ k.}$$

The load applied at the end of this stage is 4.99 kips. The corresponding top storey deflection is found from:

$$\Delta y' = \frac{\Delta W' H^3}{E\, I_{cr}} \left(\frac{11}{60} \right) \tag{5.16}$$

$$= \frac{0.33 \times 59.4^3}{4000 \times 187.5} \left(\frac{11}{60} \right) = 0.017 \text{ in.}$$

Hence, the total top storey deflection is:

$$y_p = 0.095 + 0.017 = 0.112 \text{ in.}$$

At this load level of 4.99 k, experimental top storey deflections of 0.16 in. and 0.18 in. were obtained for specimens nos. 1 and 2, respectively.

Stage 5: Ultimate Strength of Wall 2

Similarly, $\Delta W'$ is defined as the load increment which will cause wall 2 to attain its ultimate moment capacity at the base in the presence of Tu axial tension. Wall 1 may be considered as ineffective because of the formation of plastic hinge at the end of the previous stage. Thus, the maximum moment at the base of Wall 2 is:

$$M_2 \approx \frac{HI_2}{I_{cr}} \left[\left(W_y + \Delta W' + \frac{I_{cr}}{I} \Delta W''\right) \left(\frac{2}{3}\right) - 0.95\ \ell q_u \right] = M_{2,u} \qquad (5.17)$$

Solving for $\Delta W''$, one obtains:

$$\Delta W'' = \left[\left(\frac{I_{cr} M_{2,u}}{HI_2} + 0.95\ \ell q_u \right) \left(\frac{2}{3}\right) - W_u \right] \frac{I_2}{I_{cr}}$$

$$= \left[\left(\frac{184.5 \times 66.67}{59.4 \times 122.3} + 0.95 \times 24 \times 0.088 \right) \frac{3}{2} - 4.99 \right] \frac{122.3}{184.5}$$

$$= 0.371\ \text{k.}$$

Hence, the applied load at the yielding of both walls can be approximated as:

$$W'_u = 4.99 + 0.371 = 5.36\ \text{k.}$$

The top storey deflection can be accordingly approximated from the incremental deflection:

$$\Delta y_p'' = \frac{\Delta W'' H^3}{E I_2} \left(\frac{11}{60}\right) \tag{5.18}$$

$$\Delta y_p'' = \frac{0.371 \times 59.4^3}{4000 \times 122.3} \left(\frac{11}{60}\right) = 0.029 \text{ in.}$$

Hence:

$$y_p' = 0.112 + 0.029 = 0.141 \text{ in.}$$

The theoretical ultimate strength of the specimens can be considered to be at this stage of 5.36 kips total applied load, as compared to 5.3 kips and 5.0 kips obtained from experimental results for specimens nos. 2 and 1, respectively.

The theoretical load-deflection curve from stage 1 to stage 5 is plotted in Fig. 5.3. Corresponding load-deflection curves for specimens nos. 1 and 2 are also shown on the same graph for comparison purpose. The theoretical curve shows a good estimate of the applied loads and deflection values near the yielding stages of the laminas and the walls. Furthermore, it shows the stagewise behaviour in terms of the experimental load-deflection curves for both specimens.

FIG 5.3: ANALYSIS OF LOAD-DEFLECTION CURVES

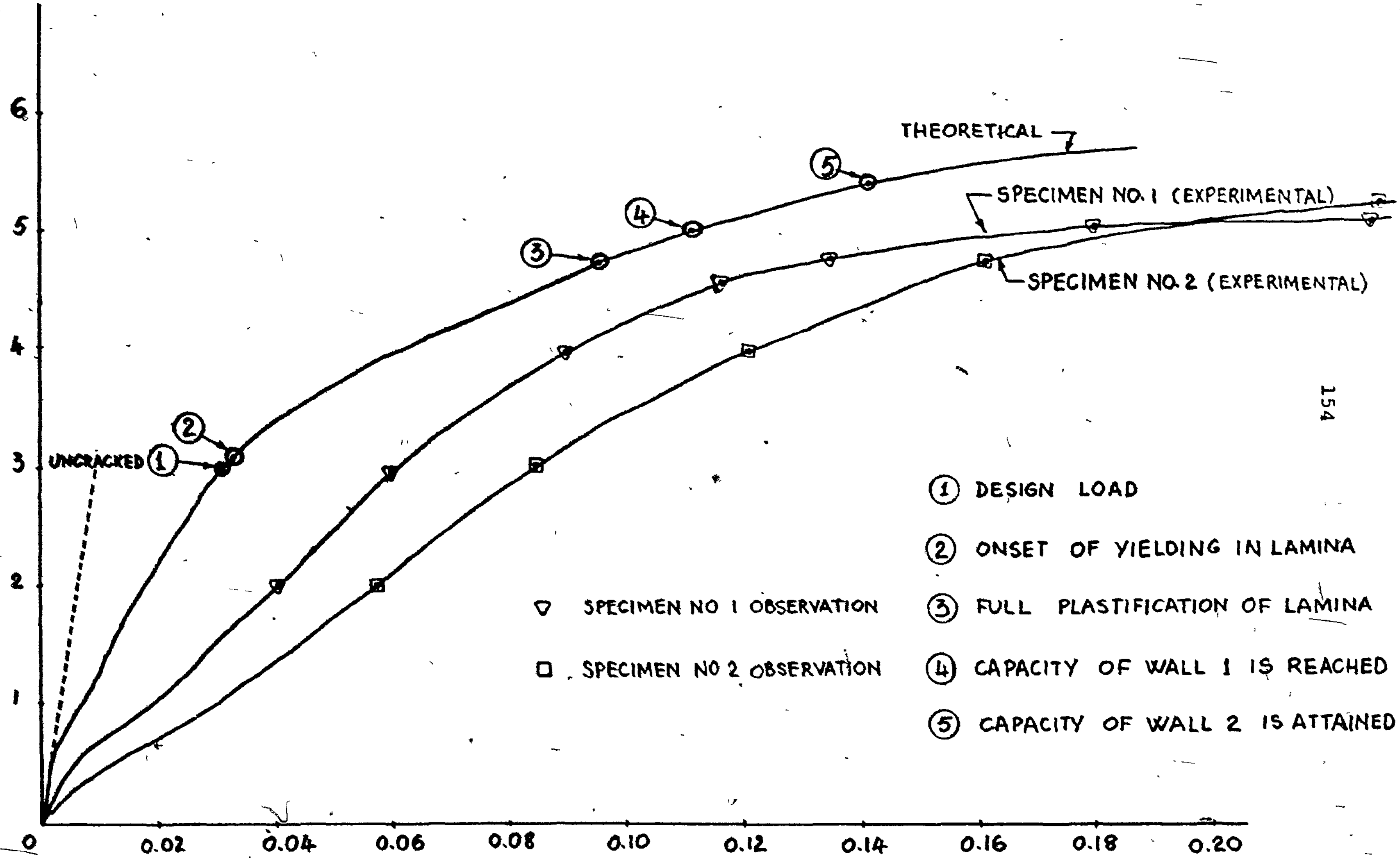

5.3 Ductility and Lateral Strength of Coupled Shear Walls

In shear wall structures resisting seismic forces, it is necessary to examine the behaviour over the entire load range, as well as ductility. Ductility implies high deformations without appreciable loss of strength, and it also implies large inelastic deformation associated with large amounts of strain energy. In this investigation, the available ductility is based on a monotonic loading condition (Table 5.1). It would be reasonable to assume that a similar amount of ductility would be available under a reversed loading cycle. It is recommended that further studies be made on shear walls subjected to reversible loadings.

The ductility of a coupled shear wall can be defined as:

$$\mu' = \frac{\Delta u}{\Delta y} \tag{5.19}$$

where

μ' = ductility factor

Δu = deflection at maximum load Pu

Δy = deflection at the total yielding of coupling beams and tension wall.

The ductility factors for the walls and coupling beams of the three test specimens are presented in Table 5.1. Ductility factors of 6.5 and 6.8 were obtained for specimens nos. 1 and 2 respectively. A moderate ductility factor of 2.14 was obtained for specimen no. 3 due to the opening of the tension cracks of wall 2. Ratios of measured deflections of other storeys, and measured rotations of different beam

TABLE 5.1

Ratios from Measured Deflections and Rotations

	$\frac{\Delta ult.}{\Delta y}$	$\frac{\Delta failure}{\Delta ult.}$	$\frac{\Delta failure}{\Delta y}$
Test Specimen No. 1			
Fourth storey deflection	6.467	2.20	14.23
Third storey deflection	7.444	2.37	17.67
Second storey deflection	7.833	2.30	17.99
First storey deflection	8.864	2.53	22.39
Wall 1 rotation (sect. $\frac{d}{2}$)	12.50	2.50	31.25
Wall 2 rotation (sect. $\frac{d}{2}$)	7.33	2.50	18.33
Beam 1 rotation (midspan)	8.33	2.03	16.88
Beam 2 rotation (midspan)	9.52	2.60	24.76
Beam 3 rotation (midspan)	10.00	2.38	23.75
Beam 4 rotation (midspan)	14.375	1.67	23.96
Test Specimen No. 2			
Fourth storey deflection	6.85	2.08	14.24
Third storey deflection	6.87	2.06	14.19
Second storey deflection	6.83	2.10	14.37
First storey deflection	7.50	2.17	16.25
Wall 1 rotation (sect. $\frac{d}{2}$)	10.71	2.21	23.70
Wall 2 rotation (sect. $\frac{d}{2}$)	9.55	1.86	17.73
Beam 1 rotation (midspan)	8.50	2.40	20.33
Beam 2 rotation (midspan)	10.87	2.80	30.43
Beam 3 rotation (midspan)	10.08	2.71	27.36
Beam 4 rotation (midspan)	13.57	2.52	34.14
Test Speciman No. 3			
Fourth storey deflection	2.14	2.67	5.72
Third storey deflection	2.01	2.79	5.62
Second storey deflection	2.09	2.90	6.06
First storey deflection	2.38	3.20	7.60
Wall 1 rotation (sect. 5½ in.)	4.07	3.78	15.37

TABLE 5.2

Summary of Calculated Design, Yield and Ultimate
'oads for the Three Test Specimens

	Design load (elastic limit)	Yield load	Ultimate load	Yield load / Design load
Specimen No. 1	3.0	5.0	6.02	1.67
Specimen No. 2	3.0	5.3	6.79	1.77
Specimen No. 3	3.0	6.0	6.59	2.00

and wall sections at ultimate and failure loads to those at yield load are also presented in the same table as a summary of their behaviour presented in Chapter IV. Ductility of coupled shear walls can be increased by suitable detailing and by considering the effects of the confinement of concrete due to closed stirrups, steel percentage, and the interaction of other structural elements as stated in section 1.2.

The observed strengths of the coupled shear wall models as compared with the theoretical elastic limit strengths are presented in Table 5.2. Ratios of the yield load to the elastic design load (theoretical strength) of 1.66, 1.77 and 2.0 were obtained for specimens nos. 1, 2 and 3 respectively. In order to obtain higher overall ductility, it is recommended that an ultimate load analysis as presented in section 5.2 be carried out in the design as a check for the ultimate load condition.

5.4 Projected Behaviour of Similar Prototype Structures

Results of this model study can be related to similar prototype structures by using the principles of similitude. For the models used in this investigation, the linear scale factor λ is:

$$\lambda = \frac{L}{L_M} = 10$$

The basic relationships between the various prototype and the model quantities are as follows:

Cross sectional area of the steel reinforcement:

$$\frac{A_s}{A_{sM}} = \lambda^2 = 100$$

The gross cross-sectional area of concrete, including steel transformed by ratio n is given by:

$$\frac{A_t}{A_{tM}} = \frac{A_g + (n-1)\ A_s}{A_{gM} + (n-1)\ A_{sM}} = \lambda^2 = 100$$

The second moment of area I for the prototype is:

$$\frac{I}{I_M} = \frac{\int y^2 dA}{\int y_M^{\ 2} dA} = \lambda^4 = 10000$$

Relationship of various types of loading; dead weight and concentrated force:

$$\frac{P}{P_M} = \frac{\sigma A}{\sigma_M A_M} = \frac{A}{A_M} = \lambda^2 = 100$$

$$\frac{W}{W_M} = \frac{uL}{u_M L_M} = \lambda^2 = 100$$

Load per unit length:

$$\frac{w}{w_M} = \frac{P/L}{P_M/L_M} = \lambda = 10$$

Cracking load, and ultimate load:

$$\frac{W_u}{W_{uM}} = \frac{W_{cr}}{W_{crM}} = \lambda^2 = 100$$

Cracking moment and ultimate moment:

$$\frac{M_u}{M_{uM}} = \frac{M_{cr}}{M_{crM}} = \frac{P_{cr}L}{P_{cr_M}L_M} = \lambda^3 = 1000$$

Deflection of the coupled shear walls:

- under point load at the top storey

$$\frac{Y}{Y_M} = \left(\frac{PH^3}{3\ EI} K_4\right) \div \left(\frac{P_M H_M^3}{3\ E_M I_M} K_4\right) = \lambda = 10$$

- under triangularly distributed load

$$\frac{Y}{Y_M} = \left(\frac{11}{120}\frac{wH^4}{EI} K_4\right) \div \left(\frac{11}{120}\frac{w_M H_M^4}{E_M I_M} K_4\right) = \lambda = 10$$

Using the principles of similitude described above, the properties of prototype coupled shear walls can be obtained and its behaviour and strength can be predicted accordingly. Table 5.3 shows the properties of prototype structures of test specimens nos. 1, 2 and 3. Applied loads at yielding of the laminas, ultimate and failure stages and corresponding deflections are also predicted in Table 5.4. Yield

TABLE 5.3 Properties of Predicted Prototypes

	Specimen No. 1		Specimen No. 2		Specimen No. 3	
Wall dimension	12.5 x 49.5 x 1.04 ft		12.5 x 49.5 x 1.04 ft		15' 10 x 50' x 1.04'	
Beam dimension	8.75 x 3.75 x 1.04 ft		8.75 x 3.75 x 1.04 ft		5' 10 x 5' 10 x 1.04'	
f'_c	5 ksi		4 ksi		4 ksi	
f_y	40 ksi		40 ksi		40 ksi	
E_s	29000 ksi		29000 ksi		29000 ksi	
n	8		8		8	
Member	steel percentage	area of reinf. steel (in.^{2})	steel percentage	area of reinf. steel (in.^{2})	steel percentage	area of reinf. steel (in.^{2})
Beam 1	0.856	4.000	0.856	4.000	0.470	4.000
Beam 2	0.744	4.000	0.744	4.000	0.470	4.000
Beam 3	0.744	4.000	0.744	4.000	0.235	2.000
Beam 4	0.744	4.000	0.744	4.000	0.236	2.000
Wall 1:						
Outside edge	0.640	12.200	0.640	12.200	0.125	2.500
Inside edge	0.133	2.530	0.133	2.530	0.125	2.500
Vert.shear/ft^2	0.210	0.310	0.210	0.310	0.200	0.310
Horiz.shear/ft^2	0.277	0.415	0.277	0.415	0.277	0.415
Wall 2:						
Outside edge	0.640	12.200	0.640	12.200	0.600	12.200
Inside edge	0.133	2.530	0.133	2.530	0.125	2.530
Vert.shear/ft^2	0.210	0.310	0.210	0.310	0.200	0.310
Horiz.shear/ft^2	0.277	0.415	0.277	0.415	0.277	0.415

TABLE 5.4

Predictions of Behaviour of Prototype Coupled Shear Walls
(scale factor = 10)

	Yield load (K)	Yield deflec. (in.)	Ult. load (K)	Ult. deflec. (in.)	Failure load (K)	Failure deflec. (in.)
Prototype S.W.No.1						
Beam 1 level	53.5	0.2	64.5	2.0	56.2	4.8
Beam 2 level	116.5	0.6	140.3	4.7	122.3	10.8
Beam 3 level	179.5	1.0	216.1	7.0	188.5	16.0
Beam 4 level	150.5	1.5	181.1	9.5	158.0	22.0
	500.0		602.0		525.0	
Prototype S.W.No.2						
Beam 1 level	56.8	0.5	72.7	0.3	62.5	6.5
Beam 2 level	123.5	0.8	158.2	7.0	135.8	12.5
Beam 3 level	190.2	1.5	243.8	11.3	209.3	19.0
Beam 4 level	159.5	2.2	204.3	14.5	175.5	28.0
	630.0		679.0		583.1	
Prototype S.W.No.3						
Beam 1 level	63.8	0.4	70.6	1.2	47.85	3.0
Beam 2 level	138.8	1.1	153.5	2.5	104.1	6.3
Beam 3 level	213.8	2.0	236.6	4.5	160.35	11.4
Beam 4 level	179.2	2.9	198.3	6.3	134.4	16.0
	595.6		659.0		446.70	

loads of 500 kips, 530 kips and 596 kips are predicted with top level deflections of 1.5, 2.2 and 2.9 in. for the corresponding three prototype structures. According to the principles of similitude, the strain values at selected positions and ductility factors of the components are expected to be the same as in the model specimens. Other quantities can also be derived from the principles of similitude.

VI CONCLUSIONS AND RECOMMENDATIONS

6.1 Methods of Analysis and Model Studies

Analytical methods have been developed to predict the behaviour of coupled shear wall structures at working and ultimate loads. The Lamina method simplifies the analysis and design of coupled shear walls with suitable design charts and can be modified for ultimate load analysis. The Equivalent Frame method utilizes an approximation to describe the behaviour of coupled shear walls in terms of an equivalent frame. With the availability of large electronic computers, the Finite Element method can be used for higher accuracy and wider applications. Photoelastic studies of coupled shear walls provide very useful information on the load distribution and stress concentrations in the system.

Direct models can be used to study not only the elastic range but also the inelastic behaviour of coupled shear wall systems. The information obtained from model tests, which are not expensive, can result in significant cost savings and improved safety considerations.

6.2 Summary of Experimental Observations

A method for direct model testing of coupled shear walls is presented in this study. The experimental set-up for this method consisted of a loading frame, a bracing system, a load distributor for upper triangularly distributed load pattern, and a load transmission system to transfer a tensile (pull) force to the specimen. Three $\frac{1}{10}$ - scale reinforced concrete models were tested under monotonically increasing loads. Complete load-deflection curves were obtained for each specimen. Early cracking in the connecting beams caused an increase in the wall moments. Further cracking in the wall bases reduced the overall stiffness of the structure. Full capacity of the connecting beams was achieved first and maintained during the test until the reinforcement at the inside edge of wall 1 failed for specimens nos. 1 and 2. Connecting beams with diagonal reinforcement showed less damage (cracking, crushing of the concrete) at failure when compared with the conventionally reinforced beams. Diagonal cracking in the deep coupling beams of specimen no. 3 was also observed. Diagonal reinforcement is considered to be a more suitable reinforcing pattern for the coupling beams.

In analyzing the load-deflection curves, an ultimate load analysis was carried out to attain the ultimate capacity of the specimens. The results of this analysis showed a good agreement with the experimental strengths. This analysis used a step by step procedure to evaluate the load and deformations of the specimens until a collapse mechanism was formed. An elasto-plastic behaviour was assumed for all critical sections.

In the first two specimens, a large ductility was observed in terms of the ratio of midspan section rotation at ultimate and yield loads. These critical connecting beams must possess a high ductility factor of at least 14 in order to ensure an overall well-behaved structure. Overall ductility factors of more than 6 were obtained for the first two specimens. A ductility factor of 2.1 was obtained for specimen no. 3 to the opening of the tension cracks at the inside edge of wall 2.

6.3 Suggestions for Design Considerations

The observations from the model studies and the overall behaviour of the test specimens suggested that:

(a) Coupled shear wall structures can be designed for adequate ductility and are able to provide adequate safety under any lateral load system (wind, earthquake, etc.).

(b) Diagonal-reinforcement pattern is more effective than conventional reinforcement pattern in transmitting load for medium and deep coupling beams.

(c) Adequate shear reinforcement, both vertical and horizontal, should be provided in the bases of the walls to ensure that their ultimate flexural capacities can be attained.

(d) Adequate bond and anchorage should be provided at the critical sections of beam-wall junctions, especially for the top beam reinforcement, and wall bases. It is suggested that the coupling beams have a ductility factor of at least 14.

(e) Adequate steel percentage at the inside edge of the compression wall should be provided for an increased moment in that wall in case of cracking and yielding of the coupling beams.

(f) In the case of deep coupling beams, the reinforcement at the inside edge and any vertical reinforcement provided should be able to resist the net tension force in the tension wall.

(g) An ultimate load analysis of the shear walls should be carried out as a check at near failure conditions.

REFERENCES

1. The Structural Engineers' Association of California Seismology Committee, "Recommended Lateral Force Requirements and Commentary",1968.

2. Chitty, L., "On the Cantilever Composed of a Number of Parallel Beams Interconnected by Cross Bars". The London, Edinburgh and Dublin Philosophical Magazine and Journal of Science, Vol. 38, Oct. 1947, pp. 685-699.

3. Beck, H., "Ein neues Berechnungs verfahren fuer gegliederte Scheiben, dargestellt am Beispiel der Vierendeeltraegers". Der Bauingenieur, Vol. 31, Heft 12, 1956, pp. 436-443.

4. Rosman, R., "Beitrag zur statischen Berechnung waagrecht belasteter Querwaende bei Hochbauter". Der Bauingenieur, Part I, Vol. 35, Heft 4, 1960, pp. 133-136; Part II, Vol. 37, Heft 1, 1962, pp. 24-26; Part III, Vol. 37, Heft 8, 1962, pp. 303-308.

5. Coull, A. & Choudhury, J.R., "Stresses and Deflections in Coupled Shear Walls", ACI Journal, Feb 1927, pp. 65-72.

6. Coull, A. & Choudhury, J.R., "Analysis of Coupled Shear Walls", ACI Journal, Sept 1967, pp. 587-593.

7. Kokinopoulos, E., "Experimental Photoelastic Determination of the Stresses and Deformations of Laterally Loaded Shear Walls with Openings", Symposium on Tall Buildings with Particular Reference to Shear Wall Structures, University of Southampton, April 1966, pp. 547-564.

8. Smith, B.S., "Modified Beam Method for Analyzing Symmetrical Interconnected Shear Walls", ACI Journal, December 1970, pp. 977-980.

9. Schwaighofer, J. & Microys, H.F., "Analysis of Shear Walls using Standard Computer Programs", ACI Journal, December 1969, pp. 1005-1007.

10. Allen, C.M., Jaeger, L.G. & Fenton, V.C., "Ductility in Reinforced Concrete Shear Walls", ACI SP-36, Response of Multistory Concrete Structures to Lateral Forces, 1972.

11. Jaeger, L.G., Fenton, V.C. & Allen, C.M., "The Structural Analysis of Buildings having Irregularly Positioned Shear Walls", 1972. Private communication.

12. Mirza, S.M. & Jaeger, L.G., "A Study of the Behaviour of Coupled Shear Wall Structures", 1972. Departmental Report. Department of Civil Engineering & Applied Mechanics, McGill University.

13. Paulay, T., "The Coupling of Shear Walls", Ph.D. dissertation, University of Canterbury, Christchurch, New Zealand, 1969.

14. Paulay, T., "The Elasto-Plastic Response of Coupled Shear Walls under Cyclic Reversed Loading". Conference on Cyclic Loading on Concrete Structures, Madrid, 1972.

15. Paulay, T., "Design Aspects of Shear Walls for Seismic Areas", Research Report No. 74-11, University of Canterbury, Oct. 1974.

16. Mamet, J.C., "Finite Element Analysis of Tall Buildings", Ph.D. dissertation, McGill University, Montreal, 1972.

17. Mehrotra, B.L., Mufti, A.A. & Redwood, R.G., "Analysis of Three-Dimensional Thin Walled Structures", Journal of Structural Division, Proceedings of the ASCE, December 1969, pp. 2863-2872.

18. "Tall Buildings", Symposium on Tall Buildings with Particular Reference to Shear Wall Structures, University of Southhampton, April 1966.

19. "Response of Multistorey Concrete Structures to Lateral Forces", ACI Special Publication 36, 1972.

20. Wilson, E.L., "Finite Element Analysis of Two-Dimensional Structures", Ph.D. dissertation, University of California, Berkeley, 1960.

21. Lee, H.H., "Stresses in Room and Pillar Mining Systems", Master's thesis, McGill University, Department of Mining Engineering, April 1969.

22. Mirza, S.M., "Structural Concrete Models - Materials, Instrumentation, Correlation", A State of the Art Report, McGill University, October 1972.

23. Franklin, H.A., "Nonlinear Analysis of Reinforced Concrete Frames and Panels", Ph.D. dissertation, University of California, Berkeley, 1970.

24. Mirza, M.S. & McCutcheon, J.O., "Bond Similitude in Reinforced Concrete Models". Paper presented to The National Structural Engineering Meeting of the ASCE, Baltimore, April 1971.

25. Harris, H.G., Sabnis, G.M. & White, R.N., "Reinforcement for Small-Scale Models of Concrete Structures". Symposium on Models for Concrete Structures, ACI SP-24, Detroit, 1970, pp. 141-158.

26. Zienkiewicz, O.C., "The Finite Element Method in Engineering Science", McGraw-Hill, 1971.

27. Pang, C.L.K.P., "Reliability of Models in the Analysis of Prestressed Concrete Beams in Flexure". M.E. thesis, McGill University, Montreal, April 1965.

28. McLeod, I., "New Rectangular Finite Element for Shear Wall Analysis". Journal of the Structural Division, Proceedings of the ASCE, March 1969, pp. 399-409.

29. Paulay, T., "An Elasto-Plastic Analysis of Coupled Shear Walls", ACI Journal, November 1970, pp. 915-922.

30. Faucher, Y., Ph.D. thesis to be published, McGill University, Montreal.

APPENDIX A

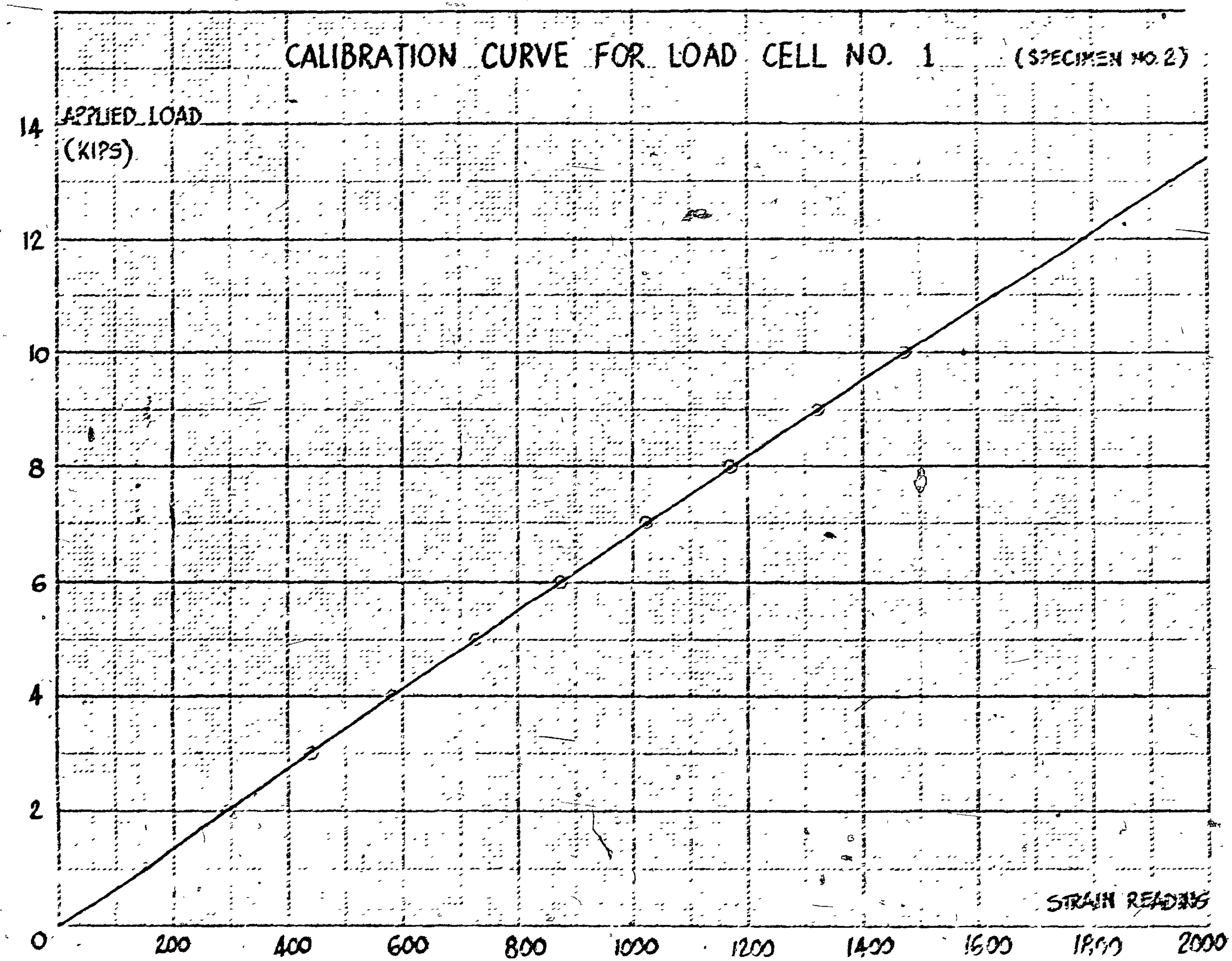
CALIBRATION CURVE FOR LOAD CELL NO. 1
(SPECIMEN NO. 2)
APPLIED LOAD
(KIPS)
STRAIN READINGS
0
2
4
6
8
10
12
14
200
400
600
800
1000
1200
1400
1600
1800
2000

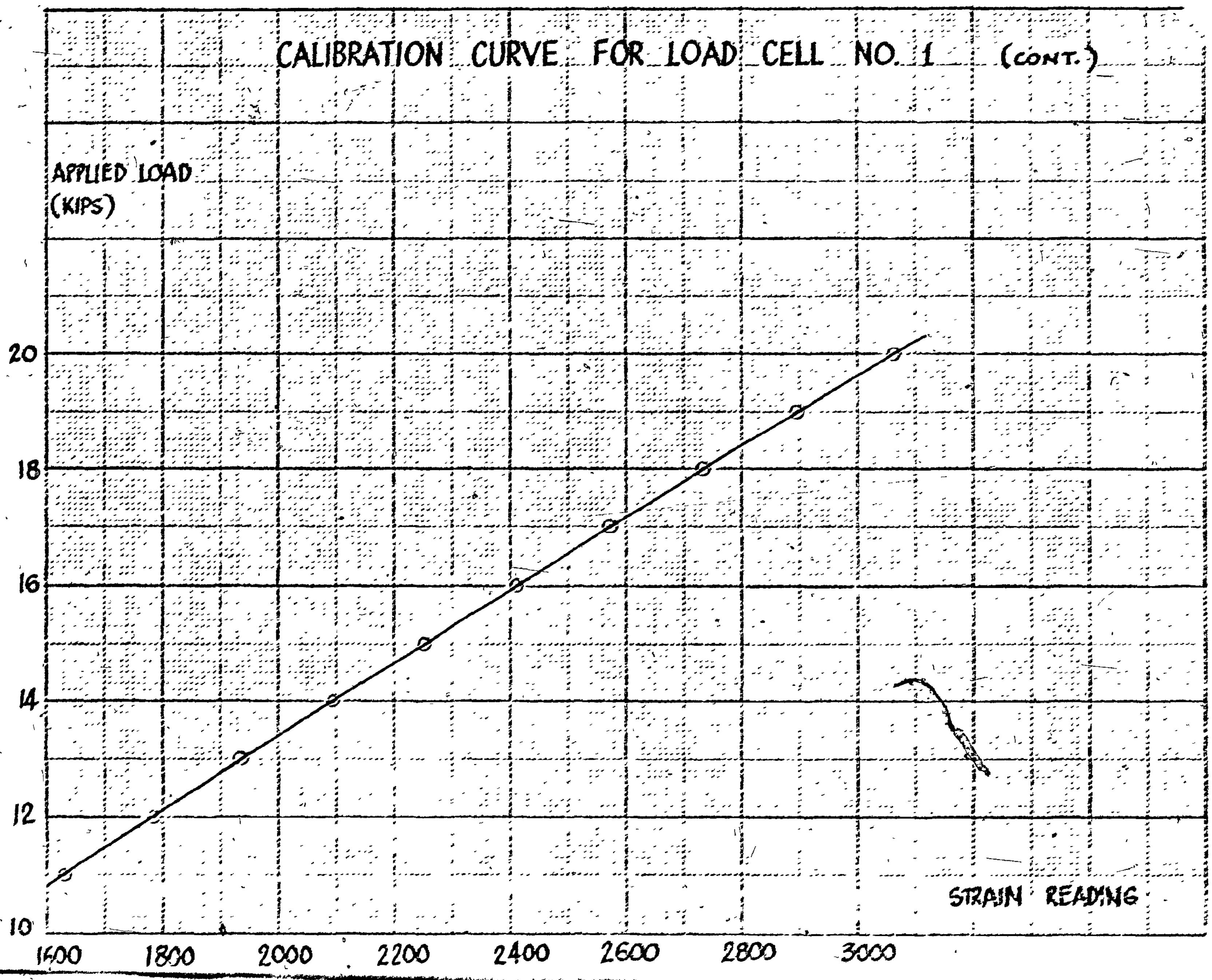
CALIBRATION CURVE FOR LOAD CELL NO. 1 (CONT.)
APPLIED LOAD
(KIPS)
STRAIN READING
10
12
14
16
18
20
1600
1800
2000
2200
2400
2600
2800
3000

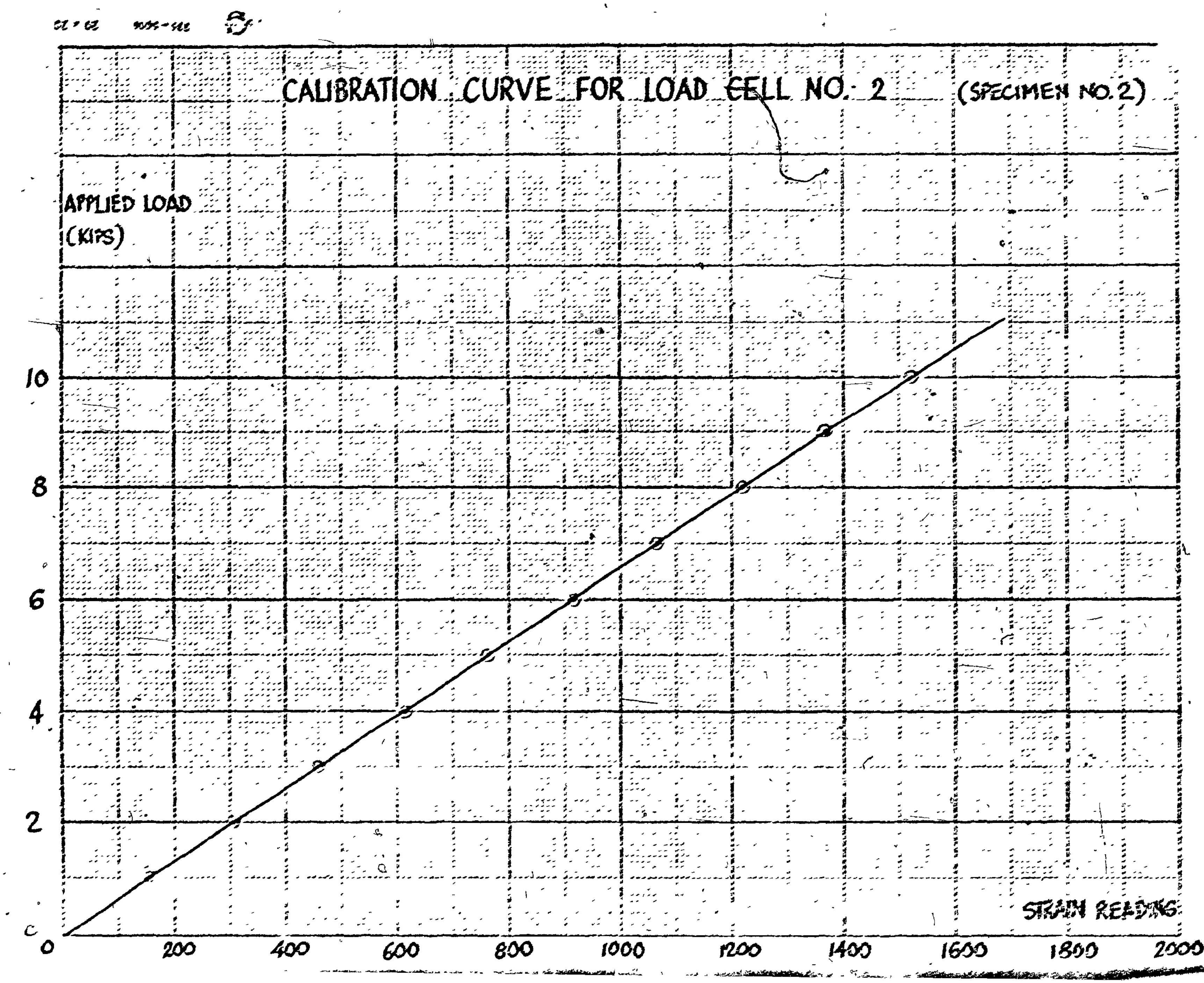
CALIBRATION CURVE FOR LOAD CELL NO. 2
(SPECIMEN NO. 2)
APPLIED LOAD
(KIPS)
10
8
6
4
2
0
200
400
600
800
1000
1200
1400
1600
1800
2000
STRAIN READING

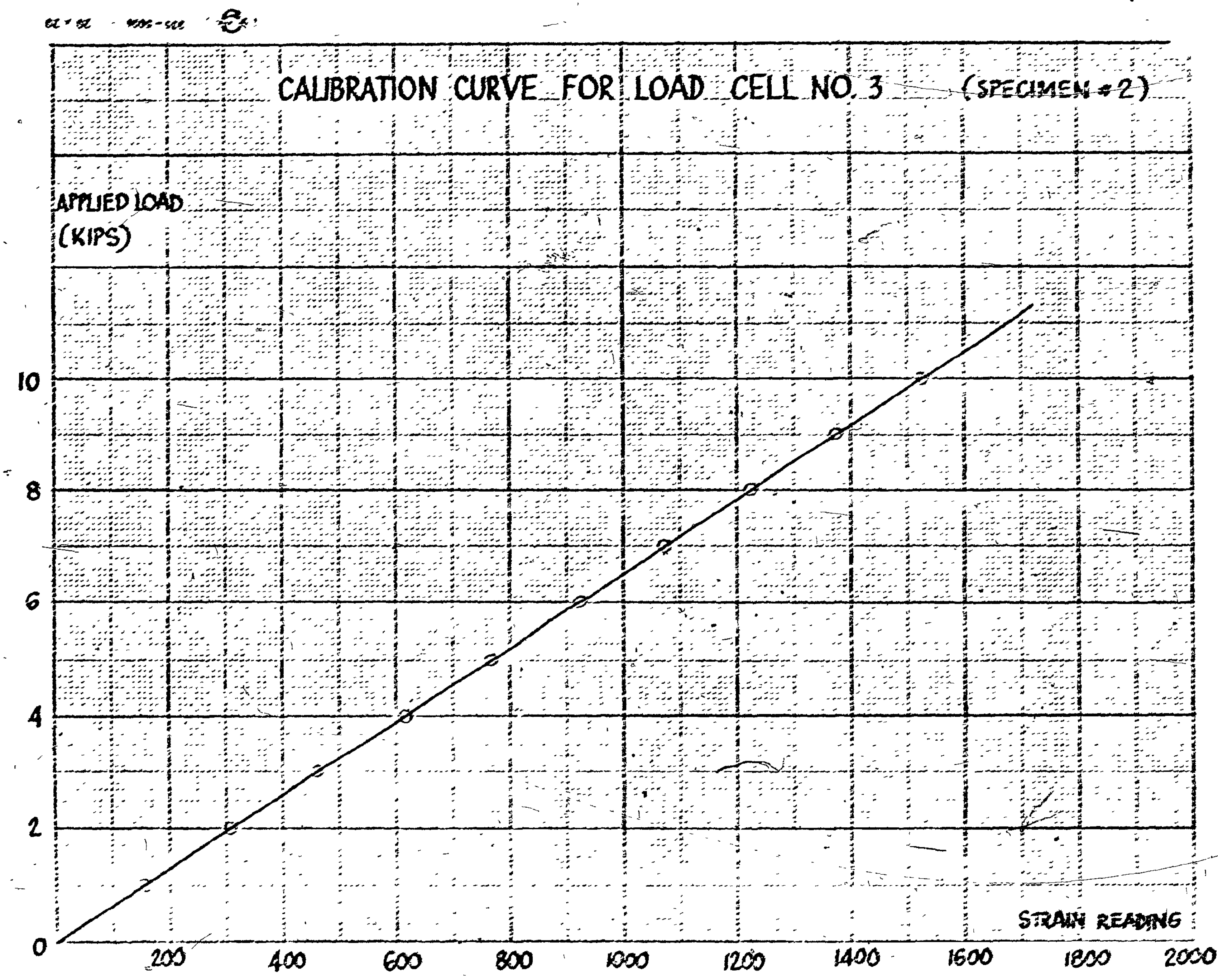
CALIBRATION CURVE FOR LOAD CELL NO. 3 (SPECIMEN # 2)
APPLIED LOAD
(KIPS)
10
8
6
4
2
0
200
400
600
800
1000
1200
1400
1600
1800
2000
STRAIN READING

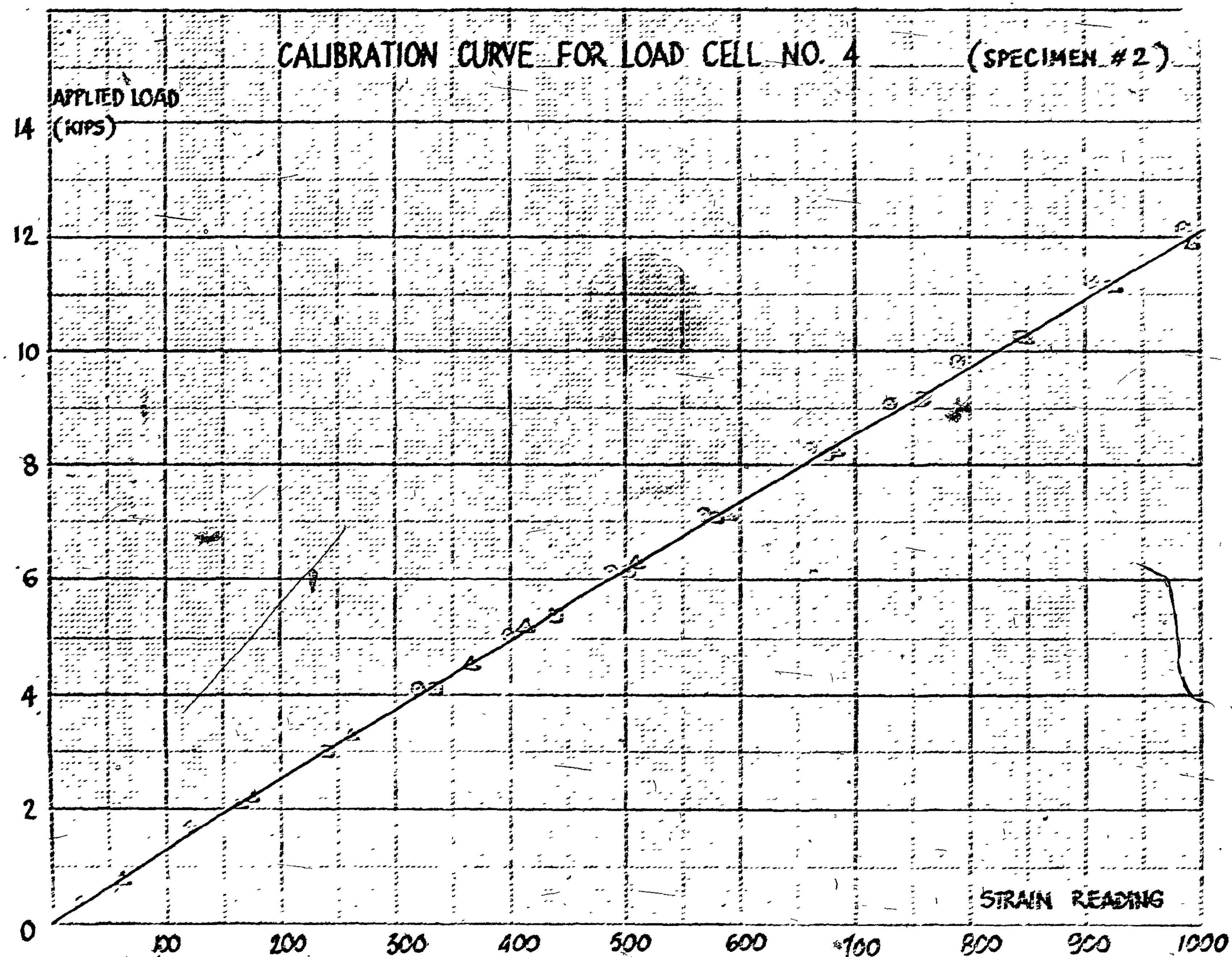
CALIBRATION CURVE FOR LOAD CELL NO. 4
(SPECIMEN #2)
APPLIED LOAD
(KIPS)
0
2
4
6
8
10
12
14
100
200
300
400
500
600
700
800
900
1000
STRAIN READING

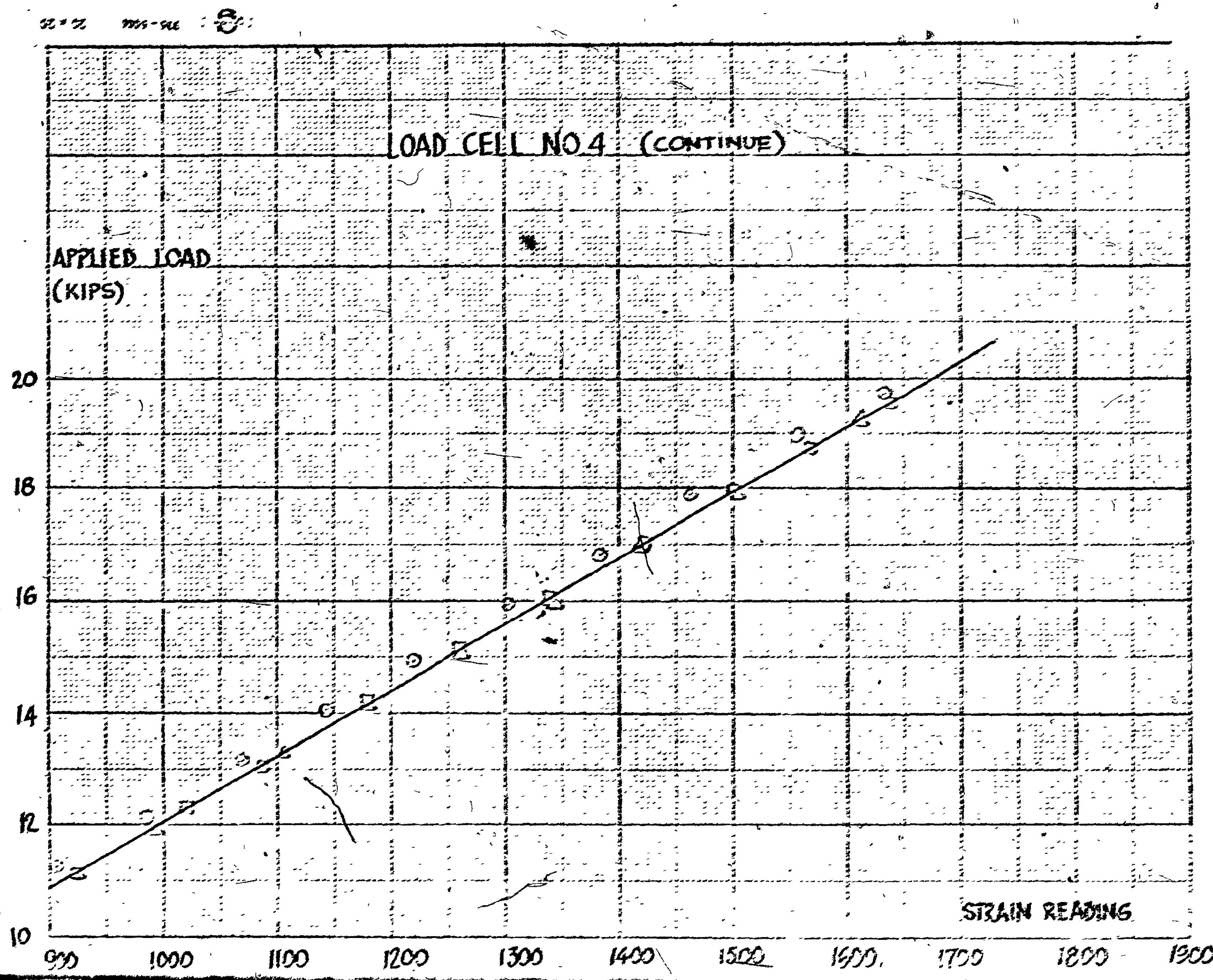
LOAD CELL NO 4 (CONTINUE)
APPLIED LOAD
(KIPS)
20
18
16
14
12
10
900
1000
1100
1200
1300
1400
1500
1600
1700
1800
1900
STRAIN READING

APPENDIX B

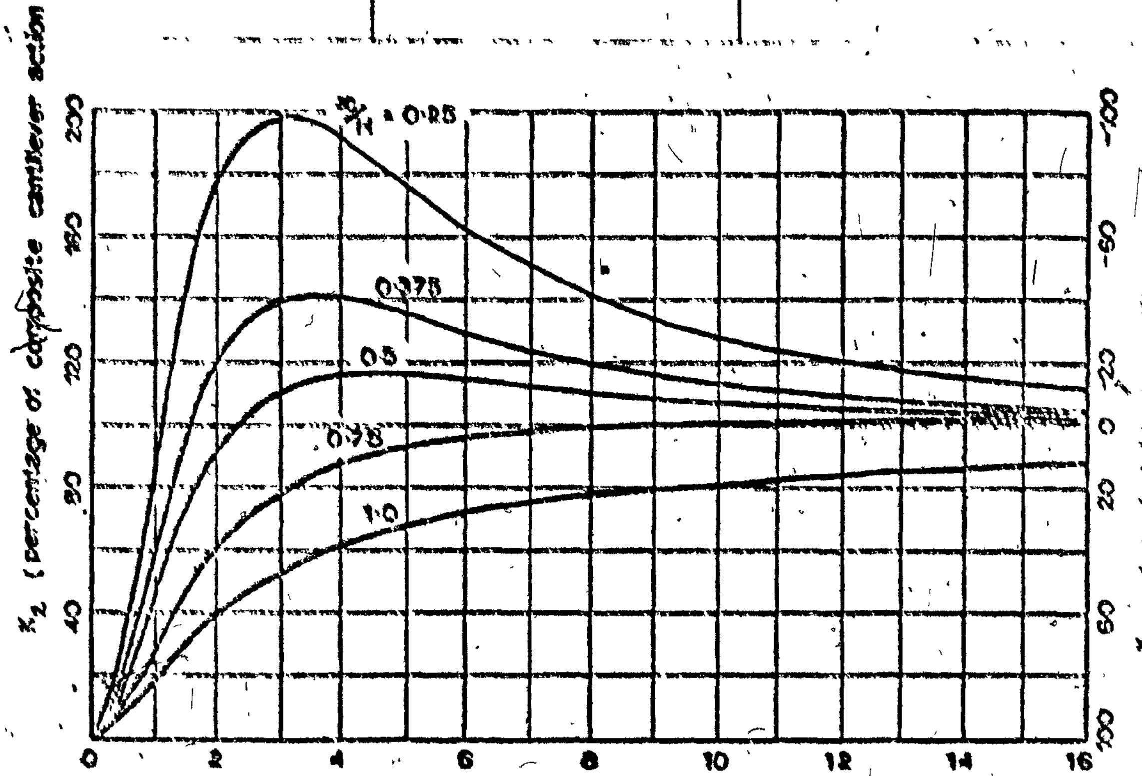

$$a^2 = \frac{12\ I}{hb^3}\ell\left(\frac{\ell^2}{I} + \frac{A}{A_1A_2}\right)$$

Fig. B.1 Variation of wall bending stress factors K_1 and K_2, Uniform Load

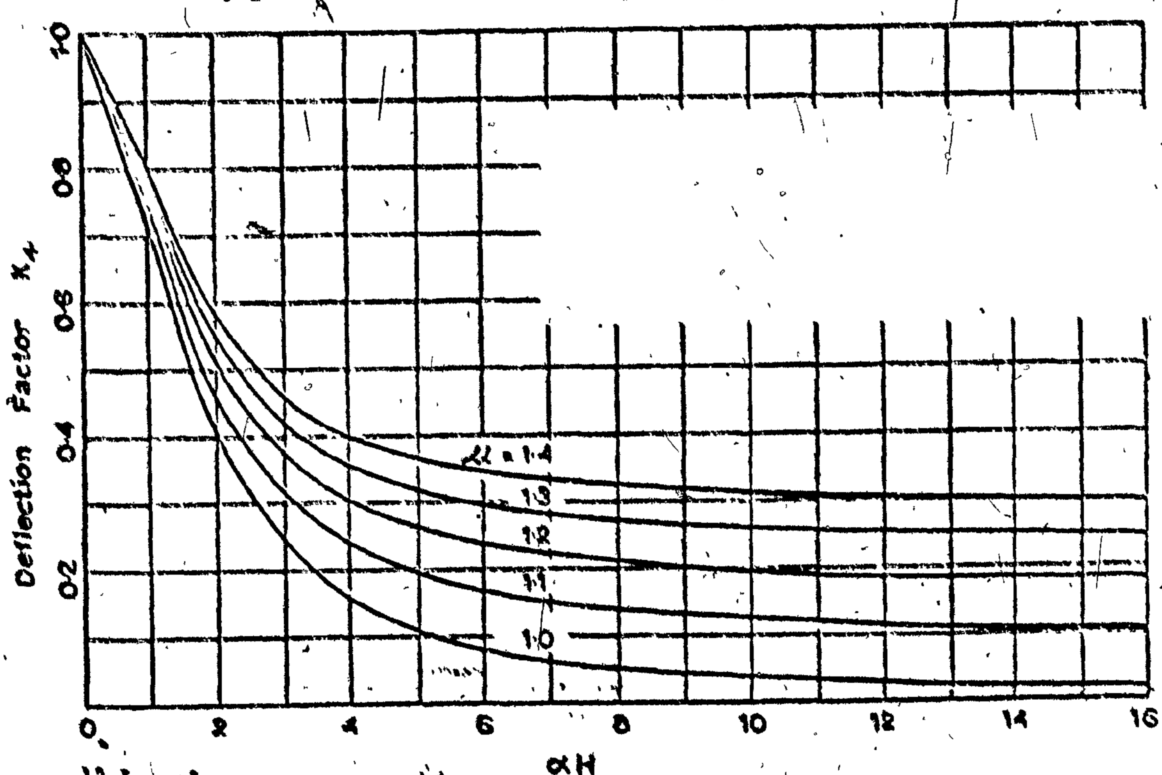

$$a^2 = \frac{12\ I}{hb}\left(\frac{\ell^2}{I} + \frac{A}{A_1A_2}\right)$$

Fig. B.2 Variation of Deflection Factor K_4, Uniform Load

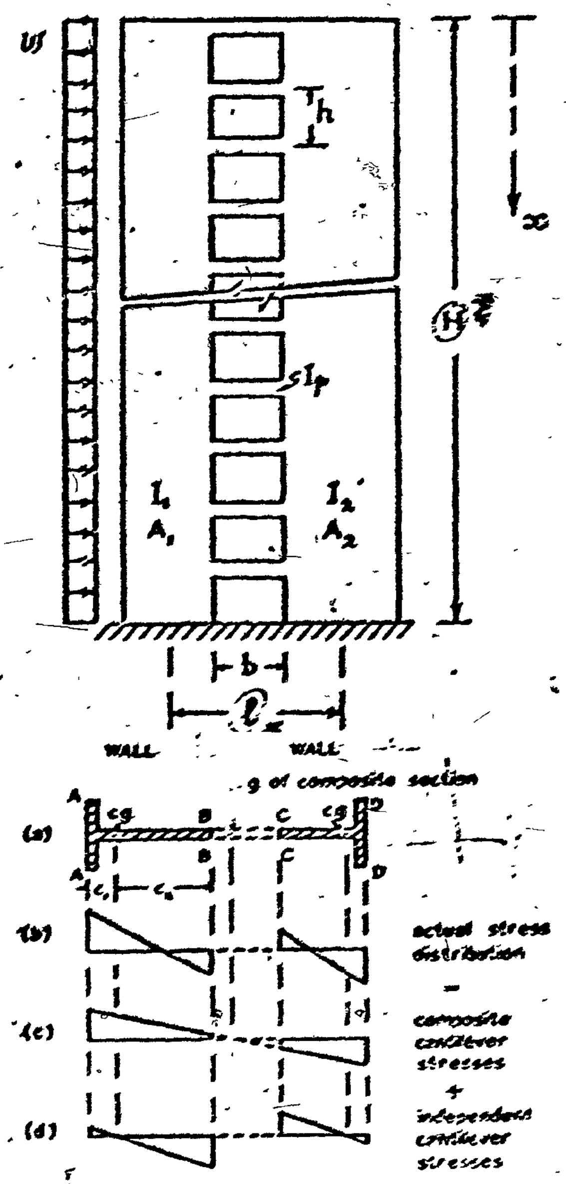

Fig. Superposition of stress distributions due to composite and individual cantilever action to give true stress distribution in walls

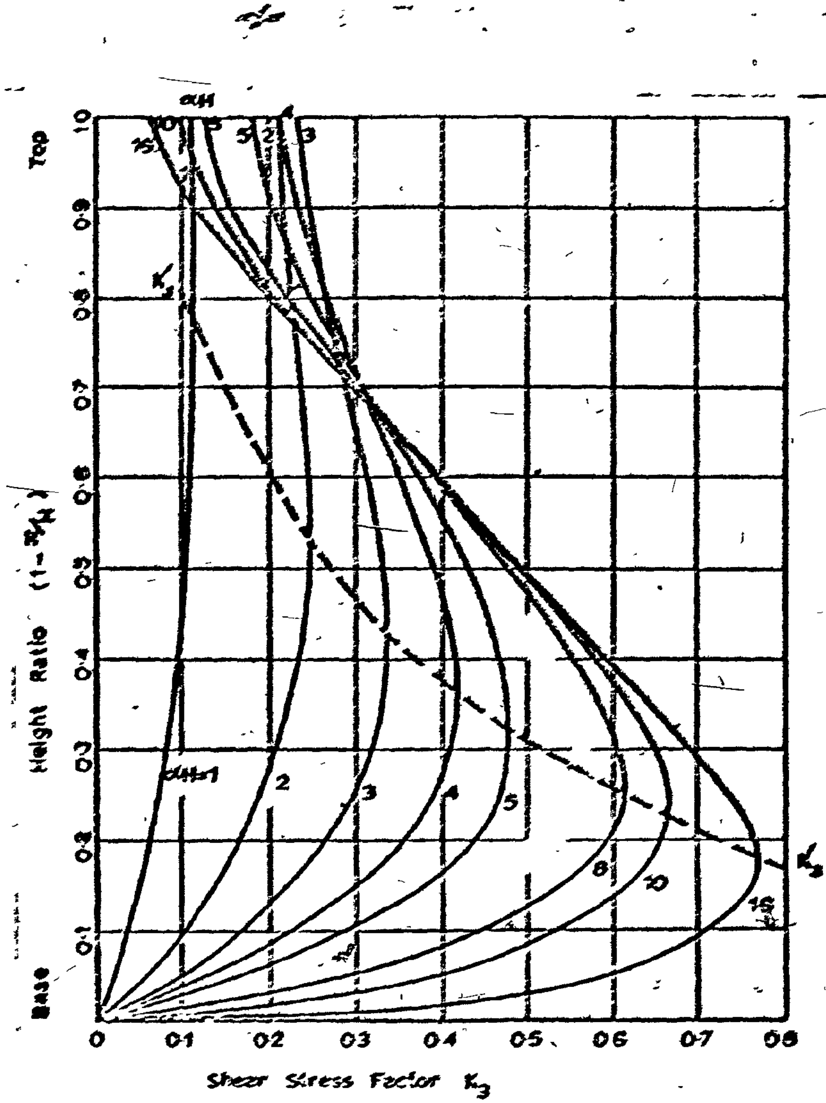

Fig. B.4 Variation of connecting beam stress factor K_3, Uniform Load.
Shear stress in connecting beams $q = w \frac{H}{l} \frac{1}{\gamma} K_3$

$$\gamma = 1 + \frac{A}{A_1 A_2} \frac{I}{l^2}$$

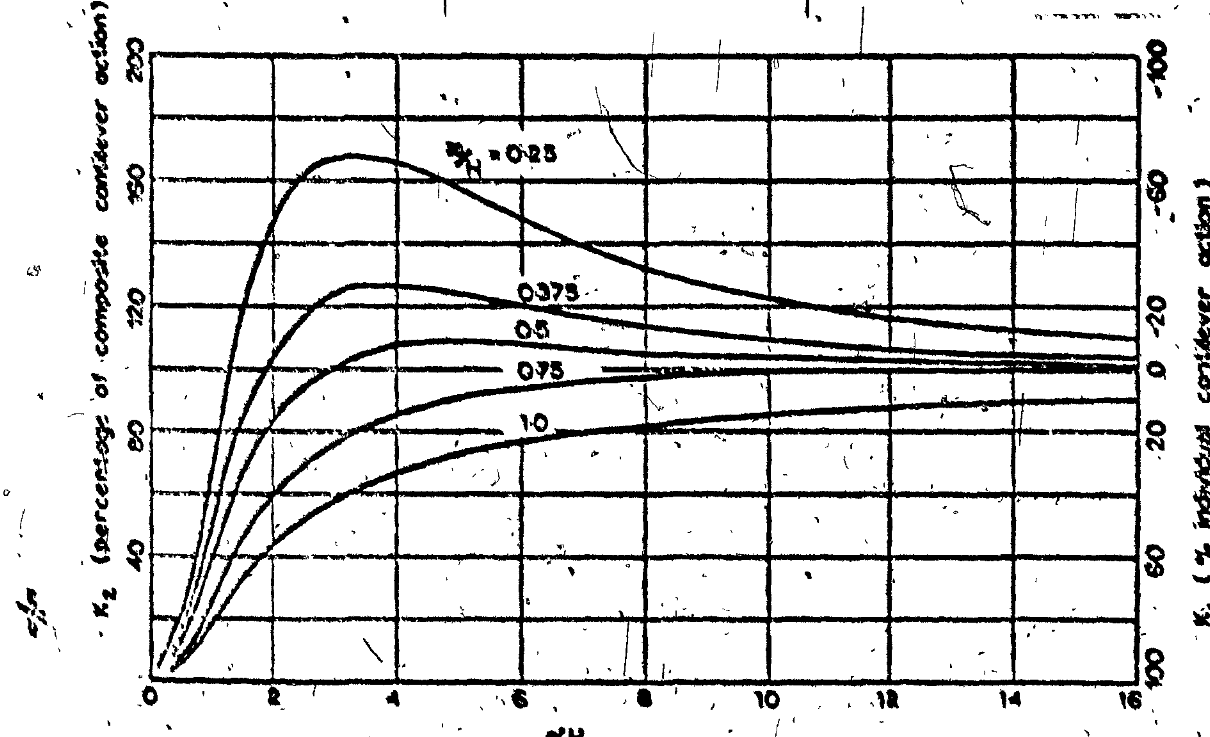

Fig. B.5 Variation of wall bending stress factors K_1 and K_2 for triangularly distributed load

$$\mu = 1 + \frac{A}{A_1 A_2} \frac{I}{\ell^2}$$

$$\alpha = \frac{12 I}{h b^3} \frac{\ell^2}{I}$$

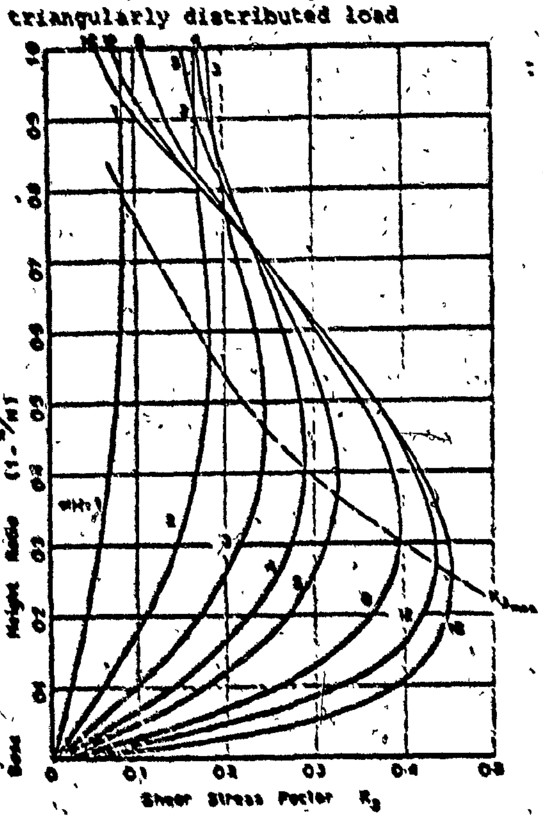

$$q = w \frac{H}{\ell} \frac{1}{\mu} K_3$$

Fig. B.6 Variation of connecting beam stress factor K_3 for triangularly distributed load

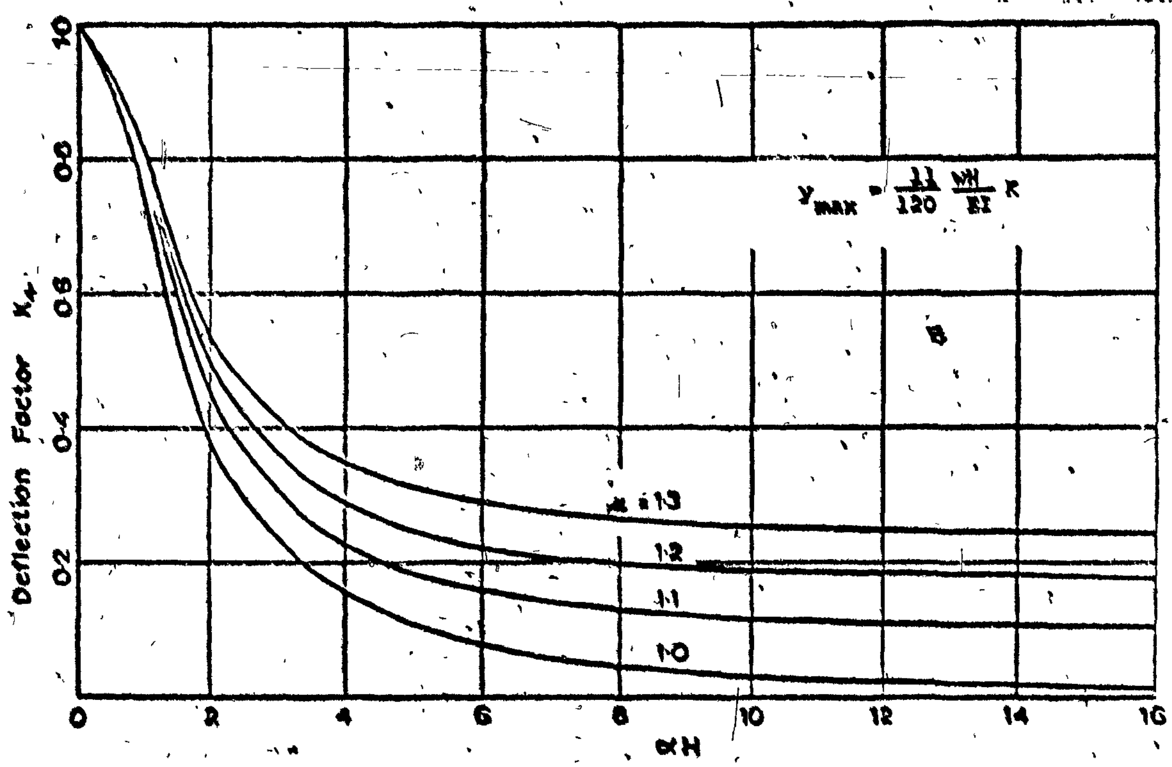

Fig. B.7 Variation of deflection factor K_4
for triangularly distributed load

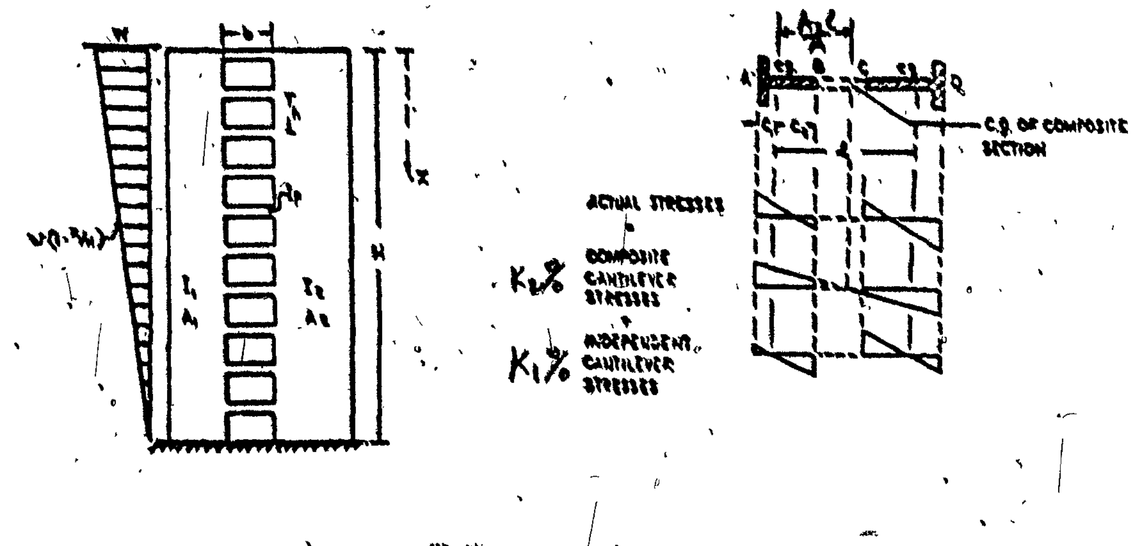

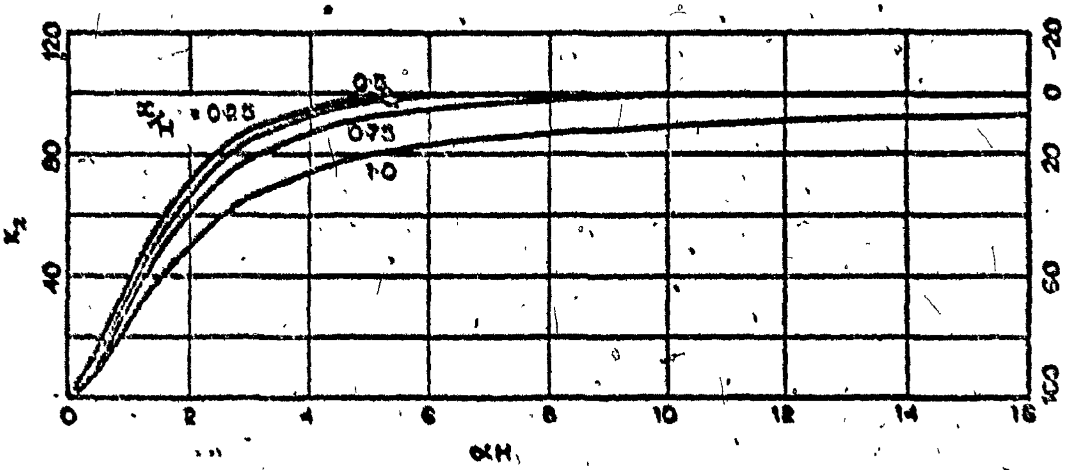

Fig. B.8 Variation of wall bending stress factors K_1 and K_2 for point load at top

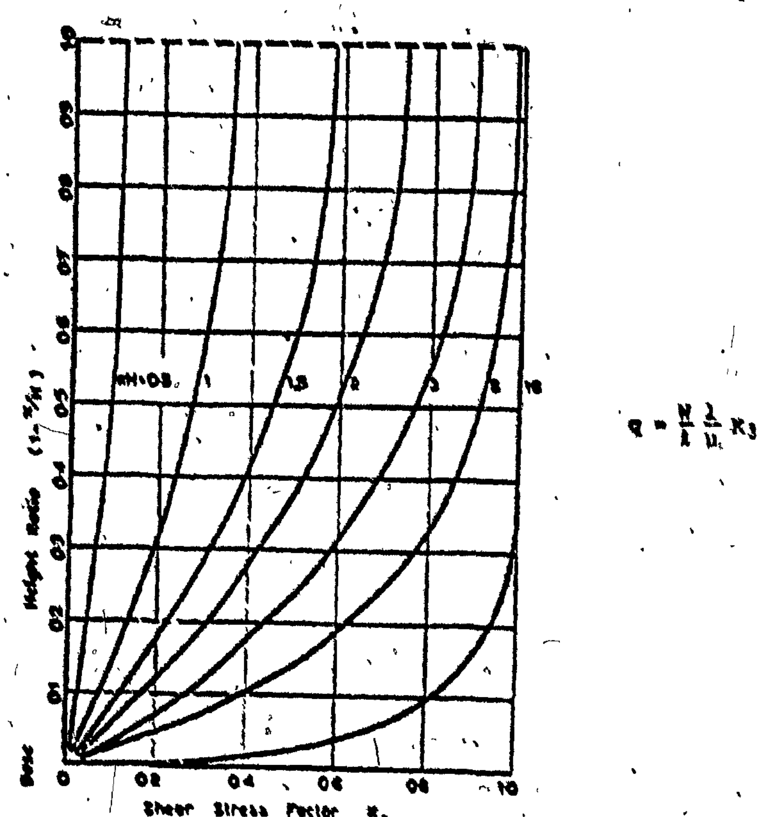

Fig. B.9 Variation of connecting beam stress factor K_3 for point load at top

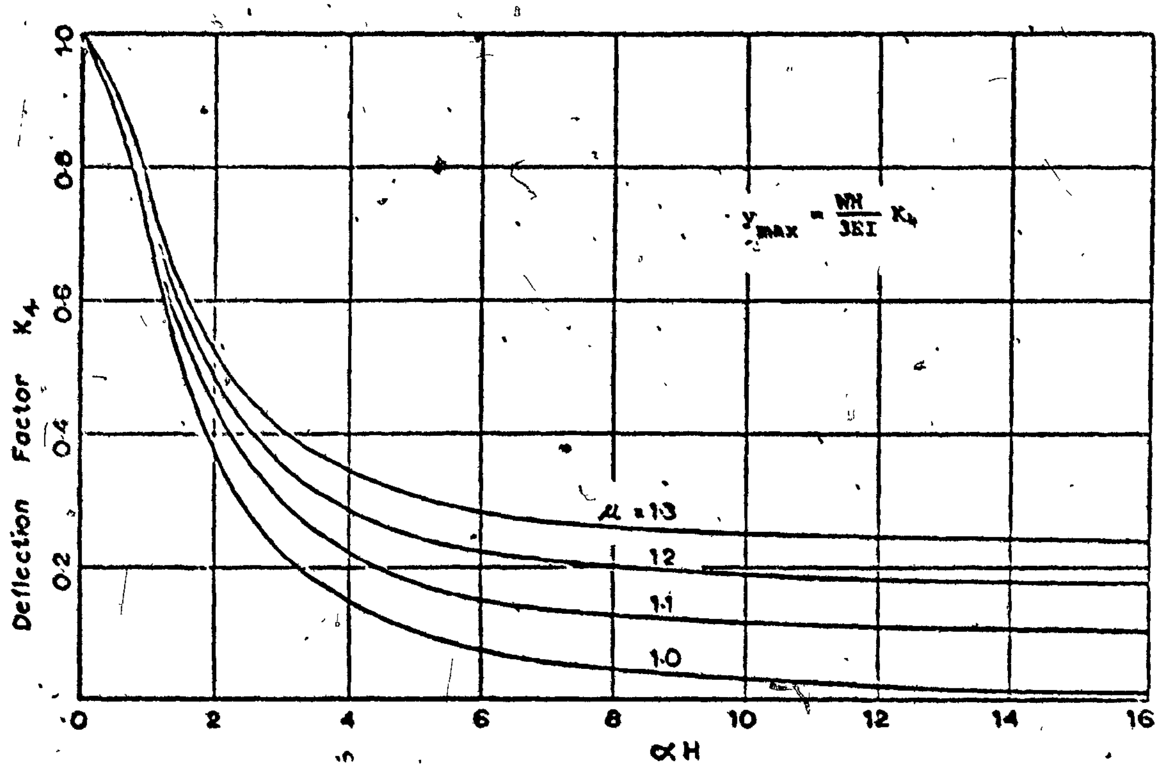

Fig. B.10 Variation of deflection factor K_4 for point load at top

APPENDIX C

SPECIMEN NO. 1

Loads on Specimen

Load Step	Load Cell #1 Total Load	Load Cell #2 (approx. side load)	Load Cell #3 (side load)	Load Cell #4 (rubber load)	Load on Specimen
0	0	0	0	0	0
1	.95	.51	.44	.1	.85
2	2.25	1.23	1.02	.24	2.01
3	3.30	1.65	1.65	.40	2.90
4	4.35	2.15	2.20	.54	3.81
5	5.35	2.68	2.67	.80	4.55
6	6.35	3.28	3.07	1.25	5.10
7					
8	7.26	3.64	3.62	1.95	5.31
9	7.55	5.80	3.75	2.15	5.40
10	7.85	3.95	3.90	2.40	5.45
11	8.12	4.05	4.07	2.65	5.47
12	8.36	4.19	4.17	2.80	5.56
13	8.62	4.31	4.31	2.95	5.67
14	8.76	4.38	4.38	3.10	5.66
15	8.93	4.48	4.45	3.20	5.73
16	9.21	4.61	4.60	3.40	5.81
17	9.47	4.73	4.74	3.65	5.82
18	9.72	4.82	4.90	3.84	5.88
19	10.09	5.00	5.09	4.19	5.90
20	10.52	5.24	5.28	4.50	6.02
21	10.88	5.45	5.43	5.00	5.88
22	11.02	5.52	5.50	5.32	5.70
23	11.75	5.88	5.87	5.93	5.82
24	11.45	5.72	5.73	6.00	5.45
25	12.18	6.06	6.12	6.75	5.43
26	12.67	6.35	6.32	7.32	5.35
27	13.35	6.68	6.67	7.85	5.50
28	13.62			8.15	5.47
29	14.00	7.05	6.95	8.55	5.45
30	14.50	7.32	7.18	9.05	5.45
31	14.70	7.42	7.28	9.33	5.37
32	14.58	7.38	7.20	9.60	4.98
33	15.10	7.65	7.45	10.12	4.98
34	15.43	7.76	7.67	10.60	4.83
35	15.95	7.88	8.07	11.06	4.89
36	17.04	8.41	8,63	11,95	5.09
37	18.53	9.17	9.36	12.25	6.28

SPECIMEN NO. 1

Lateral Deflection

	Total load	4th storey	3rd storey	2nd storey	1st storey
0	0	0	0	0	0
1	.85	.013	.007	.005	.002
2	2.01	.040	.018	.008	.005
3	2.90	.058	.084	.013	.006
4	3.81	.089	.046	.029	.011
5	4.55	.116	.0 8	.042	.015
6	5.10	.166	.102	.067	.024
7	5.25	.229	.145	.108	.033
8	5.31	.263	.167	.120	.037
9	5.40	.313	.204	.147	.046
10	5.45	.351	.232	.162	.053
11	5.47	.394	.263	.181	.057
12	5.56	.444	.299	.206	.069
13	5.67	495	.336	.231	.082
14	5.67	.543	.373	.256	.083
15	5.73	.586	.406	.277	.104
16	5.81	.635	.442	.303	.115
17	5.82	.685	.480	.327	.127
18	5.88	.734	.516	.355	.139
19	5.90	.773	.592	.404	.164
20	6.02	.933	.667	.454	.189
21	5.88	1.033	.744	.504	.212
22	5.70	1.133	.820	.555	.236
23	5.82	1.233	.907	.615	.264
24	5.45	1.333	.968	.647	.2[illegible]0
25	5.43	1.433	1.044	.703	.304
26	5.35	1.533	1.118	.752	.326
27	5.50	1.633	1.196	.805	.352
28	5.47	1.733	1.267	.851	.374
29	5.45	1.833	1.343	.903	.398
30	5.45	1.934	1.421	.955	.422
31	5.37	2.038	1.499	1.007	.448
32	4.98	2.234	1.594	1.10	.493

SPECIMEN NO.1

Dial Gauges Readings for Walls

Rotation of base at 7 1/2" from base

Loading step	WALL 1 (arm = 18 1/4") Comp.side (in.)	WALL 1 Tension side (in.)	WALL 2 (arm = 18 1/8") Comp. side (in.)	WALL 2 Tension side (in.)	Total load (kips)
0	.000	.000	.000	.000	0
1	.000	.002	.002	.002	.85
2	.001	.002	.003	.004	2.01
3	.001	.005	.004	.006	2.90
4	.002	.006	.005	.009	3.81
5	.003	.011	.006	.014	4.55
6	.006	.023	.006	.029	5.10
7	.009	.039	.008	.044	
8	.011	.050	.009	.049	5.31
9	.013	.062	.010	.059	5.40
10	.015	.074	.011	.069	5.45
11	.017	.088	.012	.080	5.47
12	.020	.100	.014	.090	5.56
13	.021	.112	.015	.099	5.67
14	.023	.125	.015	.106	5.66
15	.026	.136	.017	.113	5.73
16	.028	.149	.018	.120	5.81
17	.030	.162	.019	.129	5.82
18	.038	.174	.020	.136	5.88
19	.040	.200	.022	.154	5.90
20	.042	.226	.025	.169	6.02
21	.046	.254	.028	.190	5.88
22	.052	.281	.032	.210	5.70
23	.058	.314	.036	.226	5.82
24	.062	.333	.038	.244	5.45
25	.068	.357	.042	.267	5.43
26	.075	.382	.044	.286	5.35
27	.083	.407	.048	.311	5.50
28	.090	.430	.050	.331	5.47
29	.097	.456	.052	.354	5.45
30	.103	.483	.055	.376	5.45
31	.110	.511	.048	.401	5.37
32	.114	.535	.051	.418	4.98
33	.120	.562	.063	.435	4.98
34	.125	.587	.067	.442	5.43
35	.131	.612	.071	.450	5.95
36	.142	.663	.077	.478	

SPECIMEN NO.I

Rotation of Beams at Mid-span Sections

Loading step.	Total load	BEAM #1. (arm = 8") lower side	BEAM #1. (arm = 8") upper side	BEAM #2 (arm = 7.94") lower side	BEAM #2 (arm = 7.94") upper side	BEAM #3 (arm = 8") lower side	BEAM #3 (arm = 8") upper side	BEAM #4 (arm = 3.55" lower side
0	0	0	0	0	0	0	0	0
1	.85	.001	.001	.002	.001	.001	.002	.001
2	2.01	.002	.002	.003	.002	.002	.002	.002
3	2.90	.003	.004	.004	.003	.003	.004	.003
4	3.81	.004	.005	.005	.004	.004	.005	.004
5	4.55	.006	.006	.007	.005	.006	.006	.005
6	5.10	.011	.011	.011	.008	.009	.009	.006
7		.016	.015	.016	.013	.013	.012	.008
8	5.31	.020	.019	.020	.017	.017	.016	.010
9	5.40	.025	.022	.024	.021	.021	.020	.013
10	5.45	.029	.026	.028	.025	.025	.025	.017
11	5.47	.036	.031	.033	.030	.030	.030	.021
12	5.56	.041	.032	.037	.034	.034	.034	.024
13	5.67	.046	.036	.041	.038	.039	.038	.028
14	5.66	.050	.039	.046	.042	.043	.042	.029
15	5.73	.054	.042	.050	.044	.048	.046	.034
16	5.81	.059	.046	.055	.048	.052	.050	.037
17	5.82	.063	.050	.060	.052	.057	.054	.041
18	5.88	.068	.054	.064	.055	.062	.058	.044
19	5.90	.077	.062	.074	.063	.072	.067	.047
20	6.02	.087	.070	.083	.071	.081	.075	.063
21	5.88	.092	.079	.096	.080	.092	.083	.066
22	5.70	.092	.083	.107	.090	.102	.090	.072
23	5.82	.093	.086	.122	.101	.114	.100	.075
24	5.45	.093	.090	.127	.112	.123	.107	.078
25	5.43	.095	.093	.134	.124	.132	.117	.084
26	5.35	.099	.102	.145	.136	.138	.128	.091
27	5.50	.104	.110	.156	.147	.145	.140	.094
28	5.47	.109	.120	.165	.156	.153	.148	.097
29	5.45	.115	.130	.176	.165	.162	.157	.099
30	5.45	.124	.140	.186	.174	.174	.165	.106
31	5.37	.134	.152	.196	.183	.179	.173	.093
32	4.98	.142	.161	.204	.192	.186	.179	.087
33	4.98	.152	.171	.213	.200	.194	.186	.080
34	5.43	.160	.180	.222	.209	.202	.194	.072
35	5.45	.170	.190	.231	.217	.211		.069

SPECIMEN NO. 1

Calculated Rotational Angles

Step	Load	Wall 1 Sect.dist.7½" from base	Wall 2 Sect.dist.7½" from base	Beam #4	Beam #2	Beam #2	Beam #4
0	0	0.0	0.0	0.0	0.0	0.0	0.0
1	.85	.00011	.00022	.00025	.00035	.00030	.00027
2	2.01	.00020	.00039	.00050	.00063	.00050	.00055
3	2.90	.00033	.00055	.000875	.00088	.000875	.00082
4	3.81	.00044	.00077	.001125	.00113	.001125	.00109
5	4.55	.00077	.00110	.00150	.00151	.00150	.00137
6	5.10	.00160	.00190	.00275	.00249	.00225	.00164
7	5.25	.00265	.00287	.00388	.00366	.00313	.00219
8	5.31	.00337	.00320	.00488	.00418	.00412	.00273
9	5.40	.00414	.00380	.00588	.00567	.00513	.00355
10	5.45	.00492	.00436	.00687	.00668	.00625	.00464
11	5.47	.00580	.00507	.00837	.00795	.00750	.00574
12	5.56	.00663	.00573	.00913	.00895	.00850	.00656
13	5.67	.00734	.00628	.01025	.00995	.00963	.00765
14	5.66	.00817	.00667	.01110	.01110	.01062	.00792
15	5.73	.00894	.00717	.0120	.01185	.01175	.00929
16	5.81	.00977	.00760	.0131	.0130	.01275	.01011
17	5.82	.01060	.00816	.0141	.0141	.0139	.01120
18	5.88	.01170	.00860	.0153	.0150	.0150	.01202
19	5.90	.0132	.00970	.0174	.0173	.01735	.01284
20	6.02	.0148	.01070	.0196	.0195	.0195	.01721
21	5.88	.0166	.0120	.0214	.0222	.0219	.01803
22	5.70	.0184	.0133	.0219	.0248	.0240	.01967
23	5.82	.0205	.0144	.0224	.0281	.0268	.02049
24	5.45	.0218	.0155	.0229	.0301	.0287	.02131
25	5.43	.0235	.0170	.0235	.0325	.0312	.02295
26	5.35	.0252	.0182	.0251	.0354	.03325	.02486
27	5.50	.0271	.0198	.0267	.0382	.0356	.02568
28	5.47	.0287	.0210	.0286	.0405	.0376	.02650
29	5.45	.0305	.0224	.0306	.0430	.0399	.02705
30	5.45	.0324	.0238	.0330	.0453	.0424	.02896
31	5.37	.0343	.0248	.0358	.0478	.0440	.02541
32	4.98	.0358	.0254	.0379	.0499	.0457	.02377
33	4.98	.0376	.0275	.0404	.0521	.0475	.02186
34	4.83	.0393	.0281	.0425	.0543	.0495	.01967

SPECIMEN NO. 2

Load on Load Cells, Rubber and Shear Wall

Load step	Load Cell #1 strain reading	Load Cell #1 load	Load Cell #2 strain reading	Load Cell #2 north side load	Load Cell #3 strain reading	Load Cell #3 south side load	Load Cell #4 strain reading	Load Cell #4 rubber load	load on shear wall
0	0	0	0	0	0	0	0	0	0
1	108	.70	58	.36	64	.40	0	0	.73
2	173	1.12	94	.60	99	.61	0	0	1.16
3	232	1.54	128	.82	137	.88	0	0	1.62
4	326	2.21	180	1.16	189	1.21	3	.03	2.26
5	385	2.63	213	1.39	220	1.42	3	.03	2.69
6	446	3.05	247	1.61	253	1.63	5	.06	3.08
7	509	3.49	283	1.84	286	1.85	6	.06	3.53
8	616	4.23	343	2.23	341	2.20	16	.20	4.13
9	673	4.62	375	2.45	369	2.39	16	.20	4.53
10	766	5.26	426	2.79	416	2.70	28	.35	5.03
11	815	5.60	452	2.95	441	2.85	38	.49	5.21
12	887	6.08	490	3.20	479	3.10	53	.68	5.51
13	980	6.70	543	3.53	522	3.38	77	.98	5.83
14	1041	7.10	575	3.75	555	3.60	94	1.21	6.02
15	1085	7.40	598	3.89	580	3.75	117	1.50	6.02
16	1125	7.65	617	4.02	601	3.89	135	1.72	6.06
17	1177	8.00	644	4.20	629	4.08	152	1.93	6.21
18	1214	8.25	663	4.32	649	4.20	171	2.16	6.23
19	1249	8.50	681	4.43	668	4.32	190	2.40	6.22
20	1294	8.80	702	4.56	694	4.50	211	2.65	6.28
21	1348	9.17	730	4.75	719	4.67	234	2.93	6.37
22	1376	9.35	739	4.81	744	4.85	248	3.10	6.41
23	1446	9.81	779	5.10	782	5.10	278	3.47	6.54
24	1506	10.20	809	5.30	812	5.29	308	3.85	6.55
25	1566	10.58	834	5.48	839	5.45	333	4.12	6.64
26	1636	11.06	874	5.75	855	5.55	363	4.50	6.68
27	1696	11.41	899	5.89	906	5.89	393	4.85	6.75
28	1726	11.62	914	6.00	915	5.94	408	5.04	6.74
29	1816	12.20	964	6.31	965	6.27	453	5.60	6.79
30	1856	12.45	979	6.41	980	6.35	488	6.00	6.60
31	1911	12.82	1014	6.66	1015	6.60	518	6.47	6.57
32	1946	13.05	1029	6.75	1025	6.65	538	6.60	6.63
33	1986	13.32	1044	6.85	1050	6.82	568	6.95	6.55
34	2066	13.82	1084	7.11	1080	7.02	608	7.42	6.56
35	2111	14.11	1109	7.27	1115	7.25	632	7.71	6.61
36	2176	14.51	1139	7.47	1145	7.45	668	8.13	6.59
37	2221	14.80	1159	7.60	1165	7.59	698	8.49	6.51
38	2306	15.33	1204	7.91	1205	7.85	738	8.98	6.57
39	2361	15.66	1231	8.08	1235	8.05	778	9.45	6.44
40	2366	15.71	1234	8.10	1230	8.03	841	10.18	5.74
41	2446	16.21	1269	8.32	1250	8.15	863	10.46	5.89
42	8986		1289	8.46	1255	8.20	913	11.05	5.40
43	7166		1354	8.90	1350	8.82	1018	12.26	5.25
44	7356		1419	9.31	1410	9.22	1068	12.85	5.47

SPECIMEN NO. 2

Lateral Deflection

Loading step	Total load	4th storey deflection dial gauge reading	3rd storey deflection dial gauge reading	2nd storey deflection dial gauge reading	1st storey deflection dial gauge reading
0	0	0	0	0	0
1	.73	.016	.011	.007	.003
2	1.16	.032	.022	.014	.006
3	1.62	.050	.035	.021	.008
4	2.26	.066	.047	.028	.012
5	2.69	.080	.057	.033	.014
6	3.08	.085	.064	.038	.015
7	3.53	.108	.078	.047	.018
8	4.13	.136	.100	.062	.026
9	4.53	.153	.114	.071	.031
10	5.03	.182	.136	.086	.040
11	5.21	.215	.153	.098	.046
12	5.51	.240	.180	.119	.056
13	5.83	.303	.225	.150	.075
14	6.02	.357	.263	.176	.089
15	6.02	.413	.301	.204	.105
16	6.06	.477	.356	.234	.122
17	6.21	.517	.394	.259	.135
18	6.23	.581	.438	.284	.149
19	6.23	.642	.483	.313	.163
20	6.28	.723	.547	.352	.183
21	6.37	.786	.603	.385	.202
22	6.41	.873	.662	.421	.222
23	6.54	.935	.711	.451	.238
24	6.55	1.020	.775	.489	.258
25	6.64	1.100	.835	.524	.276
26	6.68	1.181	.896	.564	.297
27	6.75	1.268	.963	.605	.318
28	6.74	1.350	1.026	.643	.338
29	6.79	1.439	1.092	.684	.361
30	6.60	1.529	1.162	.727	.384
31	6.57	1.620	1.232	.771	.407
32	6.63	1.701	1.295	.809	.428
33	6.55	1.799	1.370	.855	.451
34	6.56	1.883	1.457	.895	.472
35	6.61	1.972	1.504	.937	.494
36	6.59	2.055	1.568	.977	.514
37	6.51	2.156	1.644	1.024	.539
38	6.57	2.244	1.712	1.066	.561
39	6.44	2.358	1.798	1.120	.590
40	5.94	2.491	1.904	1.187	.626
41	5.89	2.592	1.982	1.237	.651
42	5.40	2.747	2.099	1.207	.704
43	5.25	2.964	2.276	1.439	.782

SPECIMEN NO. 2

Dial Gauges Readings of Walls

Rotation of Section Distance 7½" from base

Load -ing step	Load on speci -men	WALL 1					WALL 2				
		Comp. side (in.)	Ang. strain	Ten-sion side	Ang. strain	Angle of rota-tion	Comp. side (in.)	Ang. strain	Ten-sion side	Ang. strain	Angle of ro-tation
0	0	0	0	0	0						
1	.73	.001	.000133	0	0	.0000573	.001	.000133	.001	.000133	.00011
2	1.16	.002	.000267	.001	.000133	.000172	.003	.000400	.003	.000267	.00023
3	1.62	.003	.000400	.002	.000267	.00028674	.003	.000400	.003	.000400	.00034
4	2.26	.004	.000533	.003	.000400	.0004014	.004	.000533	.009	.001200	.00074
5	2.69	.004	.000533	.005	.000667	.0005161	.004	.000533	.010	.001333	.00080
6	3.08	.005	.000667	.006	.000800	.0006308	.005	.000667	.011	.001467	.00092
7	3.53	.006	.000800	.008	.001067	.0008029	.006	.000800	.012	.001600	.00103
8	4.13	.007	.000933	.012	.001600	.0010896	.006	.000800	.014	.001867	.00115
9	4.53	.009	.001200	.014	.001867	.001319	.007	.000933	.016	.002133	.00132
10	5.03	.010	.001333	.019	.002533	.001663	.007	.000933	.019	.002533	.00149
11	5.21	.011	.001467	.023	.003067	.001950	.007	.000933	.029	.003867	.00207
12	5.51	.013	.001733	.031	.004133	.002581	.007	.000933	.035	.004667	.00241
13	5.83	.016	.002133	.043	.005733	.003384	.006	.000800	.053	.007067	.00339
14	6.02	.018	.002400	.051	.006800	.003957	.006	.000800	.062	.008267	.00391
15	6.02	.020	.002667	.067	.008933	.004989	.000	.000000	.088	.011733	.00506
16	6.06	.023	.003067	.081	.010800	.005964	-.012	-.001600	.216	.028800	.01174
17	6.21	.026	.003467	.093	.012400	.006824	-.018	-.002400	.231	.030800	.01225
18	6.23	.028	.003733	.105	.014000	.007627	-.019	-.002533	.235	.031333	.01243
19	6.22	.031	.004133	.120	.016000	.008659	-.019	-.002533	.241	.032133	.01277
20	6.28	.035	.004667	.140	.018667	.010036	-.017	-.002267	.246	.032800	.01318
21	6.37	.038	.005067	.160	.021333	.011355	-.015	-.002000	.250	.033333	.01362
22	6.41	.042	.005600	.179	.023867	.012674	-.013	-.001733	.271	.036133	.01484
23	6.54	.045	.006000	.196	.026133	.013821	-.011	-.001467	.284	.037867	.01571
24	6.55	.049	.006533	.218	.029067	.015312	-.006	-.000800	.296	.038467	.01669
25	6.64	.053	.007067	.238	.031733	.016688	-.003	-.000400	.308	.041067	.01755
26	6.68	.057	.007600	.258	.034400	.018065	.000	.000000	.319	.042533	.01836
27	6.75	.061	.008133	.281	.037467	.019613	.002	.000267	.335	.044667	.01939
28	6.74	.066	.008800	.300	.040000	.020989	.004	.000533	.343	.045733	.01997
29	6.79	.071	.009467	.324	.043200	.022652	.007	.000933	.355	.047333	.02083
30	6.60	.075	.010000	.348	.046400	.024258	.008	.001067	.383	.051067	.02250
31	6.57	.080	.010667	.371	.049467	.025864	.011	.001467	.403	.053733	.02362
32	6.63	.084	.011200	.393	.052400	.027355	.013	.001733	.419	.055867	.02486
33	6.55	.089		.418	.055733	.029075	.017	.002267	.430	.057383	.02572
34	6.56	.094		.441	.058800	.030681	.019	.002533	.440	.058667	.02641
35	6.61	.099		.463	.061733	.032229	.022	.002933	.454	.060533	.02739
36	6.59	.104		.484	.064533	.033720	.025	.003333	.474	.063200	.02871
37	6.51	.110		.488	.065067	.034894	.026	.003467	.490	.065333	.02969
38	6.57	.116		.534	.071200	.037276	.027	.003600	.503	.067067	.03050
39	6.44	.123		.563	.075067	.039341	.032	.004267	.520	.069333	.03077
40	5.74	.130		.607	.080933	.042265	.041	.005467	.538	.071733	.03332
41	5.89	.136		.533	.084400	.044100	.048	.006400	.552	.073600	.03453
42	5.40	.149		.666	.088800	.046738	.062	.008267	.571	.076133	.03643
43	5.25	.173		.701	.093467	.050122	.072	.009600	.609	.081200	.03919

SPECIMEN NO. 2

Rotation of Beams at Mid-span Sections

Loading step	Load applied	Beam #1 (lowest) lower side	Beam #1 (lowest) upper side	Beam #2 lower side	Beam #2 upper side	Beam #3 lower side	Beam #3 upper side	Beam #4 lower side
0	0	0	0	0	0	0	0	0
1	.73	.001	.001	.001	.001	.001	.001	.000
2	1.16	.003	.002	.001	.002	.002	.002	.001
3	1.62	.003	.002	.002	.003	.003	.003	.001
4	2.26	.004	.003	.003	.004	.004	.004	.002
5	2.69	.005	.004	.003	.004	.005	.004	.002
6	3.08	.006	.005	.004	.005	.005	.005	.003
7	3.53	.007	.006	.005	.005	.006	.006	.003
8	4.13	.008	.007	.006	.006	.007	.006	.004
9	4.53	.009	.008	.007	.007	.008	.007	.004
10	5.03	.011	.010	.008	.008	.009	.008	.005
11	5.21	.013	.011	.009	.009	.010	.010	.005
12	5.51	.016	.013	.010	.011	.012	.011	.006
13	5.83	.020	.018	.014	.015	.015	.013	.009
14	6.02	.023	.021	.018	.019	.017	.018	.011
15	6.02	.025	.024	.022	.021	.022	.021	.013
16	6. 6	.032	.026	.023	.023	.024	.023	.014
17	6.21	.033	.028	.025	.025	.026	.025	.016
18	6.23	.036	.030	.029	.029	.030	.029	.018
19	6.22	.041	.036	.035	.034	.035	.033	.022
20	6.28	.057	.043	.042	.041	.042	.039	.027
21	6.37	.055	.049	.049	.047	.051	.047	.032
22	6.41	.061	.054	.055	.053	.055	.053	.037
23	6.54	.066	.058	.060	.058	.059	.058	.040
24	6.55	.075	.063	.065	.064	.065	.063	.044
25	6.64	.077	.068	.072	.069	.071	.069	.052
26	6.68	.084	.074	.078	.075	.078	.076	.053
27	6.75	.091	.081	.086	.083	.087	.084	.061
28	6.74	.098	.087	.094	.089	.094	.092	.064
29	6.79	.106	.094	.102	.098	.103	.100	.070
30	6.60	[illegible]	.100	.109	.105	.110	.108	.075
31	6.57	.123	.108	.119	.113	.119	.117	.081
32	6.63	.131	.115	.128	.121	.128	.127	.087
33	6.55	.139	.123	.138	.132	.138	.138	.093
34	6.56	.148	.123	.149	.142	.148	.148	.098
35	6,61	.156	.132	.159	.151	.158	.157	.104
36	6.59	.167	.139	.168	.159	.167	.165	.110
37	6.51	.176	.147	.179	.169	.178	.176	.117
38	6.57	.186	.156	.189	.179	.188	.186	.123
39	6.44	.201	.165	.202	.192	.201	.199	.132
40	5.74	.222	.176	.219	.208	.219	.215	.144
41	5.89	.235	.192	.232	.220	.232	.227	.152
42	5.40	.252	.202	.250	.226	.251	.244	.165
43	5.25	.269	.216	.274	.277	.285	.262	.175

SPECIMEN NO. 2

Calculated Rotational Angles (Radians)

Loading step	Total load	Beam #1 (lowest)	Beam #2	Beam #3	Beam #4
0	0	0.00000	0.00000	0.00000	0.00000
1	.73	.00025	.00025	.00025	.00000
2	1.16	.00062	.00038	.00050	.00027
3	1.62	.00062	.00063	.00075	.00027
4	2.26	.00087	.00088	.00100	.00055
5	2.69	.00112	.00088	.00112	.00055
6	3.08	.00137	.00113	.00125	.00082
7	3.53	.00162	.00125	.00150	.00082
8	4.13	.00187	.00151	.00162	.00109
9	4.53	.00212	.00176	.00187	.00109
10	5.03	.00262	.00202	.00212	.00137
11	5.21	.00300	.00227	.00250	.00137
12	5.51	.00362	.00265	.00275	.00164
13	5.83	.00475	.00363	.00350	.00246
14	6.02	.00550	.00466	.00463	.00300
15	6.02	.00613	.00542	.00537	.00355
16	6.06	.00725	.00579	.00587	.00382
17	6.21	.00762	.00630	.00637	.00437
18	6.23	.00825	.00731	.00737	.00492
19	6.22	.00963	.00869	.00850	.00601
20	6. 8	.01250	.01047	.01013	.00738
21	6.37	.01300	.01209	.01225	.00874
22	6.41	.01440	.01360	.01350	.01011
23	6.54	.01550	.01486	.01463	.01093
24	6.55	.01730	.01625	.01600	.01202
25	6.64	.01813	.01776	.01750	.01428
26	6.68	.01975	.01928	.01925	.01448
27	6.75	.02150	.02129	.02137	.01667
28	6.74	.02313	.02305	.02325	.01749
29	6.79	.02500	.02520	.02537	.01913
30	6.60	.02680	.02696	.02725	.02049
31	6.57	.02890	.02928	.02950	.02213
32	6.63	.03080	.03137	.03188	.02377
33	6.55	.03280	.03402	.03450	.02541
34	6.56	.03398	.03666	.03700	.02677
35	6.61	.03600	.03905	.03938	.02841
36	6.59	.03738	.04119	.04150	.03005
37	6.51	.04038	.04384	.04425	.03196
38	6.57	.04275	.04636	.04675	.03360
39	6.44	.04575	.04963	.05000	.03606
40	5.74	.04975	.05379	.05425	.03934
41	5.89	.05338	.05694	.05737	.04153
42	5.40	.05675	.05996	.06187	.04508
43	5.25	.06061	.06941	.06837	.04781

SPECIMEN NO. 3

Load on Load Cells, Rubber and Shear Wall

Load step	Load Cell #1 strain reading	Load Cell #1 load	Load Cell #6 strain reading	Load Cell #6 south side load	Load Cell #3 strain reading	Load Cell #3 north side load	Load Cell #4 strain reading	Load Cell #4 load on rubber	load on shear wall
0	0	0	0	0	0	0	0	0	0
1	72	.49	9	.04	59	.39	2	.02	.44
2	381	2.55	202	1.32	168	1.12	4	.03	2.50
3	475	3.20	251	1.63	219	1.49	4	.03	3.13
4	593	3.97	313	2.05	279	1.89	5	.03	3.93
5	765	5.15	399	2.61	364	2.45	6	.03	5.08
6	923	6.22	479	3.15	446	3.02	5	.03	6.17
7	939	6.32	502	3.31	455	3.09	4	.03	6.33
8	966	6.50	505	3.33	470	3.20	8	.06	6.46
9	997	6.72	521	3.44	485	3.29	15	.14	6.59
10	1039	7.01	543	3.60	507	3.44	68	.75	6.28
11	1188	8.02	625	4.12	583	3.96	211	2.46	5.59
12									
13	1197	8.09	631	4.17	589	4.00	264	3.10	5.03
14	1324	8.94	697	4.60	650	4.41	268	3.15	5.83
15	1360	9.20	719	4.75	670	4.54	390	4.60	4.65
16	1518	10.26	807	5.33	748	5.09	486	5.75	4.59
17	1640	11.09	873	5.76	810	5.50	568	6.72	4.56
18	1634	11.06	879	5.80	802	5.45	645	7.65	3.51
19	1649	11.14	884	5.84	807	5.48	690	8.17	3.06
20	1819	12.28	979	6.45	897	6.09	760	9.00	3.41
21	1889	12.75	1019	6.72	932	6.31	795	9.40	3.49
22	2074	14.00	1114	7.35	1022	6.90	855	10.12	4.01
23	2319	15.65	1249	8.25	1152	7.76	930	11.01	6.82

SPECIMEN NO. 3

Lateral Deflection

Loading step	Total load	~~Top~~ deflection (in.)	2nd storey deflection (in.)	3rd storey deflection (in.)	4th storey deflection (in.)
0	0	0	0	0	0
1	.44	.011	.005	.002	.001
2	2.50	.083	.059	.033	.013
3	3.13	.128	.085	.049	.022
4	3.93	.178	.105	.061	.031
5	5.08	.232	.158	.085	.039
6	6.17*	.310	.207	.115	.045
7	6.33	.403	.279	.159	.068
8	6.46	.513	.350	.207	.094
9	6.59	.593	.417	.240	.107
10	6.28	.689	.480	.297	.129
11	5.59	.810	.579	.336	.157
12	-	.895	.541	.375	.177
13	5.03	1.000	.717	.420	.200
14	-	1.110	.798	.479	.227
15	4.65	1.219	.879	.521	.257
16	4.59	1.414	1.021	.608	.294
17	4.56	1.599	1.164	.697	.342
18	3.51	1.850	1.342	.805	.344
19	3.06	2.008	1.458	.875	.429
20	3.41	2.222	1.616	.970	.478
21	3.49	2.453	1.711	1.042	.507
22	4.01	2.570	1.871	1.127	.557
23	4.82	3.210	2.279	1.320	.654

SPECIMEN NO. 3

Dial Gauges Readings of Walls

Rotation of Section 5¾" from Base

Loading step	Load on specimen	WALL 1				WALL 2			
		Comp. side (in.)	Ang. strain	Tension side (in.)	Ang. strain	Comp. side (in.)	Ang. strain	Tension side (in.)	Ang. strain
0	0	0	0	0	0	0	0	0	0
1	.44	0	0	0	0	0	0	0	0
2	2.50	.001	.000174	.004	.000696	-.002	.000348	-.005	.000870
3	3.13	.001	.000174	.002	.000348	-.005	.000870	-.007	.001217
4	3.93	.001	.000174	.0005	.000087	-.008	.001391	-.010	.001739
5	5.08	.002	.000378	-.007	.001217	-.017	.002957	-.014	.002434
6	6.17	.007	.001274	-.020	.003478	-.037	.006435	-.022	.003826
7	6.33	.011	.001913	-.043	.007478	-.067	.011652	-.063	.010957
8	6.46	.016	.002783	-.069	.012000	-.104	.018087	-.119	.020696
9	6.59	.020	.003478	-.090	.015652	-.134	.023304	-.162	.028174
10	6.28	.024	.004174	-.114	.019826	-.164	.028522	-.201	.034957
11	5.59	.030	.005217	-.144	.02543	-.205	.035652	-.240	.041739
12	-	.035	.006087	-.165	.028696	-.235	.040870	-.293	.050957
13	5.03	.039	.006783	-.192	.033391	-.271	.047130	-.324	.056348
14	-	.045	.007826	-.220	.038261	-.308	.053565	-.355	.061913
15	4.65	.050	.008696	-.248	.043130	-.346	.060174	-.393	.068348
16	4.59	.059	.010209	-.297	.051652	-.413	.071826	-.435	.075652
17	4.56	.069	.01200	-.346	.060174	-.480	.083478	-.513	.089217
18	3.51	.082	.01426	-.412	.071652	-.571	.099304	-.605	.105217
19	3.06	.092	.016000	-.455	.079130	-.631	.109739	-.724	.125913
20	3.41	.099	.012712	-.510	.088696	-.706	.122783	-.786	.136696
21	3.49	.107	.018609	-.543	.094434	-.766	.133217	-.886	.154087
22	4.01	.117	.020348	-.600	.104348	-.861	.149739	-.891	.154957
23	4.82	.142	.024696	-.710	.123478	-1.011	.175583	-1.039	.180695

SPECIMEN NO. 3

Rotation of Beams at Mid-span Sections

Loading step	Load applied	Beam #4 (lowest) lower side	Beam #4 (lowest) upper side	Beam #3 lower side	Beam #3 upper side	Beam #2 lower side	Beam #2 upper side	Beam #1 lower side
0	0	0	0	0	0	0	0	0
1	.44	0	0	0	.000	0	0	0
2	2.50	.001	.001	.0005	.001	.001	.001	0
3	3.13	.002	.001	.001	.001	.001	.001	0
4	3.93	.0025	.001	.001	.001	.001	.001	0
5	5.08	.004	.001	.002	.002	.0015	.0015	.0005
6	6.17	.0055	.005	.0025	.002	.0015	.0015	.0005
7	6.33	.006	.006	.003	.002	.002	.002	.0005
8	6.46	.006	.006	.003	.002	.002	.002	.0005
9	6.59	.007	.006	.003	.002	.002	.002	.0005
10	6.28	.007	.006	.003	.002	.002	.002	.0005
11	5.59	.007	.006	.003	.002	.002	.002	.0005
12	–	.007	.0065	.003	.002	.002	.002	.0005
13	5.03	.007	.0065	.003	.002	.002	.002	.0005
14	–	.007	.0065	.0035	.002	.002	.002	.0005
15	4.65	.0075	.005	.0035	.002	.002	.002	.0005
16	4.59	.008	.005	.004	.002	.002	.002	.0005
17	4.56	.008	.005	.004	.002	.002	.002	.0005
18	3.51	.008	.005	.004	.002	.002	.001	.001
19	3.06	.007	.005	.004	.002	.002	.001	.001
20	3.41	.007	.005	.004	.002	.002	.001	.001
21	3.49	.007	.006	.004	.002	.002	.001	.001
22	4.01	.007	.005	.004	.002	.002	.001	.001
23	4.82	.007	.005	.004	.002	.002	.001	.001

SPECIMEN NO. 3

Calculated Rotational Angles of Beams

Loading step	Total applied load	Beam #4	Beam #3	Beam #2	Beam #1
0	0	0	0	0	0
1	.44	0	0	0	0
2	2.50	.000193	.000195	.000193	0
3	3.13	.000289	.000193	.000193	0
4	3.93	.000337	.000193	.000193	0
5	5.08	.000482	.000386	.000289	.000096
6	6.17	.001012	.000434	.000289	.000096
7	6.33	.001157	.000482	.000386	.000096
8	6.46	.001157	.000482	.000386	.000096
9	6.59	.001253	.000482	.000386	.000096
10	6.28	.001253	.000482	.000386	.000096
11	5.59	.001253	.000482	.000386	.000096
12	-	.001301	.000482	.000386	.000096
13	5.03	.001301	.000482	.000386	.000096
14	-	.001301	.000530	.000386	.000096
15	4.65	.001205	.000530	.000386	.000096
16	4.59	.001253	.000578	.000386	.000096
17	4.56	.001253	.000578	.000386	.000096
18	3.51	.001253	.000578	.000289	.000193
19	3.06	.001157	.000587	.000289	.000193
20	3.41	.001157	.000578	.000289	.000193
21	3.49	.001253	.000578	.000289	.000193
22	4.01	.001157	.000578	.000289	0
23	4.82	.001157	.000578	.000289	0

APPENDIX D

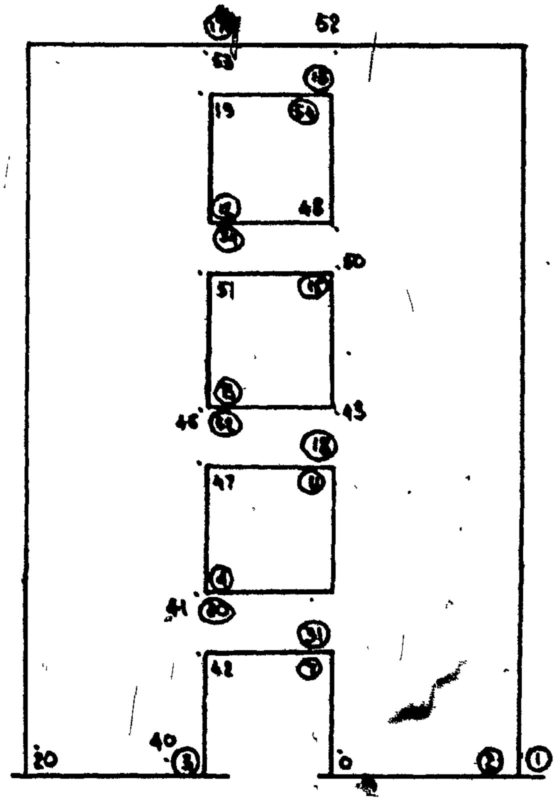

FIG. D.1 : NUMBERING OF STRAIN GAUGES
(REF: FIG. 3.21)

O CONCRETE

. STEEL

---- THEORETICAL

FIG. D.2: WALL 1, STRAIN GAUGES' READINGS

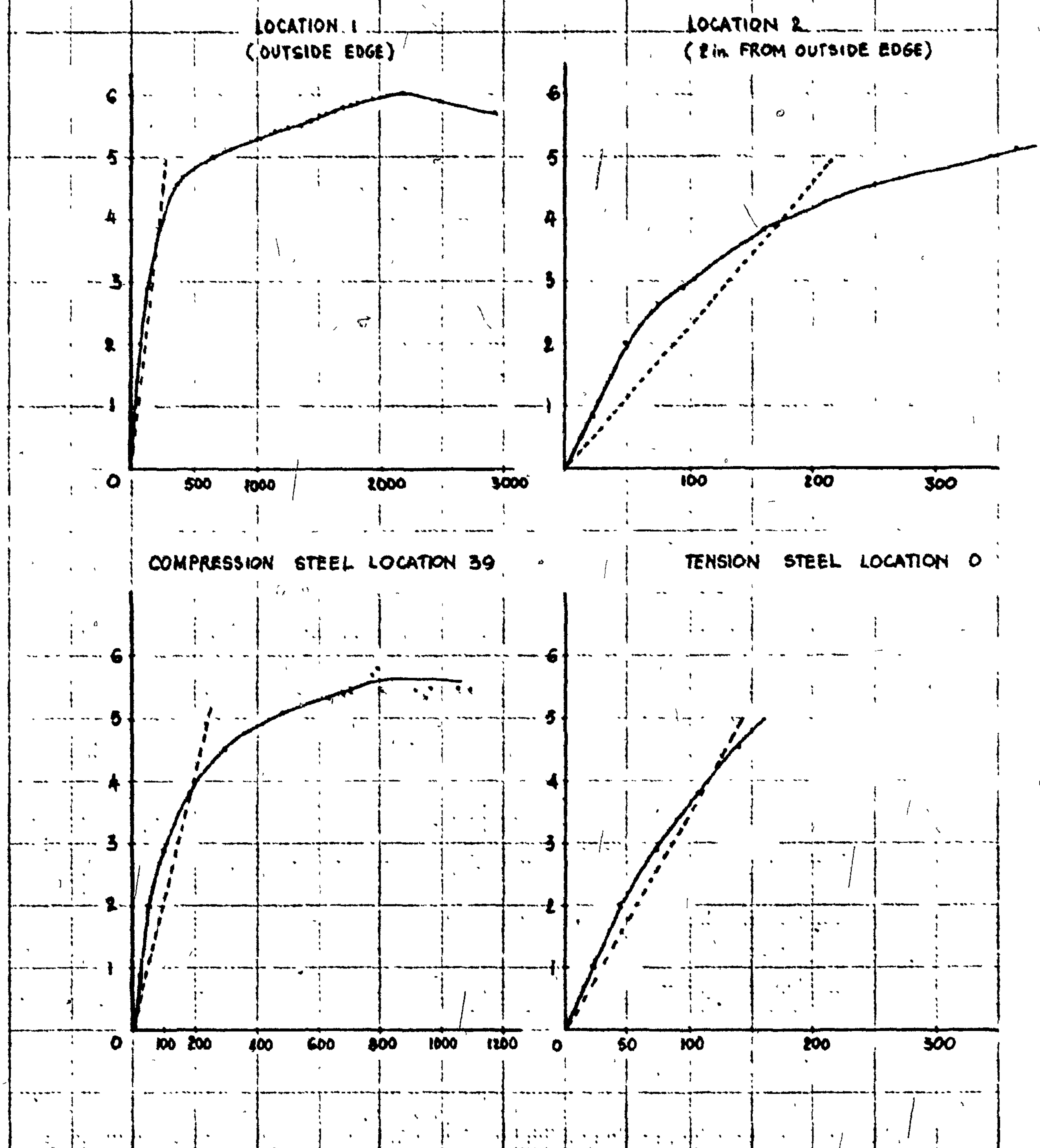

FIG. D.3 : WALL 2 STRAIN GAUGES' READINGS

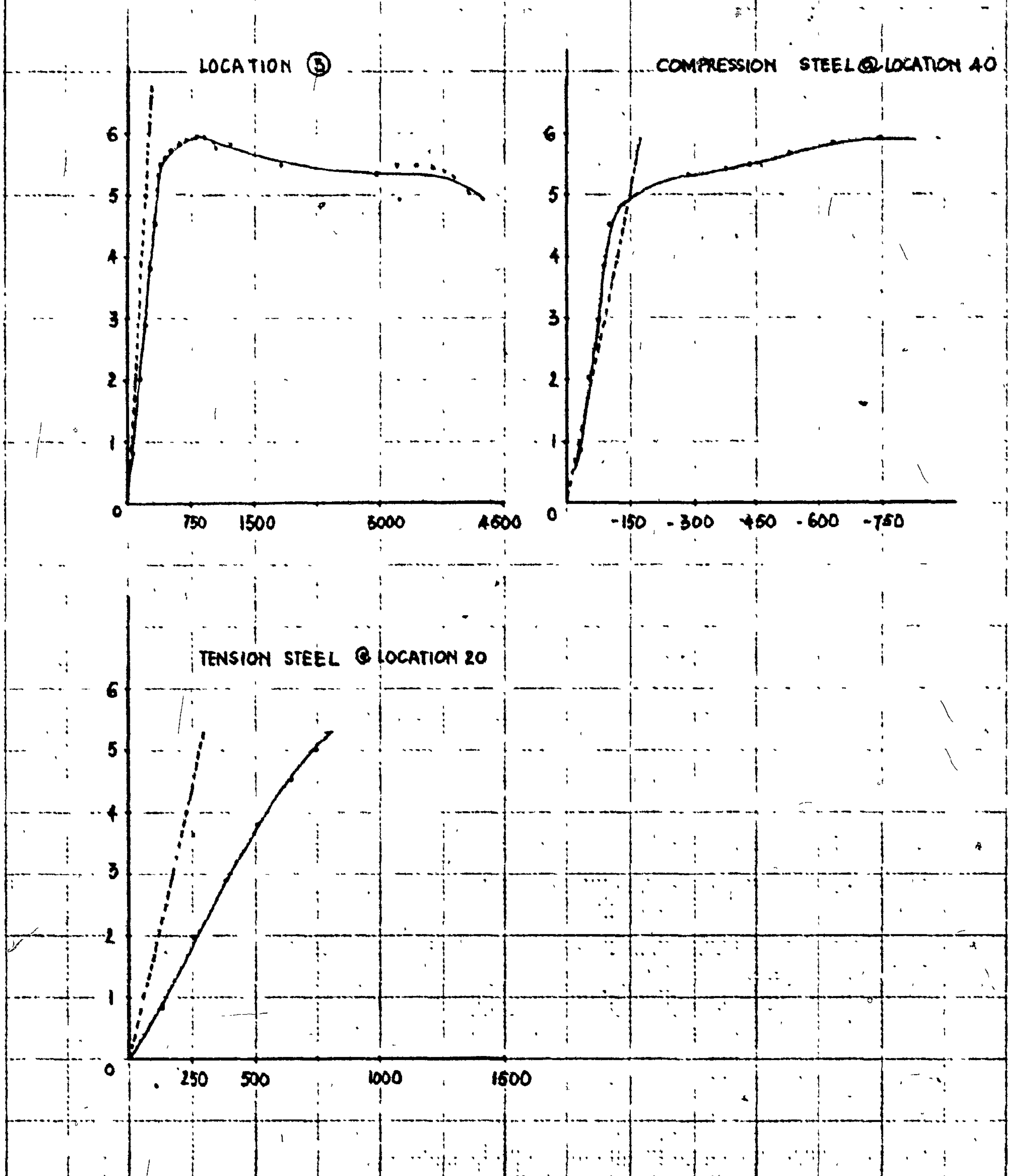

FIG. D.4 : BEAM I STRAIN GAUGES' READINGS

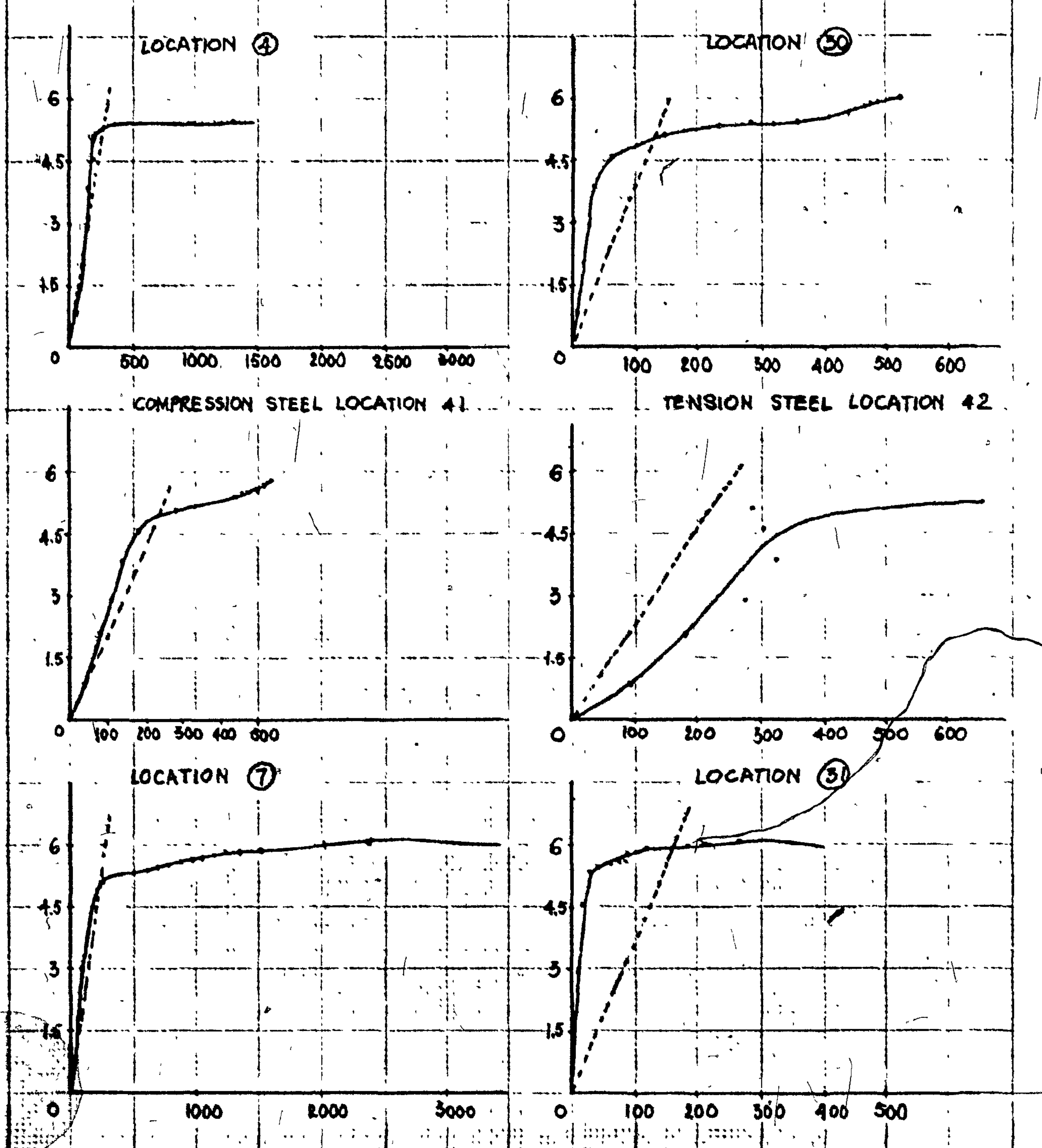

FIG. D.5 : BEAM 2 STRAIN GAUGES' READINGS

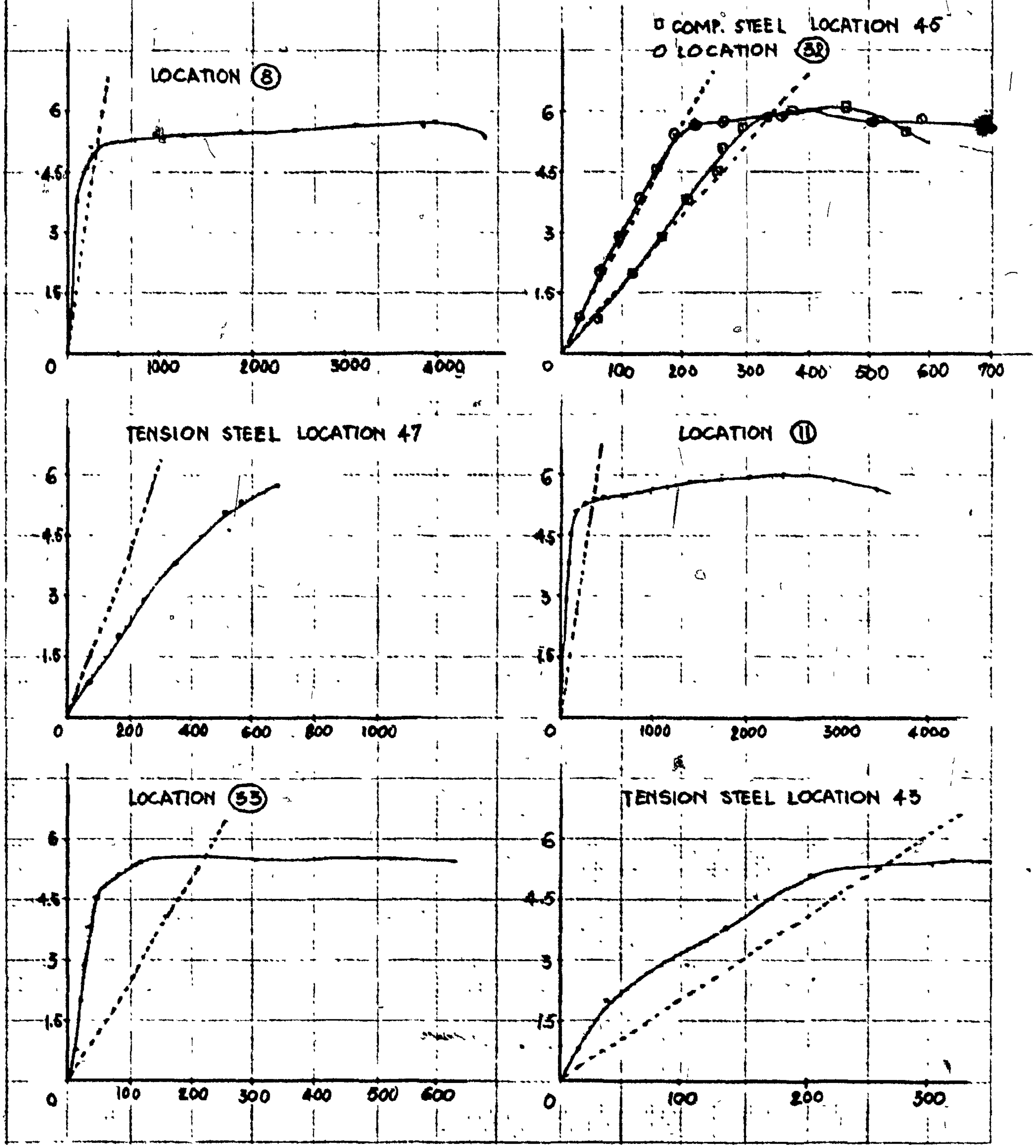

FIG. D.6 : BEAM 3 STRAIN GAUGES' READINGS

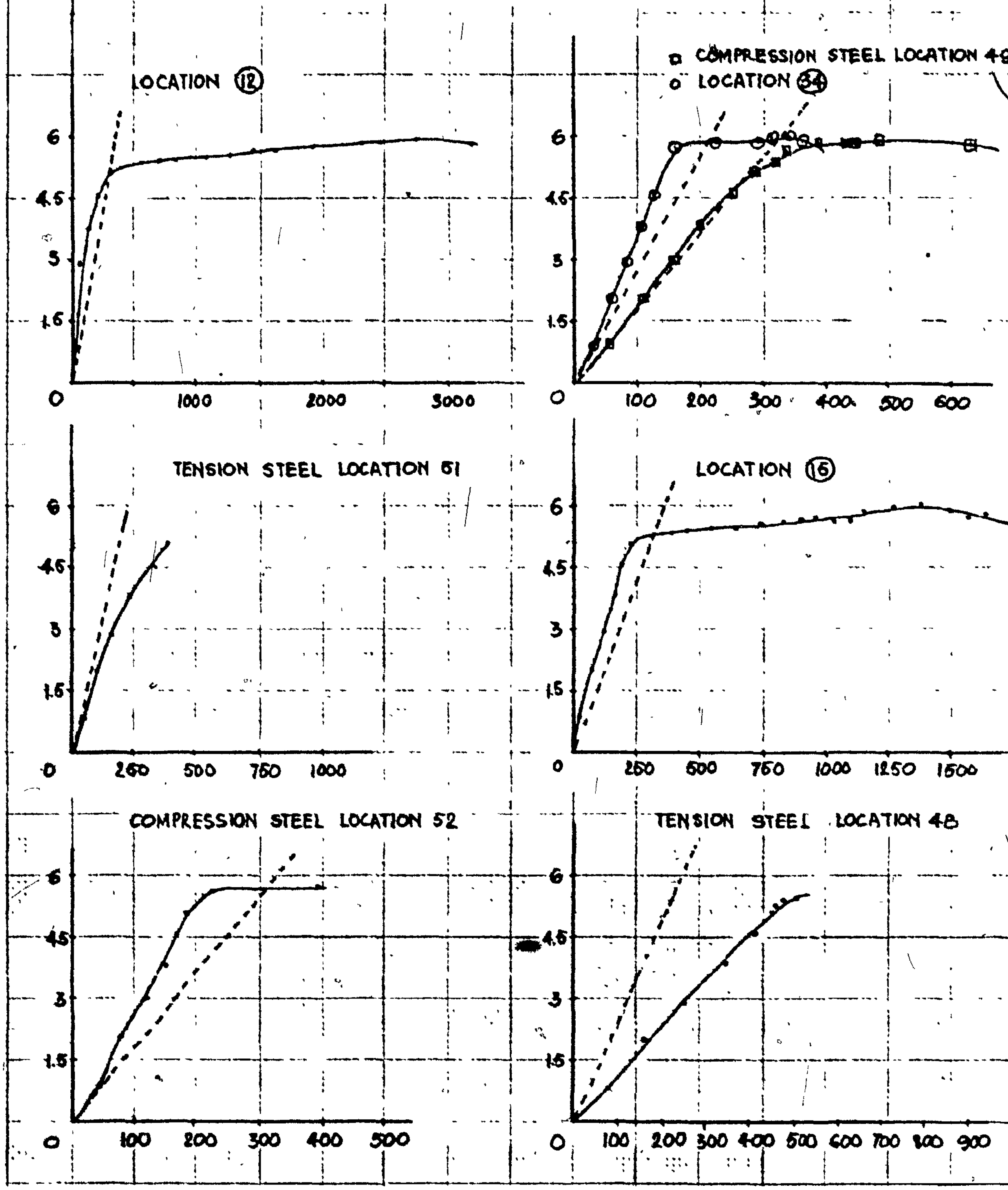

FIG. D.7 : BEAM 4. STRAIN READINGS